Final Report

Advanced Cathode Catalysts and Supports for PEM Fuel Cells

Grant No. DE-FC36-07GO17007

Submitted to the

U. S. Department of Energy, Office of Energy Efficiency and Renewable Energy, Transportation Technologies

September 30, 2012

by

3M Fuel Cell Components Program
3M Company, St. Paul, MN 55144

Prime Contractor: 3M Company, St. Paul, MN 55144

Project Title: Advanced Cathode Catalysts and Supports for PEM Fuel Cells

Principal Investigator: Dr. Mark K. Debe, 3M Fuel Cell Program

Team Members: Dalhousie University
Argonne National Laboratory
Jet Propulsion Laboratory

Key Vendor for Stack Testing: GM Fuel Cell Activities

(This page left blank intentionally)

Foreword and Acknowledgements

This report documents the work performed by 3M Company under the Grant No. DE-FC36-07GO17007, “Advanced Cathode Catalysts and Supports for PEM Fuel Cells.” The period of performance for this contract was from April 1, 2007 until June 30, 2012.

The principal objectives of the program were development of a durable, low cost, high performance cathode electrode (catalyst and support), that is fully integrated into a fuel cell membrane electrode assembly with gas diffusion media, fabricated by high volume capable processes, and is able to meet or exceed the 2015 DOE targets.

Work completed in this contract was an extension of the developments under three preceding cooperative agreements/grants Nos. DE-FC-02-97EE50473, DE-FC-99EE50582 and DE-FC36-02AL67621 which investigated catalyzed membrane electrode assemblies for PEM fuel cells based on a fundamentally new, nanostructured thin film catalyst and support system, and demonstrated the feasibility for high volume manufacturability.

All 3M MEA materials and process development were carried out by 3M Co. at its St. Paul, MN, 3M Center campus and its Menomonie, WI, pilot plant. The 3M team included primarily members from the Fuel Cell Components Program, with significant assistance received over varying periods of time from members of 3M’s Corporate Analytical Laboratory, and the Corporate Process Technology Laboratory. The principal technical team included Dr. Mark Debe as the principal investigator and technical team Leader, Mr. Andrew Steinbach as the chief operations specialist and functioning co-PI during the latter half of the contract. Dr. Radoslav Atanasoski was co-PI in the first half of the contract, Mr. Michael Kurkowski and Ms. Susan Hendricks were MEA fabrication and testing specialists, Mr. George Vernstrom was the thin film catalyst deposition specialist, Ms. Amy Hester was the project’s process engineer, and Mr. Paul Kadera the test station and utilities support technologist. Dr. James Larson led the GDL optimization work during the first half of the project before his retirement. The technical team is grateful for the significant help of Dr. Krzysztof Lewinski, Mr. Daniel Pierpont and Dr. Andrew Haug on Tasks 3, 6 and 1.3 respectively, and multiple technical aides and contract employees who assisted throughout the contract, and the invaluable contributions by the fuel cell program’s membrane development group and the manufacturing specialists and engineers at the Menomonie, Wisconsin pilot plant. Mr. Steven Kays of the 3M Government R&D Contracts department was the project’s contract administrator, with assistance from financial, controller, property accounting and sourcing experts Ms. Tara ann Witte, Ms. Anne Ringgenberg, Ms. Debra Budach and Mr. Brian Massel, respectively.

Subcontractors included Dalhousie University, Nova Scotia, Canada; NASA Jet Propulsion Laboratory, Pasadena, California; Argonne National Laboratory, Chicago, Illinois; and for final stack testing, the GM Fuel Cell Activities in Honeoye Falls, N. Y.

From our subcontractors’ organizations we are particularly indebted to Prof. Jeffrey Dahn and Dr. David Stevens of Dalhousie U.; Drs. Nenad Markovic, Vojislav Stamenkovic and Dennis van der Vliet of ANL; Drs. Charles Hays and S. R. Narayanan of JPL, and Eric Thompson of GM.

This work was funded in part by the U. S. DOE, Energy Efficiency and Renewable Energy Office of Transportation Technologies and Advanced Automotive Technologies. DOE technical and administrative oversight of the project was provided by DOE Managers Kathy Epping Martin (HQ) and David Person (GO) of the DOE Hydrogen and Fuel Cells Program, and DOE Technical Advisor Mr. Thomas Benjamin (Argonne National Laboratory).

Executive Summary

Today the world faces increasingly serious environmental challenges. Solutions to these challenges must come from a proper balance of often conflicting public policy and socio-economic drivers with the availability of appropriate new technology. The development of hydrogen fueled vehicles for transportation is one example of new technology seriously being considered to replace the internal combustion engine (ICE) in order to reduce our dependence on fossil fuels and lower emissions of greenhouse gasses.

The polymer electrolyte membrane fuel cell (PEMFC) is the ultimate electric vehicle drive technology being developed to replace the ICE. By electrochemically combining hydrogen and oxygen from air to produce water, electricity is generated by the fuel cell for powering electric motors that drive the vehicle without pollution and minimal carbon emissions depending on the source of the hydrogen. Although the concept of a fuel cell is well over a century old, only in the last two decades have sufficiently significant advances been made in the PEMFC technology to warrant substantial investments in the development of practical systems. Many materials and process challenges remain to be overcome before cost effective, fuel cell powered vehicles can be successfully commercialized at reasonably high volumes. This report summarizes the work completed over the past five years under a 3M Company/U. S. Department of Energy grant directed specifically at advancing the key fuel cell components most critical for overcoming the PEMFC performance, durability and cost barriers.

The heart of a working PEMFC, where the electrochemical reactions convert the hydrogen and air to electricity, heat and water, is called the membrane electrode assembly, or MEA. At its simplest, the MEA is a multi-layered article comprising two key components: the ion exchange membrane at its center, and the Pt based electrocatalysts on either side of the membrane (see Fig. 1), where H_2 is oxidized on the anode and O_2 is reduced on the cathode, producing water on the cathode, heat and the desired product electricity flowing through an outside load between the anode and cathode. Fig. 1 illustrates more generally the five principal components forming a three or five layer MEA depending on whether the gas diffusion components are included. The catalyst electrodes can be coated or bonded to the PEM directly, or coated onto the porous carbon gas diffusion media. The MEA components interact strongly and affect the performance and durability of the fully integrated MEA by many complex mechanisms. In practice this necessitates development of the whole MEA package in order to optimize any individual component, particularly the catalysts. The cathode O_2 reduction reaction is six or more orders of magnitude slower than the anode H_2 oxidation reaction, so most PEM fuel cell research and development focuses on the cathode catalysts and electrodes. The anode electrodes however can have a dramatic influence on the cathode performance through water management effects viz. drying or flooding of the cathode with product water; carbon support corrosion due to cathode voltage excursions from anode H_2 starvation or start-up/shut down events; and the PEM lifetime from the anode's role in peroxide production due to cross-over of gases through the PEM, particularly at open circuit potentials. The catalysts and membrane are the most expensive components of the fuel cell for reasons related to the materials necessary to obtain the performance and durability.

Today's commercialized catalysts consist of nanometer sized particles of Pt or Pt alloys dispersed onto carbon black support particles. They are formed into "inks" and applied to the surfaces of the ion exchange membranes or gas diffusion media. However, despite the world's overwhelming research focus on use of carbon black supported nanoparticles for PEM FC catalysts, they have several fundamental limitations. Within the real life automotive fuel cell environment, the carbon support particles can be rapidly corroded at the high potentials seen

during start/stop events, the Pt nano-particles (2-4 nm diameter) have a natural susceptibility to Pt dissolution due to their small radii of curvature, or they tend to surface migrate together, agglomerating or growing by Ostwald ripening and losing effective surface area. The smaller the Pt particles are made in order to increase their surface area, the lower their fundamental activity for reducing oxygen to water, the basic cathode oxygen reduction reaction or ORR. Conversely larger particles have lower surface area. Nano-sized dispersed Pt particles exhibit low specific activity for the primary oxygen reduction reaction compared to extended surface catalysts, and more recently it is found that at ultra-low cathode loadings, the limits of high current density decrease more quickly than expected based on state-of-the-art modeling.

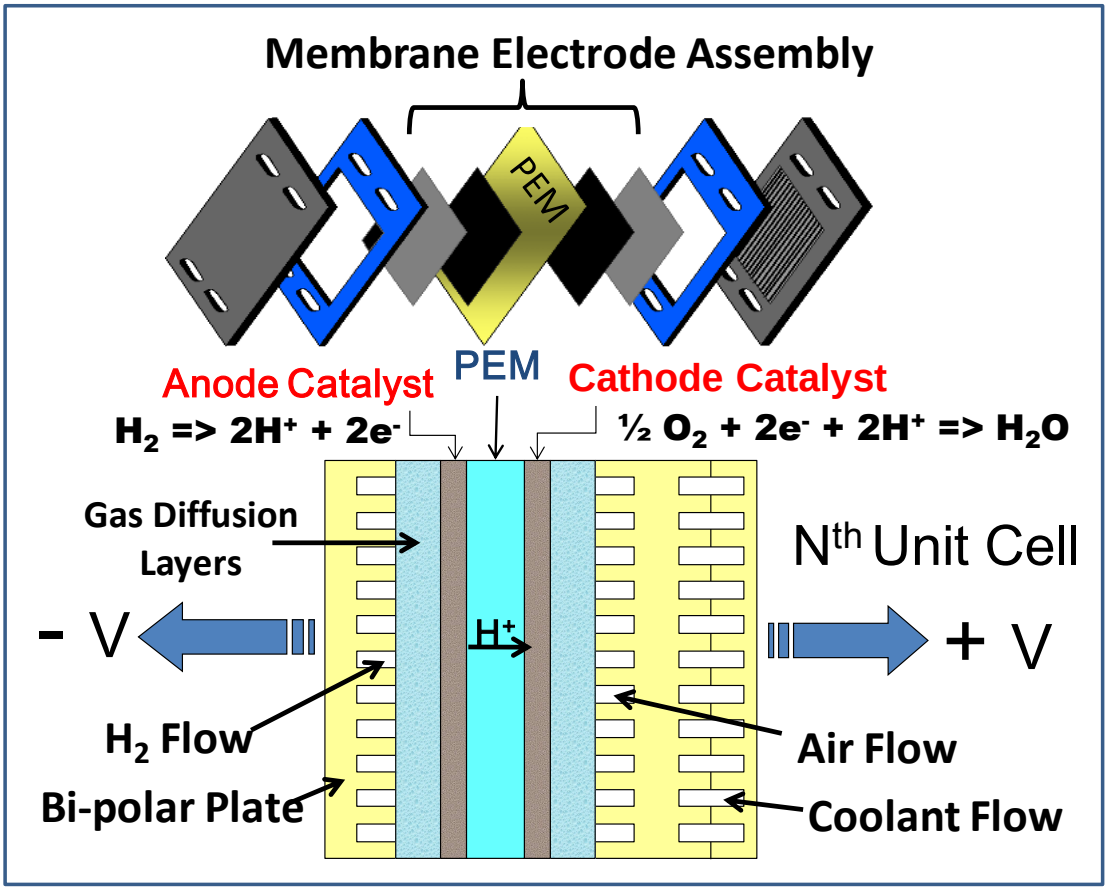

Fig. 1. Fuel cell components. Unit cell cross-section of a fuel cell stack showing the components of an expanded MEA.

Higher performing and more durable electrocatalysts at lower loadings must be developed for PEMFCs to meet the power density and lifetime hours required for fuel cell vehicles at acceptable costs. This means the catalyst activities for reducing the oxygen to water must be improved. At the same time the amount of expensive Pt catalyst must be reduced to lower the MEA costs. And while these two properties are met, the catalyst must be made more resistant to multiple degradation mechanisms to reach the necessary operating lifetimes.

In this report, we present a body of work focused on the continued development of a completely new approach to PEMFC electrocatalysts, called nanostructured thin film (NSTF) catalysts that eliminate many of the issues identified above with current catalyst technology. The carbon black supports are eliminated with this new approach and that eliminates the carbon corrosion

issue. The thin film nature of the catalyst significantly improves its robustness against dissolution and grain growth, preserving the surface area. Most important, the fundamental activity of the NSTF Pt catalysts for oxygen reduction is improved by over 500% compared to dispersed Pt catalysts. Finally, the process for fabricating the NSTF catalysts is consistent with high volume roll-good manufacturing, and extremely flexible towards the introduction of new catalyst compositions and structures. In this report we document the progress made developing new multi-element NSTF catalysts with properties that meet or exceed all the DOE Hydrogen Fuel Cells Program's 2015 targets for PEMFC electrocatalysts. The body of work completed advances the fundamental understanding of the NSTF catalyst technology, identifies and develops new NSTF-ternary catalyst materials for higher performance and durability at reduced loadings, and advances the high volume process capabilities for producing the NSTF based MEA's.

Report Organization

A list of abbreviations and acronyms for the entire report is contained in this introductory section, immediately after the high level table of contents following this introduction. The major body of the report summarizing the accomplishments towards all the project objectives and DOE fuel cell catalyst target metrics has a more detailed table of contents defining its organization, as well as its own list of references. This is followed by a summary of the project technology transfer accomplishments, including publications in technical journals, invited and contributed international presentations, and patent applications resulting from this project.

A Supplementary Section provides more detailed summaries of major aspects of the six specific work Tasks of the project.

The final Appendix reproduces fifteen of the twenty-seven total publications in peer reviewed journals that derived from this project and which we consider to be highly significant outcomes.

High Level Table of Contents

List of Abbreviations and Acronyms

ADF-STEM	Annular dark field scanning transmission electron microscopy
ANL	Argonne National Laboratory
AST	Accelerated stress test
CCB	Catalyst coated backing
CS	Constant stoichiometry
CCM	Catalyst coated membrane
CV	Cyclic voltammograms
DI	Deionized water
DOE	Department of Energy
DP	Dew point
ECSA	Electrochemical surface area
EMP	Electron microprobe
EW	Equivalent weight, polymer weight per mol of acid groups
FC	Fuel cell
GDL	Gas diffusion layer
HFR	High frequency resistance
HOR	Hydrogen oxidation reaction
HRTEM	High resolution transmission electron microscopy
Hupd	Hydrogen under-potential deposition
ICP	Inductively coupled plasma
IEC	Ion exchange capacity
MEA	Membrane electrode assembly
MPL	Microporous layer
MYDP	Multi-Year Research, Development and Demonstration Plan
NSTF	Nanostructured thin film catalyst
NSTFC	Nanostructured thin film catalyst
OCV	Open circuit voltage
OEM	Original Equipment Manufacturer
OER	Oxygen evolution reaction
ORR	Oxygen reduction reaction
PDS	Potentiodynamic polarization scan
PEM	Proton exchange membrane, polymer electrolyte membrane
PEMFC	Proton exchange membrane fuel cell
PR-149	Perylene red 149
PGM	Precious group metal
PSIG	Pounds per square inch gauge
PSS	Potentiostatic scans
Pt/C	Pt on carbon catalysts
R^2	Least squares fitting parameter
R2R	Roll to roll, as in process
RDE	Rotating Disc Electrode
RH	Relative humidity
RHE	Reversible hydrogen electrode
RRDE	Rotating ring disc electrode
SCCM	Standard cubic centimeter per minute
SEF	Surface area enhancement factor
SET	Surface energy treatment
St.	Stoichiometric
S_{min}	Minimum normalized surface area
TEM	Transmission electron microscopy
TM	Transition metal
XRD	X-ray diffraction
XRF	X-ray fluorescence

Project Overview Table of Contents

1. Introduction – Background and Overview of Scope of Work Completed

State-of-the-art proton exchange membrane (PEM) fuel cell electrocatalyst technology utilized in today's prototype fuel cell vehicles reveals limitations with respect to general durability and robustness under start-stop cycling, adequate performance with low PGM loadings, and low-cost manufacturability. To a large degree, these deficiencies are traceable to properties of the conventional carbon supported dispersed Pt catalysts in use today and issues with membrane integration. The research and development of this project were focused on overcoming these three most critical barriers for fuel cell MEA automotive deployment by using an alternative catalyst support and deposition method.

The approach to achieve the above objectives builds on a fifteen-year DOE/3M-funded development of the 3M nanostructured thin film (NSTF) catalyst and MEA technology. The NSTF catalyst is the only practical example of an extended surface catalyst, and thereby fundamentally has higher specific activity for oxygen reduction [1-11], removes all durability issues with carbon supports, demonstrates much lower losses due to Pt dissolution and membrane chemical attack [12-15], and has significant high volume all-dry roll-good manufacturing advantages [16].

The scope of work in the initial three-year 1st budget period included extensive work at 3M to increase the NSTF catalyst support film surface area, fabrication and screening of new alloys in 50 cm^2 single cells, and evaluation of multiple deposition parameters to obtain increased catalyst surface area and utilization. Complementary to this work at 3M, collaborative work included high throughput fabrication and characterization of new multi-element Pt alloys (ternaries and quaternaries) with Dalhousie University, fundamental catalyst characterization studies with ANL, and development and evaluation of a pseudo-rotating disk electrode (RDE) catalyst evaluation technique with JPL. Research in the fourth year focused at 3M on continued studies of water management improvements for cool/wet operation via optimization of materials, electrode structure and operating conditions; catalyst fabrication process improvements for increased catalyst performance and production efficiency; in-depth MEA component screening to down-select final configurations for the final short-stack testing; continued accelerated testing to benchmark the NSTF-MEA durability with each generation of MEA components; and initial fabrication of roll-good materials for initial stack testing by the GM fuel cell laboratory.

The final year focus was on a) completing the first year short stack testing to down-select a final MEA type for a 2nd (durability) stack; b) resolving specific production and MEA integration issues related to the final stack MEAs; c) 2nd stack durability protocol development and initial testing; d) extension of the improved, more cost effective P1 deposition process to the as-made NSTF-Pt_3Ni_7 catalysts; and e) development of fast roll-to-roll (R2R) capable de-alloying and annealing processes for the next generation NSTF "Pt_3Ni_7" catalysts discovered and developed under this project (17-20).

2. Project Objectives, Scope and Approach, and Task Definitions

A. Project Objectives

This project addresses the following technical barriers from the Fuel Cells section of the Fuel Cell Technologies Program Multi-Year Research, Development and Demonstration Plan: (A) Durability, (B) Cost and (C) Performance. The objectives of this project are development of a durable, low cost [both precious group metal (PGM) content and manufacturability], high performance cathode electrode (catalyst and support), which is fully integrated into a proton exchange membrane electrode assembly characterized by: a) total Pt group metal loading per MEA of $\leq$ 0.25 mg/cm^2, b) high prospects for 40,000 hours durability under operating conditions for stationary applications, c) short-stack inverse specific power density of < 0.5 g/kW_{rated}, d)

durability sufficient to operate at > 80°C for 2000 hours, ≤ 80°C for 5000 hours, with cycling for transportation applications, and e) high volume manufacturability.

B. Project Scope

State-of-the-art PEM fuel cell electrocatalyst technology utilized in today's prototype fuel cell vehicles and commercialized stationary systems are demonstrating significant limitations with respect to general durability and robustness under start-stop cycling, adequate performance with low PGM loadings, wide temperature and humidity operating windows, and low cost manufacturability. To a significant degree, these deficiencies are traceable to properties of the conventional cathode catalysts in use today. The focus of this project is development of advanced cathode catalysts and supports based on 3M's nanostructured thin film (NSTF) catalyst technology platform, which has already demonstrated catalyst specific activity and durability significantly higher than conventional carbon supported Pt catalysts. The scope of work includes fundamental catalyst studies, high throughput fabrication and characterization of new multi-element Pt alloys (ternaries and quaternaries), investigation of alternative catalyst support particles, extensive fuel cell testing in 50-cm^2 single cells and large area short stacks, and integrated MEA development using advanced 3M membranes and GDL's specific to the new NSTF catalysts.

C. Task Definitions

Task 1.0 Catalyst Activity and Utilization Improvements

Subtask 1.1 NSTF surface area optimization

The purpose of this subtask is to increase the surface area of the NSTF catalysts by increasing the surface area of the catalyst support system. The NSTF catalyst support system consists of a monolayer of oriented, high aspect ratio (length-to-width) crystalline whiskers, ~ 1 micron in length, with area number densities exceeding 3 billion whiskers/cm^2. The expected outcome will be an increase in the specific surface area of the NSTF catalysts by a factor of 2x to 3x from the current ~ 10 m^2/g-Pt.

Subtask 1.2 Fundamental studies of NSTF catalysts

The purpose of this subtask is to obtain a better understanding of the fundamental oxygen reduction reaction pathways on the NSTF ternary catalysts in order to elucidate the source of the well documented 10x gain in specific activity that NSTFC demonstrates over conventional dispersed Pt/Carbon electrocatalysts. An expected outcome of this subtask will be an understanding of the most important material parameters for obtaining further gains in NSTF electrocatalyst specific activity.

Subtask 1.3 New multi-element catalysts to increase activity and reduce impedance.

The purpose of this subtask is to obtain further increases in the NSTF catalyst specific activity (A/cm^2-Pt) for ORR by fabrication, characterization and screening of new Pt alloys. The approach will use well established methods at 3M and its collaborators for rapid throughput fabrication and characterization of new multi-element alloy catalyst compositions and constructions. An expected outcome of this subtask is a further increase in stable alloy specific activity by 50% or more over the current best PtCoMn ternary.

Task 2.0 NSTF catalyst stabilization against dissolution

The purpose of this subtask is to down-select the new catalyst compositions from Task 1 for improved stability against Pt corrosion at high potentials, high temperatures or under conditions of voltage transients or stop/start cycling. The approach will use well-documented methods, by 3M and one of its collaborators, for ex-situ and in-situ evaluation of catalyst

durability and stability. This task includes high throughput fabrication and screening of the new catalyst compositions as well for enhanced grain size stabilization which can maintain surface area. The outcome will be a subset of the higher performing catalysts which demonstrate, using these tests, increased resistance to Pt dissolution over the current PtCoMn state-of-the-art NSTF electrocatalyst.

Task 3.0 Full Size (> 250 cm^2) Single or Multi-Cell Tests

Subtask 3.1 Down-selection of cathode catalysts in 50-cm^2 cell tests

The purpose of this subtask is to evaluate MEA's made with subsets of the supports and catalysts down-selected from Tasks 1 and 2, in 50 to 100 cm^2 single cells, using well established testing protocols for performance and durability. The approach will consist of performance and durability load-cycle testing under various pressures, temperatures, stoichiometries and relative humidities. Durability testing will include the accelerated testing recommended by DOE in Appendix D of the solicitation, or more rigorous accelerated tests as may be advised at the time. The expected outcome will be the down-selected cathode catalysts which demonstrate the best overall performance and durability when evaluated as 50 to 100 cm^2 MEA's that could meet the 5000 hour lifetime targets. Overlaps with down-selection work done under subtasks 5.1 and 5.2

Subtask 3.2 Large area short stack durability tests

The purpose of this subtask is to take the down-selected cathode catalysts from Subtask 3.1 and validate with accelerated testing that the same performance and durability is achieved in large area (> 300 cm^2) single (or at most several) cells, using existing, proven stack hardware at 3M. The approach may include at least three stack builds. The expected outcome will be validation that under non-accelerated testing the full size MEA's would meet the 5000 hour targets.

Task 4.0 Alternative Support Structures

The objective of this task is demonstration of a novel catalyst support which eliminates all carbon corrosion and is optimized for cathode catalyst loadings of $\leq$ 0.2 mg_{Pt}/cm^2 so as to enable a cathode catalyst mass activity of ≥ 0.44 A/mg_{Pt} and durability against surface area and activity losses sufficient for 5000 hours operation at ≥ 80°C under cycling conditions for transportation applications or 40,000 hours under operating conditions for stationary applications.

Subtask 4.1 Durability tests of new NSTF supports

The purpose of this subtask is to specifically evaluate the stability of the new NSTF based catalyst supports derived from Subtask 1.1. The approach will use accelerated tests to evaluate stability of the catalyst activity and surface areas against corrosion of the support from high voltage cycling, stop/start cycling or fuel starvation. Both high through-put characterization methods as well as 50-cm^2 single cell tests will be included in the approach. The expected outcome is a down-selection of the new NSTF catalyst supports from Subtask 1.1 that also meet the durability requirements.

Task 5.0 Stack Testing and Optimized NSTF MEA

The objective of this task is development of durable, low cost (PGM content and manufacturability), high volume manufacturable MEA's with optimally integrated components from Tasks 2-4, which demonstrate a stack specific power density of < 0.5 g/kW_{rated}, and durability sufficient to operate at $\geq$ 80°C for 5000 hours under cycling operation for transportation applications, while using a total Pt group precious metal loading per MEA of < 0.3 mg/cm^2. The approach is to optimize the NSTF catalyst/membrane interface using lower EW

PFSA 3M membranes and GDL media optimized for the unique water management properties of the ultra-thin NSTF electrodes, followed by validation in large area short stacks.

Subtask 5.1 NSTF catalyst / low EW membrane interface integration

The purpose of this subtask is to optimize the pilot scale fabrication of catalyst coated membrane (CCM) roll-goods using the advanced cathode catalysts and supports from Tasks 1-4 in combination with new, lower equivalent weight 3M membranes developed (outside of this project) to have enhanced durability and water management properties. There is also a critical stability/durability aspect to this subtask as well due to significant effects of internal and external impurities on the catalyst/membrane interface.

Subtask 5.2 Optimized MEA components for water management

The purpose of this subtask is to develop MEA components and their interfaces, e.g. the anode and cathode GDL's, for best overall water management and high current density performance under automotive conditions, including cool/wet operation, in combination with the CCM's from Subtask 5.1. The approach will include evaluating available roll-good fabricated electrode backing materials having various 3M developed water proofing and microporous layer coatings, as well as more novel configurations. The expected outcome is a GDL configuration that best matches the CCM and stack flow field in which the integrated MEA will be tested for performance and durability.

Subtask 5.3 Short stack testing (> 10 cells, > 250 cm^2)

The purpose of this subtask is the final short-stack testing of large area MEA's developed in Tasks 1 - 5.2. The approach will be to use existing, proven 3M stack hardware and include independent validation at a specified DOE facility. The expected outcome will be a demonstration of advanced MEA's that meet the overall-project's objectives for performance and durability and were fabricated with high-volume capable processes.

Task 6.0 Reduction of Break-in Conditioning Time

The purpose of this task is to formally address a critical remaining gap for successful commercialization readiness of the 3M NSTF catalyst based MEA's.

Subtask 6.1 Break-in conditioning protocol

The purpose of this subtask is to quantify the effect of test station operating parameters on the time for break-in conditioning of the standard PtCoMn NSTF MEA's in 50 cm^2 single cell tests, to determine the best methodology to reach full performance in the shortest time using a facile protocol. The cell operating temperatures, relative humidity or liquid water flow, reactant flow rates, voltage and current density cycling ranges and speeds, will be systematically investigated. The objective is to reduce the time of break-in by a factor of two to four and simplify the protocol over the current NSTF MEA standard "thermal cycling" protocol.

Subtask 6.2 MEA component factors affecting break-in conditioning time

The purpose of this subtask is to understand the impact of specific NSTF MEA components on the break-in conditioning time to reach full performance. The current NSTF MEA standard "thermal cycling" protocol will be used for break-in conditioning while specific material changes will be studied for their effect on the break-in time. The focus will be on the catalyst composition and method of preparation, and the membrane and its method of preparation, as these are already observed to have significant impact on the number of thermal cycles required for full break-in. Improved protocols from task 6.1 will be incorporated as they occur. The objective is to reduce the overall time for full break-in conditioning by an order of magnitude.

Task 7.0 Project Management and Reporting

This task provided all aspects of the project management, documentation including six DOE Hydrogen Program Annual Merit Review presentations, seven additional annual and Go-No-go reviews requested by DOE managers, four FreedomCAR technical team reviews, twenty-one quarterly reports, five annual reports, and all financial report and documentation requirements including intellectual property development notification.

3. Project Timeline and Milestones

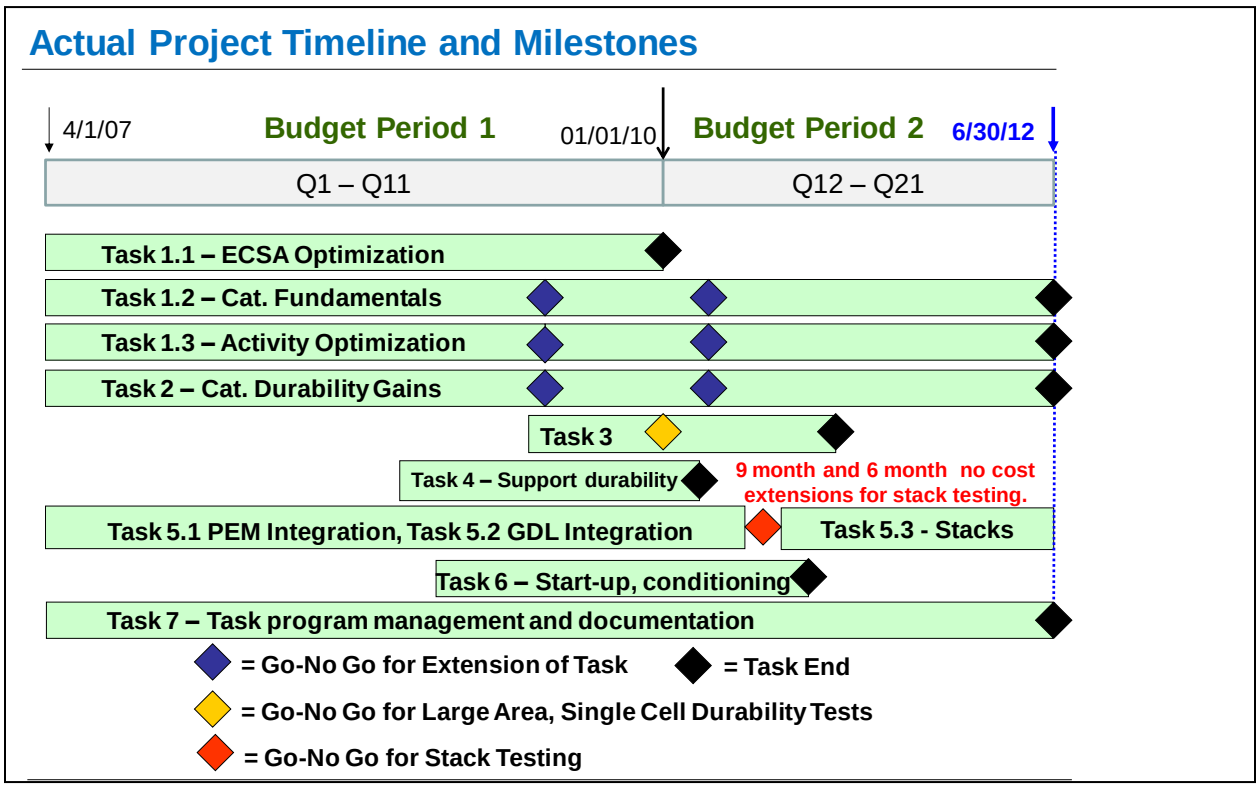

The chart above shows the actual project timeline and milestone dates for the project. The original project performance period was four years. However due to issues with preparation for and execution of the final stack testing, two no-cost extensions were granted for an additional 15 months total.

4. Subcontractors, Roles and Other Collaborators

A. Primary Collaborators by Task

TASK Collab.	1.1.1	1.1.2	1.2	1.3	2.1	2.2	3	4.1	4.2	4.3	5	6
3M	X	X	X	X	X	X	X	X	X	X	X	X
Dalhousie University		X		X	X	X		X				
JPL				X		X						
ANL			X									
GM											X	

B. Additional Collaborations (within and outside this contract)

System Integrators and stack manufacturers (partial list)

- GM Fuel Cell Activities -Honeoye Falls: Extensive collaboration outside of DOE H_2 program with materials generated at 3M under this contract. Multi-year single cell performance and activity validations, stack testing (outside Task 5.3), cold/freeze start and water management evaluations, PEM and GDL integration, durability testing, and modeling studies.
- Nuvera Fuel Cells Corporation. Technology integration project to evaluate for the first time, the combination of the 3M NSTF electrode technology with the Nuvera open flow field bi-polar plate technology.
- Proton OnSite (formerly Proton Energy Systems) – Performance testing of NSTF MEAs in electrolyzers. Ongoing testing of NSTF electrodes in short stacks for both electrolyzer cathodes and anodes.
- Giner EC Systems, LLC – Performance testing of NSTF MEAs in electrolyzers. Testing of NSTF electrodes for both electrolyzer cathodes and anodes.
- DTI, LLC – provided NSTF manufacturing related information for cost analyses.

National Laboratories

- LBNL (Weber), LANL– Participating in FFRDC Project on FC Fundamentals at Low and Subzero Temperatures, and ARPA-E funded GRIDS flow battery project.
- ANL (Ahluwalia group) - Extensive Fuel Cell Systems modeling with 3M supplied data for MEA performance under ANL defined conditions.
- ORNL (K. Moore group) – Samples supplied for TEM characterization
- NIST (Eric Stanfield group) – Samples and data supplied to NIST for optical method development under DE-EE0001047 to measure CCM Pt loadings during roll-to-roll fabrication

Other

- BASF – provided used NSTF MEA samples for Pt recovery measurements that BASF was carrying out for their own DOE project.

5. Definitions and Methodology for ORR Activity Measurements

Box 1

Definitions and activity targets

- The surface-area enhancement factor is the Pt catalyst surface area, S, measured by the charge generated from an under-potential deposited monolayer of the hydrogen atoms on the Pt catalyst surface divided by the planar area of the sample (cm^2 of Pt per planar cm^2.)
- Pt loading is the number of mg of Pt per planar cm^2 in an MEA electrode layer.
- Absolute ORR kinetic activity is currently defined as the current density measured at 900 mV under one atmosphere of fully saturated pure oxygen, at 80 ^oC. For an MEA this means 150 kPa absolute pressure due to 50 kPa of water vapor.
- The area-specific activity A_s (amps per cm^2 of Pt) is determined by dividing the absolute activity by the surface-area enhancement factor.
- The mass activity A_m (amps per mg of Pt) is determined by dividing the absolute activity by the Pt loading.
- The DOE's 2017 target for A_m is 0.44 A/mg –Pt and its 2015 target for A_s is 0.7 mA per cm^2 of Pt.

Reliable measurements of ORR activity depend on generally accepted methods and protocols. Even with these defined "standard operating procedures", laboratory to laboratory variations of 50% are not uncommon in reported ORR activities. Box 1 above gives standard definitions of the meaning of ORR absolute, mass and specific activity and the DOE targets for those quantities.

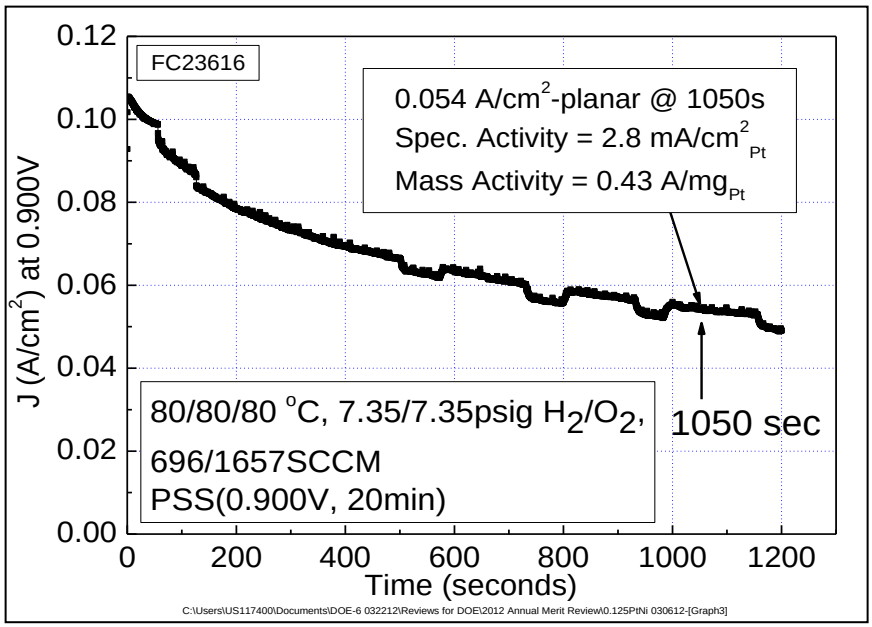

Fig. 5.1. Current density vs time trace for an MEA illustrating the protocol for measurement of ORR absolute activity. The MEA in this case is the same as used to generate the polarization curves in Figure 6.3. The current density is corrected for hydrogen cross-over and shorting currents that are measured from cyclic voltammograms taken to obtain the electrochemical surface area of each electrode.

Figure 5.1 illustrates the conditions and protocol used for the ORR measurements in an MEA used in this project; for the MEA ORR activity measurement the total current density is

recorded 1,050 seconds after setting the potential at 900 mV. The current density, in mA/cm^2_{planar}, is decreasing as the Pt is oxidizing, so the ORR activity is measured on an oxidized surface in contrast to most RDE measurements in which the current is measured on the "back-scan" from low to high potentials, i.e. from a cleaned surface substantially free of hydroxyls and other anion impurities. Just prior to the start of the time trace in Fig. 5.1, the MEA sat at a cell potential of ~ 0.4 V for 10 minutes. It is possible to obtain good quantitative agreement between the MEA and RDE measurements, as shown in Figs. 5.2 and 5.3, if instead of taking the absolute current at 1050 seconds, one takes it near the start, e.g. at 5 seconds after setting the potential at 900 mV, so the surface is still clean from having operated at near 400 mV just prior to the reset to 900 mV. In this way, the ORR activity of a clean surface is being measured in both cases.

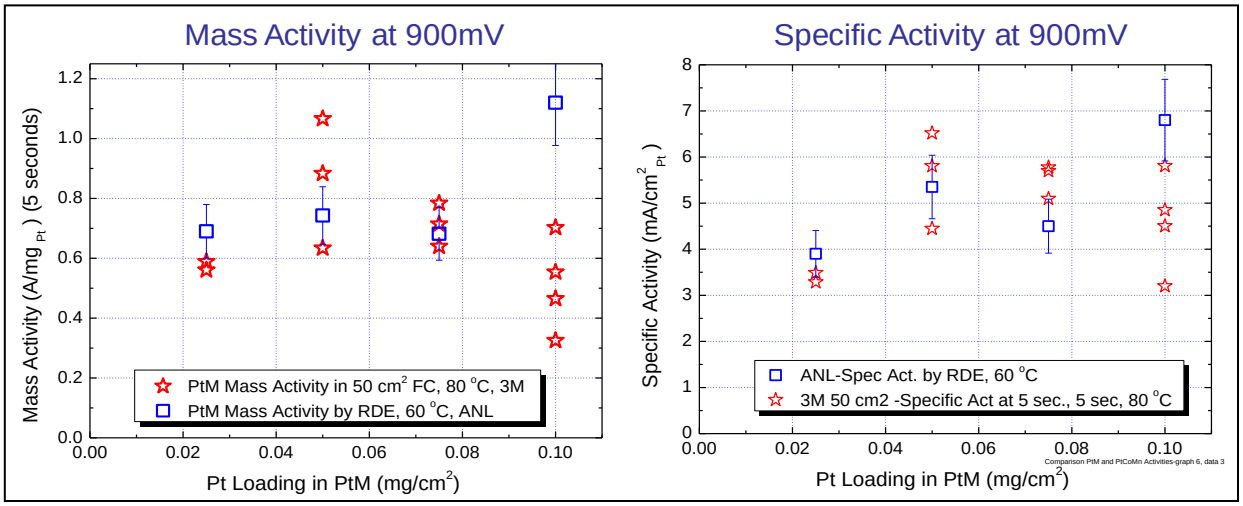

Fig. 5.2. Comparison of ORR mass and specific activity measurements at 900 mV by the RDE method at ANL and by the MEA method at 3M when the latter protocol is changed to take the current density at 5 seconds instead of 1050 seconds.

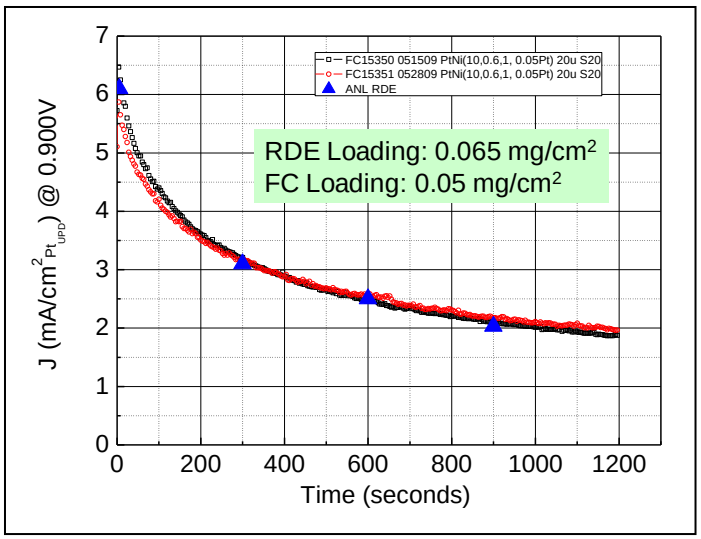

Fig. 5.3. Comparison of current versus time decay due to Pt oxidation at 900 mV during an ORR activity measurement for both the ANL RDE protocol and the 3M MEA protocol.

6. Summary of Accomplishments

We have chosen in this section to represent the advancements of this project by summarizing our judgment of the outcomes, deliverables, and technology development and transfer activities that have resulted over its 5.25 year period of performance. In addition to the usual reports, presentations and publications, there are important project outcomes we have categorized into three areas of accomplishments. These are:

A. Accomplishments towards 2017 DOE Catalyst and MEA Targets
B. Accomplishments towards Original Project Objectives
C. Accomplishments towards NSTF Technology Development

Table 1 lists the number and type of published documentation provided both as deliverables, execution of Task 7 and general technology transfer and education through publications. More important, it then lists the number (9) of patent applications generated, the number (9) of type A accomplishments meeting the 2017 DOE catalyst and MEA targets, and the number (17) of the type C major technical accomplishments enabling advanced development of the NSTF technology platform.

Table 1. Summary of Project Outcomes over the Period of Performance

Output Number	Outcomes / Technology Transfer Activities / Deliverables
1	Final Report
4	FreedomCAR Technical Team Reviews
5	Annual Reports
6	DOE Hydrogen Program AMR Presentations
7	Additional Major Annual Reviews Requested by DOE
21	Quarterly Reports
22	Contributed Presentations at International Meetings
26	Invited Presentations at International Meetings and Institutions
27	Publications in Peer Reviewed Journals
1	DOE Hydrogen Program R&D Award
2	**"Products" Developed**
9	**Patent Applications**
9	**Significant Technical Advances Meeting 2017 DOE Catalyst and MEA Targets**
17	**Major Technical Accomplishments Towards NSTF Technology Development**
2	**Number of New DOE Projects Spawned**

Also considered an important outcome is that two other follow-up projects, DE-EE0000456 And DE0005667, have been awarded as an off-shoot or direct follow-on of the work completed in this project. This project received a 2008 DOE Hydrogen Program R&D Award**,** at the DOE Hydrogen Program Annual Merit Review, June 9, 2008. Finally, although no formal 3M products have derived from this project in the sense that anyone can order them, significant quantities of roll good PtCoMn based catalyst coated membranes and as-made catalyst roll-goods of various loadings have been provided to specific automotive OEM customers under blanket purchase agreements. Also full-sized gasketed MEA's with our next generation catalyst "Pt_3Ni_7" have been sold for stack testing to a non-automotive customer.

The nine type A, five type B, and seventeen type C accomplishment titles are listed immediately below and then discussed in some depth in the following Sections 7 through 9. Finally in Section 11 we list the publication activities resulting from this project including the 27 publications in peer-reviewed journals, 26 invited presentations at international meetings and institutions, and 22 contributed presentations at international meetings.

Category A. Accomplishments towards 2017 DOE Catalyst and MEA Targets

1. Reduction of inverse specific power density, (g_{PGM}/kW)
2. ORR kinetic activity (mA/cm^2_{Pt}) increase, significantly exceeding 2015 targets
3. ORR mass activity (A/mgPt) increase, meeting 2017 targets
4. Reduction in total MEA loadings, to 0.15 mg_{PGM}/cm^2 total per MEA
5. Exceeded durability targets for catalyst support stability for 2017
6. Met durability test targets for catalyst resistance to dissolution and agglomeration under CV cycling to simulate start-stop for 2017.
7. Met durability test targets for MEA durability under OCV hold conditions
8. Demonstrated 9000 hours MEA lifetime under durability load cycling test
9. Demonstrated 0.9 W/cm^2 at 600 mV with ~ 0.2 gPt/kW in a GM 29 cell stack

Category B. Accomplishments towards Original Project Objectives

1. Total Pt group metal loading per MEA
2. Short stack inverse specific power density
3. Durability sufficient to operate at > 80^{o}C for 2000 hours with cycling for transportation
4. High volume manufacturability.

Category C. Accomplishments towards NSTF technology development

1. Discovery of unique NSTF Pt_3Ni_7 electrocatalyst
2. Development of roll-to-roll dealloying process
3. Invention and development of SET process for roll-to-roll catalyst annealing
4. Optimization of catalyst deposition process – P1 vs P4
5. Demonstration of first cell reversal tolerant anode catalyst with OER characteristics.
6. Reduction of microstructure feature size of NSTF specific Microstructured Catalyst Transfer Substrate (MCTS)
7. Discovery of the importance of the anode for effective low temperature water management.
8. Determination of how catalyst ECSA depends on NSTF whisker support characteristics
9. Discovery of a new meso-scale fundamental property of extended surface catalysts that enables higher limiting currents due to higher surface area per unit volume in the electrode.
10. Discovery and demonstration of significant effects of flow field types on NSTF MEA high current density performances.
11. First compositional screening of many new catalyst under-layers and over-layers.
12. Development of an experimental path forward to potentially realize the “entitlement” activity of NSTF alloy catalysts.
13. Study of the water and PEM impurity effects on low ECSA catalysts.
14. Discovery of dependence of limiting current on catalyst ECSA.
15. Polarization curve gains over life of contract, Cell voltage vs. A/$mg_{Total\ PGM}$
16. Knowledge and advances in break-in conditioning
17. Support for development of NSTF catalyst and CCM roll-to-roll processes

7. Accomplishments towards 2017 DOE Catalyst and MEA Targets

7.1. Gains in inverse specific power density, (g_{PGM}/kW)

When this project began, the 2005 DOE Fuel Cell Technologies Program Multi-Year Research, Development and Demonstration Plan specified the DOE targets for electrocatalysts for 2010 and 2015. Targets specified for 2010/2015 respectively for PGM total content were 0.3/0.2 g_{Pt}/kW_e rated in a stack (21). This project met those targets as reported at the 2010 DOE Annual Merit Review (AMR) (17). In January 2012, the recommended 2017 targets for PEM fuel cell electrocatalysts were revised for these characteristics and various accelerated stress tests. These new targets (0.125 g_{Pt}/kW_e) are given in Table 2, along with the status of the catalysts and MEA's developed under this project. Table 2, presented at the 2012 DOE AMR (19) shows that except for these new 2017 targets for PGM total content and loading, all the targets for ORR mass and specific activity and durability have been met or exceeded in small scale 50 cm^2 single cell tests.

Table 2. Progress towards Meeting Technical Targets for Electrocatalysts and MEAs for Transportation Applications.

Characteristic	Units	Targets 2017	**Status:** Values for roll-good CCM w/ 0.15mg_{Pt}/cm^2 per MEA or as stated
PGM Total Content	g_{Pt}/kW_e rated in stack	**0.125**	**0.14 - 0.18 g_{Pt}/kW for cell 0.6 < V < 0.65** at 80 °C and 150kPaa to 250 kPaa outlet. Pt_3Ni_7, 50 cm^2 cell w/ 0.15 mg/cm^2 total Pt.
PGM Total Loading	**mg PGM / cm^2 total**	**0.125**	**0.15 to 0.20, A+C with PtCoMn alloy** **0.15 A+C with Pt/Pt_3Ni_7**
Mass Activity (150kPa H_2/O_2 80°C. 100% RH, 1050 sec)	**A/mg-Pt @ 900 mV, 150kPa O_2**	**0.44**	**0.24 A/mg in 50 cm^2 w/ PtCoMn** **0.47 – 0.67 A/mg in 50 cm^2 with Pt_3Ni_7**
Specific Activity (150 kPa H_2/O_2 at 80°C, 100% RH)	**mA/cm^2-Pt @ 900 mV**	**0.720**	**2.1 for PtCoMn, 0.1mg_{Pt}/cm^2** **2.7-3.0 for R2R Pt_3Ni_7, 0.125 mg_{Pt}/cm^2**
Durability: 30,000 cycles 0.6 -1.0V, 50mV/sec,80/80/80°C, 100kPa,H_2/N_2	**- mV at 0.8 A/cm^2** **- % ECSA loss** **- % Mass activity**	**< 30mV** **< 40%** **< 40 %**	**10±7mV loss at 0.8 A/cm^2** **16±2% loss ECSA, PtCoMn** **37±2% loss mass activity**
Durability: 1.2 V for 400 hrs. at 80°C, H_2/N_2, 150kPa, 100% RH	**- mV at 1.5 A/cm^2** **% ECSA loss** **% Mass activity**	**< 30mV** **< 40%** **< 40%**	**10 mV loss at 1.5 A/cm^2** **10% loss ECSA** **10 % loss mass activity**
Durability: OCV hold for 500 hrs. 250/200 kPa H_2/air, 90°C, 30%RH	**H_2 X-over mA/cm^2** **% OCV loss**	**< 20** **< 20 %**	**13 ± 4 mA/cm^2 at 500 hrs (5 MEAs)** **12 ± 5 % OCV loss in 500 hrs**
Durability under Load Cycling (membrane lifetime test)	**Hours, T ≤ 80°C** **Hours, T > 80°C**	**5000** **5000**	**9000 hrs, 3M PEM (20µm, 850 EW w/ stabilizers), 50cm^2, 80/64/64 °C** **2000 hrs (OEM short stack,0.1/0.15)**

7.2. ORR mass activity (A/mg_{Pt}) increase

The DOE target for ORR mass activity has remained at 0.44 A/mg_{Pt} since first proposed for 2010 in the MY&D plan, with the assumption that the values measured by RDE methods and in an MEA would be similar. We have shown that this is not a valid assumption (9,17) due to the different protocols and state of catalyst surface cleanliness by the two methods. The RDE activities are roughly twice as large as the mass activities measured in a working fuel cell. As indicated in Table 2 and shown specifically in Table 3, we have demonstrated mass activities for our NSTF Pt_3Ni_7 catalysts that exceed the target when measured in 50 cm^2 fuel cells at both 3M and GM.

Table 3. Mass activities measured at GM of 3M CCMs having NSTF Pt_3Ni_7, roll-to-roll dealloyed and SET treated cathodes laminated to either cleaned or as-made 3M PEMs. Cathode loadings were 0.121±0.003 mg-Pt/cm^2.

Sample membrane used in CCM	Protocol used for measurement	Standard Treatment (A/mg)	With Additional Pretreatment (A/mg)
As-made PEM	GM	0.45	0.47
As-made PEM	3M	0.52	0.67
Cleaned PEM #1	GM	0.41	0.54
Cleaned PEM #1	3M	0.23	0.65
Cleaned PEM #2	GM	0.41	0.58
Cleaned PEM #2	3M	0.21	0.62

CCMs made with P1 fabricated, roll-to-roll dealloyed and SET treated Pt_3Ni_7 alloy cathodes at loadings of 0.121±0.003 mg-Pt/cm^2 were tested at GM using both their own and 3M's ORR mass activity protocols. These CCMs were made at 3M with 3M membranes that were either as-made or cleaned using both nitric acid and peroxide baths. Table II summarizes the results from the GM measurements in which the standard treatment refers to the usual NSTF thermal cycling for break-in conditioning. The last column in Table 3 shows that a proprietary GM additional pretreatment process can further substantially increase the apparent mass activities over the standard treatment, which now cover the ranges of 0.47 to 0.58 A/mg by the GM ORR protocol and 0.62 to 0.67 A/mg using the 3M protocol.

Correspondingly, the RDE mass activity values for similar NSTF Pt_xNi_{1-x} catalysts measured at ANL with x ~ 30 % atomic (55% by weight) are on the order of 0.8 A/mg$_{Pt}$ as shown in Fig. 7.1(B) and discussed more completely in reference (6).

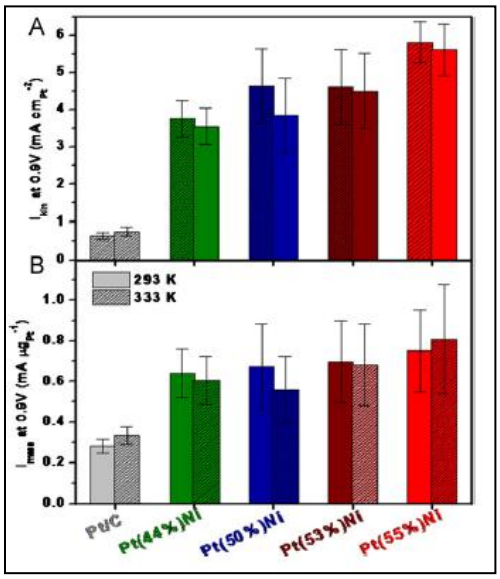

Fig. 7.1. Summary of ORR specific (kinetic) and mass activity measurements done on NSTF Pt-Ni alloy catalysts at Argonne National Laboratory using their RDE methodologies.

7.3. ORR kinetic activity (mA/cm$^2_{Pt}$) increase

The DOE kinetic or specific activity targets were 0.72 mA/cm$^2_{Pt}$ for ORR catalysts through 2015. This target was apparently dropped for 2017. As shown in Table 2, the NSTF-PtCoMn catalysts are well above these targets as is characteristic of extended surface catalysts compared to Pt/C dispersed nanoparticle catalysts. Table 2 and Fig. 7.1(A) also show that the NSTF Pt_3Ni_7 catalysts exceed these targets even further, reaching as high as 3 mA/cm$^2_{Pt}$ in 50 cm^2 single cells and over 5.5 mA/cm$^2_{Pt}$ measured by RDE methods.

7.4. Reduction in total loadings

When this project began in 2007 the typical NSTF based MEA loadings had 0.2 mg$_{Pt}$/cm^2, on each of the anode and cathode. The 2010/2015 DOE targets for PGM total loading per MEA were 0.3/0.2 mg$_{PGM}$/cm^2 respectively, and as of January, 2012 the 2017 target was reduced to 0.125 mg$_{PGM}$/cm^2. At the end of this project, our 2012 "Best of Class" MEA had 0.03 mg$_{Pt}$/cm^2 on

the anode and 0.12 mg_{Pt}/cm^2 on the cathode and generated 0.14 – 0.18 g_{Pt}/kW over the 0.6 – 0.65 V range at 80°C and 150 to 200 kPa outlet pressure H_2/air, as shown in Fig. 7.2 and summarized in Table 2.

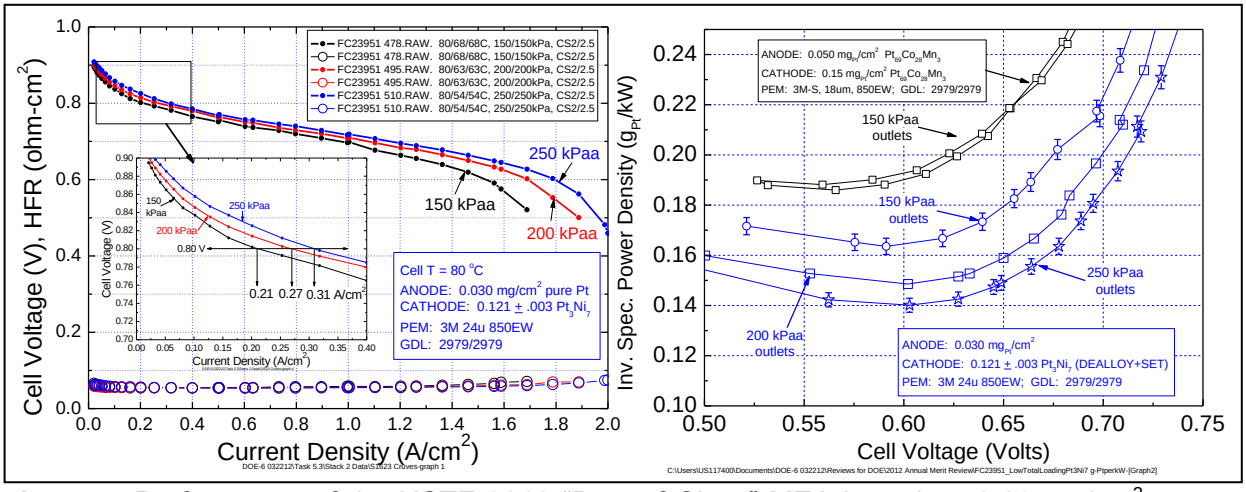

Fig. 7.2. Performance of the NSTF 2012 "Best of Class" MEA based on 0.03 mg/cm² pure Pt on the anode and 0.125 mg_{Pt}/cm^2 of Pt_3Ni_7 (dealloyed and SET processed) on the cathode, a 3M 24 μm thick 850EW PEM, quad-serpentine flow field and 3M 2979 GDL's.

7.5. Durability test for catalyst support stability.

Any new electrocatalyst alloy must have the requisite durability and stability, so we continuously tested our new MEA component compositions and process improvements against

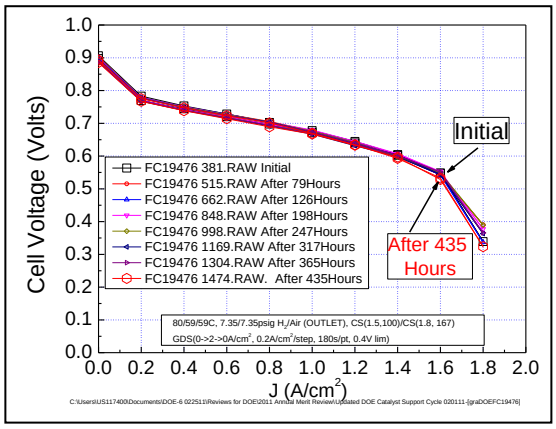

Fig. 7.3. Polarization curves versus time during the DOE 1.2 V hold durability test protocol.

the DOE recommended accelerated stress tests. The first of these DOE defined accelerated stress tests (AST), the 1.2 V hold, evaluates the stability of the catalyst support particle against high voltage corrosion. In this test the MEA cathodes are held at 1.2 V vs RHE for nominally 400 hours under 150 kPa H_2/N_2 at 80°C. It effectively measures the stability of the catalyst support perylene red whisker against corrosion. The DOE targets are that ORR activity and surface area will each drop ≤ 40%, and the performance at 1.5 A/cm² will drop less than 30 mV from initial levels. Fig. 7.3 shows the series of polarization curves (taken using DOE recommended conditions) measured periodically over a total of 435 hours at 1.2 V, for an MEA having the P1 processed (see Section 9.2) PtCoMn on the anode (0.05 mg/cm²) and cathode (0.15 mg/cm²). The MEA used a 3M made 3M-supported membrane with a chemical additive. It

is apparent that the test had only a small effect on performance. Surface area loss was 10%; specific activity was unchanged, and the performance at 1.5 A/cm^2 dropped only 10 mV, so all targets were met and repeated with a second MEA.

7.6. Durability test for catalyst resistance to dissolution and agglomeration under CV cycling to simulate start-stop.

The second DOE defined accelerated stress tests (AST) addresses one of the key durability issues facing fuel cell MEAs, namely degradation of the cathode catalysts during start/stop events. These transient events can cause cathode potentials to briefly cycle to 1.5 volts or higher before returning below 1 volt. The subsequent rapid Pt oxidation and reduction can lead to Pt dissolution and agglomeration leading to loss of surface area and Pt catalyst utilization. A recent US Drive FC tech team sanctioned accelerated stress test to evaluate catalyst electrodes for this purpose (21) was used to evaluate the final MEAs developed in this project for the final stack testing at GM, described in more detail under Task 5.3. This test imposed 30,000 cycles of a 50 mV/sec saw-tooth voltage scan on the MEA between 0.60 and 1.0 volts, with 100/100 kPa H_2/N_2 flowing at 200/200 sccm on the anode and cathode respectively, at 80^{o}C and 100%RH. The protocol called for periodic measurements of MEA performance and cathode ECSA and ORR activity during the tests. The test target criteria are given in Table 2.

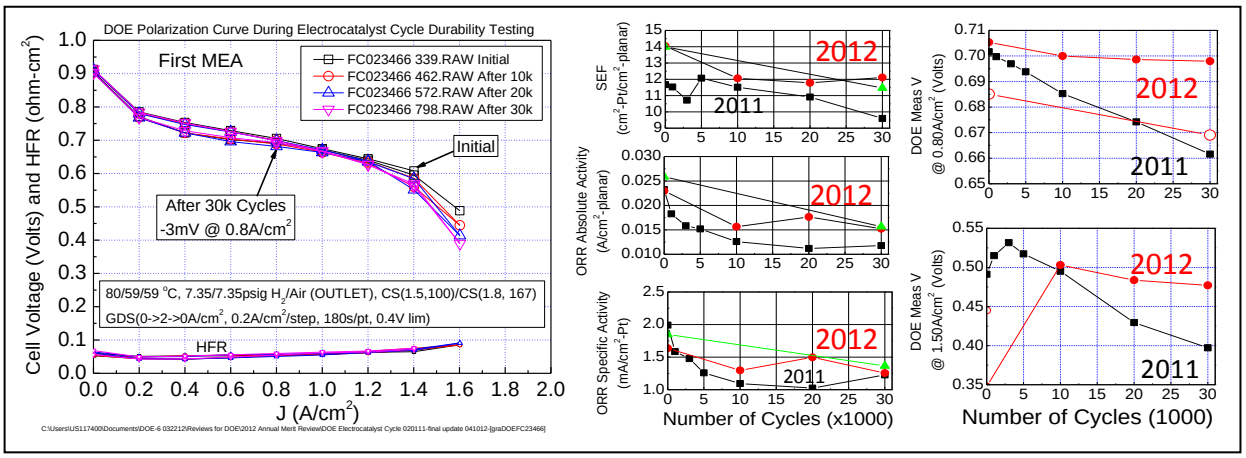

Fig. 7.4. Results of US Drive accelerated stress test, applied to NSTF MEA type used for final stack testing, involving 30,000 CV cycles from 0.6 V to 1.0 Volts to simulate start-stop degradation mechanisms that affect catalyst surface area, activity and performance.

Near the end of this project we applied this test procedure to representative MEAs of the same type and from the same lots as were used for final GM stack testing. Two MEA's were tested. These MEAs had anode/cathode loadings of 0.05/0.15 mg_{Pt}/m^2 of the NSTF $Pt_{68}Co_{29}Mn_3$ catalysts produced by the P4 deposition process with SET post processing (The P4 and SET processes are discussed in Sections 9.3 and 9.2 respectively). They used an 18 micron thick experimental 3M supported membrane with chemical additives for durability, and 3M standard 2979 GDLs on both the anode and cathode.

Fig. 7.4 (left) compares the first 50 cm^2 MEA's fuel cell initial polarization curve with that after 10k, 20k and 30k cycles. It is clear there is very little change due to the voltage cycling. The second MEA was also tested for 30,000 cycles, but only the initial and final performance and catalyst ORR metrics were measured to save time. Fig. 7.4 (right two panels) show the variation of the surface area (SEF), absolute and specific activity and fuel cell performance at 0.8 A/cm^2 and 1.5 A/cm^2 with number of cycles, for both MEAs, labeled 2012, with our MEA

attempt in 2011 with this test. The 2012 MEA's sustained surface area losses of 14% and 18%, easily meeting the DOE 2017 target of 40% loss. The polarization curve voltage losses at 0.8 A/cm^2 of 3mV and 16 mV respectively likewise easily meet the DOE target of 30 mV loss. The mass activity loss of 34% and 39% (same as absolute activity changes) also meet the 2017 target of 40% loss of initial mass activity.

7.7. Durability test for MEA durability under OCV hold conditions

The third DOE defined accelerated stress tests (AST), OCV hold, addresses another key durability issues facing fuel cell MEAs, namely degradation of the membrane due to free radical generation when the cell is off or near idle type conditions. The objective of this test is assessment of the whole MEA/membrane durability at OCV at 90^{o}C under 30% RH, 250/200 kPa H_2/air. The usual failure mode is perforation of the membrane at some point. The target is 500 hours with less than 20% loss of OCV. Using similar or the same MEA construction as in the 1.2 V hold test above, six MEA's met the 500 hour limit and cross-over targets before stopping the tests. Two MEA's were allowed to go further and exceeded 1400 hours with ~ 12% loss of OCV and acceptable H_2 cross-over. Fig. 7.5 shows OCV hold lifetime test summaries for a variety of NSTF MEA constructions. In general, chemical additives are required in order to meet the 500 hour target. For the right graph in Fig. 7.5, lifetime was estimated by visually determining the onset of rapid OCV decay below 800 mV. The PEM chemical additive was used in the 3M 850EW cast membrane. With additive, NSTF Pt_3Ni_7 lifetime is slightly better than tht of $Pt_{68}Co_{29}Mn_3$ (698±184 vs 610±40 hrs. at cathode loading of 0.1mg/cm^2). With additive and 20 μm PEM, 0.10/0.15 PtCoMn has longer lifetime (1,145±195 hrs) than 0.05/0.10PtCoMn (Av = 610±40 hrs). Thicker membrane and higher loading can meet the target with no additive.

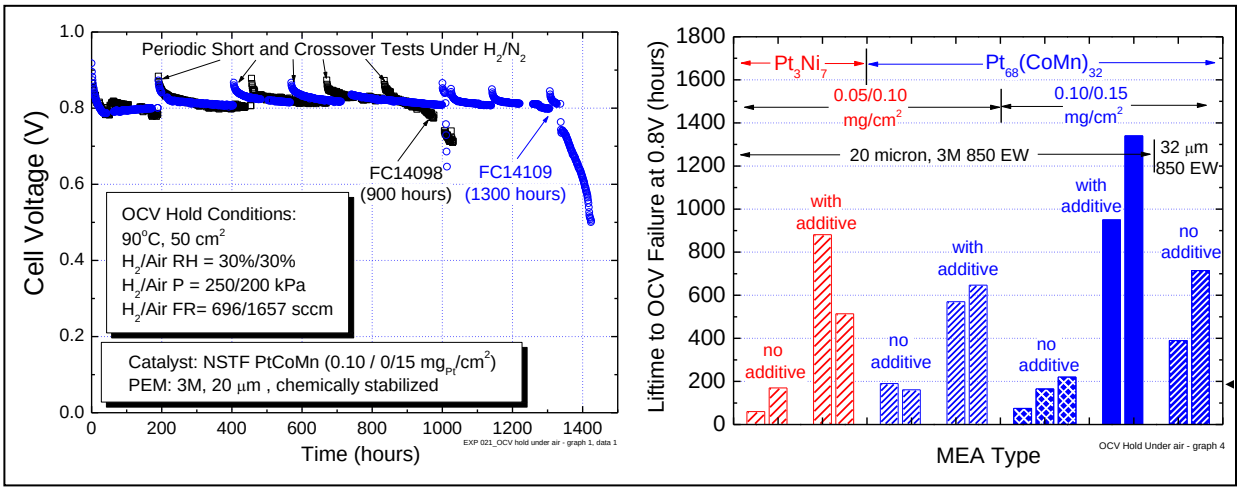

Fig. 7.5. (Left) OCV hold test versus time with periodic measurements of crossover and F^- ion release for two NSTF MEAs that contained a chemical stabilizer in the 20 μm 3M PEM. PtCoMn loadings are as stated. (Right) Summary of OCV lifetimes-to-failure at 0.8 V with various MEA constructions, showing the effect of catalyst type, loading, and membrane additives.

It is clear from Fig. 7.5 that many MEA constructions with the NSTF electrodes can meet the DOE OCV hold target at the specified AST conditions.

7.8. Durability test under load cycling

A final type of durability test is a lifetime load cycling test completed under a 3M test protocol. This test required long periods of time and as the MEA components have improved, the lifetimes increased substantially. Fig. 7.6 is an update of the load cycling tests under 80 ^{o}C that we have shown results from over the life of this project. The panel to the right of the graph in Fig. 7.6 illustrates the load cycle protocol. Cell voltages at various current densities are measured versus time under an 80^{o}C cell temperature, 64^{o}C DP, constant flow load cycling protocol. Open circuit voltages (measured daily) are used to determine end of life in this test (when the OCV falls below 0.8 V). These tests had actually began prior to the start of this contract with the NSTF state-of-the-art MEA's available at that time, with 0.2 mg/cm^2 of NSTF PtCoMn on each of the anode and cathode of a 3M 850 EW, 35 micron thick cast membrane made with no support or chemical additives. As shown in Fig. 7.6, four samples of this type dramatically lasted longer than seven conventional MEA's made with dispersed Pt/C electrodes but the same membranes and GDLs. During this project, the first two MEAs were tested with the same catalysts applied to an experimental supported membrane (solid red bars in Fig 7.6). The lifetime had increased to 7000 hours. The next two samples tested obtained ~ 5000 hr lifetimes with the 2009 best of class NSTF CCM with the 0.05/0.10 mg/cm$^2_{Pt}$ loadings on a 3M 850 EW PEM that did not contain any chemical stabilizer or mechanical reinforcement (blue crosshatched bars in Fig. 7.6). The set of black crosshatched bar graphs on the right side of Fig. 7.6 are latest results showing that MEA's with our 2009 best of class CCM, with 0.05/0.1 mg$_{Pt}$/cm^2 loadings and a 20 micron 3M PEM with a chemical stabilizer, but still no reinforcement, survived 9000 hours without failure. The NSTF electrodes have been shown to have as little as 1/1000th as much F$^-$ ion release rate as Pt/C electrodes in measurements done at 3M with the same membranes and gas diffusion layers (22).

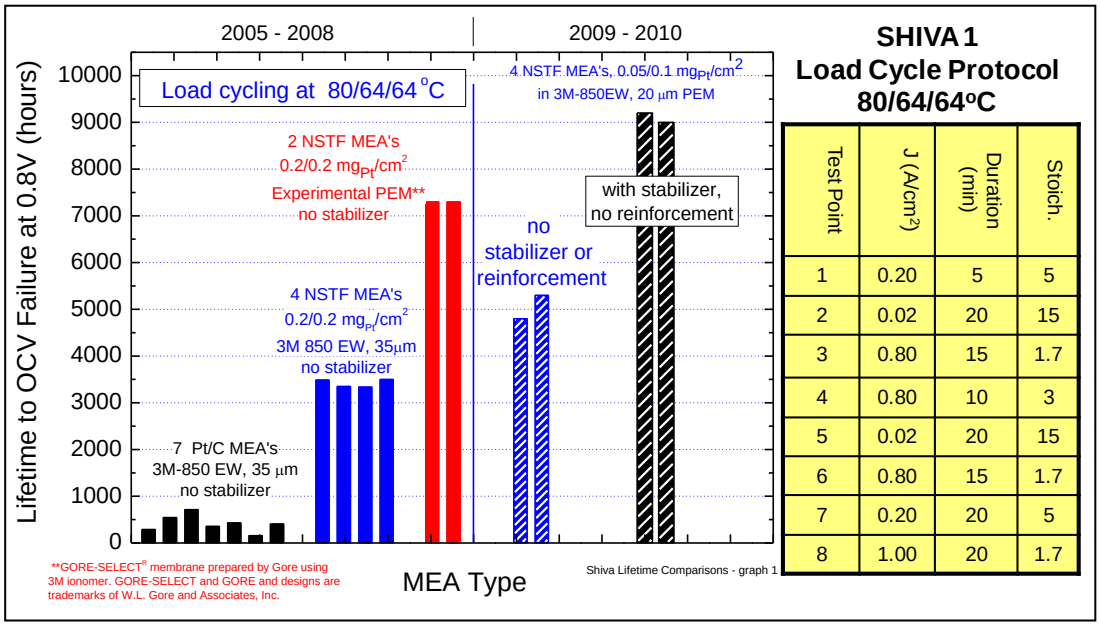

Test Point	J (A/cm^2)	Duration (min)	Stoich.
1	0.20	5	5
2	0.02	20	15
3	0.80	15	1.7
4	0.80	10	3
5	0.02	20	15
6	0.80	15	1.7
7	0.20	20	5
8	1.00	20	1.7

Fig. 7.6. Summary of lifetime versus MEA type measured over a period of 5 years with various NSTF MEA constructions. Chemical stabilizers and membrane reinforcement are important in order to obtain the longest lifetimes. The NSTF electrode based MEA's last much longer than Pt/C electrodes when no chemical additives (stabilizer) or reinforcement are used in the membranes.

A large factor of this is now known to be due to the fundamental properties of the NSTF extended surface catalyst compared to dispersed nanoparticles, as discussed in reference (23). The absence of exposed carbon support, a poor ORR catalyst, and the much higher specific activity of the NSTF catalysts also contribute to lower amounts of $2e^-$ hydrogen peroxide production and subsequent free radicals that attack the membrane.

The load cycling tests in Fig. 7.6 are primarily again an MEA or membrane lifetime test rather than a catalyst durability test. However, since the catalyst is the original source of the peroxide from incomplete oxygen reduction that gives rise to the free radicals that attach the membrane, the nature of the catalyst is important. For the above tests, a limited amount of catalyst activity and surface area measurements during the load cycling were done.

7.9. Generation of 0.78 W/cm^2 at 650 mV with 0.2 g_{Pt}/kW in a GM 29 cell stack.

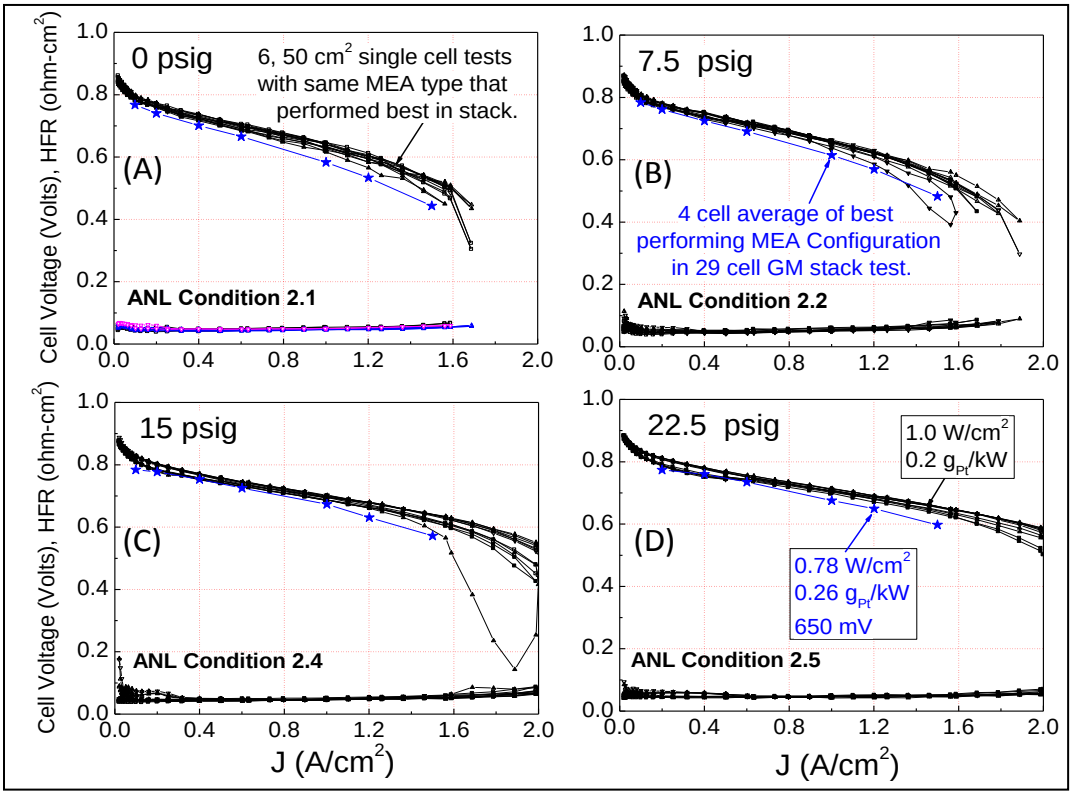

Fig. 7.7 (a) GDS polarization curve comparisons at four pressures, of the 4-cell average GM stack 1 performance (configuration-1 MEAs) with six, 50 cm^2 single-cell tests (at 3M) having the identical type MEA. GDS polarization scan: 0.02->2->0.02 A/cm^2, 10 steps/decade, 120 s/pt, 0.4 V limit, 0.1 max current density step. The test conditions used were those supplied by the systems modeling group at ANL (Ahluwalia et al.) and used by 3M for generating other MEA data requested by that group:

ANL Condition 2.1 = 80/73/73°C, 1/1 atm H_2/Air, CS(2,100)/CS(2.0, 200)
ANL Condition 2.2 = 80/70/70°C, 1.25/1.25 atm H_2/Air, CS(2,100)/CS(2.0, 200)
ANL Condition 2.4 = 80/56/56°C, 2.0/2.0 atm H_2/Air, CS(2,100)/CS(2.0, 200)
ANL Condition 2.5 = 80/40/40°C, 2.5/2.5 atm H_2/Air, CS(2,100)/CS(2.0, 200)

There were two stack tests of NSTF MEA's completed at GM at the end of Task 5.3. The first stack's objective was to compare MEA performances of six different types of MEA configurations in a rainbow stack in order to down-select to one MEA configuration for the second and final durability stack test. As explained in detail in the section on Task 5, there were significant issues in both stack tests due primarily to MEA issues we had with bad experimental membrane lots and test station water impurities. It was also not possible to obtain the same peak performance in the stacks as in 50 cm^2 single cells with the same MEA lots. This led us to suspect that flow field differences could be partially responsible. Despite these difficulties, the first stack was able to meet its objective of down-selecting to the best performing MEA configuration.

Figure 7.7 shows sets of polarization curves as a function of four different H_2/air pressures, all from MEA's assembled with the same roll-to-roll fabricated CCM lot having 0.05/0.15 mg_{Pt}/cm^2 total on the anode/cathode respectively. Each panel compares six 50 cm^2 single cell polarization curves at a given pressure, with the stack 1 average polarization curve of its four best performing MEA's (all configuration type 1). The test conditions chosen were those specified by the system's modeling group at ANL (Ahluwalia et al.) for other data sets provided to ANL. The MEA performances improve with pressure similarly in single cells and the stack, consistent with mass transport issues. The stack 1, MEA type 1 performance average underperforms the single-cell tests at all conditions, but not by too much as long as the current density is below ~1.5 A/cm^2. At higher current densities the stack 1 performance falls considerably short of the small single cells. As indicated in the 22.5 psig panel, despite the underperforming nature of the MEAs, the last two stack average data points at 1.2 and 1.5 A/cm^2 and 0.65 and 0.6 volts respectively correspond to 0.78 and 0.9 W/cm^2 and 0.26 and 0.22 g_{Pt}/kW. This is not as good as the single cells generated but it does exceed our original project goal at the start of the contract, as discussed in B. which follows. Further discussion of the stack 1 performances are given in Task 5 of the Supplementary Section as well as flow field effects discussed immediately below in Section 9.10.

8. Accomplishments towards Original Project Objectives

The above summary of accomplishments towards the DOE targets for 2015 and 2017 show that several of the original project objectives specified in section 0.2.A have been exceeded, as summarized in the following Table 4.

Table 4. Summary of Accomplishments towards Original Project Objectives

Project Objective from Slide 4	Target at Start of Project	Value at End of Project
Total Pt group metal loading per MEA	$\leq$ 0.25 mg/cm^2	0.15 mg/cm^2
Short stack inverse specific power density	$\leq$ 0.5 g-Pt/kW$_{rated}$	▪ 50 cm^2 : 0.14 to 0.18 gPt/kW$_{rated}$ ▪ GM short stack : 0.22 to 0.26
Durability sufficient to operate at > 80°C for 2000 hours with cycling, $\leq$ 80°C for 5000 hours	2000 hours @ 80°C	$\leq$ 2000 hrs. in OEM stack, testing done outside this project
High volume manufacturability	CCM processes not optimized or integrated	Full CCM and components all roll-to-roll fabricated.
High prospects for 40,000 hours durability under operating conditions for stationary applications,	N. A.	Not addressed directly, targeted automotive, but 9,000 hours in load cycle tests demonstrated with 50 cm^2 MEA's.

9. Accomplishments towards NSTF technology development

A third and very important class of accomplishments are those that refer to advancements in the development of the NSTF electrocatalyst technology itself, whether for materials, processes or cost improvements. In this section we identify and discuss seventeen accomplishments that we believe are significant towards advancing the NSTF catalyst technology platform. These are the ones listed as Category C accomplishments on page 19.

9.1. Discovery of unique NSTF Pt_3Ni_7 electrocatalyst

Near the beginning of this project, we were still screening simple binary and ternary alloy compositions for increased Pt ORR activity. While testing some Pt_xNi_y compositions at high Ni content we observed an anomalously high ORR activity. Subsequent extensive and careful investigation around this unique x:y feature showed a very novel effect, shown in Fig. 9.1 a, b, in that the ORR activity was sharply peaked at what was gravimetrically determined to be y=0.7, x = 0.3 atomic. Electron microprobe analyses at Dalhousie University determined the peak activity to be at y = 0.76 while X-ray fluorescence analyses at 3M determined the peak activity at y = 0.62. Since neither EMP nor XRF are fundamentally quantitative for mass and subject to matrix effects from the oriented NSTF structure, we have relied on the gravimetrically determined peak position of y = 0.7 for the composition that give the peak ORR activity. Subsequent SEM-EDX analysis at California Institute of Technology through JPL has validated that composition.

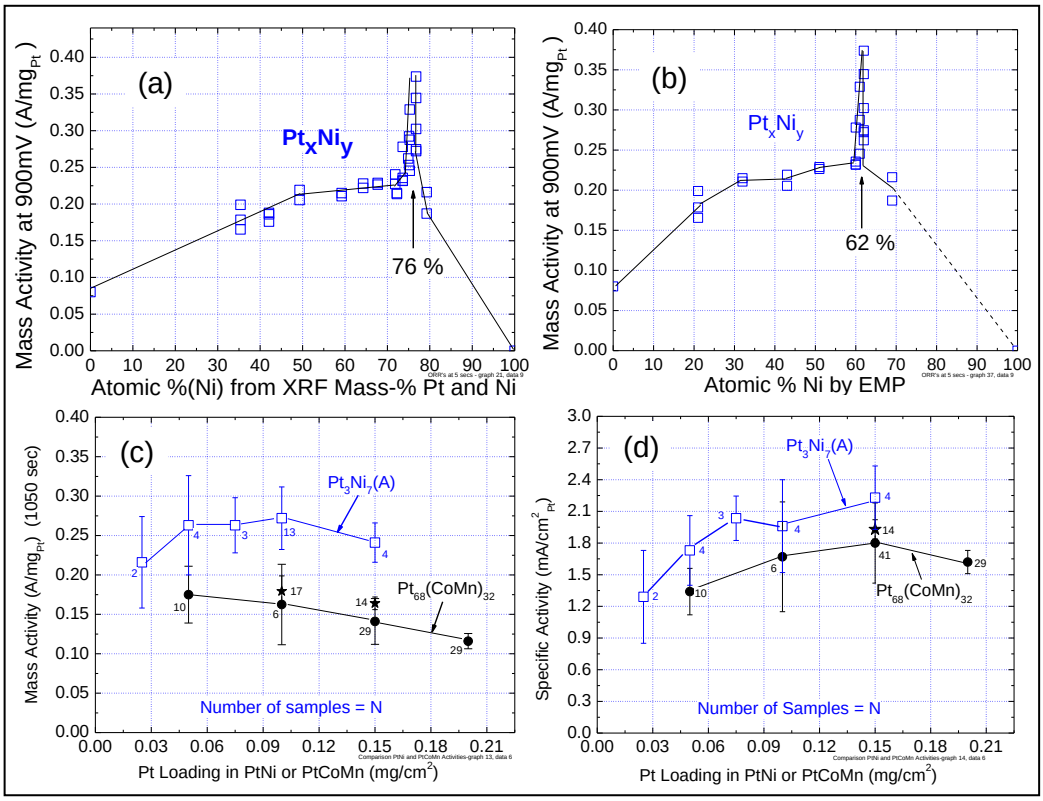

Fig. 9.1. Mass and specific activity as a function of Pt composition and loading for as-deposited NSTF PtCoMn and PtNi alloys. (a) and (b) Mass activity versus atomic % Ni measured by XRF and EMP respectively. (c) and (d) Mass and specific activity versus Pt loading for Pt_3Ni_7 and $Pt_{68}Co_{29}Mn_3$.

Fig. 9.1(c,d) show the mass activity as a function of Pt loading for these as-deposited Pt_3Ni_7 catalysts is substantially higher than our standard PtCoMn. The (A) in Pt_3Ni_7(A) in Fig. 9.1 refers to catalyst that has been deposited using our traditional multi-layer P4 process (discussed in Section 9.3 below) and was not further annealed or dealloyed prior to making into CCM's for testing. Further discussion of the unique properties of the Pt_3Ni_7 alloy system is given in the key references attached in the appendix that deal specifically with it.

9.2. Invention and development of SET process for roll-to-roll catalyst annealing

Most alloy catalysts of any type, including Pt/C, benefit from annealing. Better intermixed alloys and larger crystallite sizes generally result. Work done at ANL by Stamenkovic et al. also indicated that by annealing the NSTF PtM alloys (sent to them as powders) in hydrogen, increased ORR activity could be obtained (24). For powdered, batch processed materials, this is generally straight forward and done in a standard oven with controlled atmosphere. However, the NSTF whiskers are grown on a polyimide film substrate and restricted to temperatures below about 300 ^{o}C. This prevents use of traditional annealing methods. Since it is also critical that the annealing process be consistent with roll to roll processing at reasonable web speeds, a new approach was needed. Using another important property of the NSTF metal coated whisker films, which is that they appear highly optically black due to strong photon absorption by the whiskers, it was possible to devise a process we call the SET (surface energy treatment) process to pump energy into the catalyst coated whisker film at rapid rates while moving as a

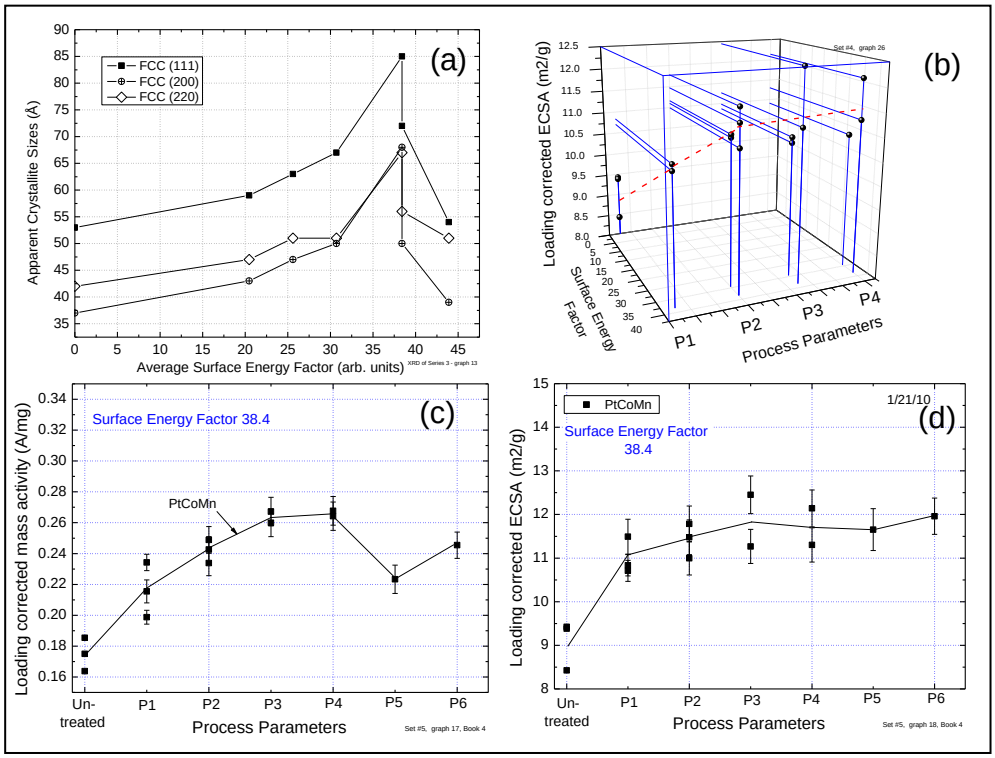

Fig. 9.2. Impact of the SET batch process parameters on NSTF PtCoMn crystallite size (a), mass activity (c) and surface area (b,d).

web. Since the NSTF catalyst process takes place in a moderate vacuum, it is also possible to control the atmosphere during the SET "annealing". We first demonstrated the feasibility for this SET process to improve the PtNi ORR activity by designing and building a small batch chamber capable of exposing 50 cm^2 sized electrodes.

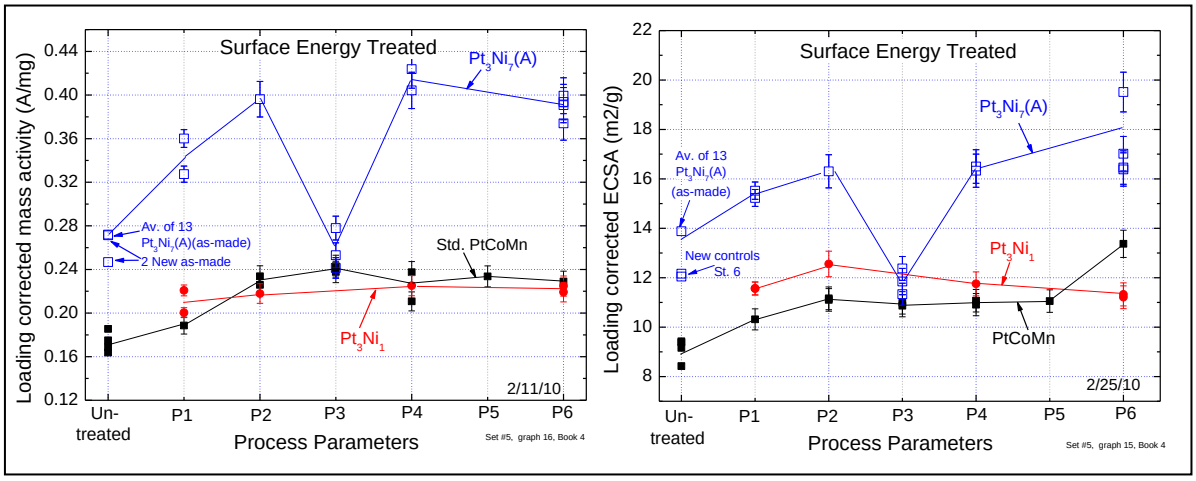

Fig. 9.3. Impact of the SET batch process parameters on the NSTF Pt_xNi_y mass activity and ECSA and comparison to the PtCoMn.

Multiple sample series with over a hundred sample exposures enabled us to determine the sensitivity to the incident energy device parameters and the environmental gas compositions and pressures. These results in turn provided the data to design a roll to roll capable SET process. Fig. 9.2 shows examples of the response of the PtCoMn catalysts to different SET batch process conditions. Fig. 9.2(a) illustrates that the XRD measured crystallite size increased dramatically with the SET fluence, while (b) illustrates the effect of both incident energy and the process environmental conditions, P1, P2,….on the catalyst surface area. Figs. 9.2(c, d) show clearly the impact of the process parameters at a fixed surface energy fluence.

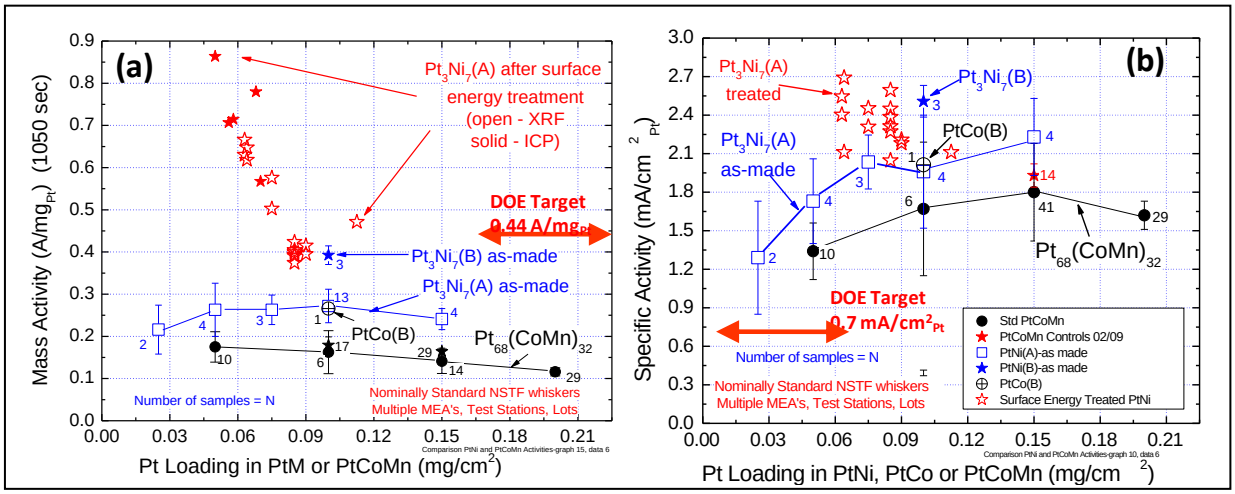

Fig. 9.4. Impact of the SET batch process at nominally the best conditions on the Pt_3Ni_7 mass (a) and specific (b) activity, as a function of loading. Loading after exposure was corrected for small amounts of Pt loss by both XRF and ICP measurements of the exposed samples.

Similarly, Pt_xNi_y also benefited from the SET process as shown in Fig. 9.3. Pt_3Ni_7 mass activity and surface area increased even more than that of PtCoMn, whereas Pt_3Ni_1 did not improve with the process parameters explored. Under many conditions used and certainly near

the peak fluence, some of the Pt was vaporized in the batch experiments and hence the loading was measured after SET treatment of each sample and this corrected loading was used for the mass activity values. Finally, in Fig. 9.4 are shown the gains in mass and specific activity when the nominal optimum batch SET process conditions are applied to the as-deposited Pt_3Ni_7 NSTF catalysts before they are made into CCM's.

9.3. Optimization of catalyst deposition process – P1

Vacuum sputter deposition has as a fundamental advantage for depositing alloys that it is as simple to deposit a mixed composition material as it is a single component material.

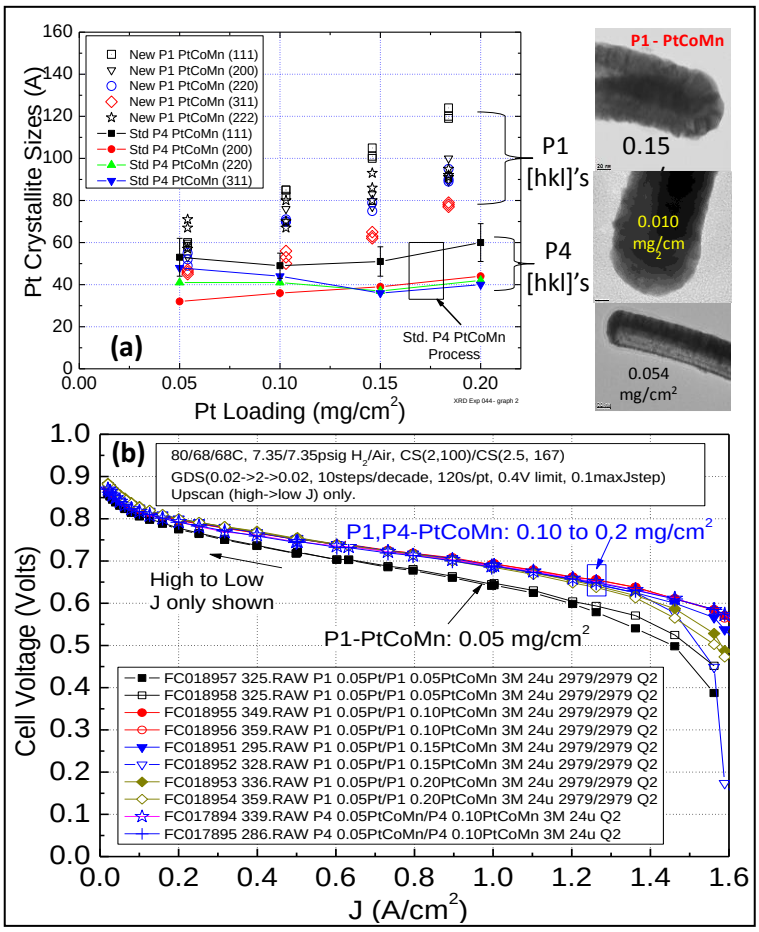

Fig. 9.5 (a). Left:PtCoMn fcc[hkl] grain sizes by XRD as a function of Pt loading for catalysts sputter coated by new process P1 versus the standard process P4. Right: TEM images of the PtCoMn coated whiskers using new deposition process P1. At all three loadings the catalyst coating is smoother than by the standard P4 process that produces whiskerettes as discussed in reference (25). **(b)** Polarization curves for PtCoMn deposited by the P1 process at ca. 0.05, 0.10, 0.15 and 0.20 mg_{Pt}/cm^2, and the P4 process at 0.10 mg_{Pt}/cm^2, under 80 ^oC cell temperature, 68^oC dew points and 150 kPa H_2/air. 3M-24 μm, 850EW PEM. 3M standard GDL's, all 50 cm^2. Actual Pt loadings of the cathodes are 0.054, 0.103, 0.146 and 0.184 mg_{Pt}/cm^2.

The differences lie within the details of how one forms the intermixed coating, either in layers from a series of single element targets or a single layer from a mixed element target, or combinations. When exploring new alloy compositions, it is economically sensible to use single element targets so a wide range of compositions can be screened with the same targets. For the NSTF alloy catalysts, all work up to about 2010/11 was done with our so called P4 process in which multiple layers were sequentially deposited from multiple targets. Key process development work completed in this project has focused on improving the NSTF-PtCoMn roll-to-roll process so that the support whiskers and sputter deposited catalyst alloy can be applied simultaneously on the moving substrate web in a single step. This new process, called P1, offers greater simplicity and more cost effective coating than the standard process called P4. It also holds the potential for better alloying due to increased intermixing and self-annealing due to higher heat of condensation with fewer layers. The key is to make sure it does not reduce performance and hopefully improves it. We have demonstrated it with PtCoMn and PtNi

targets. An example of its effectiveness is shown in a series of PtCoMn loadings deposited by the P1 process at 0.054, 0.103, 0.146 and 0.184 mg_{Pt}/cm^2. They were coated on production equipment and evaluated for structural differences by X-ray diffraction, SEM/TEM and fuel cell performance. SEM indicated no substantial differences at 40,000 magnification, but the TEM and XRD results showed significant changes. Fig. 9.5(a)(left) shows that whereas the fcc Pt[hkl] grain sizes by the standard process P4 are essentially independent of loading and 4 to 6 nm in size, the P1process produces grain sizes that increase with loading and are larger, 6 to 12 nm. Consistent with this are the TEM images, Fig. 9.5(a) (right), that show the catalyst coatings on the whiskers are smoother than those obtained by the P4 process, which produces highly oriented whiskerettes growing off the sides of the underlying whisker core, as discussed at length in reference (25). This can be understood since aspects of the P1 process provide annealing like conditions.

Fuel cell performance of the P1deposited PtCoMn is also generally the same as with the P4 process, as shown in Fig. 9.5(b). With the conditions shown in the inset of Fig. 9.5(b), in the same 50 cm^2 cell with quad-serpentine flow fields, using the same station and production lots of PEM's and GDL's, the P1 processed anodes and cathodes (0.1 to 0.184 mg_{Pt}/cm^2 loadings) show very similar performance to each other and to P4 processed 0.10 mg_{Pt}/cm^2 PtCoMn cathode. The galvanodynamic scans with the 0.054 mg/cm^2 cathodes are substantially lower (black open and closed squares) but at least as good if not better than historical results with P4 cathodes at these loadings. More careful inspection of the curves in Fig. 9.5(b), show the P1 process yields about a 10 mV improvement at 0.32 A/cm^2 and 5 mV at 1 A/cm^2 over the P4 process, but very similar performance at very low (0.025 A/cm^2) and high (1.5 A/cm^2) currents. Measurements of the absolute and specific activities at 900 mV under 150 kPa H_2/O_2 are very similar for both processes, although the P1 cathodes have slightly higher surface area than the P4 deposited materials. In conclusion, there are slight performance benefits and no penalties for the simpler, faster P1 process for depositing the NSTF alloys.

9.4. Development of roll-to-roll dealloying process

Dealloying Pt based transition metal alloy catalysts to increase their ORR mass activity is recognized increasingly in the literature as a potentially important process, particularly for extended surface type catalysts (7). Ex-situ dealloying is particularly relevant for our NSTF Pt_3Ni_7 alloy as a way to both increase its ORR activity and remove the excess Ni cations that

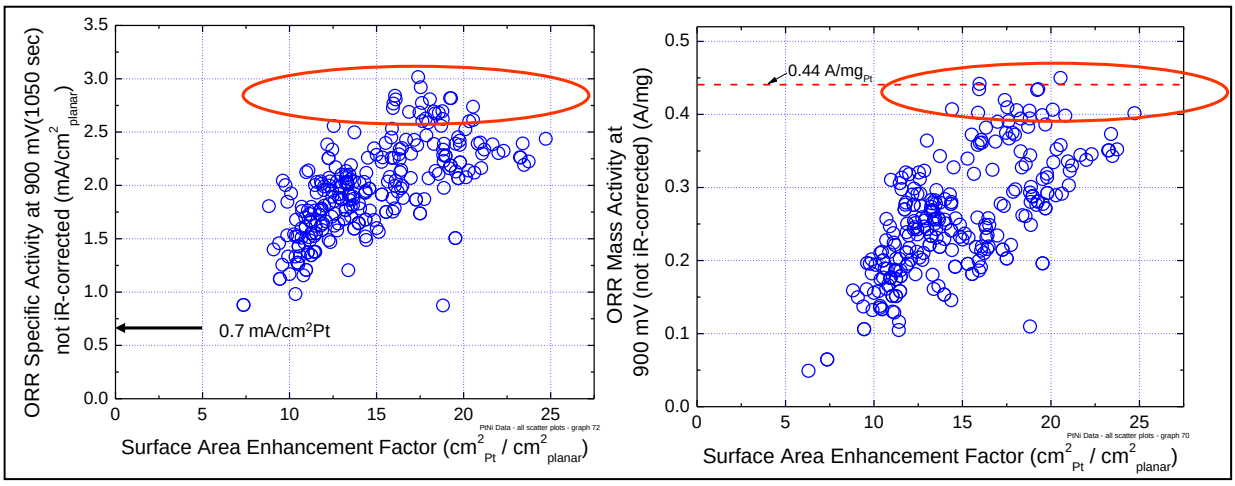

Fig. 9.6 ORR specific and mass activity as a function of surface area enhancement factor for over 100 different NSTF-PtNi cathodes derived from the as-deposited Pt_3Ni_7 catalysts for various loading, dealloying and SET post-process parameters.

will otherwise migrate to the membrane and cause issues with conductivity, water transport and charge transfer impedance, thereby significantly reducing the limiting current density achievable. Typical transition metal dealloying involves acid dissolution of the transition metal. A baseline acid bath for Ni dissolution is nitric acid. To be viable for a roll-to-roll (R2R) catalyst manufacturing process, however, we must also have an effective R2R dealloying process capable of being run at similar web speeds as the catalyst deposition. This required development of new bath chemistries, correlation of batch and R2R process experiments, and finally fuel cell testing to map myriad sample and process parameters with fuel cell performance and ORR activity.

A broad series of batch process experiments were first completed to investigate the effects of both electrochemical and passive chemical dealloying, with acid bath composition, concentrations, time and temperature as parameters. These were applied to various catalyst material factors, including Pt_3Ni_7 loading (0.075 to 0.15 mg-Pt/cm^2), alloy homogeneity (P1 vs. P4), and the SET annealing process discussed above. The objective was to try and optimize the process both to improve the limiting current density without loss of ORR activity, and to find conditions suitable for roll-to-roll processing at reasonable web speeds. Over 100 different combinations of the acid bath conditions, catalyst fabrication and process parameters were screened and tested in 50 cm^2 fuel cells in duplicate. Conditions were found that allowed speeding up the rate of dealloying by a factor of 240 over the baseline nitric acid bath soak. Using existing facilities at 3M, full-width roll-to-roll dealloying was developed with the faster process conditions. Sixteen ORR relevant kinetic and performance metrics were extracted from the fuel cell potentiodynamic and galvanodynamic polarization curves and correlated with materials and proprietary process parameters.

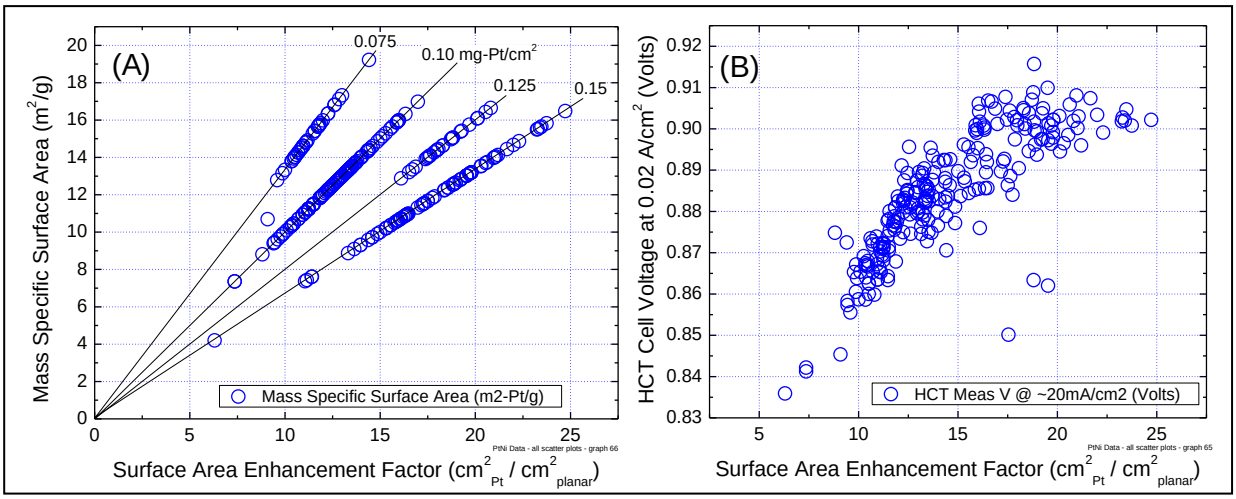

Fig. 9.7. (A) Mass specific surface area for different Pt loadings in the Pt_3Ni_7 dealloying development experiments plotted versus the surface area enhancement factor. (B) The GDS polarization curve voltage at 20 mA/cm^2 plotted versus the surface area enhancement factor.

Without disclosing proprietary process information, a total of 38 global scatter-plots can be generated to illustrate how critical metrics vary with two basic catalyst properties, surface area and loading. Figure 9.6 shows two such global metric plots of ORR specific and mass activity at 900 mV under 150 kPa saturated oxygen, versus the surface area enhancement factor in cm^2 of Pt per cm^2 of planar surface area. The scatter plot in Figure 9.6 (left) shows the high specific activity of the Pt_3Ni_7 derived catalysts, approaching 3 mA/cm^2-Pt for some samples, which far exceeds the DOE 2015 targets of 0.7 mA/cm^2-Pt. Figure 9.6 (right) is a

similar scatter plot showing that roll-to-roll dealloying and annealing conditions were found which generated mass activities of 0.44 A/mg-Pt using the 3M ORR protocol above, equivalent to the DOE 2017 target. Fig. 9.7(A) plots the electrochemical surface area versus surface enhancement factor for the dealloying sample series. It shows that mass specific surface areas of 15 to 20 m^2/g were common for the dealloyed/SET annealed catalysts with the highest mass activities. These are the highest ECSA values and SEF values we have measured for NSTF catalysts at these loadings. The increased surface area and specific activity both contributed to the improved mass activity. Finally, Fig. 9.7(B) shows the kinetic current density region (0.02 mA/cm^2) as a function of the surface area enhancement factor from GDS polarization curves for the ~ 100 samples from the R2R dealloying development and scale-up activities. The kinetic fuel cell performance mirrors the mass activity.

9.5. Reduction of microstructure feature size of NSTF specific Microstructured Catalyst Transfer Substrate (MCTS) - Task 5.1 – MEA Integration

The microstructured catalyst transfer substrate (MCTS) web developed for roll to roll vacuum coating of the NSTF whiskers and catalyst over-coating is critical for protecting the whiskers from being brushed off when passing over rollers along the web path. It also provides a square-root-of-two increase in electrochemical Pt surface area. The process for fabricating the MCTS is based on a well established 3M technology platform for manufacture of brightness enhancement film (BEF) for electronic displays. The size of the microstructure feature is different for the NSTF catalysts and the optical film applications. The initial MCTS structure developed for this NSTF fuel cell catalyst application, long before the start of this project, did have feature sizes similar to the larger BEF applications, i.e. 90^o peaks, 12 microns tall on a 24 micron pitch. This 90/24 structure was soon reduced to a 90/12 structure, 6 micron tall peaks on a 12 micron pitch to make it more appropriate for thinner membranes. The 90/12 MCTS substrate was the substrate in use prior to the start of this contract. At the beginning of this project we reduced the size of the features with a 90/6 MCTS structure. Here the peak-to-peak distances are only 6 microns and the peak heights only 3 microns. There are twice as many peaks per unit length, but only half as high, so they will penetrate into the membrane only half as deep.

Fig. 9.8 (A) shows SEM cross-sections of a catalyst/whisker coated 90/12 MCTS. Fig. 9.8 (B) shows an SEM cross-section of a fresh CCM made by lamination transfer of such a 90/12 based NSTF catalyst to both sides of a 35 micron thick membrane. Fig. 9.8 (C) shows an SEM cross-section of the CCM after fuel cell testing, illustrating how the GDL compression flattens out the micro-replicated MCTS features in the CCM surface. In so doing, the excess length of catalyst (by a factor of 1.414 ideally) has to go somewhere and is squeezed to form pockets (circled) in which the catalyst is buried as deep as ~ 4 microns into the PEM surface. Fig. 9.8 (D,E) show higher magnifications of these pockets for both a 90/12 and a 90/6 based catalyst/MCTS structure. Although with a 90/6 MCTS structure there will be twice as many such pockets per unit length, they will nominally be only half as deep. Since oxygen permeability will become more and more limited the deeper the catalyst is buried in the PEM surface, shallower pockets might be expected to perform better than the deeper pockets. That is, mass transport overpotential at high current densities would be expected to be improved.

The first 90/6 MCTS substrates were tested by putting on our standard whiskers with 0.1 mg_{Pt}/cm^2 of the PtCoMn catalyst on the anode and 0.15 mg_{Pt}/cm^2 of PtCoMn on the cathode. (We have shown at the start of this contract as reported at the 2007 DOE annual merit review meeting, that reducing the anode loading from 0.2 to 0.1 mg/cm^2 also helped the high current density mass transport.) The PEM used was 35 μm thick 830EW cast 3M. Fig. 9.9 compares the GDS polarization curves at 7.5 psig inlet pressure, from these MEA's with earlier MEA's made with higher anode and cathode PtCoMn loadings (0.2 mg_{Pt}/cm^2) on 90/12 MCTS.

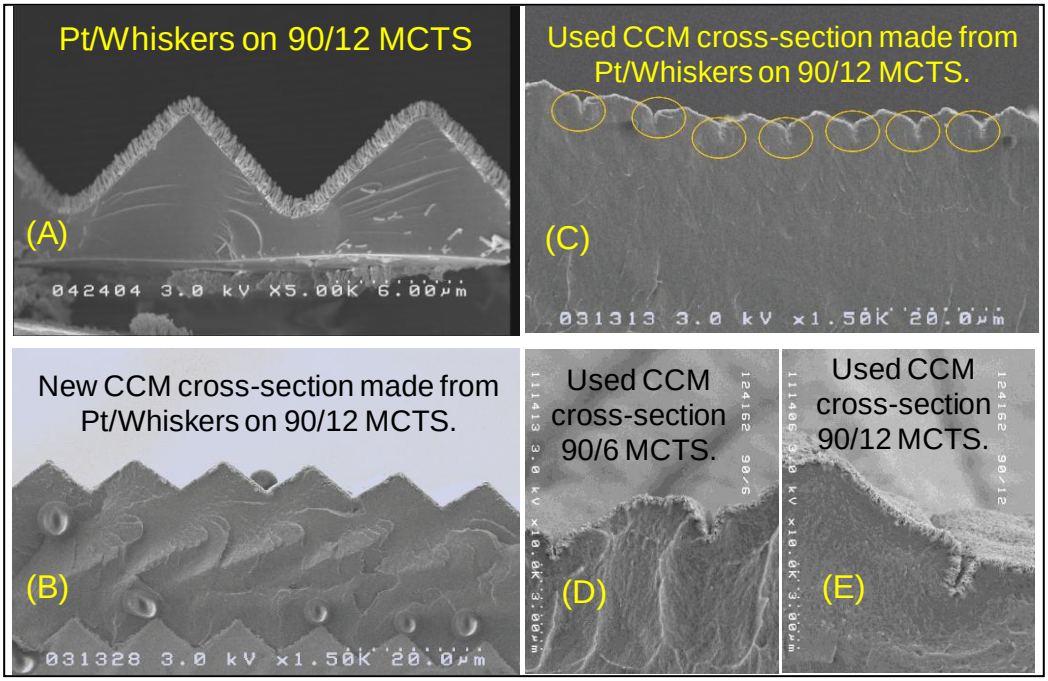

Fig. 9.8. SEM cross-sectional images of: (A) catalyst coated whiskers on a 90/12 MCTS, (B) a CCM made with NSTF catalysts formed on a 90/12 MCTS and laminated to an ~ 35 micron thick membrane. The MCTS is micro-replicated on the surface of the PEM. (C) A tested CCM showing how the micro-replicated MCTS structure is flattened out by the GDL compression and how the catalyst coated peaks are buried in the membrane, and (D,E) higher magnification images of the used CCMs made from 90/6 and 90/12 MCTS respectively.

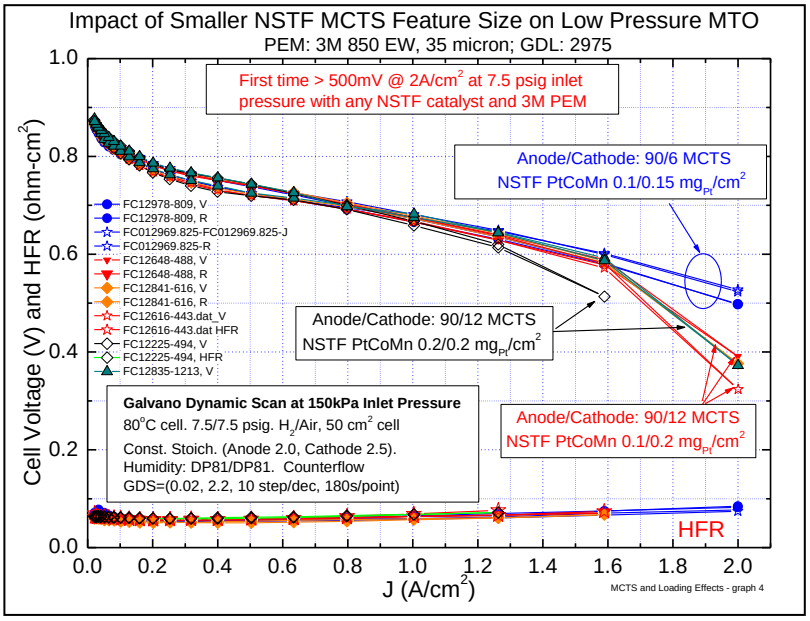

Fig. 9.9. GDS polarization curves showing the impact of using smaller 90/6 microstructure features rather than 90/12 features on the MCTS support film when making the NSTF catalyst coated webs and CCM's.

There is a clear boost in performance at high current densities from these first samples made on the 90/6 MCTS compared to the earlier 90/12 based MEAs. This was the first time we had ever obtained over 500mV at 2 A/cm^2 with only 7.5 psig inlet pressure. We attribute this benefit to the fact that the catalyst is utilized more effectively since there is in general less mass transfer overpotential with the portion of the NSTF electrode that is squeezed into the shallower pockets.

9.6. Demonstration of first cell reversal tolerant anode catalyst with OER characteristics

Start/stop events and other transient phenomena that can momentarily deplete a cell's anode of sufficient hydrogen to support the current demanded by the stack. This may produce local hydrogen starvation. The result is that a current is forced upon the anode electrode at the location of the starvation. The electrode potential quickly rises until potentials are reached where carbon, platinum and water begin to oxidize. Carbon oxidation results in degradation of carbon-supported catalyst layers and the gas diffusion media, leading to increased resistance, reduced catalyst utilization and mass transport losses. Platinum oxidation may result in formation of soluble platinum oxide species, resulting in loss of electrode surface area. In the event of anode starvation, it is preferable that the electrode's water oxidation (oxygen evolution reaction, OER, 2 H_2O -> O_2 + $4H^+$ + $4e^-$, E > E^0=1.23V.) kinetics are sufficiently fast at relatively low potential, to minimize the carbon (GDL) and platinum oxidation.

In 2008 we carried out the first measurements of the effect of adding sub-monolayer quantities of Ir onto the NSTF PtCoMn anodes to enable the anodes to support OER currents at lower reversed cell potentials, thereby potentially protecting the carbon in the GDL. Ir was sputter deposited at planar equivalent thicknesses of 5, 10, 15, 30 and 60 Angstroms onto the PtCoMn anode catalysts (0.1 mg_{Pt}/cm^2) prior to forming the CCM. Due to the approximately factor of ten increase in surface area of the PtCoMn catalyst over the planar surface area, the actual thickness of the Ir deposited once on the PtCoMn was substantially less than the planar equivalent thickness. Fig. 9.10 (A) shows a series of OER polarization curves for these thicknesses compared to the standard anode with no additional Ir. Even the case of just adding 5 Angstroms of Ir substantially increases the OER current over the range of 1.4 to 1.5 volts versus the counter electrode of Pt in 1% H_2 in N_2. For the specific case of 15 Angstroms of Ir, further analyses were done to show the effectiveness for cell reversal tolerance. First Fig. 9.10 (B) shows that the OER tests did have a small effect on the ECSA and ORR absolute activity of the PtCoMn when used as a cathode, reducing the latter from 14.2 to12.9 mA/cm^2-planar. Specific activity remained unchanged at 2.3 mA/cm^2-Pt. The small drop in ECSA, 6.3 to 5.7 cm^2Pt/cm^2_{planar}, may have been due to the Ir blocking some Pt surface area.

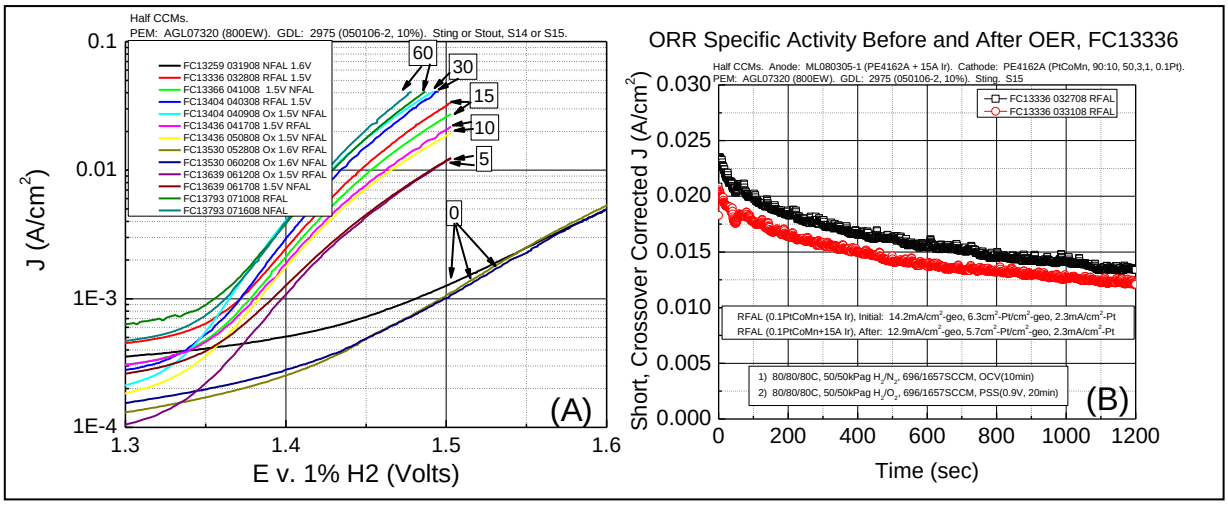

Fig. 9.10. (A) Polarization curves of oxygen evolution reaction current density versus electrode potential from a series of MEA's having NSTF PtCoMn anodes with varying amounts of additional Ir sputtered on top of the 0.1mg_{Pt}/cm^2 PtCoMn before making the CCM. The amounts shown in the boxes are in Angstroms of Ir. (B) ORR absolute activity current density measurements of the 0.1 mg_{Pt}/cm^2 PtCoMn + 15 Å Ir electrodes operated as a cathode, indicating the change caused from OER operation on the anode under a cell reversal test.

For the anode fuel starvation test, four different electrodes were compared, two NSTF and two Pt/carbon. The anode electrode was forced to support a 2mA/cm^2 oxidation current in a N_2 atmosphere for 5 hrs. All MEAs contained the same PEM and GDLs, and were evaluated with the same test station hardware. Two ½-CCMs were made with two 1.3mil 3M 800EW PEMs to reduce parasitic shorting currents. The baseline NSTF-PtCoMn ternary catalyst (anode loading = 0.1 mg$_{Pt}$/cm^2) and a modified version having 15 A of Ir added to the anode catalyst were tested in duplicate. The Pt/Carbon anodes used both 0.2 and 0.4 mg$_{Pt}$/cm^2. The test procedure consisted of first measuring the initial baseline performance, then "Corrode" the anode electrode by forcing 2 mA/cm^2 oxidation current through anode under N_2 for 5 hours, measure post-starvation baseline performance, thermal cycle the cell to recover any reversible losses, and finally measure the post-thermal cycle baseline performance. Fig. 9.11(A) shows the anode starvation voltage versus time profile for the four electrode types. The Pt/C electrodes are initially holding at around 1.35 volts but after a half hour rapidly increase to over 1.75 volts. The higher loading Pt/C electrode appears to hold twice as long as the 0.2 Pt/C before ramping up the electrode voltage. The two NSTF PtCoMn baseline MEA potentials are held to < 1.6 V, better than the Pt/C electrodes. The MEAs with anodes of NSTF-PtCoMn catalyst with the additional 15 Angstroms of Ir show a significant reduction in OER potential to ~ 1.4 V, which is stable for the 5 hours. After longer periods (3-4 hours) the Pt/C and NSTF-PtCoMn approach the potential of the NSTF PtCoMn+Ir, suggesting other avenues of corrosion current are being utilized.

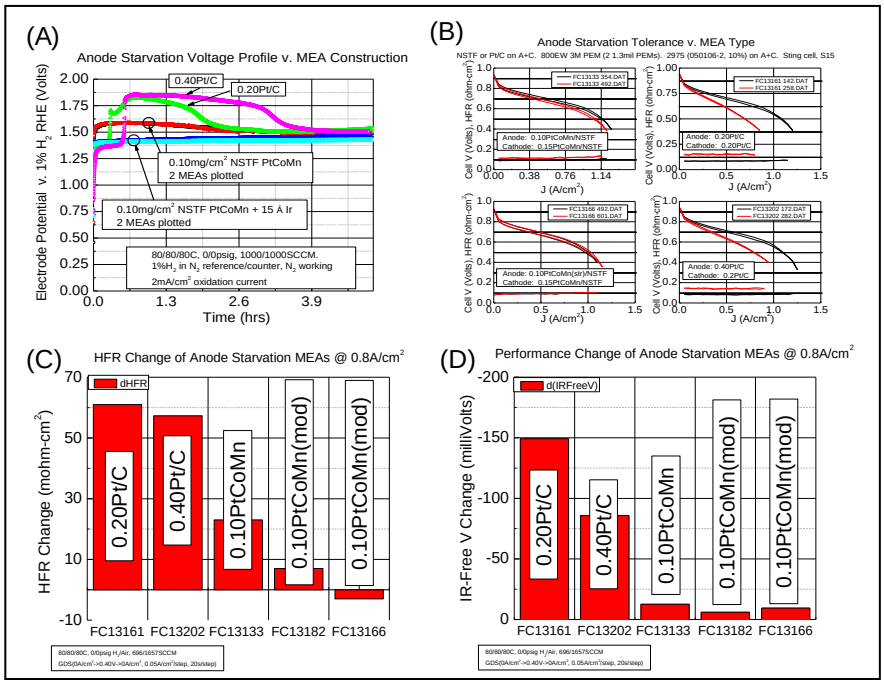

Fig. 9.11. Comparison of four types of MEA anode responses to the anode fuel starvation test in which the anodes are driven past the OER equilibrium potential. (A) Electrode potential versus time for four MEA's when forced to pass 2 mA/cm^2 for five hours. (B) Initial and post-test H_2/air polarization curves for the four types of MEA's in (A). (C) Net changes in high frequency resistance before and after the test for the four types of MEA's. (D) Net changes in iR-free cell voltage after the test for the four MEA's in (A), from polarization curves in (B).

Standard H_2/air fuel cell performance is substantially reduced immediately after the anode starvation test for all MEA's, but the extent differs for the different MEA types. Fig. 9.11

(B) compares the initial and recovered performance for the four types of MEA's. The MEAs with 0.20 and 0.40 mg/cm^2 Pt/C on the anode showed substantial decreases in performance and increased resistance that could not be recovered. The NSTF MEAs showed much less loss in performance or increase in HFR. These are more specifically plotted in Fig. 9.11(C,D). The 0.4Pt/C anode MEA appeared to suffer slightly less irreversible degradation than the 0.2Pt/C anode MEA. The extent of HFR change appears similar. The irreversible loss of the two NSTF PtCoMn MEA's is much less than the Pt/C's. The modified NSTF PtCoMn anode catalyst with 15 Å Ir shows even less irreversible loss in performance or HFR increase in either MEA tested.

9.7. Discovery of the importance of the anode for effective low temperature water management.

Membrane electrode assemblies (MEAs) utilizing the ultra-thin (<1μm) 3M nanostructured thin film catalyst (NSTFC) technology have several demonstrated advantages compared to MEAs comprising conventional, relatively thick (~10μm) carbon-supported catalyst, as noted in the introduction. However, the low temperature (0-50°C) steady state limiting current density of typical NSTFC MEAs with standard GDL's under usual operating conditions is substantially lower than that of many conventional catalyst MEAs (0.3 v. 1.6 A/cm^2 at 30°C, air cathode). This reduced low temperature performance can be attributed to the NSTFC's much higher water generation rate per unit catalyst volume or surface area (~ 6x) and to a hydrophilic electrode pore structure that is more susceptible to water condensation. Significant effort was spent studying the low temperature water management aspects of the ultra-thin layer NSTF electrode based MEA's during the first four years of this project under Task 5.2. We developed test protocols for cool start-up and steady state operation, designed and carried out many GDL materials and process design-of-experiments and then used fuel cell test protocols to evaluate the effects of both cathode and anode GDL modifications.

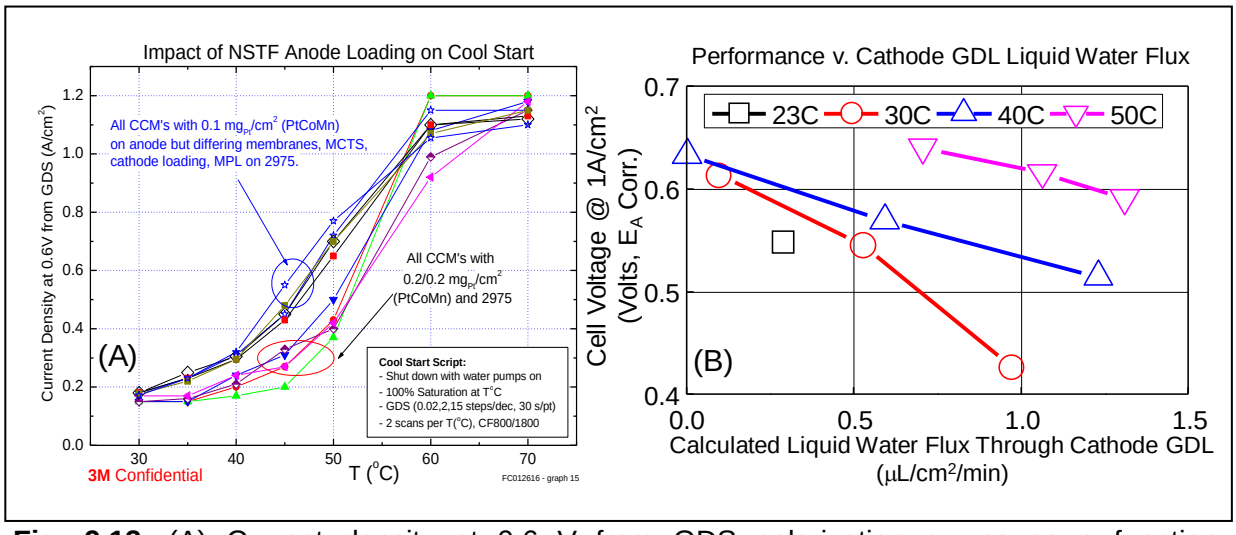

Fig. 9.12. (A) Current density at 0.6 V from GDS polarization curves as a function of temperature for two groups of MEA's differing by their anode catalyst loading. (b) Fuel cell performance versus liquid water flux out the cathode based on measurements and calculated fractions of water leaving as vapor versus liquid.

This latter work was a primary effort during the first three years with generally the focus on trying to mitigate flooding at low temperatures by modifying the cathode GDL properties of our baseline EB paper and its MPL coating, although the asymmetric anode/cathode GDLs

combinations were eventually looked at as well. The results were mixed with small improvements in high temp and low temp operation. Other work involved measuring GDL physical properties with a commercial Porotech porosimeter, as well as our own novel GDL liquid water permeation measurements for wide host of carbon paper types, and applied X-ray tomography to characterize GDL's used for above liquid water permeation studies, as discussed in more detail in the section on Task 5.2.

Eventually we began to separately identify the critical anode and cathode factors for controlling water flow and its impact on fuel cell performance. These broadened studies included quantitative water balance measurements of water exiting the anode and cathode vs their inlets; new cathode interfaces between MPL and CCM; modified NSTF (dual) hybrid cathodes; modified anode GDL's (many types of GDL carbon backing papers, hydrophobic coatings, MPL or no MPL); alternative membranes; and variable anode pressure operation. These studies led to significant improvements in low temperature water management, with the overriding result that it was the anode rather than the cathode that was key to demonstrating viable solutions, with the anode operating pressure and the anode GDL backing paper properties the biggest factors.

In retrospect, the first evidence that the anode was potentially more important for low temperature operation than traditionally thought actually came near the start of this project when we determined that reduced anode catalyst loading improved the steady state current density at operating temperatures below 60 ^{o}C. This is illustrated in Fig. 9.12 (A) which demonstrates that by reducing the anode catalyst loading from 0.2 mg_{Pt}/cm^2 (PtCoMn) to 0.1 mg_{Pt}/cm^2, the steady state current density was nearly doubled between 40 to 60^{o}C cell temperature. Furthermore, the result was not dependent on the membrane, cathode loading, type of MPL or even the MCTS structure of what was tested.

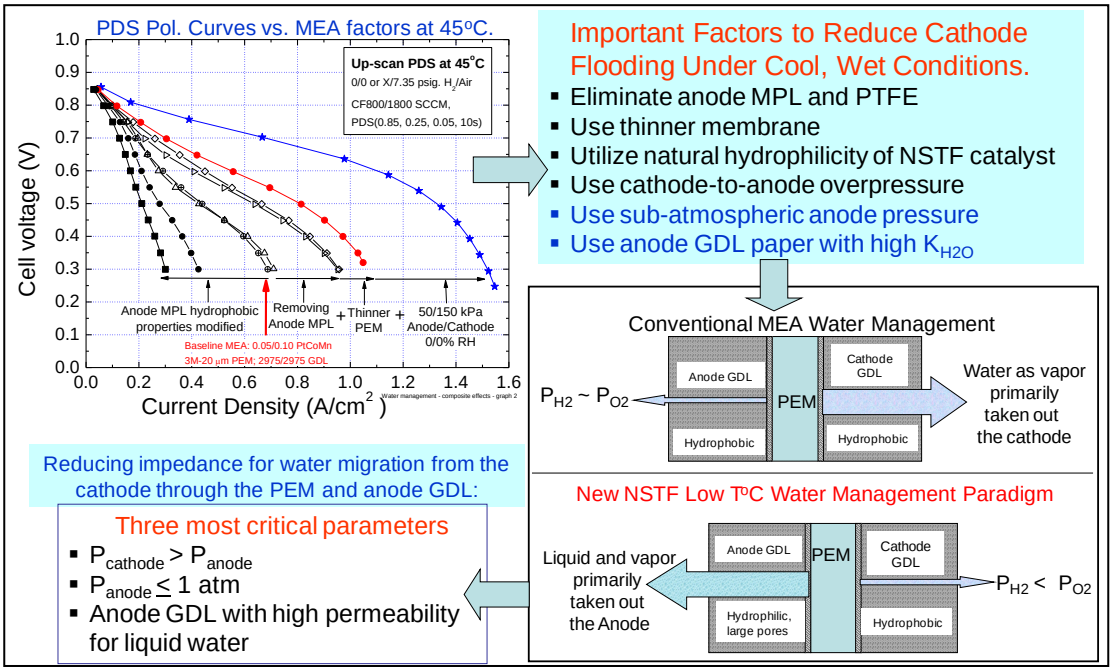

Fig. 9.13. Illustration of the new paradigm for minimizing cathode flooding with the NSTF MEAs by increased water removal out the anode. Key material and operating conditions include reduced anode pressure (even subatmospheric), thinner membranes, reduced hydrophobicity of the anode GDL backing layer, elimination of the anode GDL's MPL.

Later studies conducted to better understand water management differences between NSTF and Pt/C electrode MEAs showed that the product water effluent rate out the cathode was highest when evaluated at several conditions where NSTF MEAs typically showed reduced performance (see Fig. 9.12 (B)). By calculating the fraction of water exiting the cathode in the liquid phase and plotting against the performance loss from the 80 ^{o}C reference performance (all vapor phase water removal), reasonably quantitative agreement is observed for both NSTF and Pt/C electrode MEAs. A primary conclusion from that study was that liquid phase product water removal out the cathode is detrimental to performance for both electrode types, but at a given set of conditions the total water effluent rate out the cathode is less for Pt/C electrodes than NSTF electrodes. It also stresses that taking water out the anode rather than the cathode is a most desirable strategy if possible, since the outgoing water vapor is not interfering with the incoming oxygen, and the cross-over water can keep the membrane humidified. In light of these results, a logical path forward was based upon the premise of minimizing liquid product water removal out the cathode GDL, which is best accomplished by maximizing liquid product water removal out the anode GDL. Fig. 9.13 conceptualizes the key aspects we subsequently determined were most important for improved low temperature water management based on this new paradigm of taking water out the anode. The polarization curves in the top left show the dramatic effects of removing the MPL using a thinner PEM and operating the anode at sub-atmospheric pressure. Low temperature operation is critical for rapid stack start-up from temperatures below 60^{o}C. Fig. 9.14(A) shows steady-state current density at 0.4 volts versus absolute anode pressure at 30 ^{o}C for various combinations of anode GDL, all with no MPL except the baseline GDL (open squares). The anode absolute pressure is seen to be a very effective boundary condition for reducing cathode flooding. The Freudenberg GDL backing layers are much more effective than the baseline MRC type GDL backing layer we standardly use for improving the effectiveness of the sub-atmospheric anode pressure. We started testing the Freudenberg GDL on the anode versus the MRC baseline GDL backing layer since it had a much higher liquid water permeability (6x) from simple liquid water permeability measurements we completed earlier for a whole series of different GDL backing materials (see Task 5.2 section).

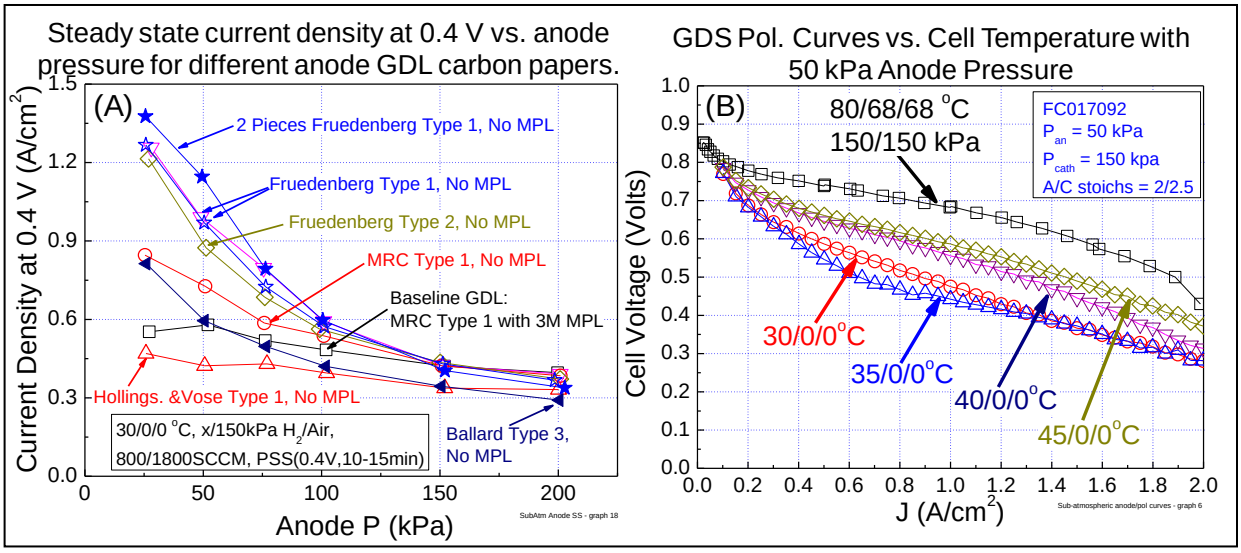

Fig. 9.14. (A) Current density at 0.4 volts as a function of absolute anode pressure under steady-state fuel cell operation at 30^{o}C, dry inlets and 150kPa H_2/air, for various anode GDL types, most without MPL's. (B) GDS polarization scans as a function of temperature and anode pressure for NSTF MEA containing the Freudenberg Type 1 GDL on the anode, 2009 best of class CCM and standard 3M cathode GDL.

Fig. 9.14 (B) shows GDS polarization curves as a function of 50 cm^2 cell temperature under 50/150 kPa anode/cathode absolute pressures of H_2/air. The MEA uses the 2009 best of class CCM and the as-received Freudenberg GDL backing layer on the anode (no MPL or PTFE treatment). With the proper anode GDL and reduced anode pressure, it is possible to run the cell stably at 2 A/cm^2 even at 30 ^oC. The high temperature curve at 80 ^oC and 68 ^oC dew points in Fig. 9.14 (B) also shows there is no impact of the anode GDL on standard higher anode pressure/temperature operation. Operating at equal anode/cathode pressures (150kPa) or higher, the same MEA will flood out at a limiting current of < 0.4 A/cm^2 at 30^oC. But if the cathode pressure exceeds sufficiently the anode pressure, then the cell can hit 2 A/cm^2 even with the anode at atmospheric pressure. This is shown in Fig. 9.15(A) for the case of a 2009 best of class CCM (0.05/0.1 $mgPt/cm^2$ of PtCoMn on anode and cathode, 24 micron thick 850 EW 3M PEM) with the anode GDL replaced by Freudenberg backing layer. Similar benefits obtain under transient load conditions as well as steady state. Fig. 9.15 (B) shows the load transient response under cooler, wet conditions as a function of anode pressure under 60^oC, 140% RH, of a 2009 best of class NSTF MEA consisting of the CCM and MPL-free anode GDL indicated, and a standard 3M cathode GDL.

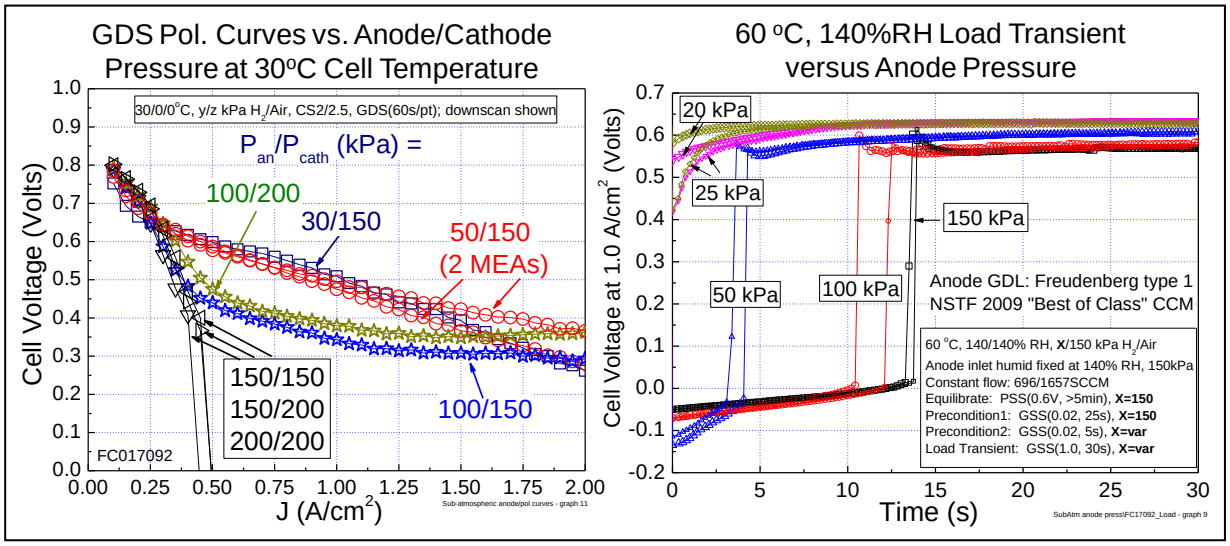

Fig. 9.15. (A) GDS polarization curves at 30^oC as a function of anode/cathode pressure ratios. (B) Transient response to a load step from 0.02 to 1 A/cm^2 as a function of anode pressure for a 2009 best of class CCM at 60^oC, 140% RH, with the MPL-free anode GDL indicated, and a standard 3M cathode GDL (MRC backing paper.)

A less system dependent and probably more practical method for improving the low temperature performance of NSTF MEAs is through materials development. In year four we focused on screening several different vendor supplied *anode* GDL backing to determine their impact on low temperature response. Fig. 9.16 (A) shows results from four tests where the anode GDL backing was varied; all GDLs contained similar hydrophobic treatments and MPLs applied by 3M. Under Test I, the MEAs with GDLs MRC A and Freudenberg A yielded similar performance whereas the MEA with electrode backing paper type MRC C had lower performance at high current density, due to higher HFR. Under Test II, a pseudo-system startup transient, the Freudenberg A GDL provided a short burst of higher performance than MRC A, but the current density dropped to the MRC A level within ~15 sec. MRC C, which had lower performance than the other GDLs under Test I, yielded transient current densities which were 50% higher than Freud A and a steady state current density approximately 3x that of the

other two GDLs. Under Test III, MEAs with either MRC A or Freudenberg A GDL had similarly low performances at 30°C. As the cell was heated, the performance with both GDLs improved, with Freudenberg A having better performance at 40°C than MRC A. MRC C, which performed well under Test II, also performed well at low temperatures under Test III. As the cell temperature exceeded 50°C, all three MEAs performed similarly. Under Test IV, MEAs with either Freudenberg A or MRC C performed similarly as the current density was stepped up from 0.02 to 1A/cm^2 when the cell temperature was 70°C, but at 60°C, Freud A was unable to provide a positive cell voltage at 1 A/cm^2 whereas MRC C only showed a slight loss relative to 70°C. These results show anode GDL properties are the most promising and effective component variable we have identified for solving low temperature cathode flooding with ultra-thin electrodes. Exactly which properties of the GDL are most critical for this function are still unclear. Measurements of standard physical properties and more involved properties such as the porosity distributions and thermal conductivities done at LBNL and through LANL have not yet been able to identify what makes the MRC type C carbon paper so unique and effective for water transport out the anode. The benefit of selecting the correct anode GDL properties is dramatically illustrated in Fig. 9.16 (b) which is a larger summary of several GDL responses to the pseudo-system startup transient Test II discussed above. It shows results with anode GDL's comprising the MRC C (GDL C in 9.16(b)) with and without MPL's, the Freudenberg A type and 3M standard GDL's. Also shown in Fig. 9.16(b) is the impact of a gradient or hybrid CCB used on the cathode (discussed in the section) with either a standard GDL on the anode or Freudenberg A or MRC C on the anode. The top three response curves in Fig. 9.16(b) are obtained with the MRC C on the anode with or without an MPL and a standard cathode GDL. This combination would seem to be the best solution to the low temperature performance issue with ultra-thin electrodes. In practice, there is still a high temperature issue with the MRC C type which is experimental from the Vendor, due to excessive HFR that remains to be solved as noted in Fig. 9,16 (a) test I. Finally, although removing the MPL from the GDL gives the best transient and steady-state cool temperature response, stray carbon fibers sticking out of the bare carbon backing paper surface plane tend to give increased DC shorting currents through the membrane leading to potentially decreased durability.

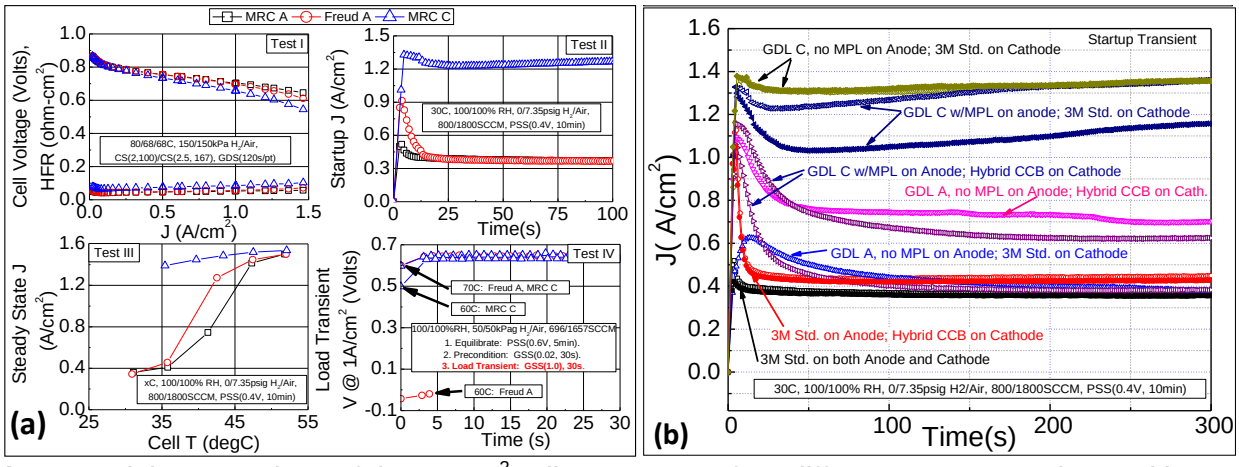

Fig. 9.16. (A) Comparison of the 50 cm^2 cell response to four different test protocols sensitive to water management: Test I is steady state high temperature performance; Test II is a pseudo-system startup transient at 30 ^{o}C; Test III is steady state current density at 0.4 V versus temperature; Test IV is a load transient current density step up from 0.02 to 1A/cm^2 at 60 or 70 ^{o}C. (B) Comparison of the 50 cm^2 cell response to a start-up transient (OCV to 0.4 V) at 30^{o}C and 100% RH for different anode and cathode GDL combinations. H_2/air pressures are 100/150 kPa. GDL type C performance with or without an MPL is far superior in transient and steady state operation to the 3M standard GDL.

9.8. Determination of how catalyst ECSA depends on NSTF whisker support characteristics

Increasing the electrochemical surface area is one sure way to increase the electrocatalyst mass activity. There are two basic approaches to potentially achieve this. One is to optimize the surface area of the catalyst support whiskers. The second is to increase the surface area of the catalyst coating applied to the whiskers. Both approaches were the key objective of Task 1.1. Subtask 1.1.1 focused on increasing the surface area of the whisker supports. Prior to this project, there had never been an attempt to systematically explore how the whisker geometric parameters and growth conditions affected the surface area of the whiskers or, more importantly, their impact on the subsequent catalyst over coating.

Our approach to do this in this project was to carry out a set of designed experiments on production pilot line web coating equipment at the Menomonie, WI, plant where the NSTF roll to roll catalysts are fabricated. These experiments consisted of a multiple series of designed process experiments, called **Whisker Area Optimization one, two, three, ... or WAO – 1,2,3,4),** in which the whisker production parameters were explored for the optimum whisker number density and dimensions, the most complete conversion of the starting material to the crystalline whiskers, and new aspects of the catalyst deposition parameters.

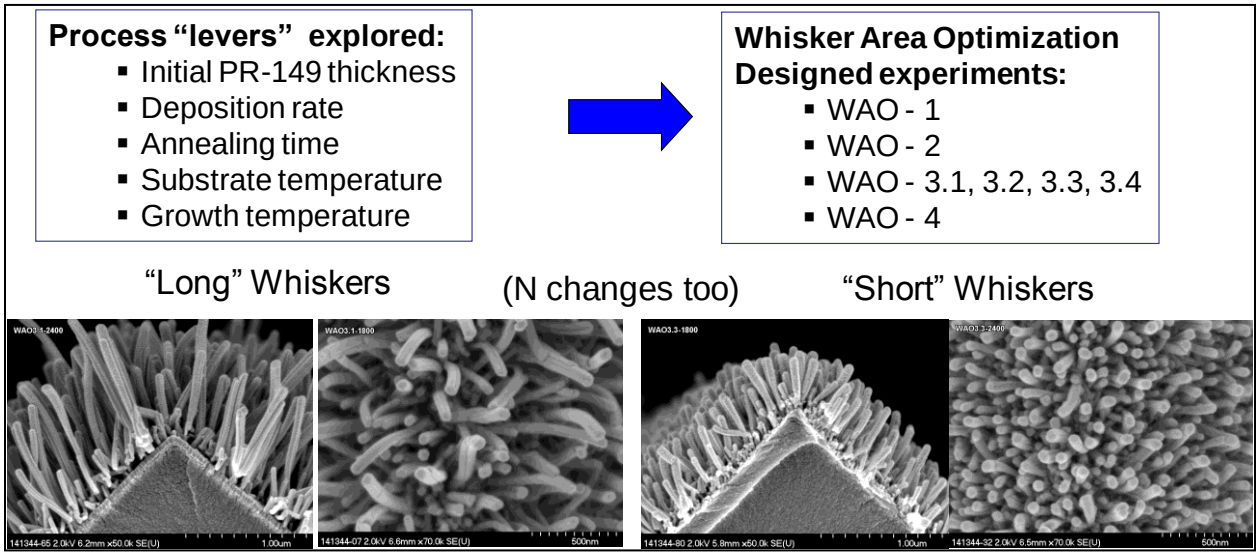

Fig. 9.17. Illustration of the whisker growth process parameters explored for their relationship to the whisker physical characteristics and the subsequent catalyst surface area. The SEM images illustrate the range of length and areal number density (number per unit area) of the catalyst coated whiskers explored in the WAO series of experiments.

Fig. 9.17 illustrates the whisker deposition and growth parameters explored in the WAO series of process experiments. A first order approximation of the geometric surface area can be imagined to be given by the simple expression,

$$S_A = 1.414 \times N[\pi d_{av} L + \pi(d_{tip}^2/2)]r_f + 1 . \quad (1)$$

This is the expression that treats the whiskers as an array of right circular cylinders, for which N is the number of whiskers per unit planar area, d_{av} is the average diameter of the coated whiskers, L their mean lengths, d_{tip} their mean diameter at their tops or tips, and r_f is a

roughness factor for the thin film catalyst coating. Good estimates of these factors were measured from many SEM images as illustrated in Fig. 9.18. Although this simple and intuitive expression for estimating the geometric surface area, S_A , of the catalyst coated whiskers is certainly close to what is measured by H_{upd} cyclic voltammetry, it does not sufficiently capture the reality of how the Pt electrochemical surface area and ORR specific activity depend on the underlying bare whisker geometric characteristics.

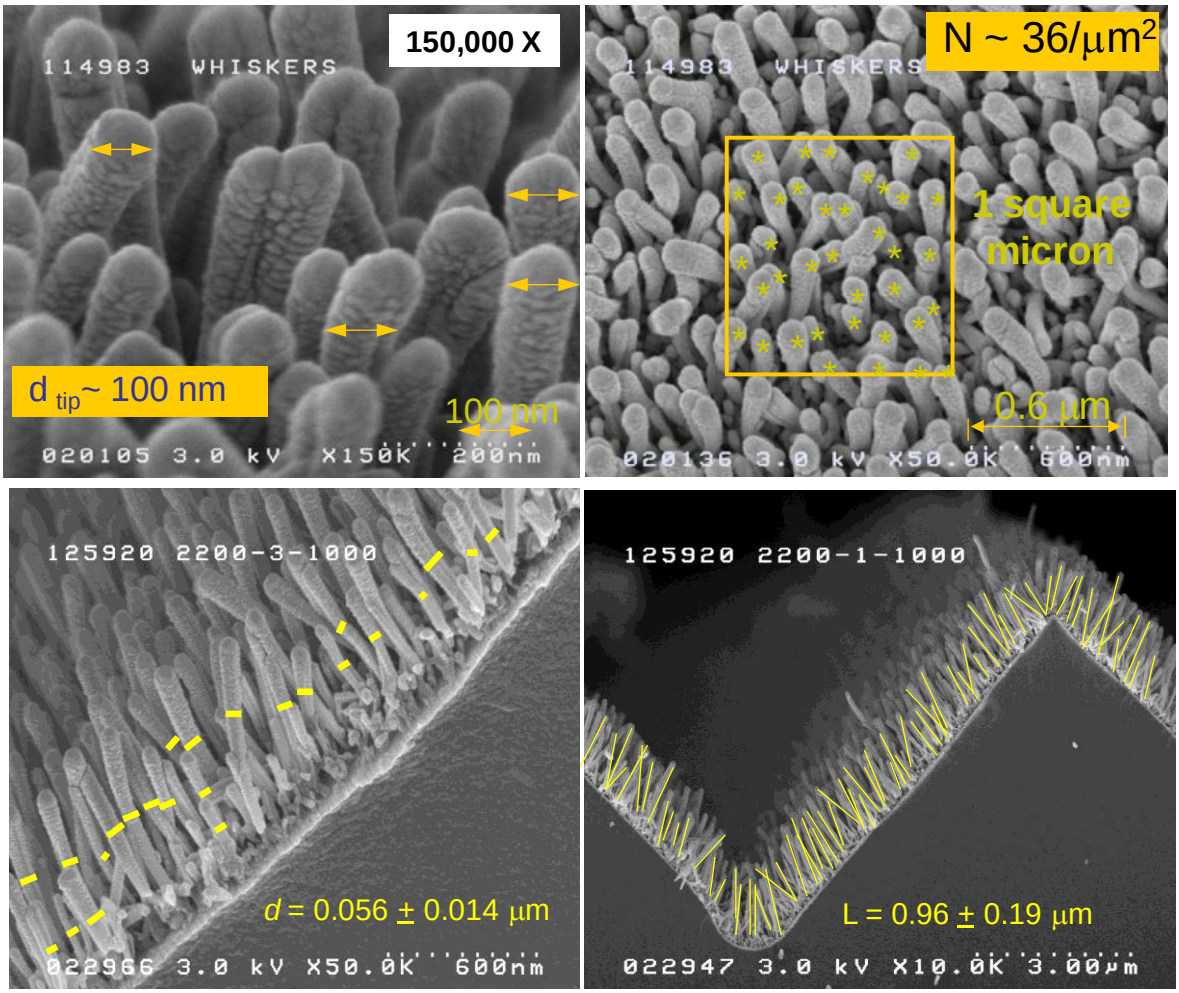

Fig. 9.18. Illustration of how distributions of the basic dimensions of the catalyst coated whiskers were determined from SEM images for the WAO-series of experiments.

The **WAO-1** series was the first designed experiment to relate process conditions to whisker geometric parameters. It used three Perylene Red (PR) pigment thicknesses, four whisker growth process conditions, and two catalyst loadings. It was used to develop a more advanced model for how catalyst electrochemical surface area depends on N, L, w, and d, and was the first study to show how catalyst particle structural properties depend on the whisker geometric characteristics.

One of the outcomes from the WAO-1 series was that not all the PR149 was converted to crystalline whiskers in the typical whisker production process. **WAO-2** as the second in the series was done to demonstrate full conversion of PR149 to crystalline whiskers was possible and also determine the potential to generate larger whisker number density and whisker

dimensions. WAO-2 employed two PR149 pigment thicknesses, seven whisker growth process conditions, and multiple catalyst loadings. WAO-1 successfully demonstrated the capability for full conversion of the as-deposited PR149 to the whisker phase, how to get increased values of N*L, but that doing so did not increase the Pt ECSA.

WAO-3.1 to 3.4 were all part of the third experiments in the WAO series, designed to correlate fuel cell activity metrics with a wider range of whisker growth conditions than considered in WAO 1 or 2. Together they utilized seven PR pigment thicknesses, covering an 18-fold range of values, three whisker growth process conditions, covering a 5-fold range of values, and one value of Pt loading, 0.1 mg/cm^2, of standard PtCoMn used on all the different whisker support types generated. They allowed many conclusions to be drawn about the impact of the whisker growth parameter process windows on fuel cell performance.

Finally, the last experiment in the series, **WAO-4**, was designed to correlate various measured ORR activity metrics with the whisker process growth temperatures. The annealing temperatures were increased in $\Delta T = X^oC$ steps from the standard conditions. One PR thickness and one PtCoMn loading were used.

One example (of many) of what was learned from WAO – 1 is the influence of whisker lengths, L, on catalyst particle growth and shape. This is illustrated in Fig. 9.19, which shows

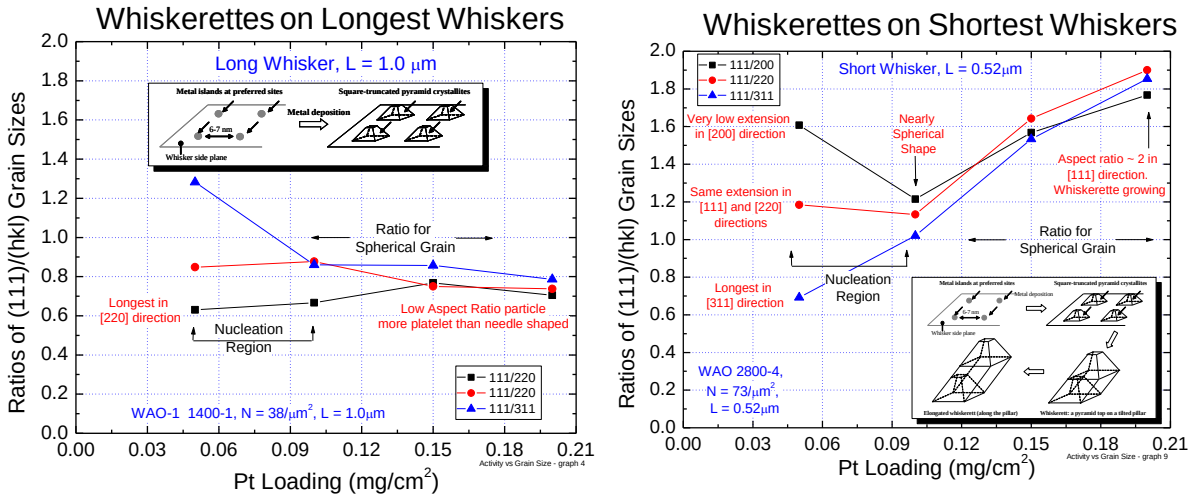

Fig. 9.19. X-ray diffraction determined fcc lattice crystallite dimensions in the (hkl) directions ratioed to the fcc(111) dimension, plotted as a function of the catalyst loading on the whiskers for two extreme whisker growth conditions used in WAO-1. The inset figures reflect the catalyst nucleation and growth of the whiskerettes that comprise the thin film coatings of catalyst on the whiskers, as described in reference (25).

X-ray diffraction determined fcc lattice crystallite dimensions in the (hkl) directions ratioed to the fcc(111) dimension, plotted as a function of the catalyst loading on the whiskers for two extreme whisker growth conditions used in WAO-1. The crystallite grains correspond to the whiskerettes that form on the sides of the whiskers, as described in (25). These ratios reflect the degree to which the whiskerette grains are elongated as they loading increases, as shown by the inset figures in each panel of Fig. 9.19. As loading increases on the longer whiskers of the WAO-1 series, how the catalyst crystallite grain morphology changes with loading is dramatically different than it is for the shortest whiskers. Below 0.1 mg/cm^2 loading, the grains are still nucleating into low aspect ratio particles, more spherical than elongated. Above 0.1 mg/cm^2, on

the longest whiskers, the whiskerettes never seem to get out of the low-aspect ratio regime, and we believe do not develop into proper whiskerettes. On the shortest whiskers, however, above 0.1 mg/cm^2, the grains begin to grow into whiskerettes with aspect ratios that increase linearly with loading, approaching 2.

As a second example of what was learned from the WAO – 1 experiment series, we introduce here an advanced model calculation of how the catalyst ECSA depends on the bare whisker geometric factors, i.e. an advanced version of equation (1) above. It assumes a thin shell model, i.e. the catalyst coats uniformly around whisker, but also accounts for Pt deposited on the back plane between the whiskers, as well as the tops and sides of whiskers. It also takes into account how the roughness factor, r_f, of catalyst coating on the whisker sides scales with increasing mass loading. The model allows for a two-parameter, x and f, fit to data, where x = fraction of catalyst coating on the whisker sides, and f is a scaling parameter for a roughness factor (1+f*d), where d=catalyst thickness. The result is the following expression for A_{geo}^{Pt}, the geometric Pt surface area per unit planar surface area: Equation (2)

$$A_{geo}^{Pt} = \sqrt{2}\left[(1-x)+2xNL(w+t)\right]+\left(m/\rho\right)\left\{(1-x)2N(w+t)+\frac{f}{2NL(w+t)}+x\left[\frac{2}{(w+t)}+f\left(1-\frac{1}{2NL(w+t)}\right)\right]\right\}+\left(m/\rho\right)^2\left[(1-x)\frac{f}{\sqrt{2}L}+\frac{\sqrt{2}xf}{NL(w+t)^2}\right]$$

where, w = bare whisker width (52.5 nm), t = bare whisker thickness,(27 nm), N = areal number density, L = bare whisker length, m= mass loading, and ρ = alloy density (e.g. 18 g/cm^3 for $Pt_{68}Co_{29}Mn_3$). The whisker widths and thickness cross-sections are fixed at values determined by the ratios of the PR149 crystalline side plane surface free energies, as discussed in references (26, 27).

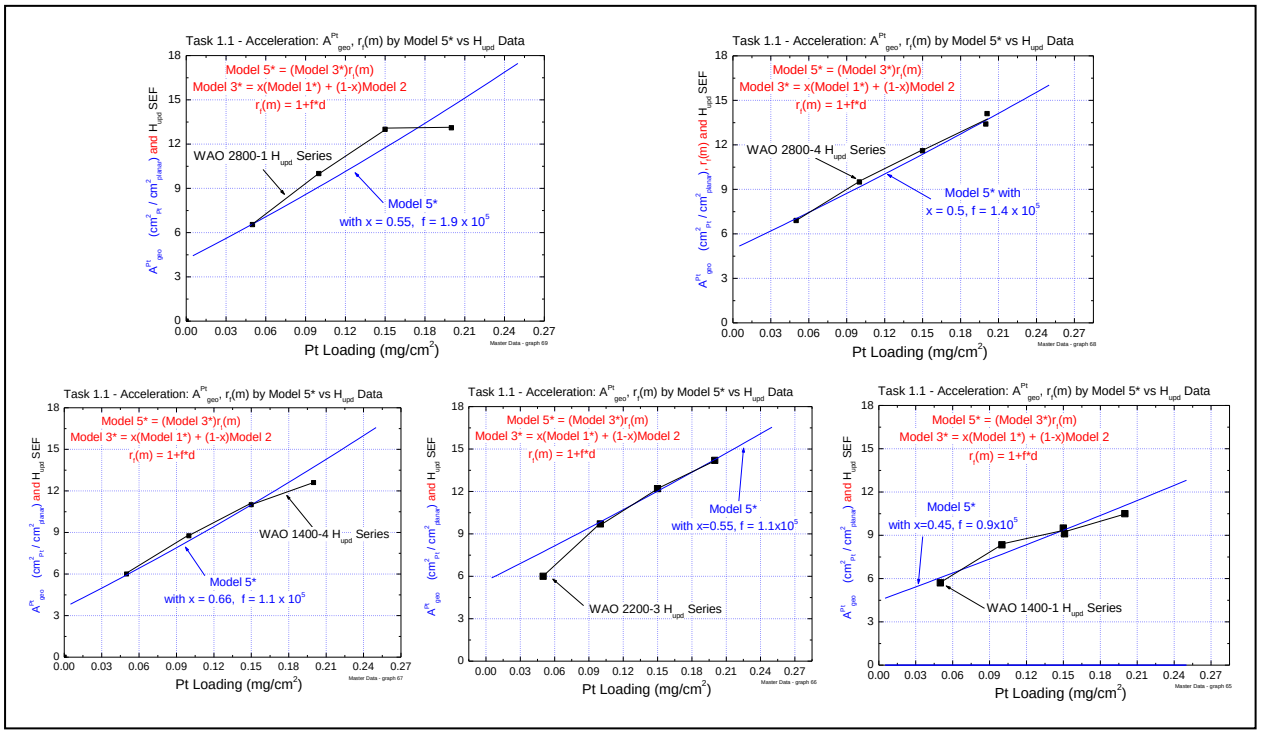

Fig. 9.20. Catalyst surface area model equation (2) comparisons to measured Hupd ECSA values versus loading, for five different WAO-1 whisker types, showing good agreement for a common set of fitting parameters (x and f).

The above model equation was tested and the two fitting parameters *x* and *f*, determined by fitting calculated surface areas to measured H_{UPD} surface area values from the WAO-1 whisker series. This is shown in Fig. 9.20. The catalyst surface area model equation (2) was able to reasonably fit the measured surface area versus loading for five whisker types in the WAO-1 series, with one set of reasonable values for parameters *x* and *f*. Determined generic values for *f* and *x* from these fits are $x = \sim 0.55$ and $f = 1.1 \times 10^5$. This value of *x* implies as much as 45% of the Pt catalyst ends up on the back plane between the whiskers and is not used as effectively as it might be. The value of the catalyst coating roughness factor (1+ *fd*) with this *f* gives a reasonable surface roughness for the coating on the whiskers of about 1.28.

With the understanding illustrated in Fig. 9.19 of how the catalyst crystallite size and shape varies with both catalyst loading and the number density and lengths of the support whiskers, combined with the complexity of the electrochemical surface area dependence on the same factors as shown in Fig. 9.20, we began to understand why increasing the Pt mass activity by increasing the support whisker geometric area was not a straightforward process. In short, the ORR specific activity will depend strongly on the distribution of Pt(hkl) surface facets and their sizes, with the Pt(111) being much more active than the others. Those factors in turn depend on the loading and N and L of the support whiskers in complex ways due to how the whiskerette structures vary with loading for a given whisker support type. Simply increasing surface area by increasing the support whisker's values of N and L for a fixed catalyst loading or composition does not lead to proportionate mass activity increases. The WAO-1 series was very successful in revealing these effects as well as correlating the whisker size distributions with the whisker growth parameters and resulting fuel cell performance metrics.

We conclude this NSTF technology accomplishment section 9 with two examples (again of many) of what was learned from the WAO – 3 series of process experiments. Fig. 9.21 (B) illustrates how the Pt surface area (SEF) (solid symbols) and the product N*L of the whisker number density and lengths (open symbols) varied with PR149 thickness. SEF increases linearly with either type of factor up to about 2000 arbitrary units of thickness, but then SEF sharply levels off with thickness even though the N*L product continued to vary with increasing thickness. This again reflects the conclusion above from the WAO-1 series that the simple geometric factors of the whisker supports do not directly determine the Pt ECSA. Fig. 9.21(A) shows that ORR mass activity does vary linearly with the measured ECSA or SEF.

Figs. 9.21(C,D) show how the fuel cell 50 cm^2 single cell polarization curves varied for the same PR149 thickness ranges but two different sets of whisker growth parameters. Two things are notable. First there is dramatic variation in fuel cell performance over the whole range of PR149 thicknesses considered, from relative values of 400 to 7200 units. Secondly, there is a relatively broad range of thickness near the peak performance curves for both growth parameter values wherein the polarization curves are independent of thickness, but strongly affected outside this 1200 to 3600 unit window. This means that the process window for the NSTF whiskers is quite broad, which is very important from process and quality control standpoints. A similar set of polarization curves exist for the intermediate set of experiments WAO-3.2 for the whisker growth parameter value 3, with the same conclusion. For the extreme values of thickness (400 and 7200 units) other factors dealing with catalyst transfer issues during the CCM fabrication contribute to the reduced performances.

Other related conclusions from these WAO-3 experiments included the following:

- All fuel cell performance metrics are quite independent of the annealing time.
- GDS voltages at all current densities from 20 mA/cm^2 to 1.46 A/cm^2 were independent of PR-149 thickness and annealing speed for thicknesses in the range of 1200 to 3600 units.
- Kinetic activity (absolute, mass and voltage at 20 mA/cm^2) vary approximately linearly with SEF.

- HFR impedance at low and high current densities are independent of PR-149 thickness, and low in value.
- Pt[111] grain sizes vary significantly with PR thickness for both 3.1 and 3.3, somewhat more for the longer 3.1 series. They decrease as whiskers lengthen (shorter whiskerettes).
- Pt[200] and [220] grain sizes are less dependent on whisker type, but appear to oscillate with increasing PR thickness.
- The grain size ratios, [111]/[hkl] vary strongly as the PR thickness changes, and more uniformly for the longer 3.1 whiskers.
- The grain size ratios, [111]/[hkl] ratios, decrease significantly and fairly uniformly as the whiskers lengthen for the longer 3.1series, but not for the shorter WAO-3.3.

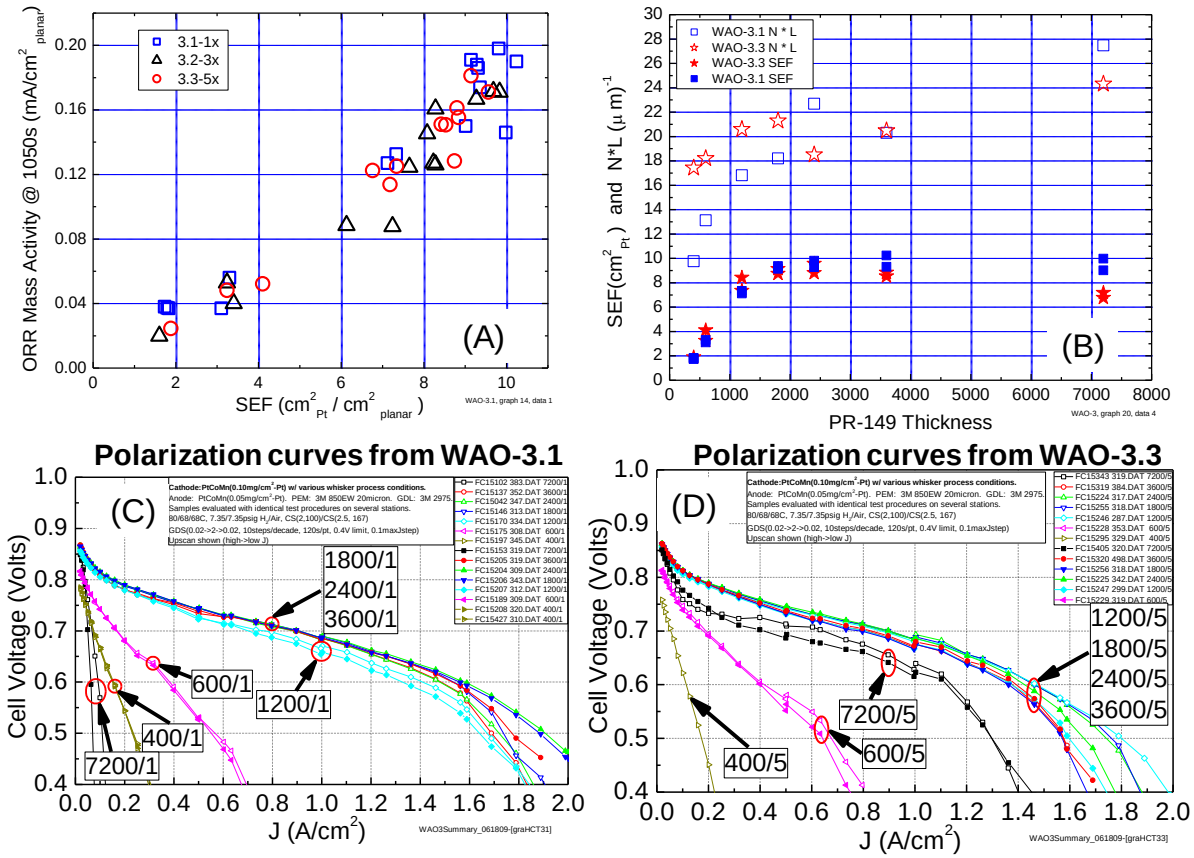

Fig. 9.21. (A) ORR mass activity versus the electrochemical Pt surface area enhancement factor (SEF) for the WAO-2.1, 3.2 and 3.3 experiments. (B) SEF and the product N*L as a function of the starting PR149 thickness (arbitrary units). (C) Polarization curves for the WAO-3.1 series of whisker growth for the thickness range of 400 to 7200 units and the growth parameter value number 1. (D) Polarization curves for the WAO-3.3 series of whisker growth for the thickness range of 400 to 7200 units and the growth parameter value number 5.

9.9. Discovery of a previously unknown fundamental meso-scale property of extended surface catalysts that enables higher limiting currents due to higher surface area per unit volume in the electrode and development of a mathematical model showing it manifested as an additional pre-exponential scaling factor in the Butler-Volmer equation.

(The accomplishment discussed in this section is discussed in depth in a paper published in the Journal of The Electrochemical Society (23). It is considered one of the key publications resulting from this project and is attached in the Appendix. We try to summarize the results and significance here.)

Commercialization of automotive fuel cells requires current densities of 1.5 A/cm^2 above 650 mV with Pt loadings of 0.1 mg$_{Pt}$/cm^2 or less. Loss of high current density with cathode loadings below 0.2 mg$_{Pt}$/cm^2 in Pt/C electrodes is an issue that current kinetic/transport models are reported inadequate to explain (see references in article attached in the Appendix). In studying these published data for dispersed Pt/C type electrodes, we realized that this effect is much less at a given loading with the NSTF catalyst type electrodes. This is basically because of the fundamentally different geometry of NSTF catalysts and their Pt surface area distribution compared to dispersed carbon supported nanoparticle type catalysts. We were then able to explain these differences using a model based on elementary kinetic gas theory and known molecule/surface interaction mechanisms that take place in the Knudsen regime, i.e. at spatial distances on the order of 80 nm above a catalyst surface within which gas phase collisions are not statistically significant. The oxygen molecule/surface collisions are then the determining factor controlling gas phase trajectories, velocity distributions and chemisorption attempts. The net result of the model is that an additional pre-exponential scaling factor $f(d_s)$ in the Butler-Volmer equation related to a distance metric d_s describing the catalyst surface area distribution:

$$J\left(A/cm^2_{planar}\right) = f(d_s)S\left(cm^2_{Pt}/cm^2_{planar}\right)[i_o(A/cm^2_{Pt})\, p_{O_2}^{\gamma}\,(1-\Theta_{ad})^{x}\exp\left(-\frac{\beta F\eta}{RT}\right)\exp\left(-\frac{\gamma\Delta G_{ad}}{RT}\right)] \qquad (3)$$

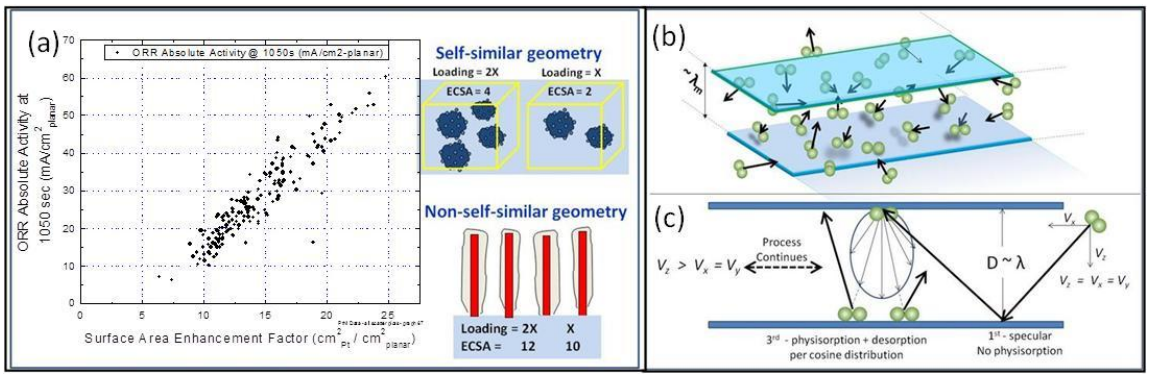

Figure 9.22. Two important properties engendered or applicable to the NSTF type geometry. (a) Self- versus non self-similar geometry can impact how the absolute activity varies with surface area. b) and c) Extended surface catalysts can impact the gas velocity distributions in the Knudsen regime within one mean free path of the surface and thereby increase the number of physisorption and chemisorption attempts per unit time (23).

We approximate this distance metric by the inverse of the surface area per unit volume of the electrode and define and test two possible functional forms for $f(d_s)$. The preferred form is able to predict the correct heat of enthalpy for O_2 physisorption and the observed ratio of current

densities at V(iR-free) = 0.7 V for NSTF compared to Pt/C dispersed electrodes in the 0.05 to 0.15 mg_{Pt}/cm^2 range from published data for eleven different catalyst types and cathode loadings below 0.2 mg/cm^2. The model has no adjustable parameters, unlike many more sophisticated MEA models based on CFD and basic transport theory that assume homogeneity down to all levels.

Fig. 9.22(a) illustrates a simple but significant impact of geometry on ORR activity at increasingly reduced loadings. Pt/C dispersed catalysts have self-similar geometries with respect to surface area and loading. That is if the electrode loading in mg/cm^2 is changed by a factor of two then the electrochemical surface area is changed by the same factor, all else being the same. NSTF catalysts are not self-similar in this way. If the catalyst loading is changed by a factor of two, resulting in approximately the same change in thickness of the catalyst coating, the surface area is observed to change by a smaller amount that depends on the whisker size and spacing parameters.

In the graph in Fig. 9.22(a) this means the absolute activity change with loading, assuming the specific activity remains unchanged will be a less sensitive function of surface area. As mentioned above the ORR area specific activity is much higher for NSTF catalysts, and this geometric factor contributes as well. The graph in Fig. 9.22(a) illustrates the absolute ORR activity at 900 mV under 1 atmosphere absolute of oxygen as a function of surface area enhancement factor for about 150 NSTF Pt-Ni alloy cathodes, near the unique Pt_3Ni_7 composition (30) but differing loadings, degrees and methods of dealloying and post-fabrication annealing. For a doubling in SEF from 10 to 20 cm^2_{Pt}/cm^2_{planar} the absolute activity increases nearly four-fold, from ~ 12 to 48 mA/cm^2.

The impact of the higher specific activity is most clearly observed by simply normalizing a fuel cell polarization curve to the Pt electrochemical surface area enhancement factor (SEF). Fig. 9.23 (A) shows this type of plot for a number of NSTF and Pt/C electrode based MEA's as described in detail in (23). The NSTF catalysts appear to be "working much harder" per Pt atom but there is more to the story than just specific activity. We show in (23) that even if the curves in Fig. 9.23 (A) are further normalized to the measured specific activities for the various cathode catalysts, there are still substantial gains from the NSTF electrodes compared to the thicker dispersed electrodes, and these gains increase as the Pt loadings are further reduced.

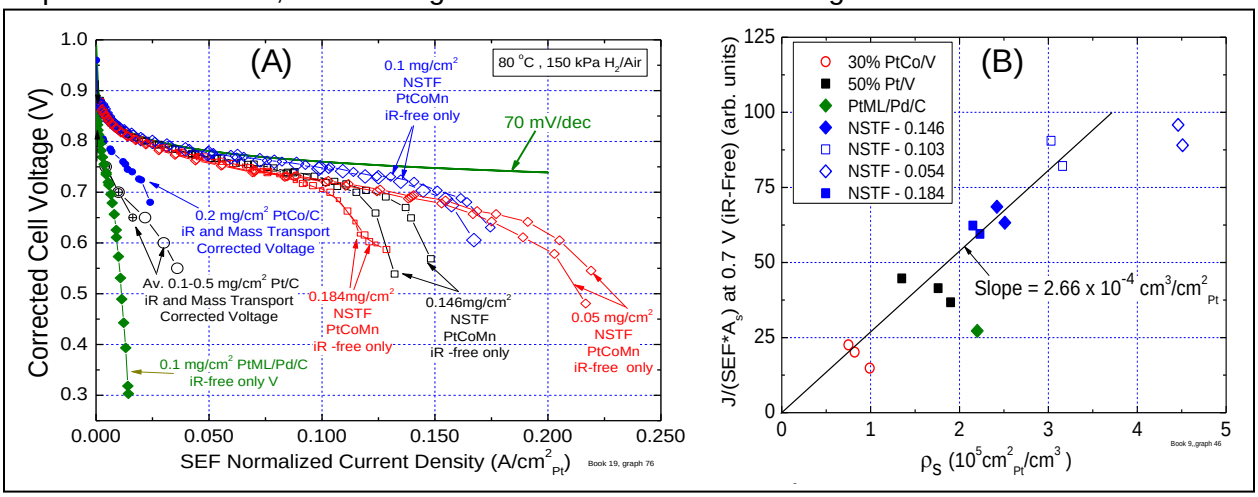

Figure 9.23. (A) Galvanodynamic polarization curves of iR-free cell voltage versus current density normalized to the surface area enhancement factor (cm^2_{Pt}/cm^2_{planar}) for a series of NSTF and Pt/C based 50 cm^2 MEA's with different Pt loadings. The Pt/C cell voltages were also mass transport corrected. (B) Surface area and specific activity normalized current density at 0.7 volts derived from (A), plotted versus the volumetric surface area density, cm^2-Pt/cm^3 for the seven

types of catalysts, derived from the electrode thickness and the measured or reported surface area enhancement factor values in Table I in reference (23). The least squares fit shown excludes the PtML/Pd/Pt and NSTF-0.054 outliers since the thickness of the former is less accurately known and the iR-free cell voltage for the latter is decreasing due to other factors.

This observation forced us to look for some alternative mechanisms which we attribute to another fundamental geometry difference not previously appreciated before. The mechanisms are dependent on the electrode's surface area per unit volume density (cm^2_{Pt}/cm^3) and the ability of the catalyst surfaces' spatial distributions to influence the number of chemisorption attempts per unit time in the Knudsen regime by virtue of their impact on the O_2 molecules physisorption precursor events per unit time. The end result is an additional pre-exponential scaling factor in the Butler-Volmer equation that accounts for the impact of those effects on the O_2/Pt surface collision frequency. This effect is enhanced by the close-packed nature and parallel orientation of the extended NSTF catalyst surfaces as seen e.g. in Fig. 9.17. These effects combine the statistical physics of ideal gases within one mean free path of the catalyst surface with the impact of Knudsen's cosine law for desorption on their velocity distributions resulting in an enhancement in the collision rate as illustrated in Fig. 9.22 (b,c) for gases between ideal parallel extended surfaces.

Based on these mechanisms we have developed a model to explain the significant difference in current density normalized by both surface area and specific activity, observed between low loaded catalyst electrodes having widely differing volumetric surface area densities, specifically dispersed Pt/C and NSTF electrodes. The model is based on the premises that the average time spent by oxygen molecules in physisorption states plus the mean time in transit between physisorption events determines a surface collision frequency factor that contributes directly to the rate of successful chemisorption and oxygen reduction, and also that the surface area distribution can impact this collision frequency. The rate of physisorption events is related to the gas phase molecular velocities in the Knudsen regime over distances of one mean free path, and a distance metric describing the spatial distance between catalyst surface area sites. Using kinetic gas theory and approximating the distance metric by the inverse volumetric surface area density, we tested two functional forms for a pre-exponential collision scaling factor introduced into the Butler-Volmer equation. The preferred scaling factor is able to satisfy two criteria: i) correct prediction of the desorption heat of 4.77 kCal/mole for O_2 from physisorbed states, and ii) prediction of the observed ratio of current densities at 0.7V (iR-free) of published polarization curves from similar MEA's containing eleven Pt/C, PtCo/C and NSTF-PtCoMn cathodes with Pt loadings below 0.2 mg/cm^2. The scaling factor was found to have a quadratic dependence on volumetric surface area density and for the fuel cell data used to determine it, numerically ranged from a low of 0.66 to 0.93 for the catalysts having ρ_s in the range of 0.75×10^5 to 4.5×10^5 cm^2_{Pt}/cm^3. It suggests that electrode surface area densities of at least 3×10^5 cm^2_{Pt}/cm^3 are most desirable to minimize the effect. The enhanced current density for the extended surface area NSTF catalysts is intuitively consistent with the electrode structure's better ability to "entrap" adsorbing oxygen molecules due to the alignment, length to width ratios and spacing of the catalyst coated whiskers in conjunction with Knudsen's cosine law which serves to increase the molecule/surface collision rate per unit time. This concept may not have been considered previously for conventional electrodes and we suggest that a more sophisticated application of the model may be able to partially explain the excessive loss of high current density performance at low loadings seen with conventional Pt/C electrodes.

9.10. Discovery and demonstration of significant effects of flow field types on NSTF MEA high current density performances.

The under-performance observed in Task 5.3 of the MEAs in the GM stack compared to the 50 cm^2 single cell MEAs suggests there is still a question of the possible impact of flow field differences between the quad-serpentine 50 cm^2 cells used at 3M and the flow field design of the GM stack. Flow fields have never before been systematically optimized for the NSTF type ultra-thin electrodes yet can clearly have a strong effect that might not be considered an issue with conventional thick layer electrodes. To establish a baseline of these effects we initiated tests of NSTF MEA's having the same construction as our 2009 best of class in a series of six alternative flow field designs. This was the last major activity of this project. The 50 cm^2 flow field graphite blocks were all tested in one set of 3M cell hardware or one set of OEM cell hardware (OEM HW). Figure 9.24 compares the galvanodynamic scan (GDS) polarization curves from six alternative flow fields with the standard quad-serpentine (QS or FF5), completed at the end of this project. As shown there is a large impact of the flow field type on the limiting current density, and several that perform better than our standard quad serpentine. The HFR differences are small and not responsible for the differences when the graphite blocks are all in the same set of 3M Al cell hardware (3M HW). Cathode and anode pressure drops were also measured for the different flow fields, and can explain the high current density performance gain

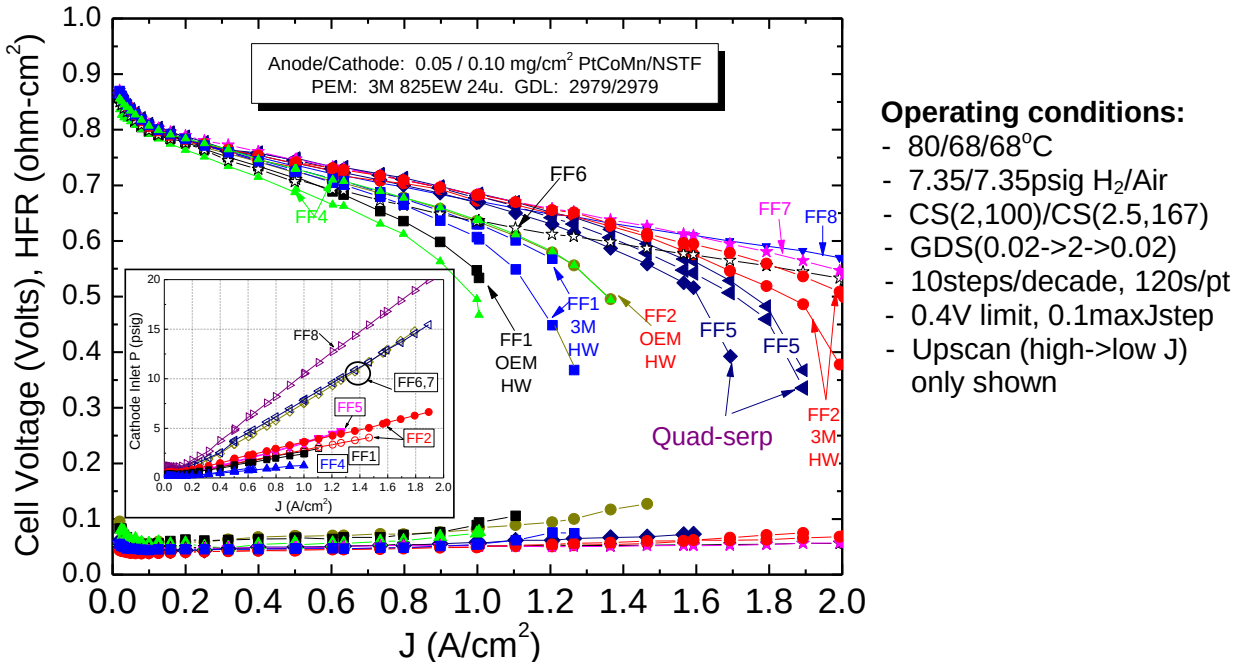

Fig. 9.24. Comparison of single cell (50 cm^2) GDS polarization curves from the standard quad serpentine flow field (**FF5**) with six alternative flow fields: **FF1** = 6 serpentine channels, 2 loops, 2 mm channel width, 2 mm land width, ~0.3 mm channel depth; **FF2** = 24 serpentine channels, 2 loops, 0.5 mm channel width, 0.5 mm land width, ~0.25 mm channel depth; **FF4** = 9 serpentine channels, 4 loops, 1 mm channel width, 0.6 mm land width, 1 mm channel depth; **FF5** (**quad-serpentine)** = 4 serpentine channels, 10 loops, 0.8 mm channel width, 0.8 mm land width, 1 mm channel depth; **FF6** = single channel 3M Zig-Zag (21); **FF7** = 2 serpentine channels, 21 loops, 1 mm channel width, 1 mm land width, 1 mm channel depth; **FF8** = single serpentine, 43 loops, 0.8 mm channel width, 1.0 mm land width, 1.5 mm channel depth.

with the single channel flow fields FF7 and FF8 relative to the standard FF5. However, the FF2 flow field blocks used in the 3M hardware significantly out-performed the standard FF5 with similar or slightly lower pressure drops. Polarization curves taken using ANL specified test conditions with our 2009 best of class MEA in this FF2 generated 2 A/cm^2 at ambient outlet pressure with a stoichiometric flow ratio of two. This is shown in Fig. 9.25. This is a significant result and the first time we have ever obtained 2 A/cm^2 at ambient pressure, particularly at a stoichiometric flow ratio of 2 on the cathode. It is notable that the FF2 gain in performance over the QS (FF5) is most dramatic at lower pressures. The three FF types in Fig. 9.25 differ significantly in the number of loops and channels, yet it appears that the land and channel widths are the most significant factor. This suggests that the smaller (0.5 mm) channel and land width dimensions of the FF2 are key to improved performance and a guide to optimizing the flow field for NSTF MEA's.

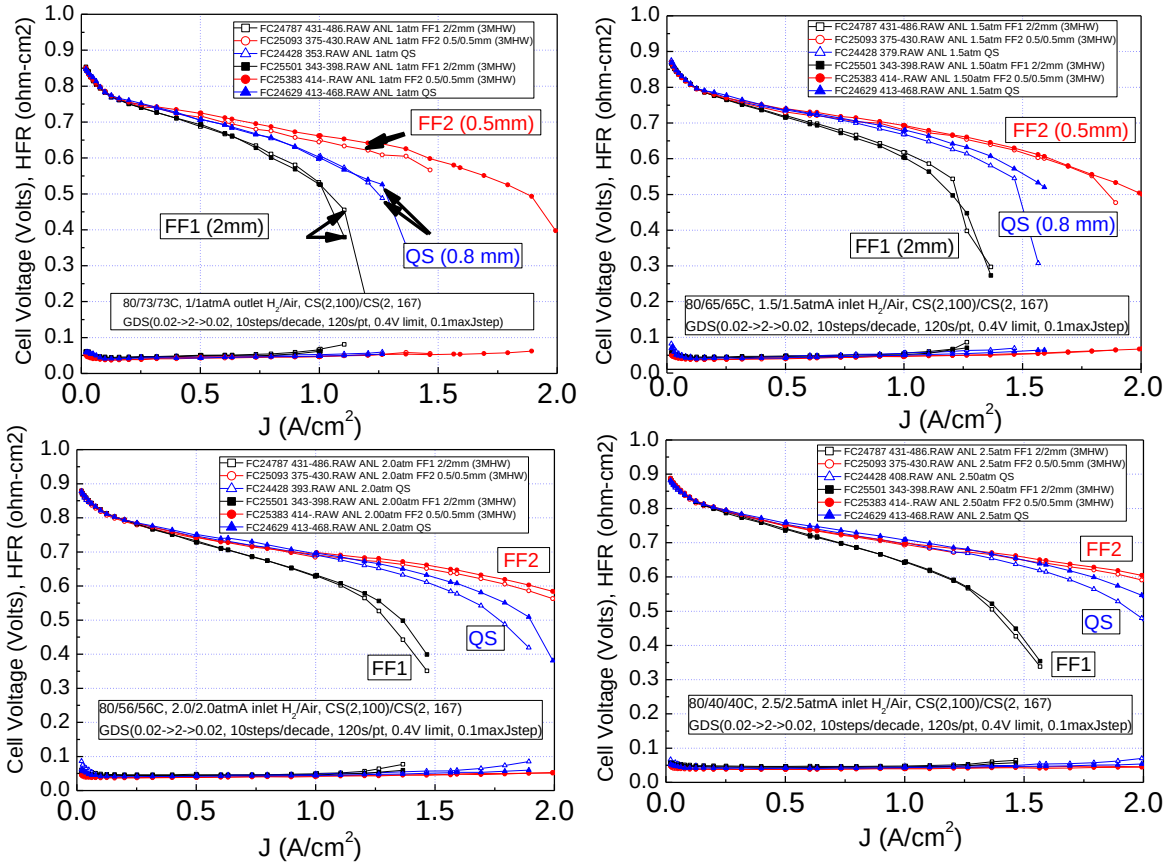

Fig. 9.25. Polarization curves under the ANL specified pressure and flow conditions for identical MEA's (2009 NSTF best of class) in three flow fields, showing the effect of pressure and flow field type. QS is the standard quad-serpentine flow field type FF5 in Fig. 6.23.

9.11. First compositional screening of many new catalyst under-layers and over-layers.

Dalhousie participated closely with 3M on Tasks 1.1.2, 1.3, 2, and to a smaller degree Task 4, during the first four years of the project. The primary focus was to generate higher activity NSTF catalysts with increased surface area and increased durability. Towards this end they used a unique approach for generating and characterizing new compositional spreads of catalysts in 64 element arrays that could then be electrochemically studied in a 64 channel cell unique to their design (ref.)

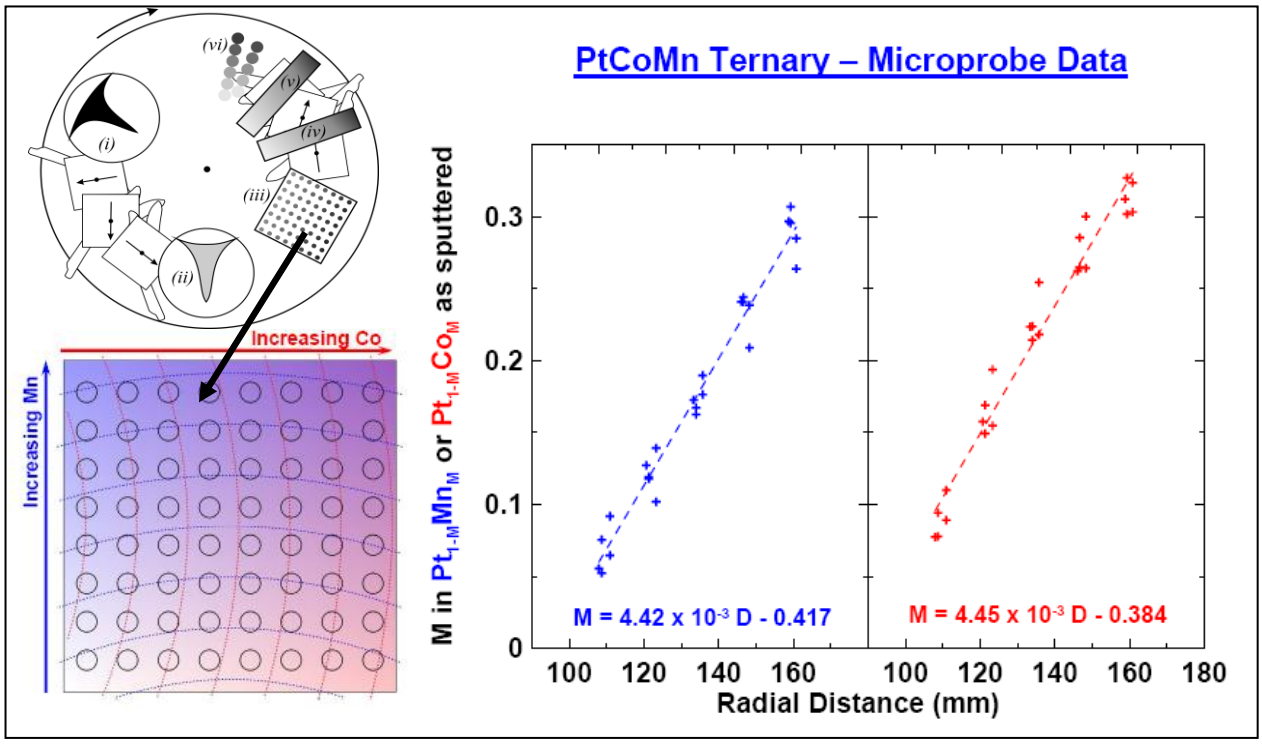

Fig. 9.26. (left) Schematic of how Dalhousie coated catalyst compositional spreads of PtM onto 50 cm^2 samples of NSTF whiskers provided by 3M. The top diagram shows a plan view of their batch vacuum coater with masks at locations of different sputter target types by which gradient compositions were deposited continuously over the whole sample area. The enlarged array of circles shows positions of electrodes when installed in their 64 channel cell for ECSA and ORR activity measurements. The curved lines represent contours for constant Mn or Co respectively. (Right) Electron microprobe data showing how the atomic percentages of the Mn or Co varied with radial position on the sample array for PtMn (blue) or PtCo (red) binaries.

In our approach, they generated compositional spreads of Pt with various metals and inorganic materials to form new alloys, intermixed layers, inert underlayers, and inert overlayers with the objective to control Pt crystallite grain size, increase surface area, increase specific activity and enhance resistance to Pt corrosion. Key to this approach was that they also used sputter deposition to apply the catalysts to the NSTF whisker supports. 3M supplied rolls of the NSTF standard whisker supports that were then used as substrates for Dalhousie to apply the new catalyst compositional spreads, underlayer and overlayer constructions using the coating methodology illustrated in Fig. 9.26. Multiple sheets of any one type of compositional spread coated onto the whiskers were prepared by Dalhousie at the same time and used for their XRD, electron microprobe and other characterizations. One of each of the compositional gradient spreads of catalyst coated 50 cm^2 sheets of NSTF whiskers were then returned to 3M for

transfer to a membrane to form the cathode of a catalyst coated membrane. These CCM's were then returned to Dalhousie for fuel cell testing in their 64 channel cell. This process worked extremely well despite the involved sounding supply chain. For specific compositions chosen for more detailed study at 3M, Dalhousie coated the desired composition onto the entire 50 cm^2 area and returned it to 3M where it was made into a CCM for characterization in 3M's single cells. Near the end of the project, 3M also grew whiskers directly onto glassy carbon disks received from Dalhousie, where they were subsequently coated by catalysts and studied by RRDE methods. In total approximately 200 MEA's were made with compositional spreads from Dalhousie and evaluated in their 64 channel cells or in 3M 50 cm^2 cells. For each sample array, composition at 64 positions was measured as a function of position by electron microprobe analysis, and crystallite grain sizes by XRD. From the 64 channel cell, cyclic voltammograms as a function of position provided measures of Pt surface area at the beginning of life, stability of the surface area with cyclic voltage cycling accelerated stress tests, and relative measures of fuel cell ORR polarization curves. Extracting ORR activity from the multi-channel cells turned out to be more difficult than first envisioned, in part due to "cross-talk" between adjacent sampling sites from the common anode electrodes.

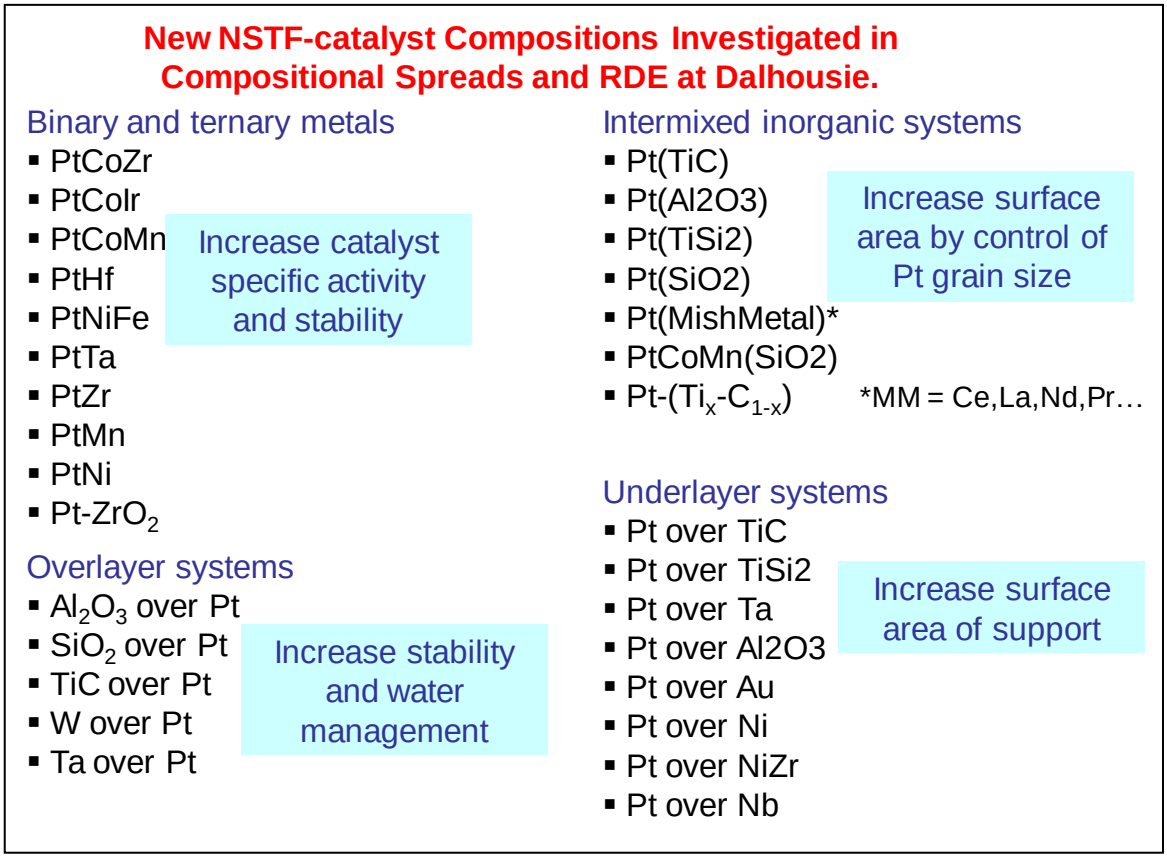

Fig. 9.27. New catalyst compositions investigated with Dalhousie, prepared as compositional spread arrays coated onto NSTF whiskers and characterized in their 64 channel cell. For the overlayer systems, the coating was applied after the Pt was sputtered onto the whiskers. The intermixed inorganic systems and the binary and ternary metal alloys were deposited in multi-layer constructions of the component materials. The non-Pt underlayer components were deposited onto the whiskers before the Pt.

Fig. 9.27 lists the new catalyst compositions investigated with Dalhousie, prepared as compositional spread arrays coated onto NSTF whiskers and characterized in their 64 channel cell as described above. Four types of catalyst coating constructions were investigated for different possible end results. Although perhaps counter intuitive, for the overlayer systems, the coating was applied after the Pt was sputtered onto the whiskers, with the objective to look for any increased stability or different water management behavior. The intermixed inorganic systems and the binary and ternary metal alloys were deposited in multi-layer constructions of the component materials with the goal to look carefully for any impact on ORR activity or crystallite grain size stability. The non-Pt underlayer components were deposited onto the whiskers before the Pt with the objective to explore any effect of increased surface area of the support whisker by "fattening" it. In this respect this latter sample category fit the objectives of Task 4. Fig. 9.28 illustrates just some of the data output from the Dalhousie work for one example of the list in Fig. 9.27.

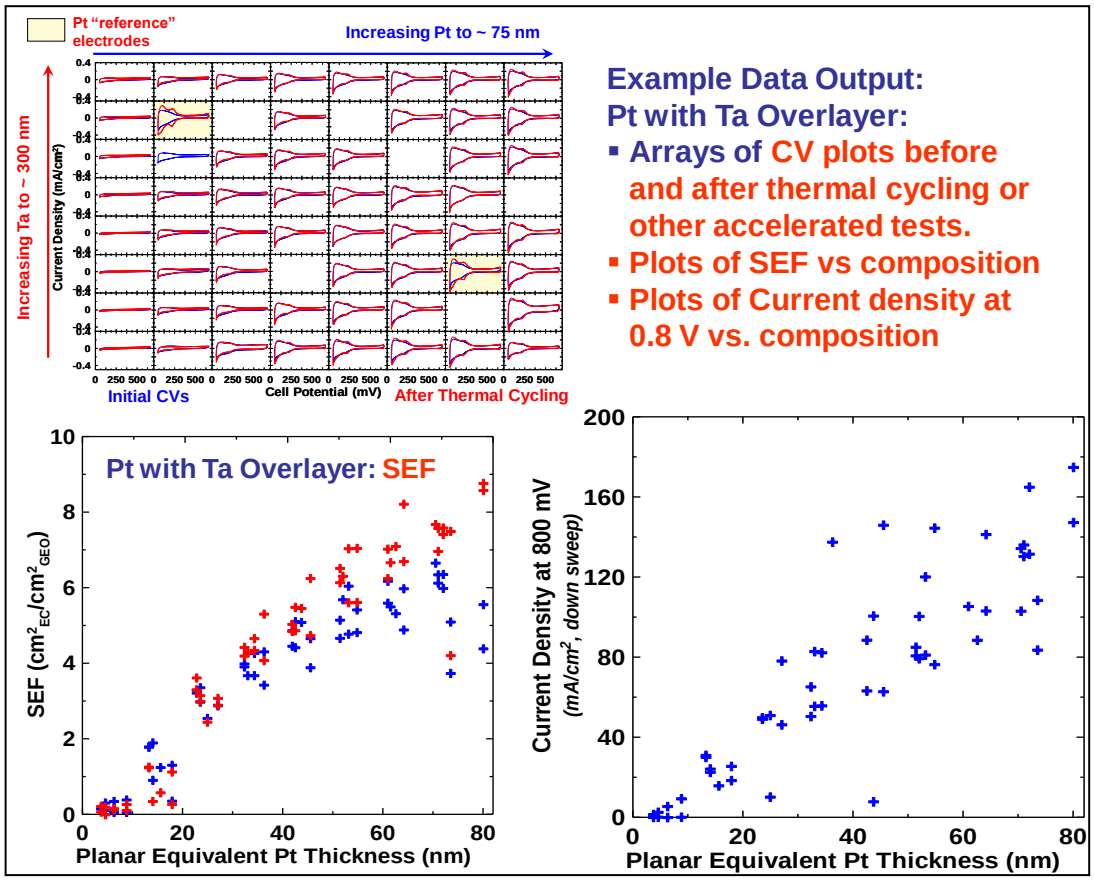

Fig. 9.28. Example of data output from the Dalhousie 64 channel cell for a Pt with Ta overlayer spread. Top left shows the array of cyclic voltammograms before and after thermal cycling. Bottom left shows the SEF versus Pt thickness extracted from the CV arrays above it. Bottom right shows the current density at 0.8 V as a function of Pt thickness extracted from polarization curves obtained with each of the 64 channels.

Finally, we conclude with an incomplete summary example in Fig. 9.29, of how the four categories of new catalyst constructions identified in Fig. 9.27 were evaluated with respect to a number of important characteristics relevant to fuel cell performance and durability.

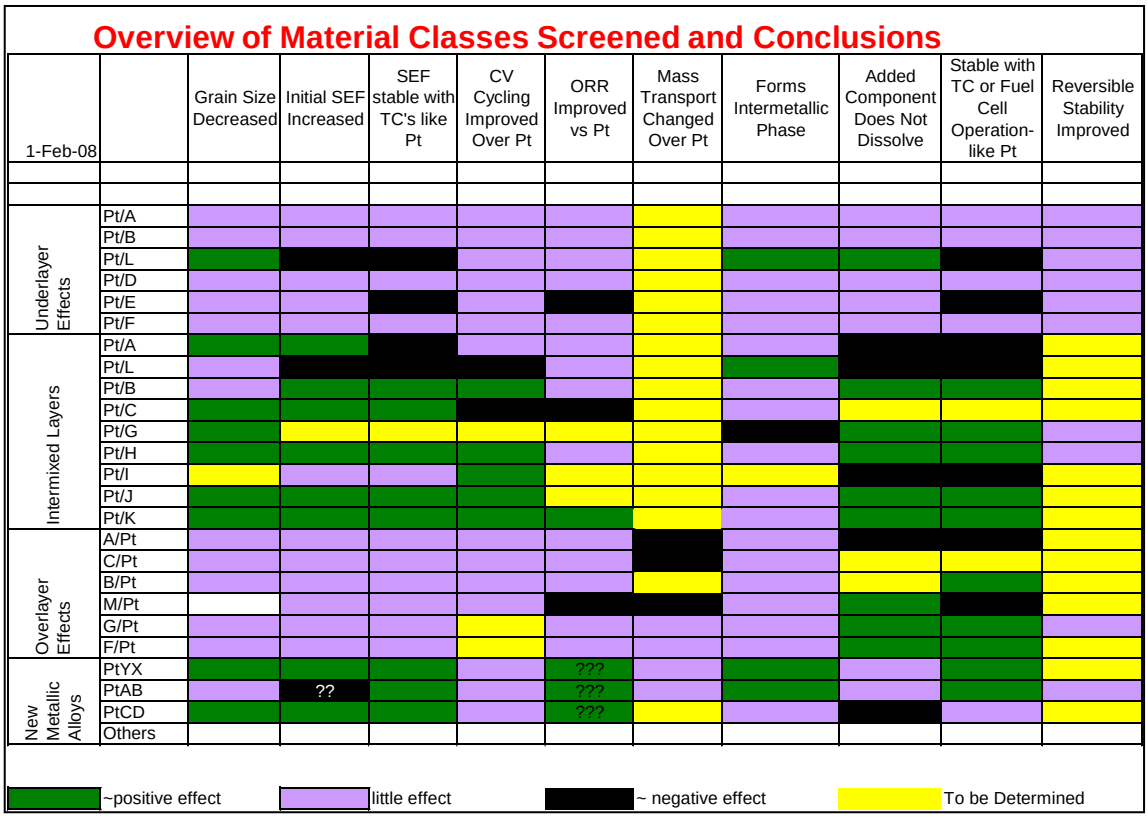

Fig. 9.29. Example of relevant fuel cell properties for the four categories of catalyst constructions listed in Fig. 9.27 that were extracted from the 64 channel compositional spread studies done at Dalhousie University.

Much was learned from these in-depth and first of their kind catalyst constructions and analyses, and significant amounts of it has already been published in references (28 - 38). However, no dramatic improvements in catalyst performance was found with the exception of the PtNi series which were done after discovery of and in conjunction with the Pt_3Ni_7 alloy work at 3M. Four of the Dalhousie originated journal articles are considered significant and have been included in the Appendix.

9.12. Development of an experimental path forward to potentially realize the "entitlement" activity of NSTF alloy catalysts.

Advances in PEM fuel cell electrocatalyst activities have been significant in the past few years. Five key concepts leading to these improvements included use of PtNi alloys; modulated surface composition and lattice strain; extended surface area catalysts; controlled de-alloying; and core-shell catalysts (9). As shown by Stamenkovic et al. (40) of ANL, the Pt_3Ni_1 system is unique in showing the highest ultimate potential ORR activity in bulk single crystal RDE measurements, with specific activities that are reported to be 90 times that of state-of-the-art Pt/C catalysts. This is illustrated in the graph portion of Fig. 9.30, a diagram prepared by V. Stamenkovic of ANL to compare their RDE specific activity measurements of various polycrystalline Pt alloys with that of the $Pt_3Ni_1(111)$ single crystals and commercial Pt/C catalysts. Key to this high kinetic activity is the formation of large area flat fcc[111] facets on the surface with a modulated surface composition in the top three surface layers. Also included on the graph are their measured values of the NSTF PtCoMn, NSTF PtNi and hydrogen annealed NSTF PtNi values (red star).

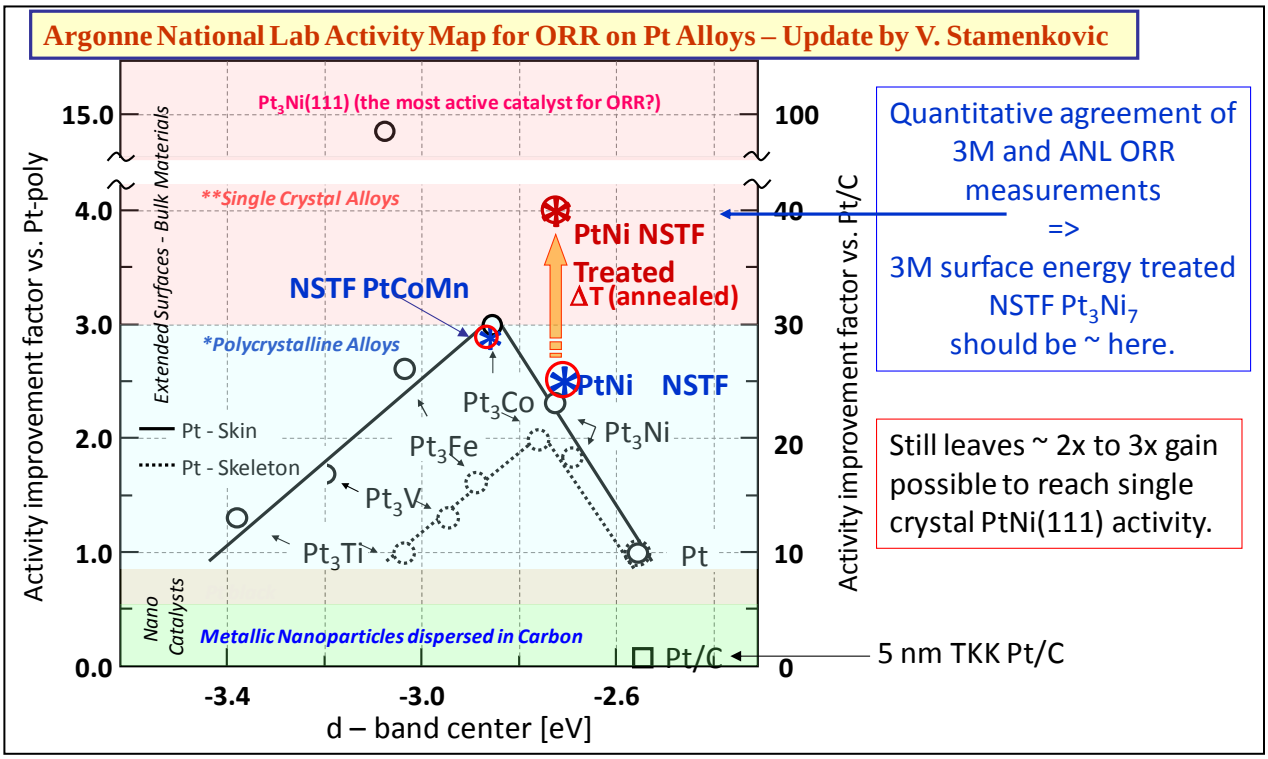

Fig. 9.30. Specific activity improvement factors via RDE measurements by ANL of various alloys with Pt skin or Pt skeleton bulk surfaces, over Pt/C catalysts. Also shown are their measured values of the NSTF PtCoMn, NSTF PtNi and hydrogen annealed NSTF PtNi values (red star).

Because of the good quantitative agreement between their RDE and our MEA ORR activity measurements as shown in Fig. 5.2, we have projected that our SET treated and dealloyed Pt_3Ni_7 catalysts' activities (see e.g. Fig. 7.1 and Table 3) would also correspond to the level of the arrow shown in Fig. 9.30. This would mean that there could potentially be a factor of 2x to 3x further gain in activity to be realized in the optimum NSTF electrodes in order for their activity to reach that of the bulk single crystal $Pt_3Ni_1(111)$ surface.

How we believe it should be possible to achieve those last remaining gains is illustrated in Fig. 9.31.

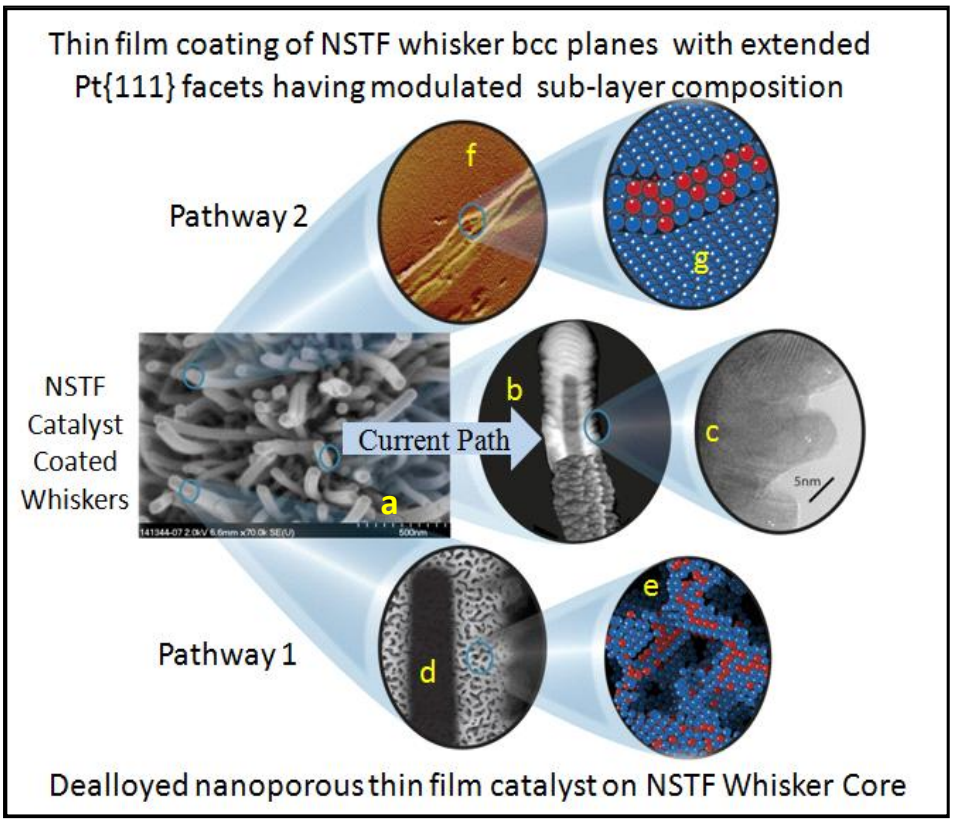

Fig. 9.31. Illustration of two NSTF catalyst advancement pathways combining several of the most promising catalyst concepts in practice today; (a, b, c) shows the current status with NSTF as-made whiskerette surface morphology. (d, e) show pathway 1 using optimized *ex-situ* de-alloying to increase the surface area while maintaining alloy activity gains. (f, g) show pathway 2 on which the alloy coating morphology on the body-centered crystalline lattice of the NSTF whisker core is optimized like bulk single crystalline Pt_3Ni_1 with modulated surface composition in the outer three layers.

Fig. 9.31 illustrates two possible NSTF advanced pathways for incorporating all five of the electrocatalyst concepts mentioned at the start of this section. The whiskerette structure illustrated in inset (c) of Fig. 9.31, is the result of the current pathway and is probably not the best due to the large number of un-coordinated Pt surface atoms on the small [111] facets.

Pathway 1 in Fig. 9.31 with controlled dealloying of high Ni containing Pt alloys has already been pursued in this project as discussed in Section 9.3, to the point of having successfully developed roll to roll dealloying, with significant gains in activity and surface area of the Pt_3Ni_7 alloy. However we do not know that the resulting dealloyed catalyst is optimized as proper *ex-situ* dealloying methods are necessary to obtain the ideal nanoporous structure and composition of the NSTF-PtNi catalyst surface so that it retains the high surface area and develops the modulated composition in the outer surface layers necessary for proper surface lattice strain and d-band structure also believed critical to generating high specific activities (ref (39). Fig. 9.32 shows recent TEM HAADF images obtained by ORNL of samples of the SET and dealloyed NSTF Pt_3Ni_7 electrodes from tested CCM's that we provided to them. They show

clearly that the catalyst coatings on the whiskers are highly porous, and no doubt a strong contributor to the large gain in surface area we achieved with this unique alloy.

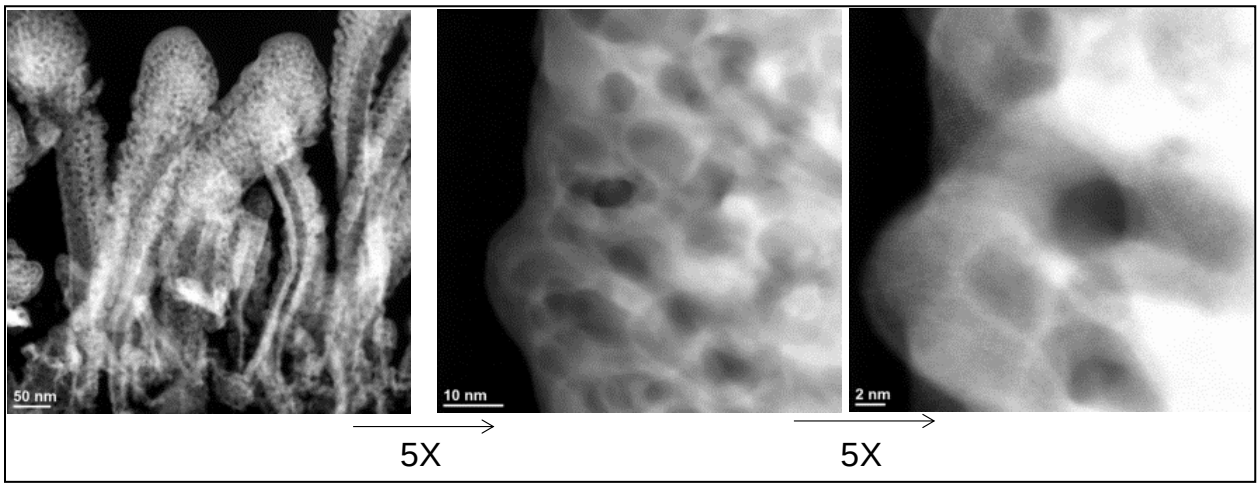

Fig. 9.32. TEM HAADF images of whiskers in the cathode of a fuel cell CCM after break-in conditioning. The catalyst coating the whiskers was dealloyed, SET treated NSTF Pt_3Ni_7 as discussed in Section 7.4 and Fig. 7.2 The scale of the images increases by 5x from left to right for each pair. (Images courtesy of David Cullen **o**f ORNL)

Surface facets are evident at the 2 nm scale resolution in the right-most image of Fig. 9.32. By EDS the dealloyed composition is ~ $Pt_{62}Ni_{38}$. ORNL also reports that there is evidence of Pt skin seen in the highest magnification TEM images which could account for some of the ORR specific activity gain we measure with this unique Pt_3Ni_7 catalyst. It is still not known, however if the surface composition of the topmost layers is modulated as is believed to be important for the ANL Pt_3Ni_1(111) single crystal surfaces that set the standard for most active surfaces, or if the dealloying is optimum.

Another, even more intriguing pathway potentially feasible is pathway 2 illustrated in Fig. 9.31 by insets (f, g). Inset (g) is drawn to represent large, flat (111) surface facets on the coatings of Pt_3Ni_1 catalyst encapsulating the NSTF whisker cores which have the ideal surface composition modulation like that matching the Pt_3Ni_1(111) single crystal results. If the PtNi alloy coating on the NSTF whiskers can be made to model that of the single crystal Pt_3Ni_1(111) surfaces, with negligible uncoordinated surface Pt and nearly 100% (111) facets, the activity would presumably be optimum. We do not know if this is possible or not, as the surface energy of Pt is very high, unlike for Au which easily forms large flat facets in vapor deposited films applied to the NSTF whiskers.

9.13. Study of the water and PEM impurity effects on low ECSA catalysts

Impurities, from sources either external to the MEA and its catalysts (water, air) or internally generated (PEM decomposition) can seriously affect the MEA performance, usually from direct contamination of the catalyst surface. The first in-depth studies of the effects of externally doped impurities on the NSTF MEA performance (reversible and non-recoverable decay) were completed near the beginning of the project. The standard NSTF MEA at that time had 0.2 mg/cm^2 of PtCoMn on both the anode and cathode. These were tested for sensitivity to chloride and sulfide anions at concentrations of tens of micromoles per liter, introduced into the humidification water (supplied as liquid via chromatography pumps.) Desorption of the adsorbed impurities can be generally accomplished by simply thermally cycling the MEA (effectively a cooled shut-down of the cell with flowing clean water moving through the cell and a restart, all repeated three or four times.). This allows cell recovery for the most part, but after multiple such exposures and recoveries, there is some permanent, non-reversible decay observed. Comparative studies were also completed for MEAs having standard Pt/C catalyst electrodes with 0.2 and 0.4 mg$_{Pt}$/cm^2 loadings. These studies have been reported in depth in publications in ECS Transactions and are included as numbers four and five included in the Appendix. The following few figures and discussion however illustrate and summarize the main conclusions of this impurity effects study.

Fig. 9.33 illustrates the performance over time of NSTF-PtCoMn (0.2mg$_{Pt}$/cm^2), with deionized water (DI) (left column), versus 20 µM HCl (middle column), and 20µM Na_2S (right column) added to the water. The top row shows current density at 0.7 V versus time. The middle row shows the decay and recovery by thermal cycling, and the bottom row shows the initial, poisoned and then recovered polarization curves.

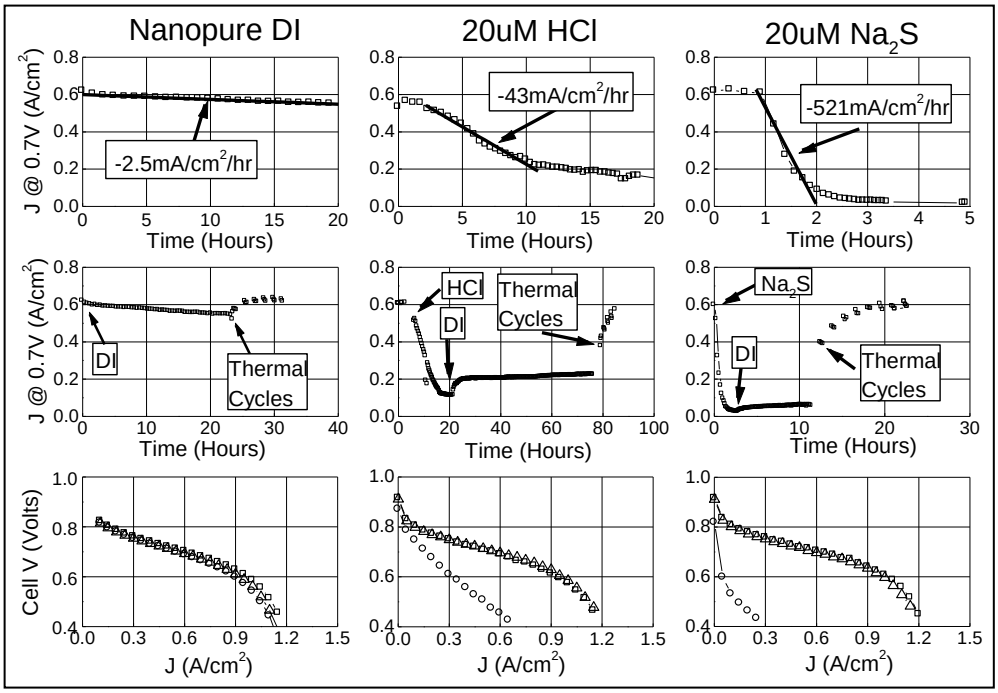

Fig. 9.33. Examples of polarization curve performances over time as a result of exposure of the MEA's to HCl and Na_2S added to the inlet humidification water.

In general, the effect of the Na_2S is much worse than the HCl, but complete recovery of the cell performance is possible with the simple thermal cycles.

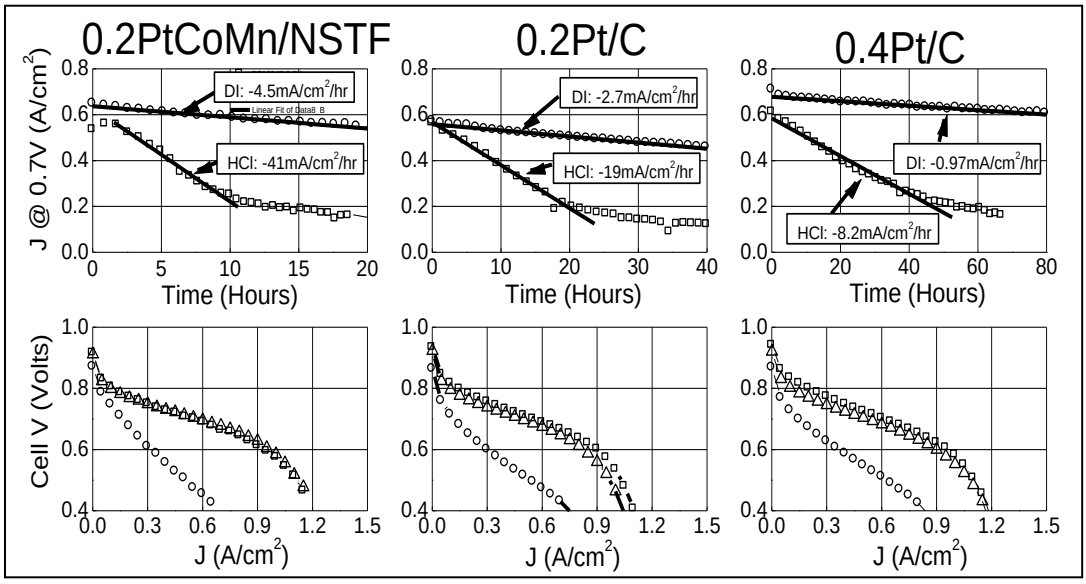

Fig. 9.34. Examples of polarization curve performances from Pt/C and NSTF based MEA's over time as a result of exposure of the MEA's to 20 μM HCL added to the inlet humidification water.

Fig. 9.34 compares the effect of 20μM HCl on polarization curve performances from Pt/C and NSTF based MEA's over time. The Cl^- ions cause performance of both catalyst types to rapidly decay. Table IV summarizes the NSTF and carbon supported dispersed Pt (Pt/C) electrodes' current density reversible decay rates due to doping the fuel cell inlet water with 20 μM Cl^- ions. NSTF decays faster than the Pt/C but has many times lower surface area. All decays can be recovered to some extent, but more so for the NSTF MEA's. All MEA's show some reversible decay even on nanopure water.

Table 4. Summary of reversible decay rates and initial current density for MEAs operated with either DI or 20μM HCl humidification solution. The number in parentheses indicates the number of MEAs evaluated.

Catalyst (# of MEAs)	Humid. Solution	Current Decay Rate @ 0.70V ($mA/cm^2/hr$)	Initial J @ 0.70V (mA/cm^2)
0.2Pt/C (5)	DI	-2.0± 0.7	597±42
0.2Pt/C (4)	20μM HCl	-18±3	610 ±23
0.2PtCoMn/NSTF (12)	DI	-4±2	611 ± 27
0.2PtCoMn/NSTF (5)	20μM HCl	-63±27	596±31
0.4Pt/C (2)	DI	-0.5 ± 0.1	702 ±12
0.4Pt/C (1)	18.6μM HCl	-8.96	610

Table 5 summarizes the effect of exposure and recovery of NSTF and Pt/C MEA surface areas to the 20 μM HCl just discussed. To within statistical variability of surface area measurements, the NSTF surface area loss from chloride (and sulfide) adsorption is essentially

recoverable. The NSTF surface area losses are ~ 0% to 10% respectively. The 0.2 and 0.4 Pt/C cathodes lose ~ 30% and 50% of their surface area respectively. Non-reversible performance loss appears to be primarily due to permanent loss of surface area.

Table 5. Variation in cathode Pt Surface area Enhancement Factor (SEF) in initial, poisoned, and recovered state for the 0.2PtCoMn/NSTF, 0.2Pt/C, and 0.4Pt/C MEAs from Fig. 9.34. SEF values are ± 10% or ± 1, whichever is larger.

Catalyst	**Initial SEF (m^2-Pt/m^2-geo)**	**Poisoned SEF (m^2-Pt/m^2-geo)**	**Recovered SEF (m^2-Pt/m^2-geo)**
0.2PtCoMn/NSTF	10.6 ± 1.1	9.0 ± 1	9.8 ± 1
0.2Pt/C	75 ± 8	44 ± 4	51 ± 5
0.4Pt/C	150 ± 15	63 ± 6	70 ±7

Following the above studies, the effect of the Cl^- ion concentration was shown to be directly proportional to surface area. Fig. 9.35 (Left) shows the cell current density at 0.7 V response of the 0.2 mg_{Pt}/cm^2 Pt/C MEA's to a series of HCl-doped water levels from 0 to over 1000 μM.

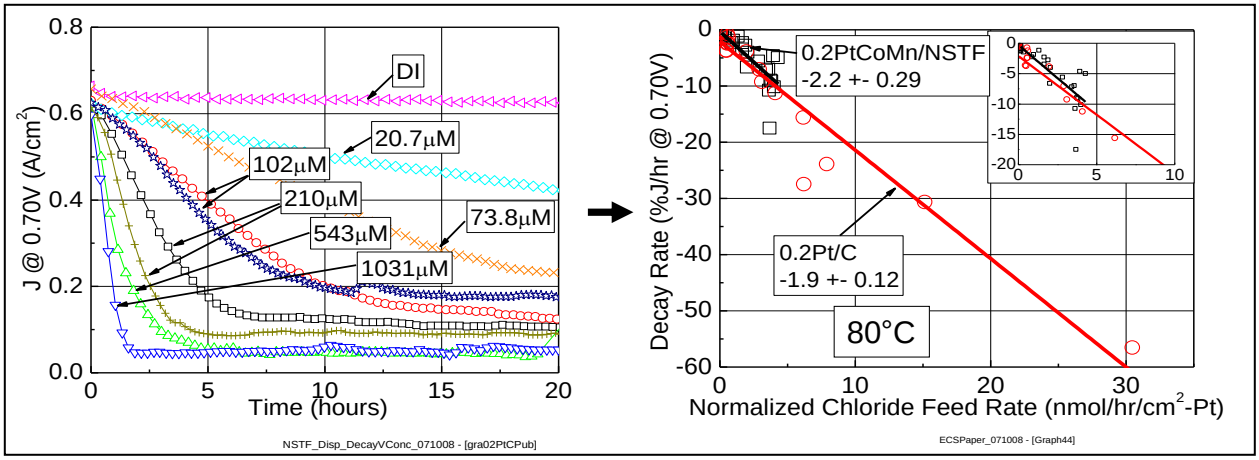

Fig. 9.35 (Left) Cell response of current density at 0.7 V to the 0.2 mg_{Pt}/cm^2 Pt/C based MEAs to a series of HCl-doped water levels. 20 μM = 0.71 ppm. (Right) Decay rates plotted versus the surface-area-normalized chloride ion feed rates.

The graph on the right in Fig. 9.35 plots the decay rate data versus the surface-area normalized chloride ion feed rates, showing a common slope for both types of electrodes. It is apparent that chloride, provided to the fuel cell via the humidification water at micro molar concentration dramatically increased the rate of reversible performance decay for MEAs with 0.2 mg/cm^2 Pt/C (above left) electrodes, as it did for the 0.2 mg_{Pt}/cm^2 PtCoMn/NSTF electrodes. With identical operating conditions and Cl^- concentration, the reversible decay rate of the Pt/C MEAs decreased **~7x** more slowly than the NSTF MEAs. Fig. 9.36 (right) shows the decay rate in percentage current density loss, extracted from the left figure, plotted versus the surface area-normalized chloride feed rate in nano-Moles per hour per cm^2 of Pt surface area. Normalizing to the Pt surface area accounts for the ~7x difference in catalyst surface area between the MEA types, and the reversible performance decay rate increase with SEF-

normalized chloride feed rate was very similar for both the NSTF and Pt/C electrode types. The universal line slope gives a decay rate sensitivity factor of ~2% current density (J) lost per (nmol Cl^- fed per cm^2-Pt).

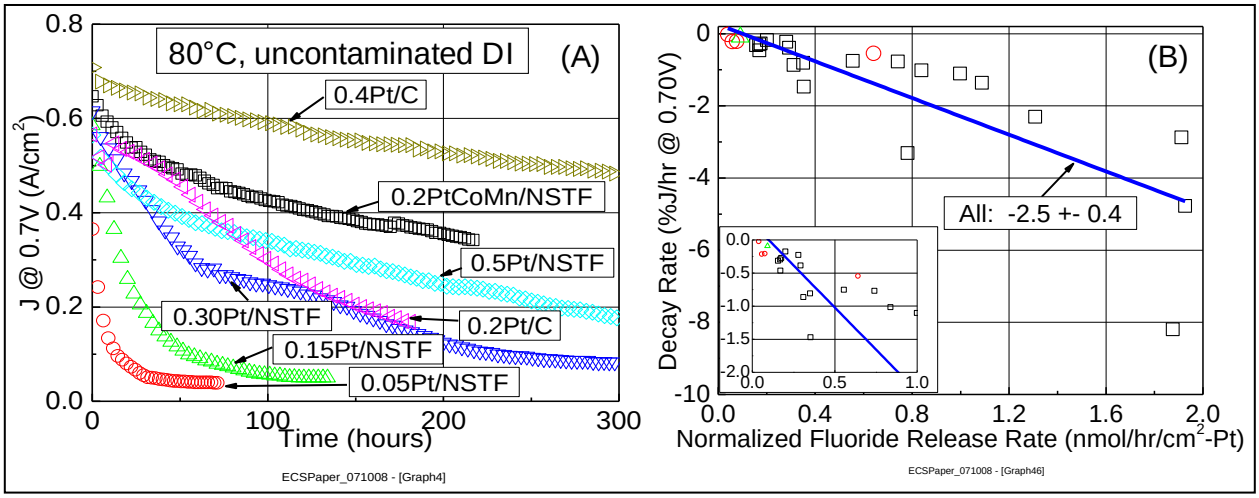

Fig. 9.36. (A) Current density at 0.7 volts versus time for various NSTF and Pt/C electrode based MEA's when exposed to just the incoming nominally pure DI water. (B) Decay rates from graph A versus the surface-area-normalized fluoride ion release rates measured in the cell exit water.

So it is very clear that the effect of Cl^- contamination can be simply understood as due to adsorption and poisoning of the Pt surface, regardless of the catalyst type. But even with nominally pure inlet water, there is reversible decay. Fig. 9.36 (A) shows how the current density at 0.7 volts versus time varies for various NSTF and Pt/C electrode based MEA's when exposed to just the incoming nominally pure DI water. The decay rates vary substantially with the catalyst loading and surface area. Again all the data suggest a worsening decay rate with lower surface area for a given catalyst type, even with nominally pure DI. But the performance decay rate data variations between catalysts types cannot be explained by just external low-level residual contaminants, as the variation could not be explained by surface area alone. This is clearly seen in Fig. 9.36 (A) where the MEA with 0.2 mg/cm^2 Pt/C electrodes, with 7x higher SEF, decayed faster than 0.2 mg/cm^2 PtCoMn/NSTF electrodes. So something internally generated as an adsorption impurity has to be considered. The decay rate data can be explained by normalizing to Pt surface area and the internal production rate of fluoride ions measured in the exit water. The F^- ion rates vary with catalyst surface area, composition, and support type, and can be up to 1000 times less for NSTF vs Pt/C catalysts (22). Fig. 9.36 (B) plots the percent current density (at 0.7 V) decay rates versus the surface-area-normalized fluoride ion release rates measured in the cell exit water. F^- itself is not a contaminant, but rather is a correlated indicator to one or more internally-generated species, such as PEM decomposition products. Different PEMs (e.g. 3M 1000EW v. Nafion™ 112), with all other components fixed, caused the "F^-" decay rate sensitivity factor to vary up to 4x, likely due to differences in PEM decomposition (different species produced per unit F^- ratios). Identifying the exact composition(s) and chemical nature of these internally generated (likely membrane decomposition products) is a key need to reduce the reversible decay at low catalyst loadings.

With 0.2 mg/cm^2 PtCoMn/NSTF + 3M 1000EW PEM MEA's, the absolute decay rate due to the internally-generated species was measured and found to increase super-linearly with operating temperature, while the F^- production rate also increased. The decay rate temperature sensitivity was found to be linear with temperature, increasing to 0.1% per °C above 62°C and zero below this temperature. Limited data from the earlier Cl^- studies suggested a minimum

sensitivity temperature of ~28°C with 20μM Cl^- and a lower rate of increase with temperature than the internally-generated (F^- ion) species.

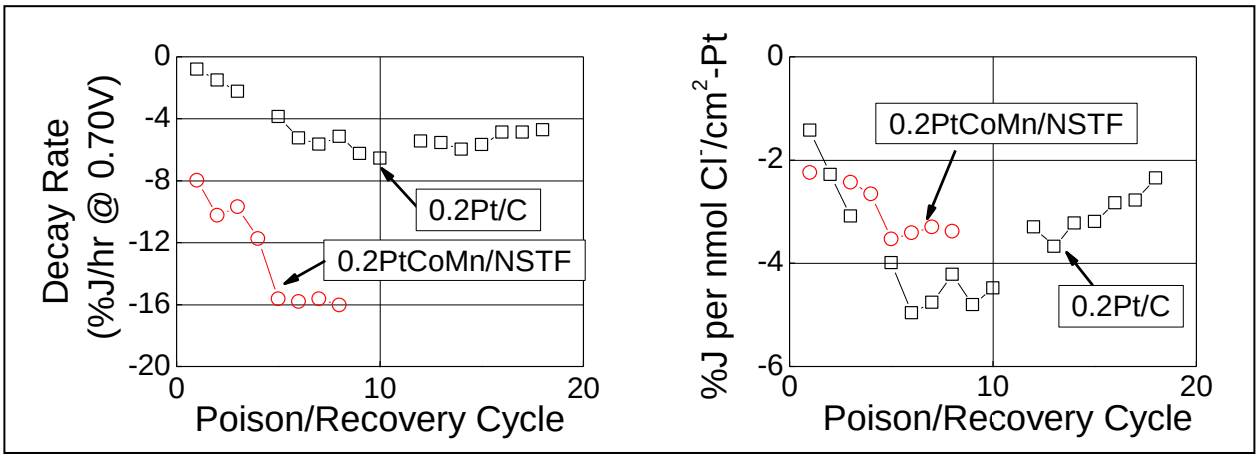

Fig. 9.37. Effect of repeated Cl^- ion poisoning and recovery cycles on both Pt/C and PtCoMn/NSTF electrodes at same 0.2 mg_{Pt}/cm^2 loading.

Finally, the impact of multiple exposures to poisoning with Cl- ions and subsequent recovery was evaluated. Repeated poison/recovery cycles with 20μM Cl^- caused the absolute decay rates of both 0.2 mg/cm^2 PtCoMn/NSTF and 0.2 mg/cm^2 Pt/C MEA's to increase, as shown in Fig. 9.37. Both MEAs' decay rate sensitivity factors increased with repeated cycles, but the Pt/C MEAs' rate and extent of sensitivity increase was larger, due to the Pt/C MEAs' 2x and 3x larger rate and extent of surface area loss with poison/recovery cycles. Identical experiments with DI confirmed that 20μM Cl^- did not increase the rate of surface area loss for either MEA.

9.14. Dependence of limiting current on ECSA

Traditionally, surface area is only considered to affect the kinetics. In 2010, we identified a correlation between cathode absolute surface area and H_2/Air limiting current density for MEA's with Pt/NSTF and PtCoMn/NSTF cathodes. Limiting current density was observed to decrease monotonically with Pt loading and hence surface area, below a certain threshold. This impact on the fuel cell polarization curves is shown in Fig. 9.41. Over time we observed that the trend holds for beginning of life MEA's and for MEA's even after several types of durability tests which led to surface area loss, as shown in the right side plot in Fig. 9.38.

In the plot on the right side of Fig. 9.38, the current density value at 0.5 V (one metric for the limiting current density) appears to stop increasing with the cathode Pt surface area above about 8 or 9 cm^2_{Pt}/cm^2_{planar}. This is presumably is because some other factor is limiting this fuel cell performance metric rather than surface area. One example is the type of flow field such as discussed in Section 9.10. The significant gain in high current density provided by the flow field type FF2 in Figs. 9.24 and 9.25 would suggest that with such a flow field, the plot on the right side of Fig. 9.38 would continue to increase with SEF before again flattening out.

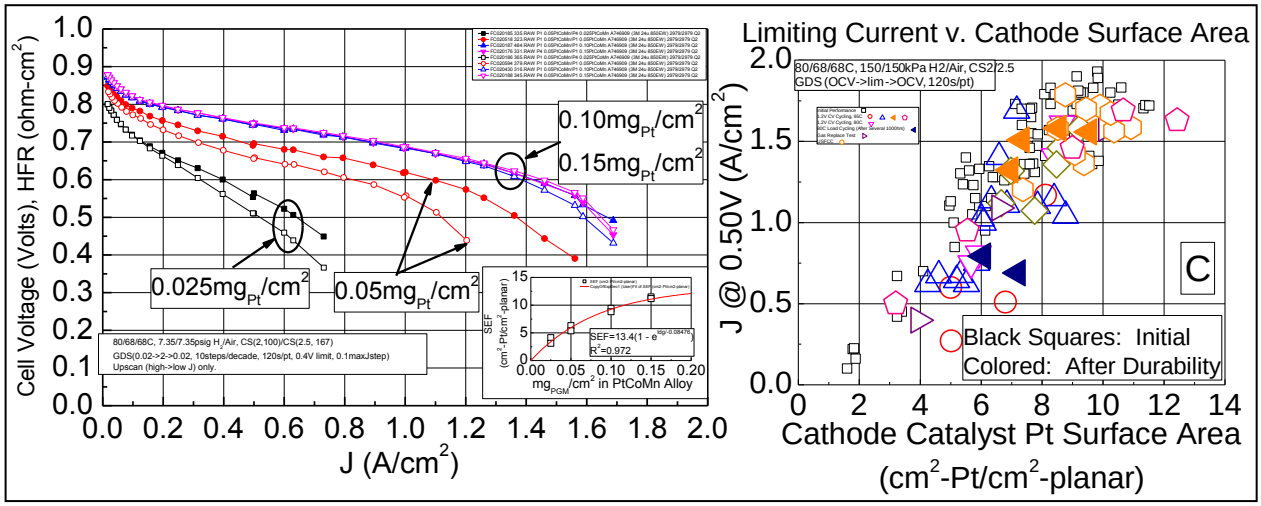

Fig. 9.38. (Left) Polarization curves show the effect of reduced Pt loading on the fuel cell and especially the limiting current densities. **(Right)** Cumulative plot over many types of MEA's and cathodes and tests, including durability stress tests and beginning of life tests, showing that the current density at 0.5 V (one metric approximating limiting current) varies linearly with cathode Pt surface area up to a limit that reflects other performance limiting factors.

It remains to be understood what exactly is the cause for this dependence of limiting current density on loading, which is also seen with conventional dispersed Pt/C electrodes as discussed in Section 9.9. The difference is that whereas this increased reduction of high current density with Pt/C electrodes appears to begin at loadings below 0.2 mg/cm^2, for the NSTF loadings as Fig. 9.38 shows, do not lose appreciable current density until the loading drops below 0.1 mg/cm^2.

9.15. Polarization curve gains over life of contract, Cell voltage vs. A/mg$_{\text{Total PGM}}$

As discussed in technology development accomplishment number 11 above, at the end of this project we completed the first systematic study of flow field effects on the NSTF MEA performances. As shown in Fig. 9.24, the land and channel dimensions have a large impact on the high current density performance with the flow field type FF2 having 0.5 mm wide lands and channels giving the best results. When tested with our 2009 best of class (BoC) PtCoMn MEA, having 0.05/0.10 mg$_{Pt}$/cm^2 loadings on the anode and cathode, the high current density performance is particularly improved. This coupled with our material improvements since the start of the project give a significant overall improvement in cell voltage versus the Pt loading normalized current, A/mg$_{Pt}$, as shown in Fig. 9.39. Fig. 9.39 (A) compares the polarization curve at 23 psig (2.5 atma) from the 2009 BoC MEA in FF2 under the ANL test conditions shown in Fig. 7.7, with that from our standard PtCoMn NSTF MEA at the start of the project which had 0.2 mg$_{Pt}$/cm^2 on both the anode and cathode. The latter polarization curve was shown in slide 8 of this project's presentation given at the 2007 DOE HFCIT Kick-off meeting on Feb. 13-14, 2007, in Washington, D.C. In Fig. 9.39 (B) the current density has been normalized to the MEA total Pt loading. At 0.6 V, we can demonstrate a three-fold gain in A/mg. In addition, the cathode stoichiometry is lower for the end of project data (2.0 vs 2.5) and the test condition drier.

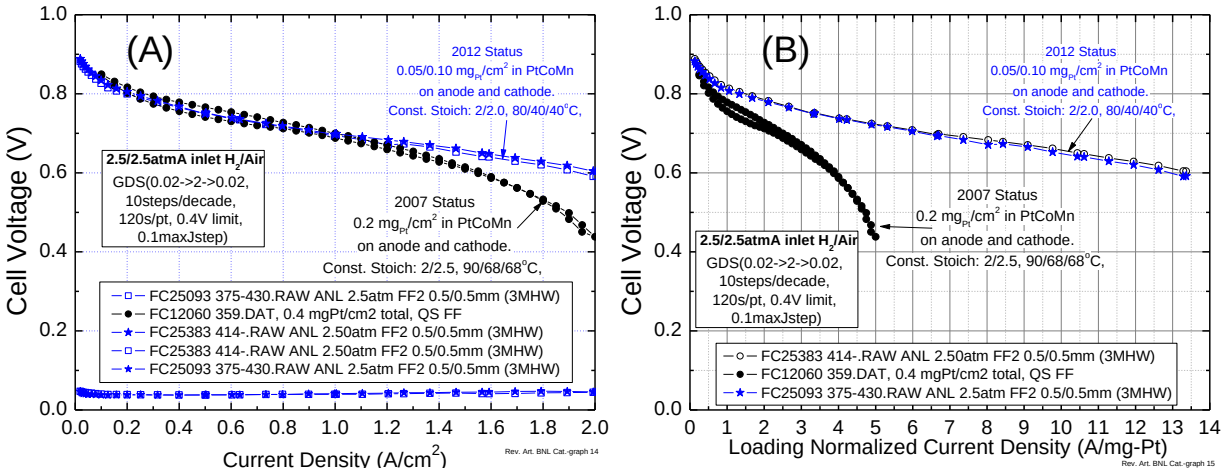

Fig. 9.39. (A) Comparison of polarization curves at 23 psig (2.5 atma) from the 2009 BoC MEA in FF2 (blue symbols), taken under the ANL test conditions shown in Fig. 7.7, with that from our standard PtCoMn NSTF MEA at the start of the project which had 0.2 mg$_{Pt}$/cm^2 on both the anode and cathode. (B) Polarization curves in A replotted with the current density normalized by the total MEA Pt loading.

9.16. Knowledge and advances in break-in conditioning

One of the characteristics determined early in our development of the NSTF electrodes is that the MEA's require very specific break-in conditioning protocols in order to reach full performance. Early studies found that the residual impurities from the membrane casting solvents clearly affected how much conditioning was required. Since then many other factors have been found influential. Around the beginning of this century we devised an effective thermal cycling procedure which allowed dramatic gains in beginning of life performances. The issue was that exceptionally long times for this break-in conditioning, usually 24 – 40 hours, were required for the best performance. This was attributed to the low loading and low surface area of NSTF electrodes. It was believed that the details of the protocol could be very important for accelerating whatever processes were happening to activate the catalysts and clean up the membrane. Many experiments were consistent with the break-in conditioning being tied to removal of residual impurities in the membrane, such as organic anions, that poisoned the catalyst or affected the electrode charge transfer impedance. But one clear observation was that the catalyst kinetics peaked first and relatively quickly, while the remainder of the time was spent to bring up the limiting current density, such as discussed in Section 9.14.

There was a need to find a more effective break-in condition protocol that acted more quickly and was also could be easily implemented in stacks. This activity was incorporated into this project in 2009 as a new Task 6. It consisted of two subtasks focused on test station protocols and materials:

Subtask 6.1 - Break-in conditioning protocol - quantify the effect of test station operating parameters on the time for break-in conditioning of the standard PtCoMn NSTF MEA's in 50 cm^2 single cell tests

Subtask 6.2 - Component Factors - Identify MEA component factors having greatest effect on break-in conditioning time

Significant work prior to the current project had identified many MEA component materials and their processes, and test station protocols that strongly affect the time for break-in conditioning of new MEA's (see Fig. 9.40).

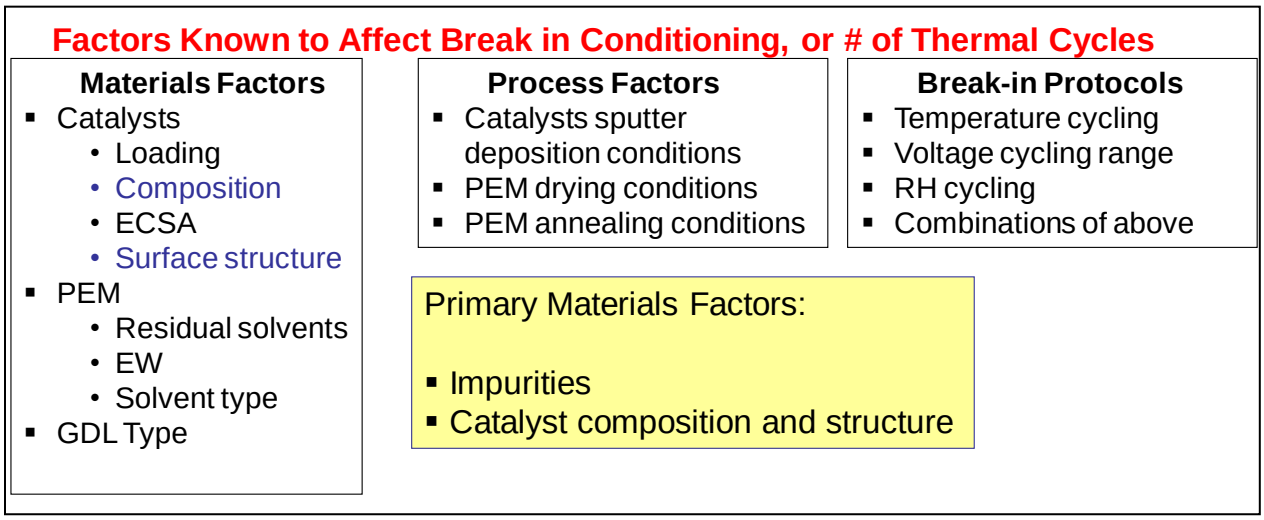

Fig. 9.40. Factors found to affect break-in conditioning time and effectiveness by the standard thermal cycling protocol.

These included catalyst composition, surface area, fabrication conditions, membrane processing solvents and drying conditions, and GDL types. Our standard thermal cycling protocol with liquid water injection has been used for years to break-in new NSTF MEA's to obtain full performance. The new task 6 now focused on both materials effects and the protocol effects in order to significantly reduce the time and simplify the procedures for conditioning a new MEA.

Protocol Effects

In 2009 new test station protocol work was successful in reducing the conditioning time with our current test stations (i.e. the time to full performance at 0.4 V during GDS polarization scans) from over 24 hours to less than six hours. In the 2009-2010 timeframe protocols were developed that both reduced the time for reaching full power and were more stack friendly to implement. From 2009 to 2010 over 40 new protocols were investigated.

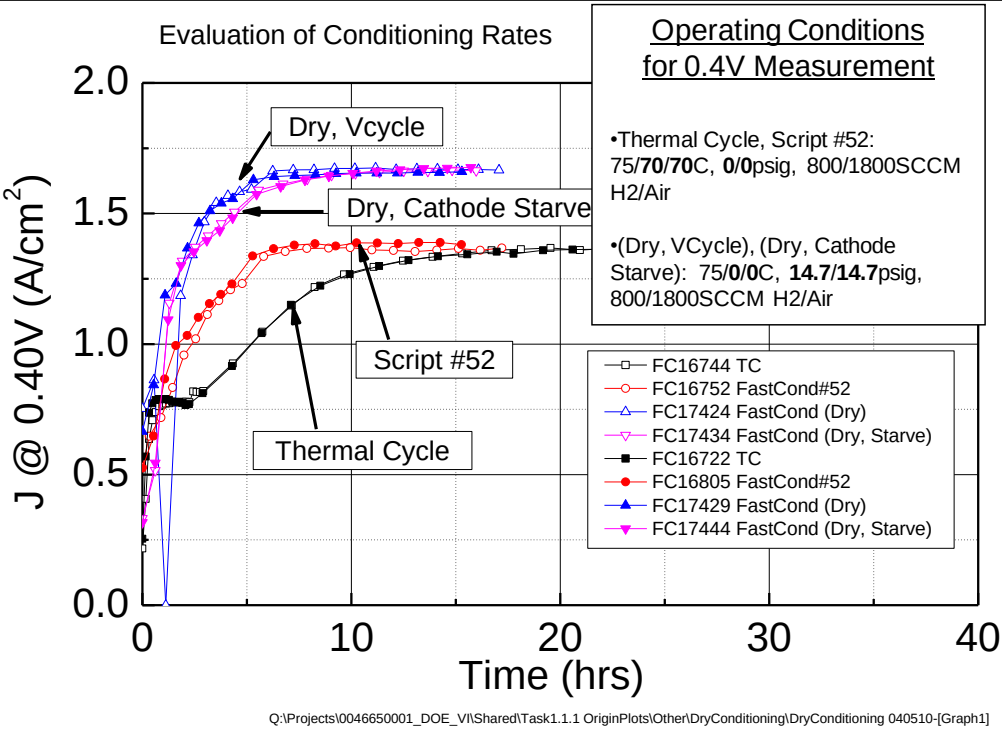

Script #52		
Tcycle	**LoadCycle**	**Duration**
{50/45/45C, 800/1800SCCM, 100/100kPa}, {30/60/60C, 200/400SCCM, 100/100kPa}	OCV(2s), 0.5V(2s), 0.25V(10s) 1 PDS Curve per Tcycle (at max T)	1hr
{75/70/70C, 800/1800SCCM, 100/100kPa}, {55/90/90C, 200/400SCCM, 100/100kPa}	OCV(2s), 0.5V(2s), 0.25V(10s) 1 PDS Curve per Tcycle (at max T)	3hr
{75/70/70C, 800/1800SCCM, 100/100kPa}, {30/60/60C, 200/400SCCM, 100/100kPa}	OCV(2s), 0.5V(2s), 0.25V(10s) 1 PDS Curve per Tcycle (at max T)	16hr

Fig. 9.41. Log plots of current density versus time at 0.4 V as extracted from PDS polarization scans, showing examples of "Stack-Capable" FAST Conditioning Protocol Effects compared to the standard thermal cycling protocol. The table describes the Script 52 protocol.

Examples of this are illustrated in Fig. 9.41, which compares log plots of current density at 0.4 V versus time extracted from potentiodynamic polarization scans taken during the break-in conditioning. The time for the cell current density to reach within 90% of its peak value is much less for the "Script 52" protocol compared to the standard thermal cycling protocol, both of which use ambient pressure outlets. The "dry protocols" in Fig 9.41 (cathode starve and V-cycle) reach higher ultimate performance values due to their higher operating pressure, but they clearly also condition faster, nominally fully conditioned in <8 hours. FAST conditioning has not always achieved performance parity with the slower, historical 3M thermal cycling procedure, and we have seen a test station dependence on their effectiveness that is not understood. Further systematic study is needed to determine how to resolve the performance gaps, but clearly these faster, simpler conditioning protocols are an effective approach.

Material Factors

Understanding how the break-in conditioning protocols depend on material factors listed in Fig. 9.40 is also key to finding the complete solution. Both the catalyst composition and the nature of the alloying component can have a large influence on the rate of break-in conditioning.

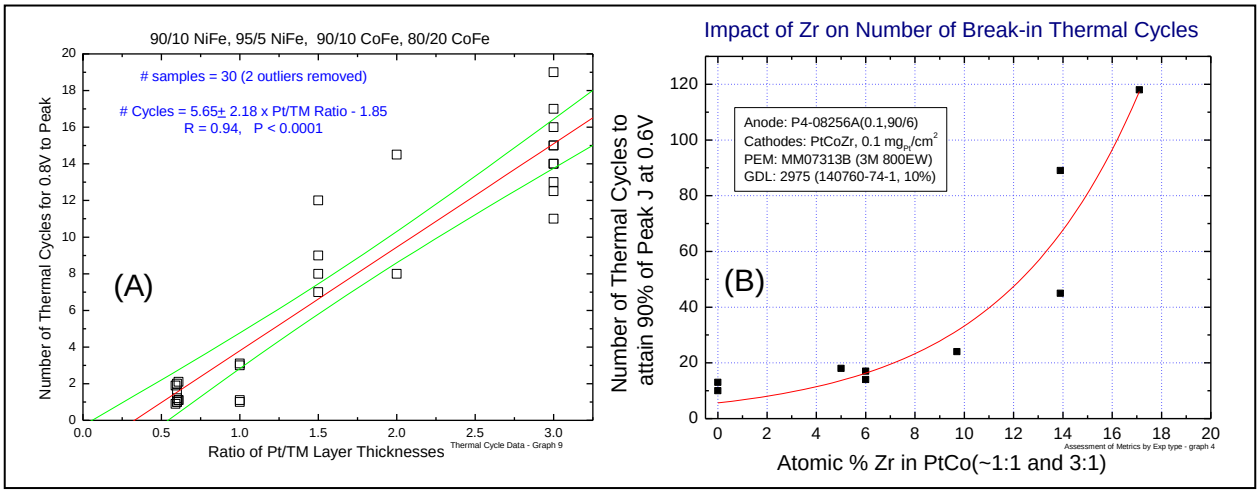

Fig. 9.42. (A) Data from the previous 3M/DOE contract preceding the current one, showing how the number of thermal cycles varies as a function of the ratio of the Pt/TM layer thicknesses for a PtCo and PtNiFe alloy series. (B) Impact on the atomic percentage of Zr added to PtCo alloys (PtCo or Pt_3Co) on the number of thermal cycles required for break-in conditioning by standard thermal cycles (data from the current project.)

Fig. 9.42(A) shows data from the previous 3M/DOE contract preceding the current one. It shows the number of thermal cycles as a function of the ratio of the Pt/TM layer thicknesses for a PtCo and PtNiFe alloy series. The higher the amount of transition metal, Co or Ni, the faster full kinetic performance was achieved. Fig. 9.42 (B) shows a very surprising result from this project. Small amounts of Zr in two PtCo alloys have an enormous effect on the number of standard thermal cycles required to reach peak performance. As little as 17 at% Zr increased the number of thermal cycles required by an order of magnitude. Surface area and activity were not decreased by the Zr, so clearly some other mechanism is occurring. No other material effect has been seen to be as strong. Equally as interesting is that a post fabrication process

applied to the NSTF PtCoZr has a dramatic impact on the conditioning time of the Zr-containing cathode catalyst. This is illustrated in Fig. 9.43.

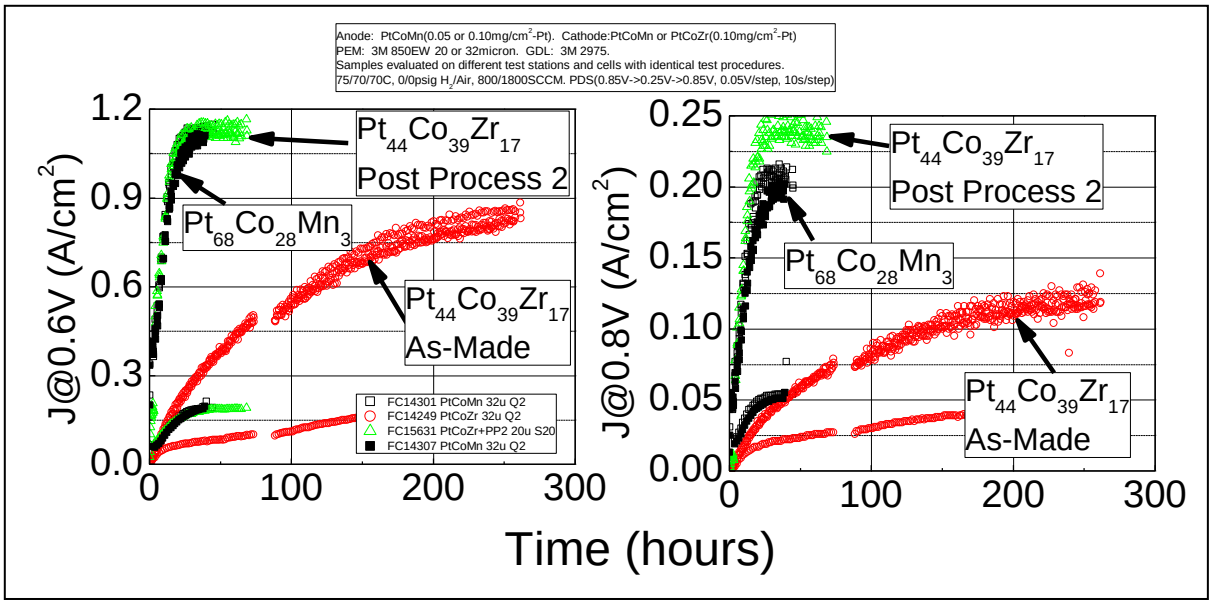

Fig. 9.43. Examples of the effect of an electrochemical post-deposition process on start-up performance for NSTF PtCoZr alloys. Current density at 0.6 V (left) and 0.8 V (right) increases with time of thermal cycling in a dramatically different way depending on whether the PtCoZr is as-made or if a post-process was made prior to forming the CCM and fuel cell testing.

As-made, PtCoZr requires significantly longer conditioning time than standard PtCoMn and the ultimate kinetic performance is also suppressed. After application of an electrochemical post process, the conditioning time w/ PtCoZr appears comparable or faster than standard PtCoMn, and may have similar or improved kinetic performance. This illustrates that there is a very rich area of material science process and composition yet to be studied in order to fully understand and thereby achieve the requirements for fast, stack friendly break-in conditioning. At the very least these examples for both protocol effects and material effects shown in Figs. 9.41-9.43 illustrate that there is not likely to be anything fundamentally limiting NSTF electrodes from rapid conditioning, as long as the surface area is sufficiently high.

9.17. Support for development of NSTF catalyst and CCM roll-to-roll processes

Process improvements were continuously being implemented for roll-to-roll NSTF catalyst and CCM fabrication, quality and cost. This project was a major driver for these process improvements. Over 260,000 linear ft combined of a) NSTF substrate (MCTS), b) whisker support coated substrates, c) catalyst coated whisker supports, and d) catalyst coated membrane were produced since production tracking started in 2006, for process development, qualification and customer use. Fig. 9.44 shows the yearly increases in the total of a) through d) during the period of this project.

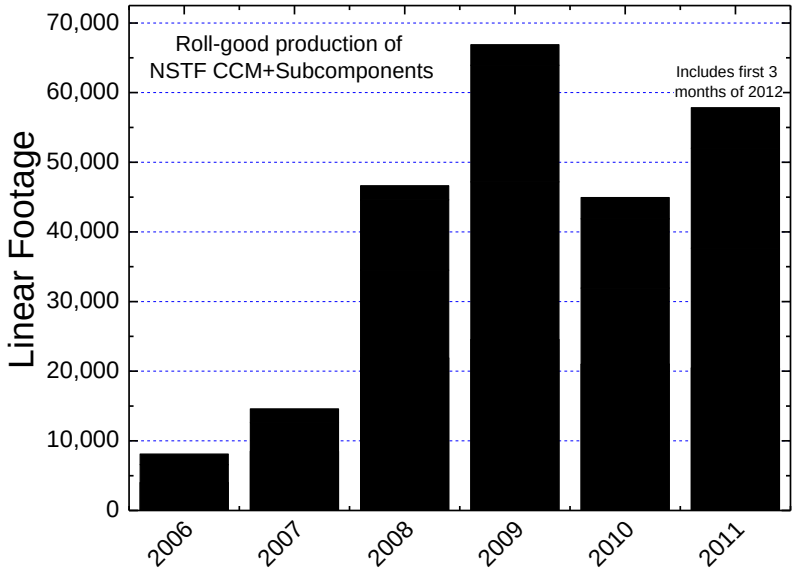

Fig. 9.44 Summary of the total combined linear footage of NSTF CCM and its components manufactured yearly since production reporting began in 2006. The components refer to the four components of the MCTS substrate, whisker coated substrate, catalyst coated substrate, and CCM.

10. References for Sections 1 - 9

1. Arman Bonakdarpour, Krystal Stevens, George D. Vernstrom, Radoslav Atanasoski, Alison K. Schmoeckel, Mark K. Debe, and Jeff R. Dahn, "Oxygen Reduction Activity of Pt and Pt-Mn-Co Electrocatalysts Sputtered on Nanostructured Thin Film Support," Electrochimica Acta **53** (2007) 688-694.
2. D. Van der Vliet, D. Strmcnik, C. Wang, R. Atanasoski, M. Debe. N. Markovic and V. Stamenkovic, "Multimetallic Catalysts for Oxygen Reduction Reaction," 216th ECS Meeting, Vienna, Austria, Oct. 4-9, 2009.
3. K. J. J. Mayrhofer, D. Strmcnik, B. B. Blizanac, V. Stamenkovic, M. Arenz, N. M. Markovic, "Measurement of oxygen reduction activities via the rotating disc electrode method: From Pt model surfaces to carbon-supported high surface area catalysts," *Electrochimica Acta* **53** (2008) 3181-3188.
4. Liu, Gary C-K.; Sanderson, R. J.; Vernstrom, G; Stevens, D. A.; Atanasoski, R. T.; Debe, M. K.; Dahn, J. R., "RDE Measurements of ORR Activity of Pt_{1-x} Ir_x ($0<x<0.3$) on High Surface Area NSTF-Coated Glassy Carbon Disks," *J. Electrochem. Soc.* (2010), **157**(2), B207-B214.
5. Gary Chih-Kang, D. A. Stevens, J. C. Burns, R. J. Sanderson, G. D. Vernstrom, R. T. Atanasoski, M. K. Debe and J. R. Dahn, "Oxygen reduction activity of dealloyed $Pt_{1-x}Ni_x$ catalysts." *J. Electrochem. Soc.* **158**(8) B919-B26 (2011).
6. Dennis van der Vliet, Chao Wang, Mark Debe, Radoslav Atanasoski, Nenad M. Markovic and Vojislav R. Stamenkovic, "Platinum-alloy Nanostructured Thin Film Catalysts for the Oxygen Reduction Reaction," *Electrochimica Acta*. **56** 8695-8699 (2011).
7. A. K. Schmoeckel, G. D. Vernstrom, A. J. Steinbach, S. M. Hendricks, R. T. Atanasoski and M. K. Debe, "Nanostructured Thin Film Ternary Catalyst Activities for Oxygen Reduction," 2006 Fuel Cell Seminar, Honolulu, Hawaii, Nov. 13-17, 2006.
8. M. Debe, A. Steinbach, G. Vernstrom, S. M. Hendricks, M. J. Kurkowski, R. T. Atanasoski, P. Kadera, D. A. Stevens, R. J. Sanderson, E. Marvel and J. R. Dahn, "Extraordinary oxygen reduction activity of Pt_3Ni_7," *J. Electrochem. Soc.* **158**(8) B910-B918 (2011).
9. Mark K. Debe, "Electrocatalyst Approaches and Challenges for Automotive Fuel Cells," invited review article, *Nature*, **486**(9401) 43-51(2012).
10. Mark K. Debe, "Nanostructured Thin Film Electrocatalysts for PEM Fuel Cells – A Tutorial on the Fundamental Characteristics and Practical Properties of NSTF Catalysts," *ECS Transactions* **45**, April, 2012.
11. R.K. Ahluwalia, X. Wang, A. Lajunen, A.J. Steinbach, S.M. Hendricks, M.J. Kurkowski, and M.K. Debe, "Kinetics of Oxygen Reduction Reaction on Nanostructured Thin-Film Platinum Alloy Catalyst," *Journal of Power Sources* **215** (2012) 77-88.
12. Debe, M. K.; Schmoeckel, A.; Hendricks, S.; Vernstrom, G.; Haugen, G.; Atanasoski, R., *ECS Transactions* **1**(1), 51 (2006).
13. Debe, M. K.; Schmoeckel, A. K.; Vernstrom, G. D.; Atanasoski, R., *Journal of Power Sources* **161**, 1002 (2006).
14. Steinbach, A.J.; Noda, K.; Debe, M. K., *ECS Transactions* **3**(1) 835 (2006).
15. Bonakdarpour, A.; Lobel, R.; Atanasoski, R. T.; Vernstrom, G. D.; Schmoeckel, A. K.; Debe, M. K.; Dahn, J. R., *Journal of The Electrochemical Society* **153**, A1835 (2006).
16. M. Debe, A. Hester, G. Vernstrom, A. Steinbach, S. Hendricks, A. Schmoeckel, R. Atanasoski, D. McClure and P. Turner , in proceedings of the 50th Annual Technical Conference of the Society of Vacuum Coaters, Louisville, KY, May 1, 2007.
17. Mark K. Debe, Project review at the DOE 2010 Vehicle Technologies and Hydrogen Programs Annual Merit Review, June 8, 2010, Washington, D.C., number FC 001. http://www.hydrogen.energy.gov/pdfs/review10/fc001_debe_2010_o_web.pdf
18. M. K. Debe, A. J. Steinbach, G. D. Vernstrom, S. M. Hendricks, M. J. Kurkowski, R. T. Atanasoski, P. Kadera, D. A. Stevens, R. J. Sanderson, E. Marvel and J. R. Dahn, "Extraordinary oxygen

reduction activity of Pt_3Ni_7," *J. Electrochem. Soc.* **158**(8) B910-B918 (2011), and *ECS Trans*., **33** 143 (2010).
19. Mark K. Debe, Project review at the DOE 2012 Vehicle Technologies and Hydrogen Programs Annual Merit Review, May 15, 2012, Washington, D.C., number FC 001. http://www.hydrogen.energy.gov/pdfs/review12/fc001_debe_2012_o.pdf
20. A. Steinbach, M. Debe, M. Pejsa, D. Peppin, A. Haug, M. Kurkowski and S. Maier-Hendricks, "Influence of Anode GDL on PEMFC Ultra-thin Electrode Water Management at Low Temperatures," *ECS Transactions*, **41**(1) 449-457 (2011).
21. Target Tables from the US Drive Fuel Cell Technical Team, Revised January 25, 2012.
22. Greg Haugen, Sara Barta, Mike Emery, Steven Hamrock and Mike Yandrasits, "Open Circuit Voltage Fuel Cell Durability Testing Using Multiple PEM MEA's," in Fuel Cell Chemistry and Operation, eds. Andrew M. Herring, Thomas A. Zawodzinski Jr., and Steven J. Hamrock, *ACS Symposium Series 1040*, page **137** (2010).
23. Mark K. Debe, "Effect of Electrode Structure Surface Area Distribution on High Current Density Performance of PEM Fuel Cells," *J. Electrochemical Society* **159**(1) B54-B67 (2011).
24. Dennis van der Vliet, Chao Wang, Dusan Tripkovic, Dusan Strmcnik, Xiaofeng Zhang, Mark Debe, Radoslav Atanososki, Nenad M. Markovic and Vojislav R. Stamenkovic, "Metallic Nanotubes with Tunable Composition and Structure as Advanced Electrocatalysts," *Nature Materials*, in press (2012).
25. Lajos Gancs, Takeshi Kobayashi, Mark K. Debe, Radoslav Atanasoski, and Andrzej Wieckowski, "Crystallographic Characteristics of Nanostructured Thin Film Fuel Cell Electrocatalysts – A HRTEM Study," *Chemistry of Materials* **20**, 2444-2454 (2008).
26. M. K. Debe, R. J. Poirier, "Post deposition growth of a uniquely nanostructured organic film by vacuum annealing," *J. Vac. Sci. Technol.* **A 12**(4, Pt. 2), 2017-22 (1994).
27. M. K. Debe, A. R. Drube, "Structural characteristics of a uniquely nanostructured organic thin film," *J. Vac. Sci. Technol.* **B 13**(3), 1236-41 (1995).
28. Arnd Garsuch, D. A. Stevens, R. J. Sanderson, S. Wang, R. T. Atanasoski, S. Hendricks, M. K. Debe, and J. R. Dahn, "Alternative Catalyst Supports Deposited on Nanostructured Thin Films for Proton Exchange Membrane Fuel Cells," *J. Electrochemical Society* **157**(2) B187-B194 (2010).
29. D. A. Stevens, J. M. Rouleau, R E. Mar, R. T. Atanasoski, A. K. Schmoeckel, M. K. Debe and J. R. Dahn, "64-Electrode PEM Fuel Cell Studies of CO-Tolerant Hydrogen Oxidation Catalysts," *ECS Transactions* **3**(1) 355-360 (2006).
30. D. A. Stevens, J. M. Rouleau, R. E. Mar, A. Bonakdarpour, R. T. Atanasoski, A. K. Schmoeckel, M. K. Debe, J. R. Dahn, "Characterization and PEMFC Testing of $Pt_{1-x}M_x$ (M=Ru, Mo, Co, Ta, Au, Sn) Anode Electrocatalyst Composition Spreads," *J. of the Electrochem. Soc.* **154**(6), B566-B576 (2007).
31. Arman Bonakdarpour, Krystal Stevens, George D. Vernstrom, Radoslav Atanasoski, Alison K. Schmoeckel, Mark K. Debe, and Jeff R. Dahn, "Oxygen Reduction Activity of Pt and Pt-Mn-Co Electrocatalysts Sputtered on Nanostructured Thin Film Support," *Electrochimica Acta* **53** (2007) 688-694.
32. Arman Bonakdarpour, Tara R. Dahn, Radoslav Atanasoski, Mark K. Debe, and Jeff R. Dahn, "H_2O_2 Release During Oxygen Reduction Reaction on Pt Nano Particles," *Electrochemical and Solid-State Letters*, **11,** B208-B211 (2008).
33. Gary C-K. Liu, R. J. Sanderson, G. Vernstrom, D. A. Stevens, R. T. Atanasoski, M. K. Debe, J. R. Dahn, "RRDE Measurements of ORR Activity of Pt_{1-x} Ir_x ($0<x<0.3$) on High Surface Area NSTF-Coated Glassy Carbon Disks," *J. Electrochem. Soc.* **157**(2), B207-B214 (2010).
34. Gary Chih-Kang, D. A. Stevens, J. C. Burns, R. J. Sanderson, G. D. Vernstrom, R. T. Atanasoski, M. K. Debe and J. R. Dahn, "Oxygen reduction activity of dealloyed $Pt_{1-x}Ni_x$ catalysts." *J. Electrochem. Soc.* **158**(8) B919-B26 (2011).
35. D. A. Stevens, R. Mehrotra, R. J. Sanderson, G. D. Vernstrom, R. T. Atanasoski, M. K. Debe and J. R. Dahn, "Dissolution of Ni from high Ni content $Pt_{1-x}Ni_x$ alloys," *J. Electrochem. Soc.* **158**(8) B905-B909 (2011).

36. D. A. Stevens, S. Wang, R. J. Sanderson, G. C. K. Liu, G. D. Vernstrom, R. T. Atanasoski, M. K. Debe and J. R. Dahn, "A combined rotating disk electrode/X-ray diffraction study of Co dissolution from $Pt_{1-x}Co_x$ Alloys," *J. Electrochem. Soc.* **158**(8) B899-B904 (2011).
37. J.E. Harlow, D.A. Steven, R.J. Sanderson, G. C-K Liu, L.B. Lohstreter, G.D. Vernstrom, R.T. Atanasoski, M.K. Debe, and J.R. Dahn, "The oxygen reduction reaction activity of a $Pt_{1-x}Mn_x$ binary composition spread," *J. Electrochemical Society* **159** (6) B670-B676 (2012).
38. D. A. Stevens, S. Wang, R. J. Sanderson, A. Garsuch, M. K. Debe, S. M. Hendricks, R. T. Atanasoski, J. R. Dahn, "Assessing the Pt_{upd} Surface Area Stability of $Pt_{1-x}M_x$ (M=Re, Nb, Bi) Solid Solutions for Proton Exchange Membrane Fuel Cells," *Journal of the Electrochem. Soc.* **157**(5), B737-B743 (2010).
39. P. Strasser, S. Kohr, T. Anniyev, J. Greeley, K. More, C. Yu, Z. Liu, S. Kaya, D. Nordlund, H. Ogasawara, M. Toney and A. Nilsson, "Lattice-strain control of the activity in dealloyed core-shell fuel cell catalysts," Nature Chemistry **2**, 454 (2010).
40. Stamenkovic, V. R. et al., "Improved oxygen reduction activity on $Pt_3Ni(111)$ via increased surface site availability. Science **315**, 493 - 497 (2007)."

11. Publication Activities

11.1. Publications in peer-reviewed journals

1. A . Bonakdarpour, K. Stevens, G. D. Vernstrom, R. Atanasoski, A. K. Schmoeckel, M. K. Debe, and J. R. Dahn, "Oxygen Reduction Activity of Pt and Pt-Mn-Co Electrocatalysts Sputtered on Nanostructured Thin Film Support," *Electrochimica Acta* **53** (2007) 688-694.
2. K. J. J. Mayrhofer, D. Strmcnik, B. B. Blizanac, V. Stamenkovic, M. Arenz, N. M. Markovic, "Measurement of oxygen reduction activities via the rotating disc electrode method: From Pt model surfaces to carbon-supported high surface area catalysts," *Electrochimica Acta* **53** (2008) 3181-3188.
3. Lajos Gancs, Takeshi Kobayashi, Mark K. Debe, Radoslav Atanasoski, and Andrzej Wieckowski, "Crystallographic Characteristics of Nanostructured Thin Film Fuel Cell Electrocatalysts – A HRTEM Study," *Chemistry of Materials* **20***,* 2444-2454 (2008).
4. Liu, Gary C-K.; Sanderson, R. J.; Vernstrom, G; Stevens, D. A.; Atanasoski, R. T.; Debe, M. K.; Dahn, J. R., "RDE Measurements of ORR Activity of Pt_{1-x} Ir_x (0<x<0.3) on High Surface Area NSTF-Coated Glassy Carbon Disks," *J. Electrochem. Soc.* (2010), **157**(2), B207-B214.
5. Gary Chih-Kang, D. A. Stevens, J. C. Burns, R. J. Sanderson, G. D. Vernstrom, R. T. Atanasoski, M. K. Debe and J. R. Dahn, "Oxygen reduction activity of dealloyed $Pt_{1-x}Ni_x$ catalysts." *J. Electrochem. Soc.* **158**(8) B919-B26 (2011).
6. Dennis van der Vliet, Chao Wang, Mark Debe, Radoslav Atanasoski, Nenad M. Markovic and Vojislav R. Stamenkovic, "Platinum-alloy Nanostructured Thin Film Catalysts for the Oxygen Reduction Reaction," *Electrochimica Acta*. **56** 8695-8699 (2011).
7. Mark K. Debe, "Electrocatalyst Approaches and Challenges for Automotive Fuel Cells," invited review article, *Nature,* **486**(9401) 43-51(2012).
8. Mark K. Debe, "Nanostructured Thin Film Electrocatalysts for PEM Fuel Cells – A Tutorial on the Fundamental Characteristics and Practical Properties of NSTF Catalysts," *ECS Transactions* **45**, April, 2012.
9. R.K. Ahluwalia, X. Wang, A. Lajunen, A.J. Steinbach, S.M. Hendricks, M.J. Kurkowski, and M.K. Debe, "Kinetics of Oxygen Reduction Reaction on Nanostructured Thin-Film Platinum Alloy Catalyst," *Journal of Power Sources* **215** (2012) 77-88*.*
10. M. K. Debe, A. J. Steinbach, G. D. Vernstrom, S. M. Hendricks, M. J. Kurkowski, R. T. Atanasoski, P. Kadera, D. A. Stevens, R. J. Sanderson, E. Marvel and J. R. Dahn, "Extraordinary oxygen reduction activity of Pt_3Ni_7," *J. Electrochem. Soc.* **158**(8) B910-B918 (2011), and *ECS Trans*., **33** 143 (2010).
11. M. K. Debe, and A. J. Steinbach, "An empirical model for the flooding behavior of ultra-thin PEM fuel cell electrodes," ECS Transactions 11(1) 659-673 (2007).
12. A. J. Steinbach, M. K. Debe, J. L. Wong, M. J. Kurkowski, A. T. Haug, D. M. Peppin, S. K. Deppe, S. M. Hendricks, and E. M. Fischer, "A New Paradigm for PEMFC Ultra-Thin Electrode Water Management at Low Temperatures," ECS Trans., 33(1), 1179-1188 (2010).
13. A. Steinbach, M. Debe, M. Pejsa, D. Peppin, A. Haug, M. Kurkowski and S. Maier-Hendricks, "Influence of Anode GDL on PEMFC Ultra-thin Electrode Water Management at Low Temperatures," *ECS Transactions*, **41**(1) 449-457 (2011).
14. M. K. Debe, R. T. Atanasoski, and A. J. Steinbach, "Nanostructured Thin Film Electrocatalysts – Current Status and Future Potential, ECS Transactions, 41(1) 937-954 (2011).
15. Mark K. Debe, "Effect of Electrode Structure Surface Area Distribution on High Current Density Performance of PEM Fuel Cells," *J. Electrochemical Society* **159**(1) B54-B67 (2011).

16. Arnd Garsuch, D. A. Stevens, R. J. Sanderson, S. Wang, R. T. Atanasoski, S. Hendricks, M. K. Debe, and J. R. Dahn, “Alternative Catalyst Supports Deposited on Nanostructured Thin Films for Proton Exchange Membrane Fuel Cells,” *J. Electrochemical Society* **157**(2) B187-B194 (2010).
17. D. A. Stevens, J. M. Rouleau, R. E. Mar, A. Bonakdarpour, R. T. Atanasoski, A. K. Schmoeckel, M. K. Debe, J. R. Dahn, “Characterization and PEMFC Testing of $Pt_{1-x}M_x$ (M=Ru, Mo, Co, Ta, Au, Sn) Anode Electrocatalyst Composition Spreads,” *J. Electrochem. Soc.* **154**(6), B566-B576 (2007).
18. Arman Bonakdarpour, Tara R. Dahn, Radoslav Atanasoski, Mark K. Debe, and Jeff R. Dahn, “H2O2 Release During Oxygen Reduction Reaction on Pt Nano Particles,” *Electrochemical and Solid-State Letters*, **11**, B208-B211, 2008.
19. D. A. Stevens, R. Mehrotra, R. J. Sanderson, G. D. Vernstrom, R. T. Atanasoski, M. K. Debe and J. R. Dahn, “Dissolution of Ni from high Ni content Pt1-xNix alloys,” *J. Electrochem. Soc.* **158**(8) B905-B909 (2011).
20. D. A. Stevens, S. Wang, R. J. Sanderson, G. C. K. Liu, G. D. Vernstrom, R. T. Atanasoski, M. K. Debe and J. R. Dahn, “A combined rotating disk electrode/X-ray diffraction study of Co dissolution from Pt1-xCox Alloys,” *J. Electrochem. Soc*. **158(**8) B899-B904 (2011).
21. J.E. Harlow, D.A. Steven, R.J. Sanderson, G. C-K Liu, L.B. Lohstreter, G.D. Vernstrom, R.T. Atanasoski, M.K. Debe, and J.R. Dahn, “The oxygen reduction reaction activity of a $Pt_{1-x}Mn_x$ binary composition spread,” *J. Electrochemical Society* **159** (6) B670-B676 (2012).
22. Dennis van der Vliet, Chao Wang, Dusan Tripkovic, Dusan Strmcnik, Xiaofeng Zhang, Mark Debe, Radoslav Atanasoski, Nenad M. Markovic and Vojislav R. Stamenkovic, “Metallic Nanotubes with Tunable Composition and Structure as Advanced Electrocatalysts,” *Nature Materials*, **in press** (2012).
23. M. K. Debe, A. E. Hester, G. D. Vernstrom, A. J. Steinbach, S. M. Hendricks, A. K. Schmoeckel, R. T. Atanasoski, D. J. McClure, and P. L. Turner, “Nanostructured Thin Film Catalysts for PEM Fuel Cells by Vacuum Web Coating, in proceedings of the 50th Annual Tech. Conference of the Society of Vacuum Coaters, Louisville, KY, May 1, 2007**,** 175-185 ISSN 0737-5921.
24. D. A. Stevens, J. M. Rouleau, R. E. Mar, R. T. Atanasoski, A. K. Schmoeckel, M K. Debe, J. R. Dahn, “Enhanced CO-Tolerance of Pt-Ru-Mo Hydrogen Oxidation Catalysts,” *Journal of the Electrochem. Soc.* **154**(12), B1211-B1219 (2007).
25. A. J. Steinbach, C. V. Hamilton, Jr., and M. K. Debe, “Impact of Micromolar Concentration of Externally-Provided Chloride and Sulfide Contaminants of PEMFC Reversible Stability,” *ECS Transactions* **11**(1) 889-902 (2007).
26. D. A. Stevens, S. Wang, R. J. Sanderson, A. Garsuch, M. K. Debe, S. M. Hendricks, R. T. Atanasoski, J. R. Dahn, “Assessing the Pt_{upd} Surface Area Stability of $Pt_{1-x}M_x$ (M=Re, Nb, Bi) Solid Solutions for Proton Exchange Membrane Fuel Cells,” *Journal of the Electrochem. Soc.* **157**(5), B737-B743 (2010).
27. M. K. Debe, S. M. Hendricks, G. D. Vernstrom, M. Meyers, M. Brostrom, M. Stephens, and Q. Chan, Jason Willey, Monjid Hamden, and Cortney K. Mittelsteadt**,** Christopher B. Capuano, Katherine Ayers and Everett Anderson, “Initial Performance and Durability of Ultra-low Loaded NSTF Electrodes for PEM Electrolyzers,” *J. Electrochem. Soc*., **159**(6) K165-K176 (2012).

11.2 Invited presentations at international meetings and institutions

1. M. K. Debe, 2008, and 2009 to 2011 *DOE Hydrogen Program Annual Merit Reviews*, Washington, D.C.
   http://www.hydrogen.energy.gov/pdfs/review09/fc_17_debe.pdf
   http://www.hydrogen.energy.gov/pdfs/review10/fc001_debe_2010_o_web.pdf
   http://www.hydrogen.energy.gov/pdfs/review11/fc001_debe_2011_o.pdf
   http://www.hydrogen.energy.gov/pdfs/review12/fc001_debe_2012_o.pdf
2. M. Debe, A. Hester, G. Vernstrom, A. Steinbach, S. Hendricks, A. Schmoeckel, R. Atanasoski, D. McClure and P. Turner, invited, 50th Annual Technical Conference of the Society of Vacuum Coaters, Louisville, KY, May 1, 2007.
3. M. K. Debe, "Solving Durability and Performance Issues of PEMFC's by Eliminating Carbon Supports and Highly Dispersed Catalysts," Fuel Cells Durability and Performance 2007, Knowledge Foundation's 3rd Annual International Conference, Miami, FL Nov. 15-16, 2007, invited.
4. M. K. Debe, "Meeting Durability, Performance and Cost Targets for Automotive Fuel Cells by using Thin Film Catalysts, Ultra-thin Electrodes and Eliminating Carbon Supports, "NRC Institute for Fuel Cell Innovation, Vancouver, BC, Canada, March 17-18, 2008, invited.
5. M. K. Debe, "Nanostructured Thin Film Electrocatalysts for PEM Fuel Cells - Fundamental Characteristics and Practical Properties to Meet Automotive Requirements," 213th ECS meeting, Phoenix, AZ, May 18-23, 2008, invited.
6. R. Atanasoski, M. Debe, and T. Wood, "High Performance Platinum and Non-precious Metal Catalysts for PEM Fuel Cell Application", Opening key-note presentation at the 7th International Symposium on New Materials and Nano-Materials for Electrochemical Systems, June 24-27, 2008 Montréal, Canada.
7. Radoslav Atanasoski and Mark Debe, "Nano-Structured Thin Film - NSTF Catalysts for PEM Fuel Cells: Fundamentals and Application" ACES Electromaterials Symposium "Nanostructured Electromaterials", University of Wollongong, NSW, Australia, 4-6 February 2009, invited.
8. Radoslav Atanasoski, "Fuel Cell Catalysts of Tomorrow**":** XXth Congress of Chemist and Technologist of Macedonia, Ohrid, Macedonia, September 16–21, 2008, invited.
9. A.J. Steinbach, "Influence of Contaminants, MEA Components, and Temperature on PEM Fuel Cell Stability", Invited, Canada – USA PEM Network Research Workshop, February 16 and 17, 2009, NRC for Fuel Cell Innovation, Vancouver, BC, Canada.
10. D.A. Stevens, R.J. Sanderson, A. Garsuch, S. Wang,R.E. Mar and J.R. Dahn, Invited, "High Throughput Screening of PEM Fuel Cell Catalysts", Canada – USA PEM Network Research Workshop, February 16 and 17, 2009, NRC Institute for Fuel Cell Innovation, Vancouver, BC, Canada.
11. Mark K. Debe, "Ultra-high activity electrocatalysts based on nanostructured organic films and sputtered Pt alloys," Invited, *238th Am. Chem. Soc. Meeting,* Washington, D.C. August 16, 2009.
12. Mark K. Debe, "Update of the activity, performance, durability and water management of the 3M NSTF catalyst based MEA's for PEM fuel cell," Invited, MEA Fuel Cell Modeling and Characterization Workshop, NRC Institute for Fuel Cell Innovation, Vancouver, BC, Canada, Nov. 12-13, 2009.
13. Radoslav Atanasoski and Mark Debe, "Nano-structured thin film-NSTF catalysts for PEM fuel cells: focus on durability," Invited, Ulm Electro Chemical Talks 2010 and 2015 Technologies on Batteries and Fuel Cells, Ulm, Germany, June 16, 2010.
14. D.A. Stevens, T.D. Hatchard, R.J. Sanderson, R.T. Atanasoski, M.K. Debe and J.R. Dahn, (invited), "PEMFC Electrocatalyst Development," 218th ECS meeting.

15. M. K. Debe, "Nanostructured Catalyst Developments," invited, 2nd CARISMA Conference, Montpellier, France, Sept. 2010.
16. M. K. Debe, R. T. Atanasoski and A. J. Steinbach, "Nanostructured Thin Film Electrocatalysts – Current Status and Future Potential," Invited , 220th ECS Meeting, Boston, MA, Oct. 9-14, 2011.
17. Radoslav Atanasoski, "Fundamental and practical aspects of Nano-structured thin film - NSTF catalysts for PEM fuel cells: Durability under Transient Conditions," Invited, 61st ISE – Electrochemical Energy Conversion and Storage, Nice, France, Sept. 2010.
18. M. K. Debe, "NanoStructured Thin Film Catalysts -15 (or is it 28?) Years on an Alternative Path for PEM Fuel Cell Electrocatalysts," Invited, Fuel Cell Seminar and Exposition R&D Award presentation, San Antonio, TX, Oct. 19, 2010.
19. M. K. Debe, "Nanostructured Thin Film Catalysts for PEM Fuel Cells: Status and Path Forward to Meet Performance, Durability and Cost Targets for High Volume Automotive Applications," Invited, Workshop on PEM Fuel Cell Catalyst & MEA Preparation and Characterization, HySA Catalysis Competence Center and University of Cape Town, Cape Town, Rondebosch, South Africa, March 28-29, 2011
20. M. K. Debe, "NSTF Catalyst Technology for Energy Applications," Invited, Northwest University, Potchefstroom, South Africa, March 25, 2011.
21. M. K. Debe,"A General Introduction to Nano-Structured Thin Film Catalyst (NSTFC) Technology for Hydrogen and Fuel Cell Applications," Invited, Council for Scientific and Industrial Research (CSIR) , Pretoria, South Africa, March 24, 2011.
22. Mark K. Debe, "Designing Electrocatalysts for Fuel Cell Vehicles-It's going to Take More than Just High Activity," Invited, Cornell University Annual Energy Materials Symposium, August 12, 2011.
23. M. K. Debe , "PEM Fuel Cell Performance Factors Determined by Electrocatalyst Structure Characteristics," Invited, Zing International Hydrogen and Fuel Cell Conference, Riviera Maya, Mexico, Dec. 1, 2011.
24. Mark K. Debe, "A New Generation of Catalysts and Electrode Designs for PEM Water Electrolysis: Fundamentals and Practical Examples," Invited, Hydrogen Production and Water Electrolysis Short Course, North-West University, Potchefstroom, South Africa, April 18-19, 2012.
25. Mark K. Debe, "Nanostructured Thin Film Electrocatalysts for PEM Fuel Cells – A Tutorial on the Fundamental Characteristics and Practical Properties of NSTF Catalysts," Invited, 221st ECS Meeting, Seattle, Washington, May 8, 2012.
26. Mark K. Debe, "Looking to the Future and Assuming Success – Are current approaches for MEA electrocatalyst and membrane integration on a path to meet cost and high volume manufacturing requirements for automotive PEM fuel cells?," Invited, 6th International Fuel Cell Workshop, Yamanashi University, Kofu, Japan, August 2-3, 2012.

11.3 Contributed presentations at international meetings

1. D. Van der Vliet, D. Strmcnik, C. Wang, R. Atanasoski, M. Debe. N. Markovic and V. Stamenkovic, "Multimetallic Catalysts for Oxygen Reduction Reaction," 216th ECS Meeting, Vienna, Austria, Oct. 4-9, 2009.
2. A. K. Schmoeckel, G. D. Vernstrom, A. J. Steinbach, S. M. Hendricks, R. T. Atanasoski and M. K. Debe, "Nanostructured Thin Film Ternary Catalyst Activities for Oxygen Reduction," 2006 Fuel Cell Seminar, Honolulu, Hawaii, Nov. 13-17, 2006.
3. D. Van der Vliet, D. Strmcnik, C. Wang, R. Atanasoski, M. Debe. N. Markovic and V. Stamenkovic, "Catalysts with Multifunctional Active Sites: From well-defined to nanoscale surfaces**,"** 216th ECS Meeting, Vienna, Austria, Oct. 4-9, 2009.
4. A. J. Steinbach, K. Alade-Lambo, H. Le and M. K. Debe, "Investigation of Cation-Induced Performance Losses in PEM Fuel Cells," 2008 Fuel Cell Seminar and Exposition, Phoenix, AZ, Oct. 27, (2008) Extended Abstract GHT35a-22.
5. A. J. Steinbach, C. V. Hamilton, Jr. and M. K. Debe, "Impact of Micro-molar Concentrations of Externally-Provided Chloride and Sulfide Contaminants on PEMFC Reversible Stability," presented at the 212th ECS meeting, Washington, D.C. October 7-12, 2007.
6. M. K. Debe and A. J. Steinbach, "An Empirical Model For The Flooding Behavior Of Ultra-Thin PEM Fuel Cell Electrodes," ECS Transactions 659 (2007), and presented at the 212th ECS meeting, Washington, D.C. Oct. 7-12, 2007.
7. G. Vernstrom, A Schmoeckel, R. Atanasoski, S. Hendricks, A. Steinbach, and M. Debe, "Oxygen Reduction Activities of Nanostructured Thin Film Alloy Electrocatalysts", Fuel Cell Seminar, Oct. 13–17, 2008, Phoenix, Abst. 1365.
8. Gary C-K Liu, R.J. Sanderson, G. Vernstrom, D.A. Stevens, R.T. Atanasoski, M.K. Debe and J.R. Dahn,"RRDE measurements of ORR activity of $Pt_{1-x}Ir_x$($0<x<0.3$) on high surface area NSTF-coated GC disks," 216th ECS Meeting, Vienna, Austria, Oct. 4, 2009.
9. C.C. Hays, J.G. Kulleck, B.E. Haines and S.R. Narayan, "Thin Film Platinum Alloys for Use as Catalyst Materials in Fuel Cells," Abstract for 216th ECS Meeting, Vienna, Austria, Oct. 4, 2009.
10. A.J. Steinbach, H. Le, K Alade-Lambo, C.V. Hamilton Jr., M.J Kurkowski and M.K. Debe, "Reversible Performance Stability of Polymer Electrolyte Membrane Fuel Cells," 238th Am. Chem. Soc. Meeting, Washington, D.C. August 16, 2009.
11. D. Stevens, A. Bonakdarpour, R. Sanderson, S. Wang, R. Atanasoski, M. Debe and J. Dahn, "Development of Multi-component PEM Fuel Cell Catalysts for Enhanced Stop-Start Protection", 217th ECS meeting, Vancouver, BC, Canada, Aril 28, 2010.
12. Gary Chih-Kang Liu, R. Sanderson, D.A. Stevens, G. Vernstrom, R.T. Atanasoski, M.K. Debe and J. R. Dahn, "RRDE measurements of ORR activity of $Pt_{1-x}Ni_x$ ($0 < x < 1$) on high surface area NSTF-coated GC disks," 218th ECS meeting, Las Vegas, NV, Oct. 14, 2010
13. A. J. Steinbach, M. K. Debe, J. L. Wong, M. J. Kurkowski, , A. T. Haug, D. M. Peppin, S. K. Deppe, S. M. Hendricks and E. M. Fischer, "A New Paradigm for PEMFC Ultra-Thin Electrode Water Management at Low Temperatures," 218th ECS meeting, Las Vegas, NV, Oct. 14, 2010.
14. M. K. Debe, A. Steinbach, G. Vernstrom, S. Hendricks, R. Atanasoski, P. Kadera, "Extraordinary ORR activity of Pt3Ni7." 218th ECS meeting, Las Vegas, NV, Oct. 14, 2010.
15. A. Steinbach, M. Debe, M. Pejsa, D. Peppin, A. Haug, M. Kurkowski and S. Maier-Hendricks, "Influence of Anode GDL on PEMFC Ultra-thin Electrode Water Management at Low Temperatures," 220th ECS Meeting, Boston, MA, Oct. 9-14, 2011.

16. Gary Chih-Kang Liu, R.J. Sanderson, D.A. Stevens, G. Vernstrom, R.T. Atanasoski, M.K. Debe and J.R. Dahn, "De-alloying of $Pt_{1-x}M_x$ [M = Ni, Co] (0 < x < 1) catalysts and impact on surface area enhancement, " Presentation at the 218th ECS meeting, Las Vegas, NV, Oct. 12, 2010.
17. D.A. Stevens, S. Wang, R.J. Sanderson, G.C.K. Liu and J.R. Dahn, G. D. Vernstrom, R.T. Atanasoski and M.K. Debe, "A Combined Rotating Disk Electrode/X-Ray Diffraction study of Co Dissolution from $P_{1-x}Co_x$ alloys," Poster paper at the 218th ECS meeting, Las Vegas, NV, Oct. 13, 2010.
18. A. J. Steinbach, M. K. Debe, J. L. Wong, M. J. Kurkowski, A. T. Haug, D. M. Peppin, S. K. Deppe, S. M. Hendricks and E. M. Fischer, "A New Paradigm for PEMFC Ultra-Thin Electrode Water Management at Low Temperatures," Presentation at the 218th ECS meeting, Las Vegas, NV, Oct. 14, 2010.
19. M. Debe, S. M. Hendricks, G. Vernstrom, J. Wiley, M. Hamden, C. Mittelsteadt, C. Capuano, K. Ayers and E. Anderson, "Initial Performance and Durability of Ultra-low Loaded NSTF Electrodes for PEM Electrolyzers," Presentation at the 220Th ECS Meeting, Boston, MA, Oct., 2011.
20. A. Steinbach, M. Debe, M. Pejsa, D. Peppin, A. Haug, M. Kurkowski and S. M. Hendricks, "Influence of Anode GDL on PEMFC Ultra-thin Electrode Water Management at Low Temperatures," Presentation at the 220th ECS Meeting, Boston, MA, Oct. 2011.
21. M. Debe, S. M. Hendricks, G. Vernstrom, J. Wiley, M. Hamden, C. Mittelsteadt, C. Capuano, K. Ayers and E. Anderson, "Initial Performance and Durability of Ultra-low Loaded NSTF Electrodes for PEM Electrolyzers," 220th ECS Meeting, Boston, MA, Oct. 2011.
22. X. Wang, R. K. Ahluwalia, A. J. Steinbach, and M. K. Debe, "Dynamic Performance of Automotive Fuel Cell Systems with Low Platinum Loadings," 220th ECS Meeting, Boston, MA, Oct. 2011.

12. Intellectual Property Developments

Title	Investigators	Date Reported to DOE	Patent Application #
Fuel Cell Nanocatalyst with Voltage Reversal Tolerance	Steinbach, Verstrom, Debe, and Atanasoski	23-Sep-08	12/546775 (61/091643)
Catalyst Particle Size Control with Organic Pigments	Debe, Bender, Sowatzke	1-Oct-09	12/766304 (61/172111)
Catalyst Property Control with Intermixed Inorganics	Debe, Atanasoski, and Hendricks	1-Oct-09	12/766359 (61/172118)
Platinum Nickel Catalyst Alloy	Debe	18-Apr-11	US2011/033949 (61/328049)
Fuel Cell Electrode with Nanostructured Catalyst and Dispersed Catalyst Sublayer	Haug	25-May-10	12/976168 (61/288882)
Membrane Electrode Assemblies including Mixed Carbon Particles	Haug	25-May-10	12/976303 (61/288950)
Annealed Nanostructured Thin Film Catalysts	Debe, Smithson, Studiner, Hendricks, Kurkowski, Steinbach, and David Johnson	18-Apr-11	US2011/033972 (61/328064)
Fuel Cell Electrode Construction with Enhanced Properties	Debe, Hendricks, Vernstrom, Kurkowski. Steinbach, and Hester		(61/581351)
Fuel Cell Water Management via Sub-Atmospheric Anode Reactant Pressure	Steinbach, Debe, Haug, Thomas, Wong and Lee	18-Apr-11	US2011/033913 (61/328058)

13. Products developed and advanced under this project

No formal 3M products have derived from this project in the sense that anyone can order them. But significant quantities of roll good PtCoMn based catalyst coated membranes and as-made catalyst roll-goods of various loadings have been provided to automotive OEM customers under blanket purchase agreements. Stack sized gasketed MEA's with dealloyed and SET treated "Pt_3Ni_7" have been sold for stack testing to non-automotive customers as well.

14. Awards Received

A **2008 DOE Hydrogen Program R&D Award** was received at the DOE Hydrogen Program Annual Merit Review, June 9, 2008, Washington, D.C.

Supplementary Task Information

Supplementary Task Information

Over the course of this project the PI and co-PI had the opportunity to prepare and present 1,611 power point slides at 17 requested summary reviews for DOE fuel cell program management, the DOE AMR meetings and the FreedomCAR technical team at USCAR. In addition, at least 400 pages of word documents were provided in the 26 quarterly and annual reports. It is not possible to capture in this final report the extent of the work completed during the 5.25 years that even those reviews were summarizing. In this Section on Supplementary Task Information we provide some additional documentation on specific subjects that either further illustrate the type of work completed, are instructive for understanding the uniqueness of the NSTF electrocatalyst technology, or present what we believe are useful and intriguing results that the PEM fuel cell field as a whole might benefit from knowing.

Contents **Page**

Task 1

Selected Supplementary Information

Task 1.1 NSTF surface area increase – NSTF support whisker optimization

Introduction (see also Section 9.8)

Despite the higher surface area per unit volume, the thinness of the NSTF catalyst layer prevents the absolute Pt surface area from being nearly as high as that of nanoparticles dispersed on carbon black. The NSTF ECSA is critically dependent on two basic aspects of the electrode structure – the surface area of the underlying layer of PR149 support whiskers, and the roughness factor of the catalyst coating applied to those whiskers. The former in turn will depend on the geometric properties of the PR149 whisker layer, i.e. the number of whiskers per unit area, N and their dimensions, lengths L and cross-sectional dimensions d. The latter will depend on the catalyst layer porosity and any overt crystallite growth structure formed when the catalyst is deposited. In this project we carried out the first systematic attempt to determine how the observed ECSA depends on the whisker support layer geometric properties (and to some extent the process conditions), and catalyst loading for the PtCoMn system. We also correlated these factors to the 50 cm^2 fuel cell performance. The net result was a detailed model development with some surprising results of how catalyst ECSA actually depends on the physical properties of the catalyst layer, realization that there are conflicting factors that prevent a simple optimization of surface area by just adjusting the N, L and d of the whiskers, and that the fuel cell performance is very weakly dependent on these and the process parameters for producing the NSTF whisker support layer, i.e. the process windows are wide.

Approach: Designed experiments on Pilot line web coating equipment in Menomonie, WI

Because the whisker growth properties are very dependent on the process equipment and parameters used to make them, it was important to do the various experiments on the process line used for roll-good production of the NSTF whisker supports. We defined and executed a series of designed process experiments, called Whisker Area Optimization (WAO – 1,2,3,4), in which the whisker production parameters were explored for the optimum whisker number density and dimensions, the most complete conversion of the starting material to the crystalline whiskers. Fig. 9.17 indicates the high level process parameters that were controlled in defining the WAO experiments.

Various performance metrics were extracted from the fuel cell measurements and correlated with the WAO experimental whisker parameters, as shown in Fig. S1. From these performance metrics and the various whisker parameters, three different plot types could be made, as indicated in Fig**.** S1, viz. global, experiment specific and model comparison plots. Figs. S2 and S3 show two other example plots from an early stage of the WAO series.

In Section 9 we discussed an example of the modeling results. Fig. 9.20 in Section 9 shows an example of the modeling comparison plots for surface area. From such a graph it was apparent the model and experimental fits were fairly good, over the 0.05 to 0.15 mg/cm^2 Pt loading range. So the mean or approximate values of *x* and *f* in equation (1) below could be used to explore a general model able to project how the surface area, A^{Pt}_{geo} , would vary with N and L for a given loading.

Equation (1):

$$A_{geo}^{Pt} = \sqrt{2}\left[(1-x)+2xNL(w+t)\right]+\left(m/\rho\right)\left\{(1-x)2N(w+t)+\frac{f}{2NL(w+t)}+x\left[\frac{2}{(w+t)}+f\right]\right\}+\left(m/\rho\right)^2\left[(1-x)\frac{f}{\sqrt{2}L}+\frac{\sqrt{2}xf}{NL(w+t)}\right]$$

To do this the overall expression for A^{Pt}_{geo} in equation (1) was reduced as follows (cont. after Fig. S3):

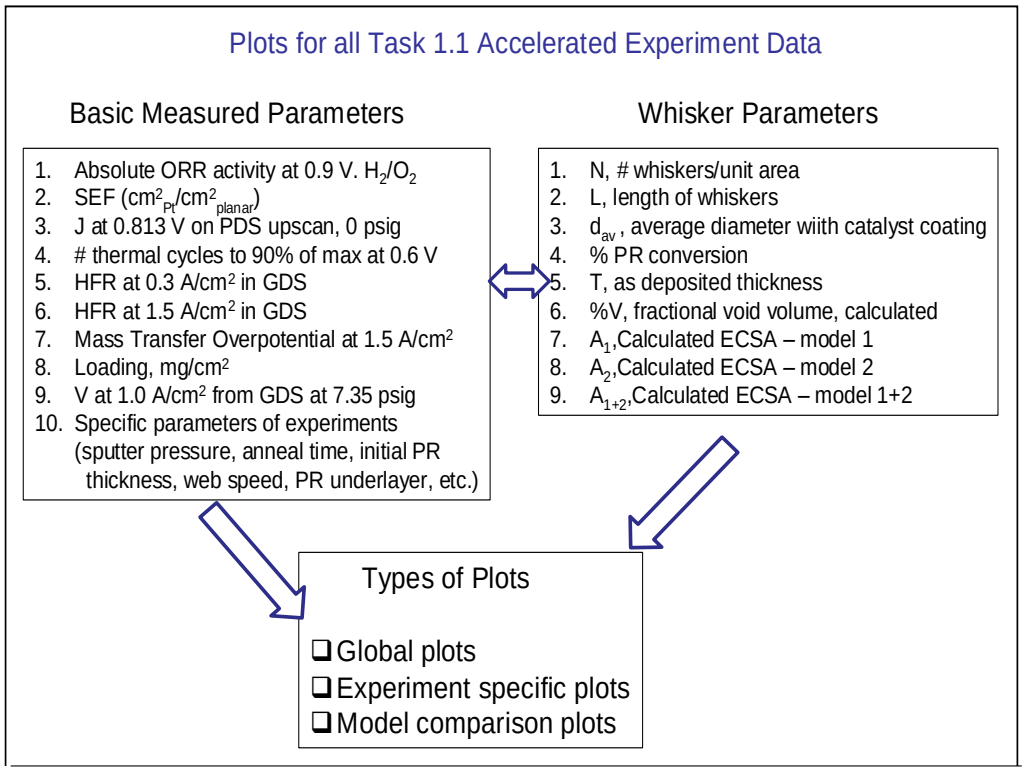

Fig. S1. Basic measured parameters, whisker and model parameters investigated in the WAO-series of experiments and the three types of data plots that were used to assess the results.

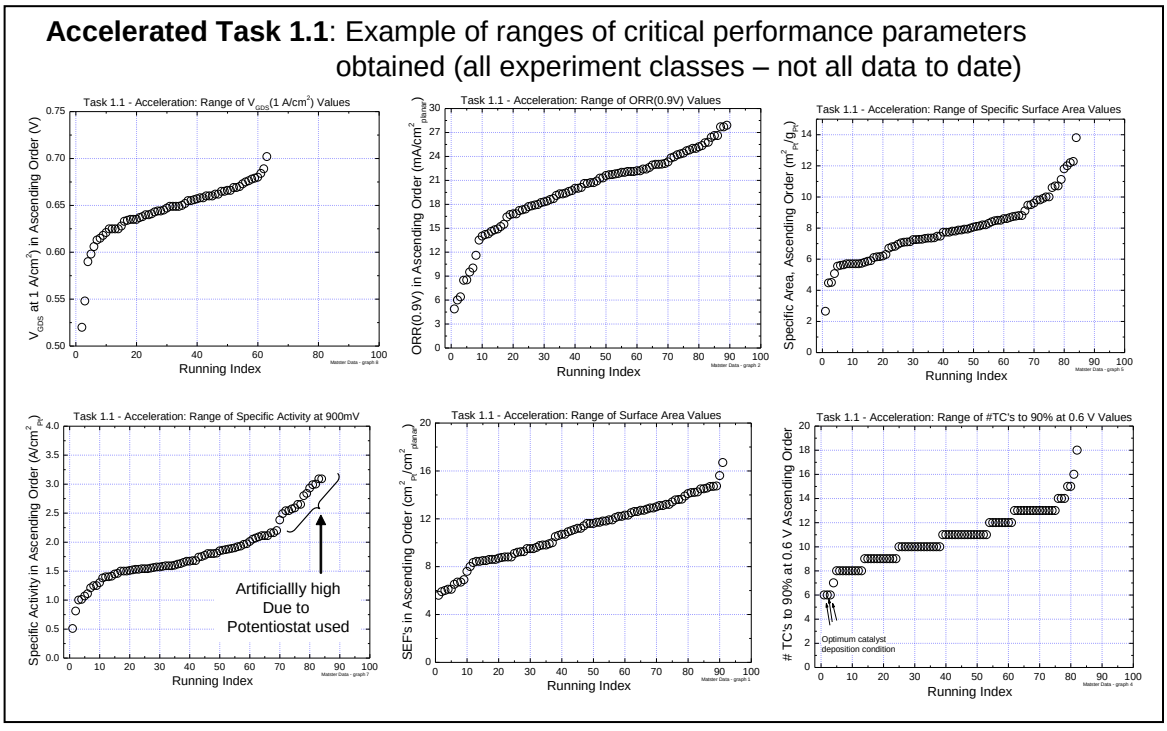

Fig. S2. Example of a global plot of various fuel cell performance metrics from the results of 118 MEA's, showing the ranges of the metrics for one material parameters varied.

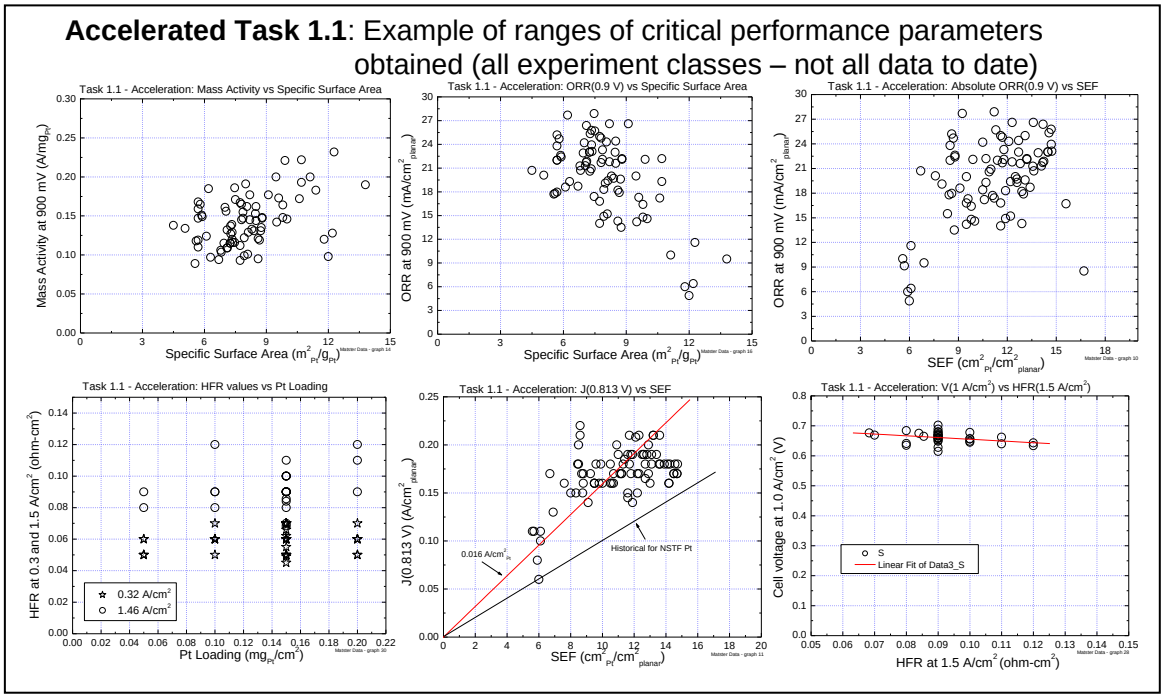

Fig. S3. Example of a global plot of various fuel cell performance metrics from the results of 118 MEA's, showing the ranges of the metrics as a function of surface area, Pt loading or HFR.

Using representative values for $f = 3\text{x}10^5$ and x=2/3, resulting from the modeling graphs, and known fixed values for w and t of the bare whiskers, A^{Pt}_{geo} can be expressed as a function of N for 10 < N < 50 with L as a parameter in the range of 0.3 < L < 3 microns. Equation 1 then reduces to the following quantitative expression, where N is in units of numbers of whisker per square centimeter and L is in units of centimeters:

(2) $$A^{Pt}_{geo} = 2.52 + 1.067\text{x}10^{-5}\ NL + 2.98\text{x}\ 10^{-11}\ N + 1.05\text{x}10^{5}/NL + 2.2\text{x}10^{-6}\ /\ L$$

This result of A^{Pt}_{geo} can be plotted vs N for various L are shown in Fig. S4. The cross-hatched box indicates the small relative range of N, L parameters screened by the WAO-1 data series. Surprisingly, the predicted surface area is still a monotonically increasing function of N for all L above the smallest values of N and L. Clearly the range of values scanned by WAO-1 is very small, and although not all the ranges of N and L will likely be obtainable, there should be definite benefits to determining the maximum values of N and L likely to be obtainable simultaneously.

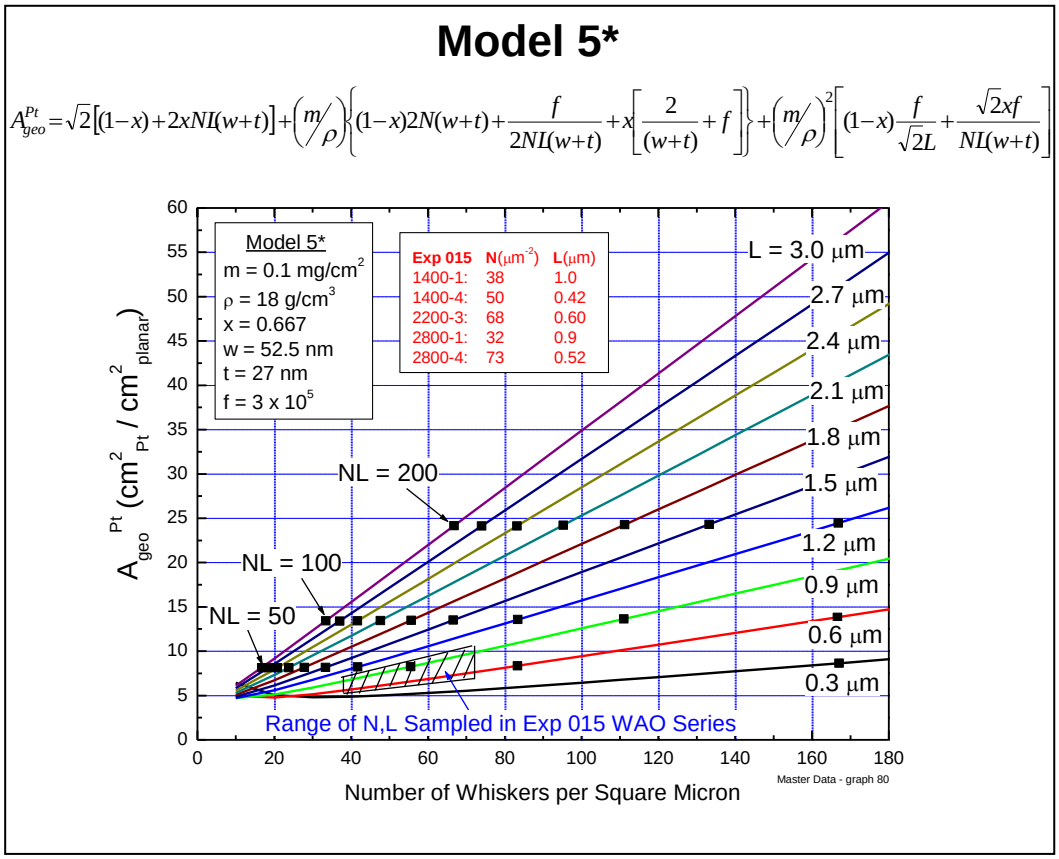

Fig. S4. Predicted Model 5* electrochemical Pt surface area from equation (2) based on the parameters in the legend.

Task 1.2 Fundamentals of NSTF catalytic activity

Task 1.2. Re-assessment of 3M NSTF catalyst entitlement ORR activity

- Measurements of NSTF alloy activities at ANL using RDE methods show significantly higher fundamental activities than state-of-the-art Pt dispersed on carbon, confirming 3M fuel cell measurements.
- ANL data shows also that H_2 annealing the NSTF alloys produces similar increases seen with their segregated surface composition profiles produced by H_2 annealing bulk polycrystalline and single crystal samples.
- **But are these NSTF activities near the entitlement values?**

Specific Activity Measurements by ANL Rotating Disc Electrode (RDE) System

V. Stamenkovic,
Dennis van der Vliet,
N. Markovic

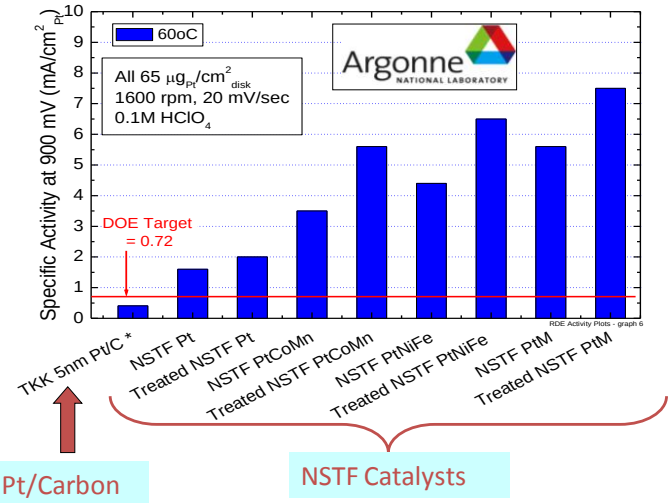

3M Advanced Cathode Catalysts and Supports..... DOE Review, March 16, 2010

Task 1.2. Re-assessment of 3M NSTF catalyst entitlement ORR activity

- Joint ANL/3M presentation at the fall 2009 ECS meeting showed this "Volcano Plot"
- Compares ANL measured NSTF alloy activities and ANL extended surface (bulk) catalyst activities to TKK 5nm Pt/C dispersed catalyst, all measured at ANL.

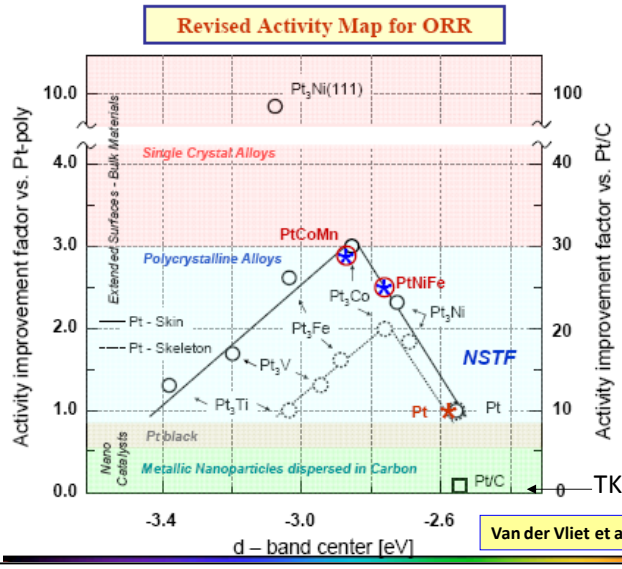

- $Pt_3Ni_1(111)$ single crystal surface activity is ~100 x more active for ORR than the Pt/C by ANL.
- 3M NSTF PtCoMn and PtNiFe appeared to fit their model for polycrystalline alloys
- Still potential for > 3X more to make NSTF equal to single crystal.

Van der Vliet et al., 216th ECS Meeting, Vienna, Oct. 2009

Task 1.2. Re-assessment of 3M NSTF catalyst entitlement ORR activity

Updated, Revised Activity Map for ORR on Pt Alloys

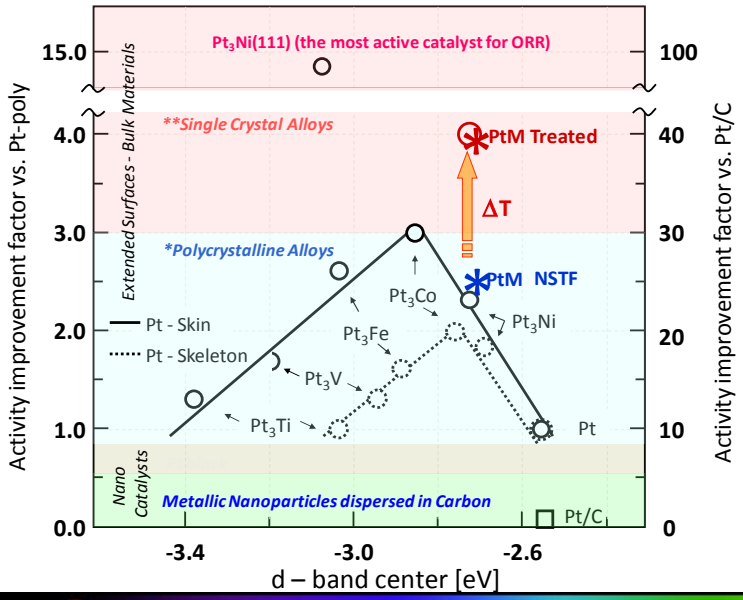

- Recently updated version from Voja of their slide showing the effect of their annealing the NSTF PtM alloys. Now NSTF PtM treated is less than 2.5 X from the bulk $Pt_3Ni(111)$ alloy.
- Is the bulk crystal surface $Pt_3Ni_1[111]$ activity value Nature's fundamental upper limit? Consider the following:

Argonne NATIONAL LABORATORY

*Stamenkovic, Markovic et al., Nature Mat 6(2007) 241

**Stamenkovic, Markovic et al., Science 315(2007) 493

Nanosegregated Surfaces as Superior Catalysts

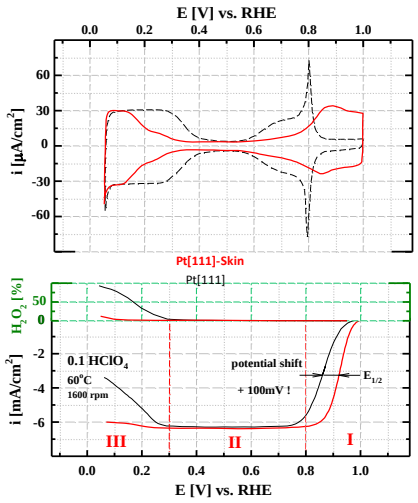

Pt(111)-Skin is the most active catalyst for the oxygen reduction reaction, and it is ~100 times more active than the state-of-the-art Pt/C catalysts

Stamenkovic, Markovic et al. Science 315(2007) 493

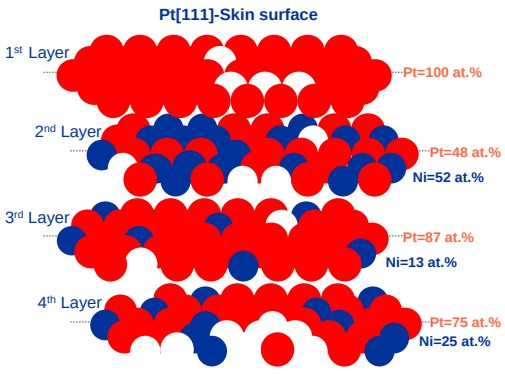

Nanosegregated Pt[111]-Skin Surface formed over Pt_3Ni alloy has oscillatory concentration profile in the first four atomic layers, which induces unique electronic and superior catalytic properties.

Argonne NATIONAL LABORATORY

UChicago ▸ Argonne LLC

Office of Science U.S. DEPARTMENT OF ENERGY

Task 1.2. Re-assessment of 3M NSTF catalyst entitlement ORR activity

- Based on ANL work on single crystals, the activity of bulk Pt_3Ni_1(111) alloy surfaces is ~ 9 times higher than bulk Pt_3Ni_1 (100) and 3.6 times higher than Pt_3Ni_1 (110), and many times higher than pure Pt if one has the nano-segregated surface composition profile structure in the top 4 layers.
- Do we have this yet on the NSTF Pt alloy surfaces? Do we even have mainly Pt(111) surface facets?

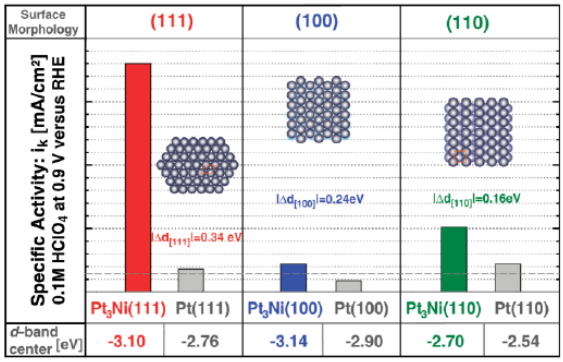

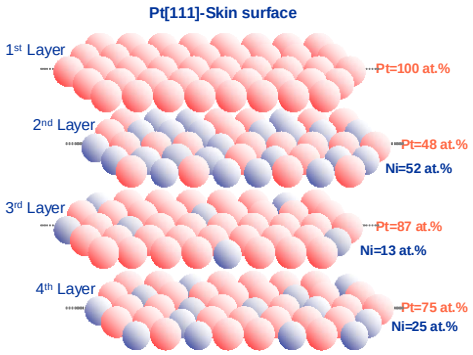

Stamenkovic et al., Science 315(2007) 493

3M Advanced Cathode Catalysts and Supports…… DOE Review, March 16, 2010

Task 1.2. Re-assessment of 3M NSTF catalyst entitlement ORR activity

- Stamenkovic et al. have used vicinal single crystal surfaces to study the effect of activity on terrace width. ORR activity drops off if terrace is too small.
- So this is another factor for extended surface area catalysts that is important.

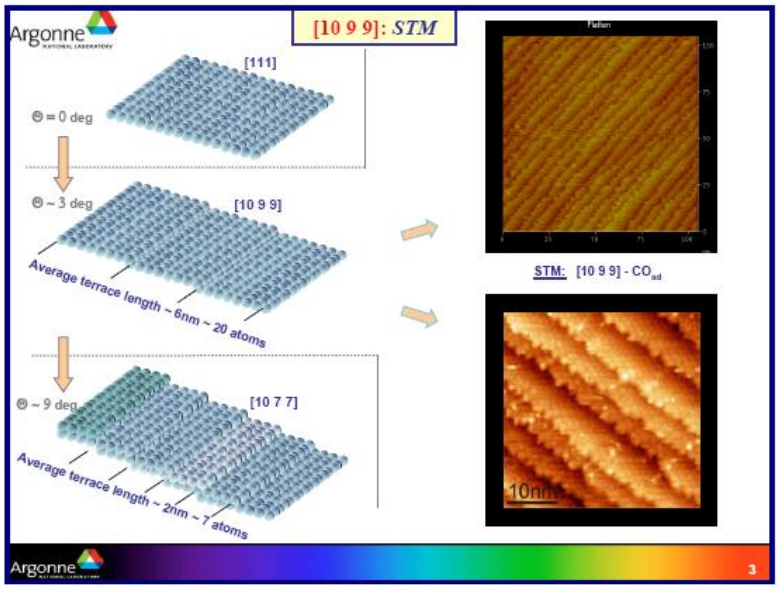

Task 1.2. Re-assessment of 3M NSTF catalyst entitlement ORR activity

Stamenkovic et al. have used vicinal single crystal surfaces to study the effect of activity on terrace width.

ORR on Pt(hkl) Surfaces

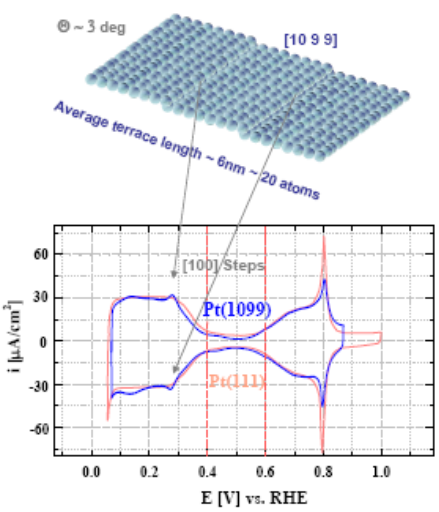

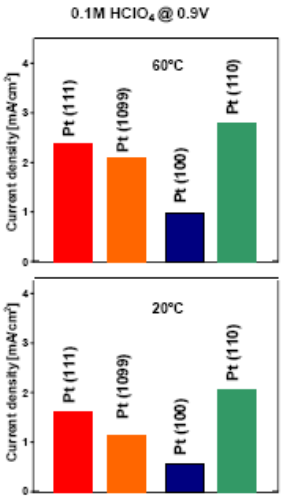

Therefore, 3 things to optimize for NSTF:

- Besides maximizing the proportion of Pt(111) facets, and segrating the surface structure, are those facets large enough is another question:

3M Advanced Cathode Catalysts and Supports..... DOE Review, March 16, 2010

Task 1.2. Re-assessment of 3M NSTF catalyst entitlement ORR activity

TEM studies of NSTF catalysts at 3M suggest current sputtered Pt alloy catalysts have activities that may be far below the entitlement potential.

- Low magnification TEM image of NSTF PtM catalyst coated whiskers, showing metal coating comprises small grains ~ 5-10 nm in size.
- XRD shows apparent crystallite grain sizes in similar range:
  - Pt[111] = 7.7 nm
  - Pt[200] = 5.1 nm
  - Pt[220] = 5.3 nm
  - Pt[311] = 6.3 nm
- Suggests each grain consists primarily of a single crystal.
- Are the grain surface facets the right (preferred) orientation for ORR? Are they large enough? How much of the total whisker surface area is good stuff?

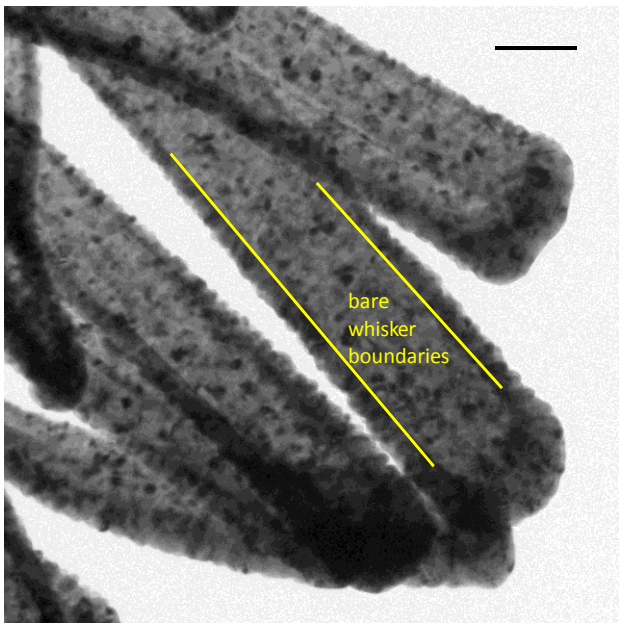

Task 1.2. Re-assessment of 3M NSTF catalyst entitlement ORR activity

Composite TEM images to define terms and elements (not from the same whisker)

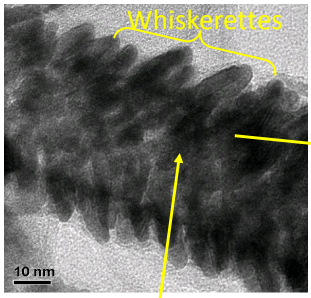

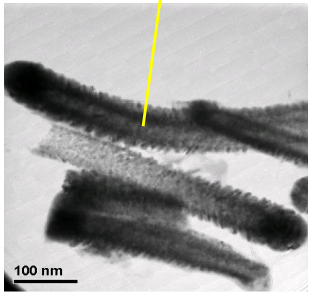

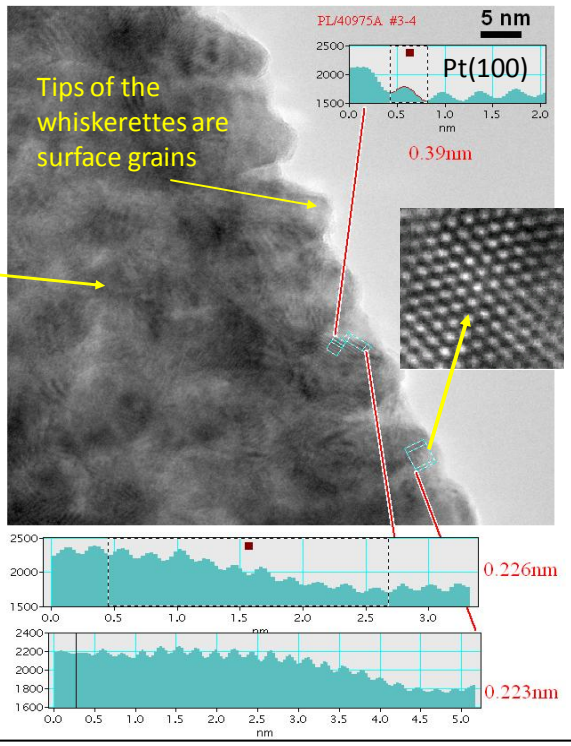

Task 1.2. Re-assessment of 3M NSTF catalyst entitlement ORR activity

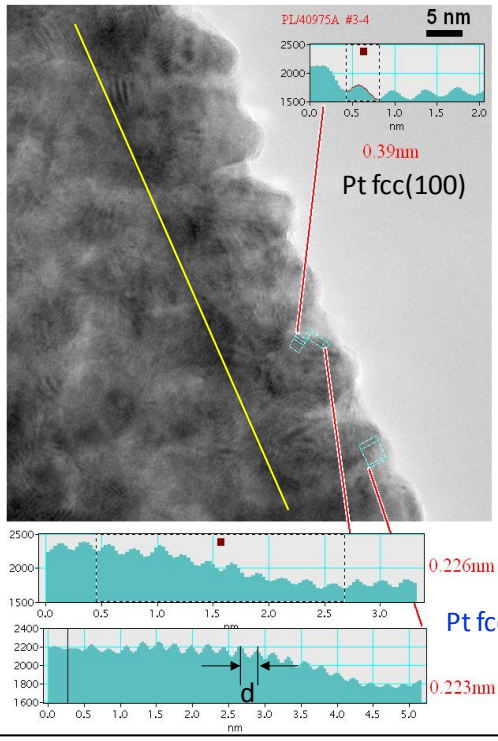

TEM image of one edge of a portion of a standard NSTF catalyst coated whisker of sputter deposited PtCoMn at a loading of 0.1 mg_{Pt}/cm^2.

- Surface facets of the grains are mixed, not all the preferred [111].
- Facets are small, ~ 5 nm.
- No large flat terraces apparent.
- Probably a lot of "junk surface" in between the good surface facets.

PtCoMn fcc lattice constant = 3.88 Å:

Pt(111) d = 3.88 / $(3)^{1/2}$ = 2.24 Å

Task 1.2. Re-assessment of 3M NSTF catalyst entitlement ORR activity

TEM image of the tip of a standard NSTF catalyst coated whisker of sputter deposited PtCoMn at a loading of 0.1 mg_{Pt}/cm^2.

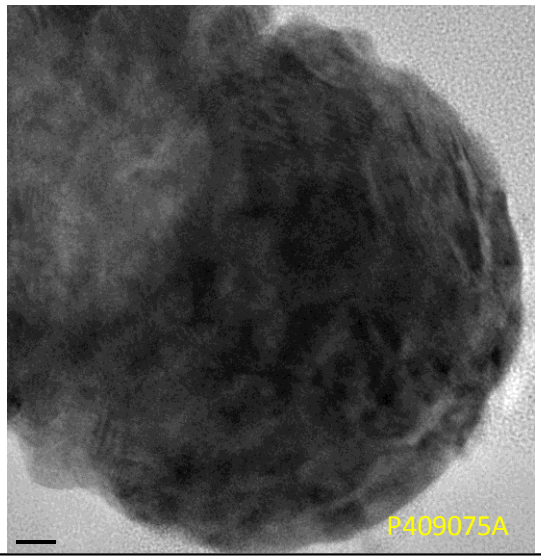

- No clear, well defined facets on the whisker tips.
- Some coarse Moire fringes apparent indicating some overlapping lattice fringes.
- Tips represent a small fraction of the total surface area, but still could be important if it were highly fcc(111) faceted.

3M Advanced Cathode Catalysts and Supports…… DOE Review, March 16, 2010

Task 1.2. Re-assessment of 3M NSTF catalyst entitlement ORR activity

- Vapor deposited Au using e-beam deposition gives very different surface structure.
- There is significant surface coverage of Au(111) terraces.
- Very different from sputter deposited PtCoMn.

- TEM overview of a Au coated whisker end.
- Note smoothness of surface.
- Some grain boundaries are marked in red.

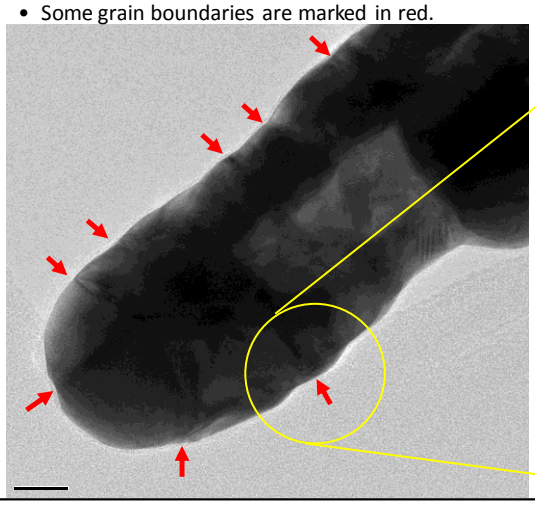

- 3 different gold grains showing 111 lattice fringes in different directions.
- Note the atomically smooth surface, circled.

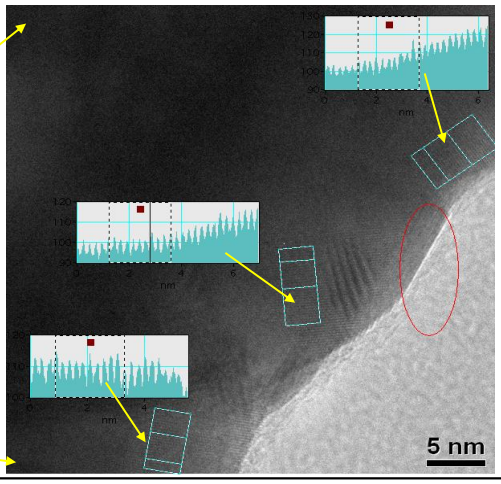

Task 1.2. Re-assessment of 3M NSTF catalyst entitlement ORR activity

- Vapor deposited Au using e-beam deposition gives significant surface coverage of fcc(111) terraces.
- The terraces can be atomically flat over large distances.

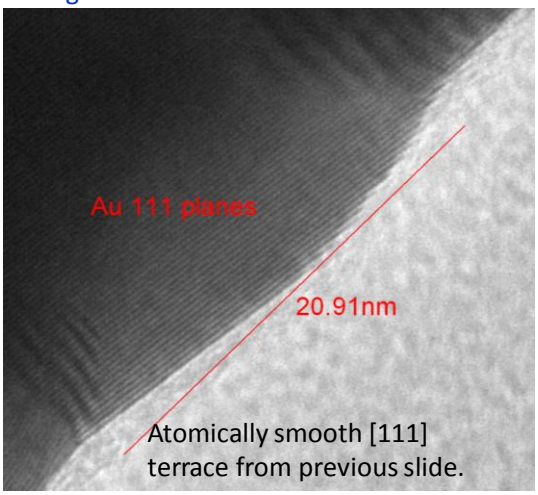

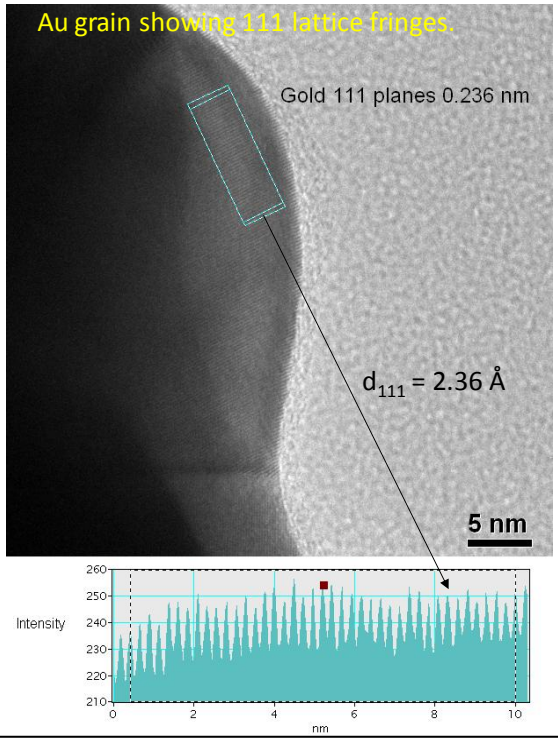

Task 1.2. Re-assessment of 3M NSTF catalyst entitlement ORR activity

- Vapor deposited Pt using e-beam deposition gives very different surface structure again.
- Pt coating consists of a high level of distinct crystalline grains.
- Very different from sputter deposited PtCoMn or vapor coated Au..

0.2 mg_{Pt}/cm^2 of pure Pt (images from 2000-2001)

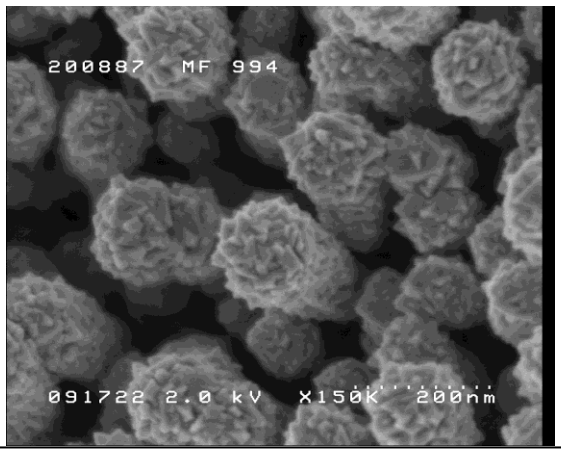

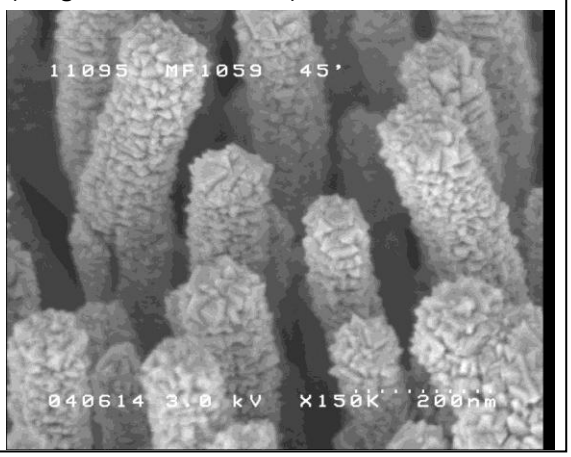

Task 1.2. Re-assessment of 3M NSTF catalyst entitlement ORR activity

Summary

- We have shown excellent correlation of NSTF fuel cell activity measurements with the fundamental ANL rotating disk electrode measurements.
- The surface morphology of the NSTF catalyst coatings can be dramatically varied depending on the materials used and the deposition process conditions.
- The current standard NSTF Pt and Pt alloy catalyst coatings appear far from ideal based on the fundamental single crystal and polycrystalline surface catalysis and surface structure determination done at ANL by Markovic, Stamenkovic et al.
  - Activity for ORR of bulk Pt_3Ni_1[111] surfaces are 9 x larger than Pt_3Ni_1[100] and 3.6 x larger than Pt_3Ni_1[110] surfaces
  - The [111] terraces must be sufficiently large to realize the full activity potential, > 6 atoms.
  - The nano-segregated bulk Pt[111]-Skin Surface formed over bulk Pt_3Ni_1 alloy has an oscillatory concentration profile in the outer four atomic layers, which induces unique electronic and superior catalytic properties. This was obtained at ANL by annealing single crystals of Pt_3Ni_1 in hydrogen.
- So there appears to be significant opportunity yet to optimize the NSTF catalysts based on fundamental assessments of extended surface area bulk catalysts.

3M Advanced Cathode Catalysts and Supports…… DOE Review, March 16, 2010

Task 1.2. Re-assessment of 3M NSTF catalyst entitlement ORR activity

How would we measure the amount of NSTF surface area that is in the preferred fcc(111) orientation, vs other fcc(hkl) or garbage surface area?

- TEM – very specific and definitive, but laborious and difficult to get an average ensemble measurement over the whole whisker, or
- ANL's In-situ FTIR rapid scan CO adsorption and oxidation

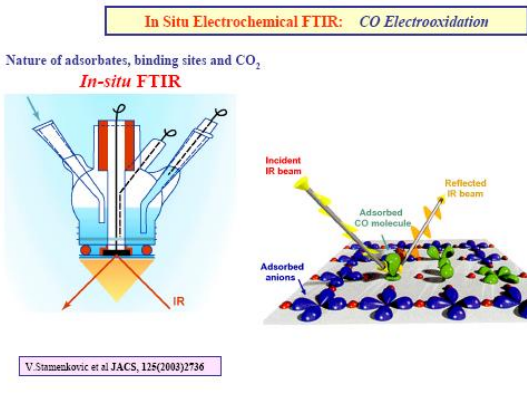

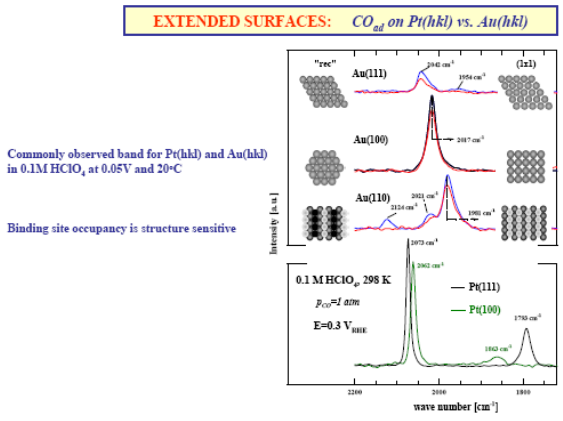

Pt(hkl) SURFACE MORPHOLOGY: CO_{ad} Oxidation on Pt[hkl] - Rapid In-Situ FTIR

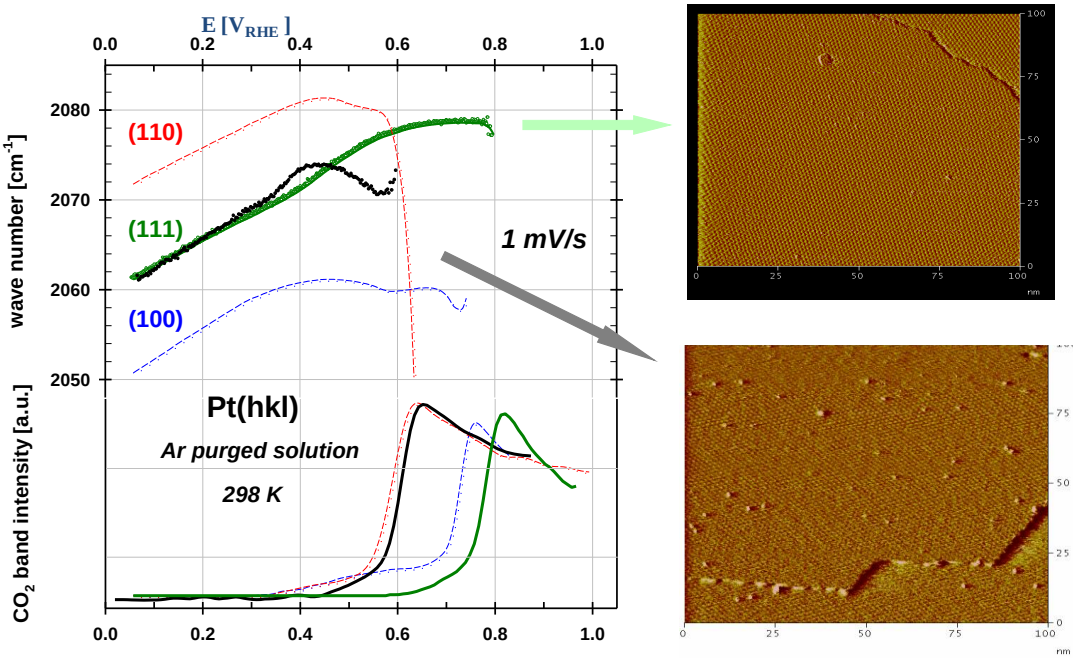

L-H: $CO_{ad} + OH_{ad} \rightarrow CO_2 + H^+ + e^-$

Argonne NATIONAL LABORATORY

Pt-NSTF: Surface Morphology by in-situ FTIR

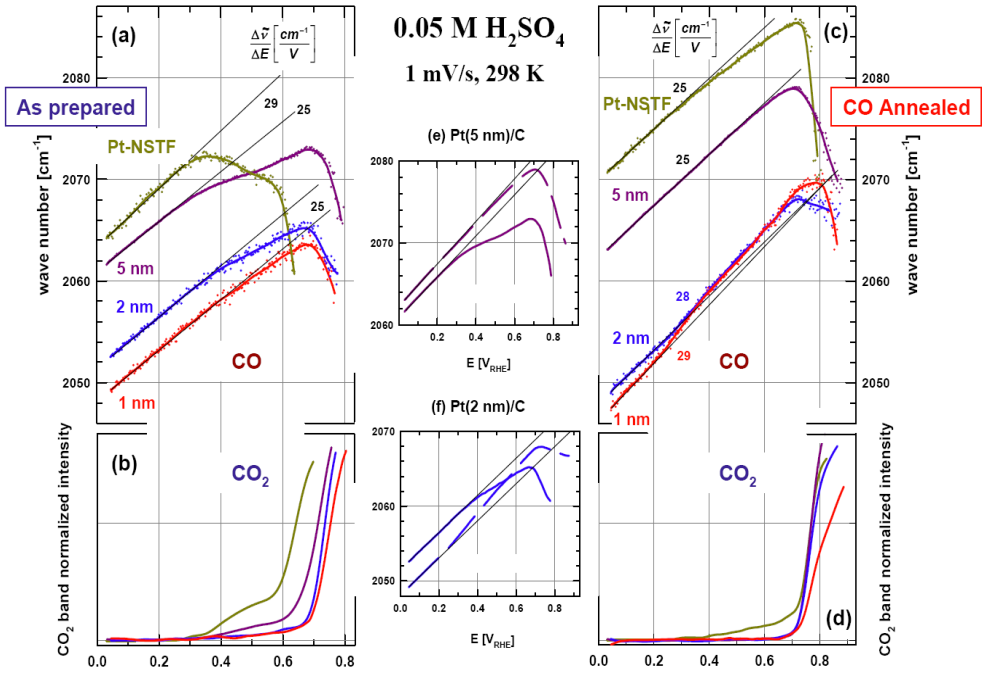

Argonne NATIONAL LABORATORY

ANL, *Unpublished*

Task 1.2. Re-assessment of 3M NSTF catalyst entitlement ORR activity

- ANL's In-situ FTIR studies of the electrochemical oxidation of CO adsorbed on well defined single crystal bulk surfaces and on NSTF-Pt, suggest that NSTF-Pt behaves for CO adsorption like Pt[110].
- This would suggest that a majority of our surface structure is not the preferred Pt[111].

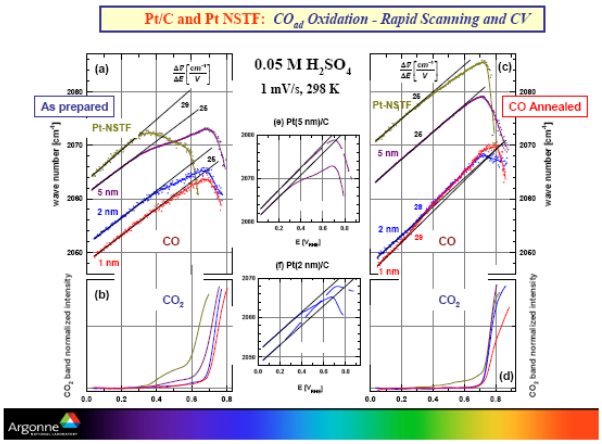

3M Advanced Cathode Catalysts and Supports…… DOE Review, March 16, 2010

Task 1.2. Re-assessment of 3M NSTF catalyst entitlement ORR activity

Future NSTF Catalyst Development Path

- There appears to be significant opportunity to increase the activity of the NSTF catalysts by maximizing, to the entitlement value:
  1) the fraction of the whisker surface area covered by fcc(111) facets,
  2) forming the fcc(111) facets to be of sufficient size to realize the full activity per unit area seen in single crystal surfaces,
  3) developing the segregated surface composition profile in the outer layers of the Pt alloys.
- Items 1) and 2) will be addressed by modifications to the catalyst deposition process and process parameters, trying to generate a similar surface as e-beam deposited Au. Will require a good metric to assess relative amounts of [hkl] facet areas. TEM is limited. ANL's FTIR–CO fast scan may be better.
- Item 3) may be addressed by roll-good compatible energetic surface treatment processing that simulates the hydrogen annealing of bulk single crystals. As shown on earlier slides we have demonstrated ~ 50% increase in mass activity of the PtM and PtCoMn alloys.

Task 1.3 New multi-element catalysts to increase activity

Technical Accomplishments and Progress

Supplemental Slide

Task 1. NSTF Catalyst Activity, Surface Area, Fundamentals

- Dalhousie is also capable of excellent RRDE characterization. Now applied to NSTF routinely.
- New aspect is that 3M grows the whiskers directly on the glassy carbon disk.
- Dalhousie applies the catalyst to be studied to the whiskers by sputtering. Then characterizes in multi-RRDE facilities.

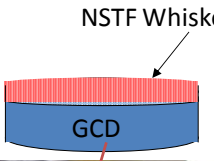

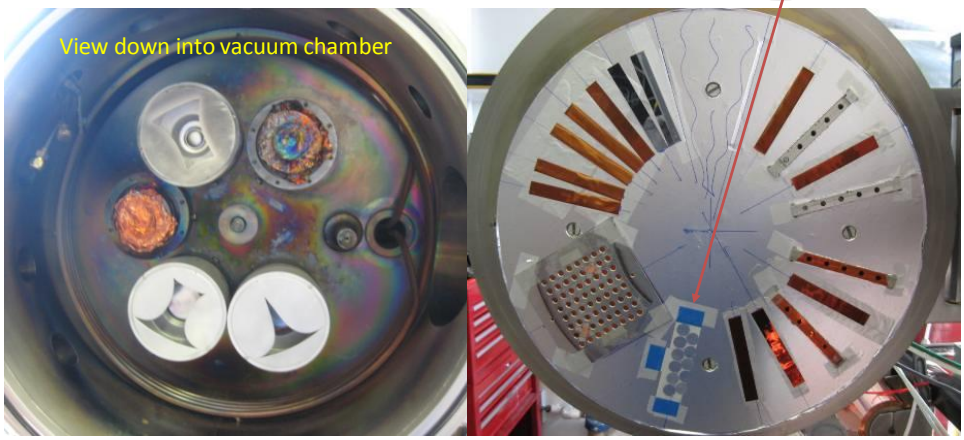

Task 1.3 – New catalysts for increased ORR activity and stability

❑ Dalhousie University Activities

2) PtNi dealloying kinetics – Part of Gary C. K. Liu Ph.D thesis, results presented at 218th ECS meeting

Nickel dealloys from the Pt_3Ni_7 material at a potential higher than 600 mV .

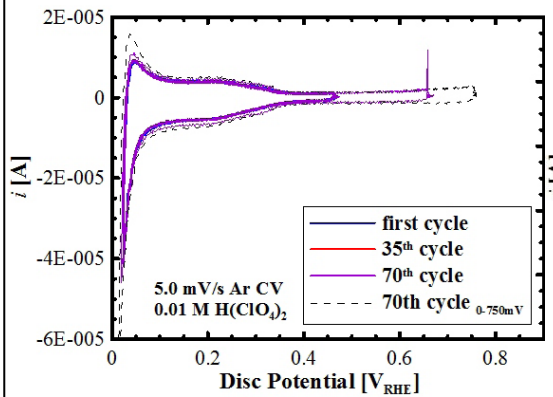

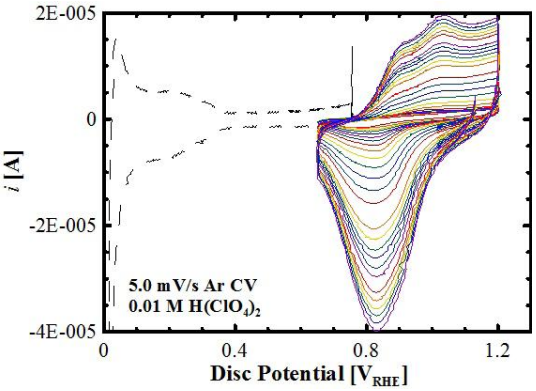

CV of Pt Ni in lower potential regions where pure nickel dissolves fastest. There are no changes to the CV shapes, indicating no dealloying.

CV of Pt Ni in higher potential regions where pure nickel would have already dissolved. There is an apparent increase in the active surface area, indicating dealloying.

Task 1.3 – New catalysts for increased ORR activity and stability

❑ Dalhousie University Activities – 1) C. K. Liu PtNi on NSTF RDE study

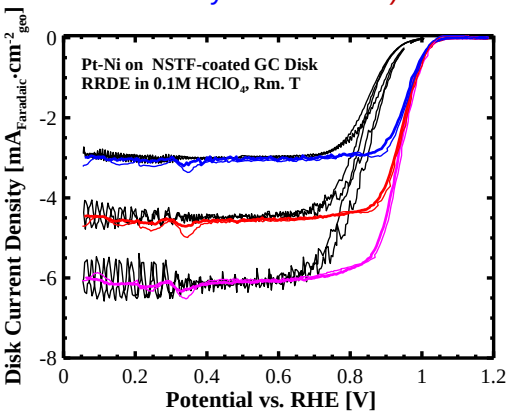

ORR measurements of the sputtered catalysts on different substrates, measured at different rotating rates (400, 1000 and 1600 rpm) at different potential sweep rates (20 and 50 mV/s)

- 400 rpm 20mV/s
- 1000 rpm 20mV/s
- 1600 rpm 20mV/s
- 400 rpm 50mV/s
- 1000 rpm 50mV/s
- 1600 rpm 50mV/s
- Pt_{poly} on mirror-GC

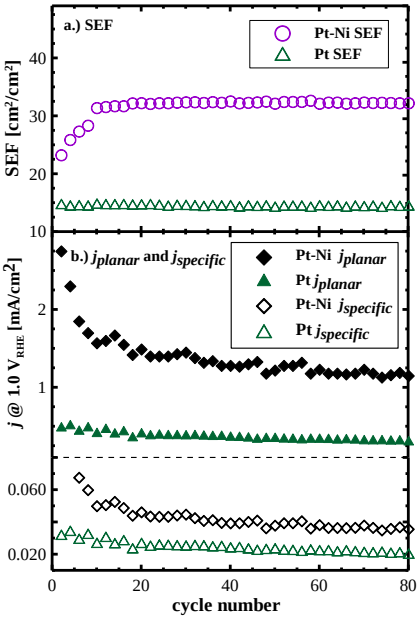

Summary of catalytic activity (SEF, j_{planar} and $j_{specific}$ extracted at 1.0VRHE) of the Pt and Pt-Ni samples measured over 80 potential cycles.

3M Advanced Cathode Catalysts and Supports…… DOE Review, March 16, 2010

Task 1.3 – New catalysts for increased ORR activity and stability

❑ Dalhousie University Activities

2) PtNi dealloying kinetics – Part of Gary C. K. Liu Ph.D thesis, results presented at 218th ECS meeting

Ni dissolution characterized by CV (A) and electrolysis (potential hold) method (B) shows the Ni dissolution reaction is most active between 200mV and 600 mV .

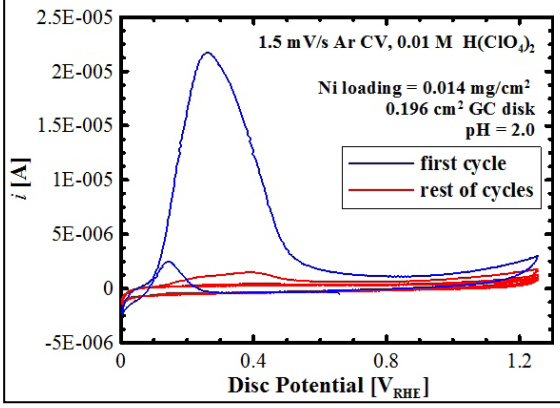

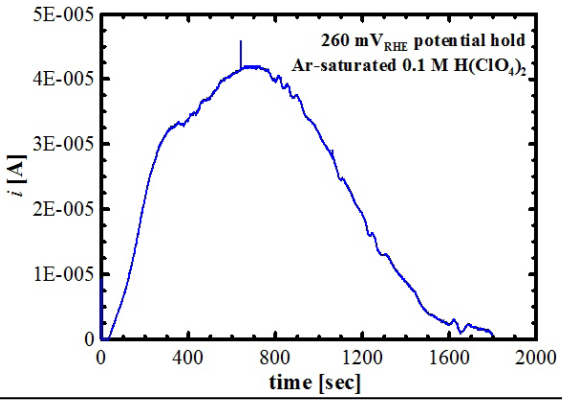

Task 1.3 – New catalysts for increased activity and stability - hi thru-put studies

Objective: Control grain size, lattice spacing, and surface composition to increase activity, catalyst surface area, stability under high voltage cycling,

- We have continued to focus on the binary, ternary and intermixed inorganic materials systems – no further under- or over-layer work.
- There have been no "home runs" resulting yet from the compositional spread, high throughput work at Dalhousie.
- IP has been filed though on systems and methods to control alloy crystalline grain size and lattice parameters.
- Several new material systems have been studied, and also sputtering process parameter effects.
- Most recently, we have asked them to help focus on the PtNi system, as described in Task 1.2.

New composition spreads studied:

- Pt-W-C, Pt-Ta-C, Pt-C
- Pt-TiO_2, Pt-ZrO, Pt-Re, Pt-Hf, all as intermixes and as 50cm^2 for 3M
- PtCoMn sputtered vs pressure
- Pt sputtered in various gases
- Pt-Ni
- Pt-Co
- Pt-Pb
- Pt-Nb

11

The additional compositional spreads listed on this slide are in addition to those listed in Fig. 9.27 in Section 9.

Task 1.3 – New catalysts for increased activity and stability - cat. deposition

Background

- STEM work at ORNL during this contract on our standard multi-layer PtCoMn construction showed clearly that the bi-layer Pt/TM thickness of 50 Angstroms was preserved on the whisker tips (very tiny fraction of surface area)
- But layering was still visible on the upper whiskerettes.

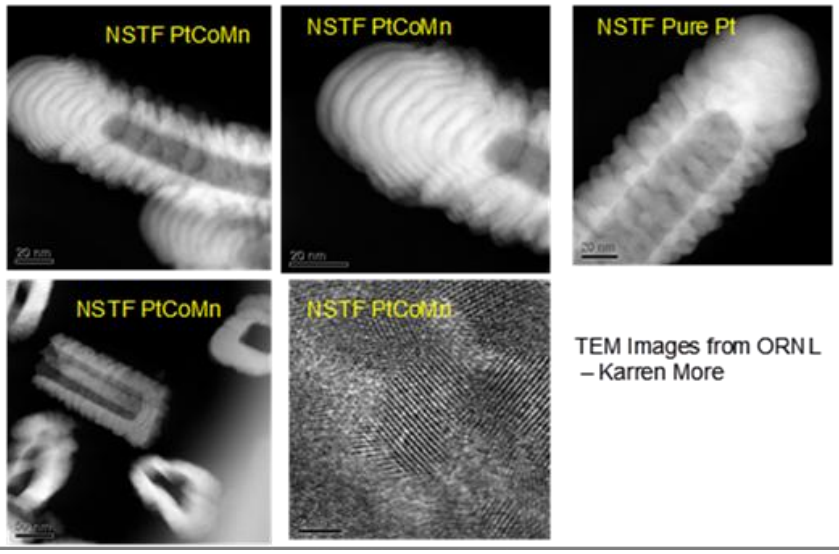

TEM Images from ORNL
– Karren More

Task 1.3 – New catalysts for increased activity and stability - JPL

JPL Electrochemical Cell with Rotating Electrolyte (RDE Simulation)

JPL Original Concept:

Novel multi-electrode electrochemical cell with rotating electrolyte to simulate rotating disc electrode measurements.

JPL

Charles C. Hays, S. R. Narayanan

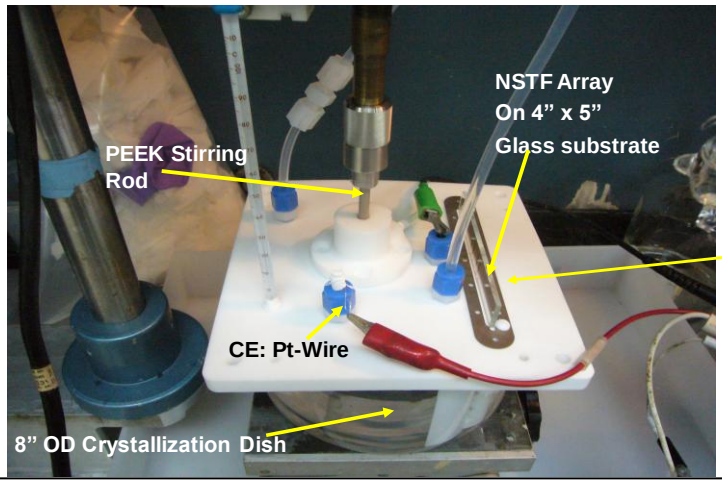

Multi-element sample array

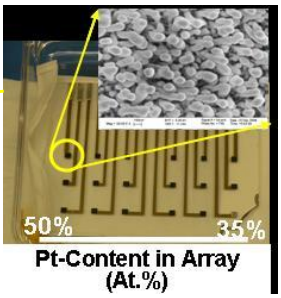

3M Advanced Cathode Catalysts and Supports…… DOE Review, June 30, 2009

Task 1.3 – New catalysts for increased activity and stability - JPL

JPL Catalyst Array Fabrication

Co-sputtering of Alloy NSTF

JPL applies sputtered alloys to 3M NSTF whisker supports in compositional spread over multi-electrode array.

JPL

Charles C. Hays, S. R. Narayanan

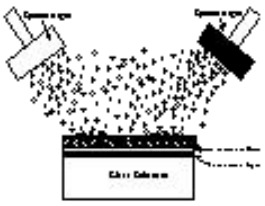

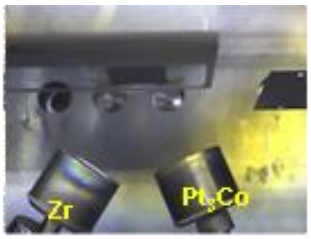

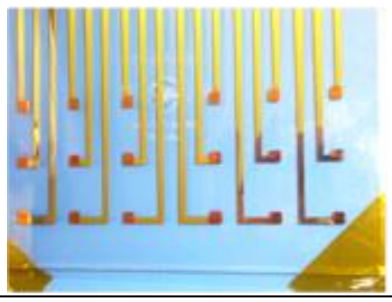

Task 1.3 – New catalysts for increased activity and stability - JPL

JPL Catalyst Array Fabrication

JPL

Approach:

- JPL sends glass substrate with array of gold-electrodes to 3M
- 3M applies bare NSTF whiskers to JPL substrates
- JPL sputters catalyst onto NSTF whiskers using multiple ion guns
- JPL characterizes the catalysts ex-situ and electrochemically

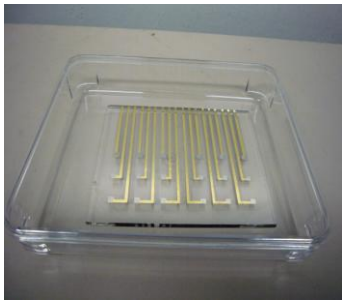

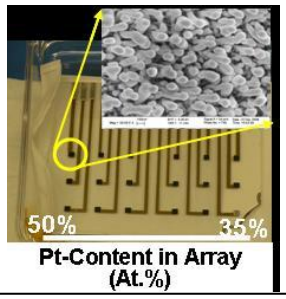

Characterization by JPL:

- Ex-situ: XRD, SEM, AFM,
- In-situ electrochemical
  - •Surface area by Hupd
  - •ORR – via Rotating Electrolyte

3M Advanced Cathode Catalysts and Supports…… DOE Review, June 30, 2009

Task 1.3 – New catalysts for increased activity and stability - JPL

- **Status of thin film synthesis and characterization at end of 2008**
  - – Sputtering Systems: all systems working
  - – Sputtering Process: jig assembly validated
  - – Catalyst synthesis : 4- and 18-electrode substrates demonstrated with Pt, PtCo, PtZr, PtCoZr
  - - Characterization completed: Composition, SEM Images, XRD results, AFM
- **Status of electrochemical testing at end of 2008**
  - – Multi-electrode technique hardware completed
  - – Cyclic voltammetry on multi-electrodes demonstrated
  - – Surface areas by Hupd and ORR scans demonstrated
  - – CV cycling for durability of PtZr completed

Electrochemical Surface Area

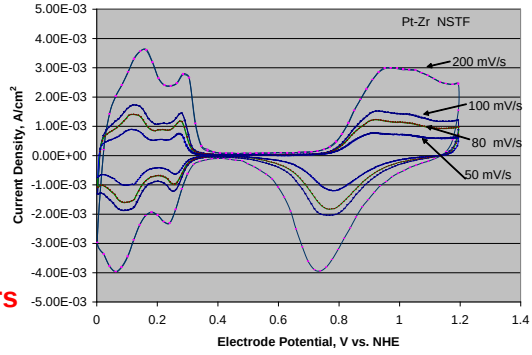

- **Surface area measurements from the novel CV apparatus were as expected.**
- **However, the magnitudes of the ORR currents were anomalously low by orders of magnitude.**

Task 1.3 – New catalysts for increased activity and stability - JPL

Polarization Curves for ORR with JPL rotating electrolyte apparatus

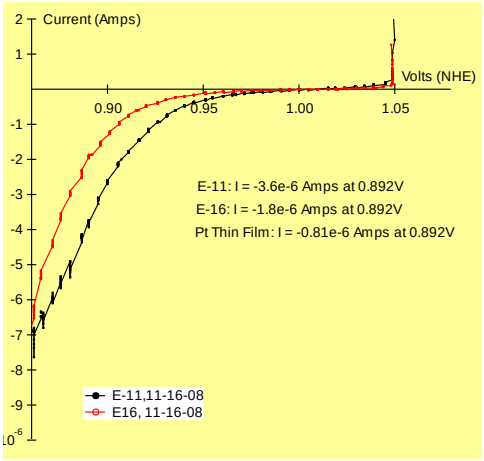

Limiting currents (not presented) are about three times less than RDE measured at Dalhousie on the same NSTF configuration at 400 rpm.

Scan Rate Measurements for ORR on PtCoZr NSTF

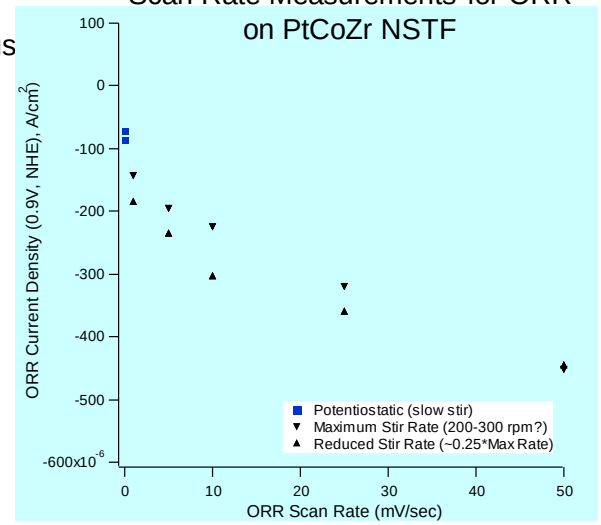

The current at 0.9 V at 50 mV/s is 3 – 4 times that measured at 1 mV/s.

3M Advanced Cathode Catalysts and Supports…… DOE Review, June 30, 2009

Task 1.3 – New catalysts for increased activity and stability - JPL

This issue of the JPL device currents caused us to re-examine the fundamentals of the concept approach:

- RRDE measurements of Pt coated GCD's (with and without NSTF whiskers) at Dalhousie were used to estimate the equivalent disk rotation speed of the JPL device's rotating electrolyte (next slide).
- Conclusion was that the equivalent rotation speed of the JPL system is only 10% of the normal RDE system. This meant that the JPL system was dominated by the boundary layer transport properties, not the ORR kinetics of the catalyst surface.
- Further round-robin samples have been made at 3M and Dalhousie for comparison testing at JPL and Dalhousie.

Task 1.3 – New catalysts for increased activity and stability - JPL

Estimating Equivalent Rotating Disk Speed of JPL Method

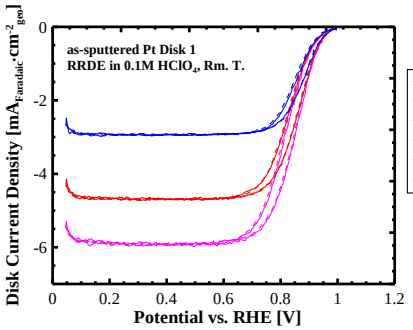

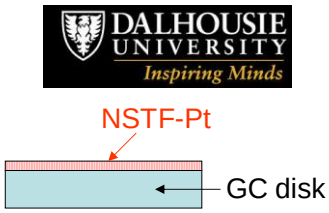

Rotating disk data on smooth Pt and NSTF-Pt coated glassy carbon disks for 1:1 comparison with the JPL rotating electrolyte technique. (from Dalhousie)

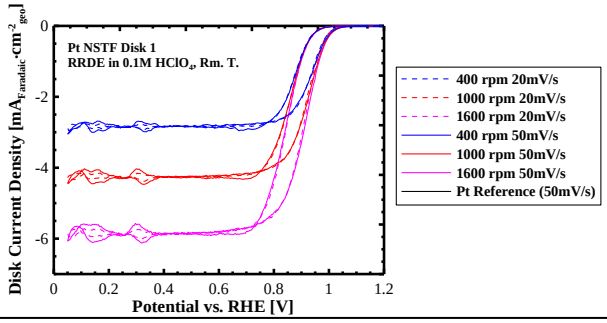

Based on the values of the limiting currents at 400 rpm, the equivalent rotation rate by JPL method is ~ 44 rpm.

Task 1.3 – New catalysts for increased ORR activity and stability

JPL

- JPL/Cal Tech Activities – Charles Hays and Carol Garland (Cal Tech sub.)

Microstructural Characterization of Note To Date

Transmission electron microscopy (TEM) Characterization of $Ni_{70}Pt_{30}$ NSTF :

- Subcontract set up with Caltech for TEM work with Carol Garland
  - Phillips – FEI Technai Field Emission Microscope, Model TF30UT - 300 kV Ultrathin
  - SEM at JPL with Dr. Jim Kulleck, using FEI NOVA Nano SEM 600.

1st Sample Set: $Pt_{30}Ni_{70}$ coated NSTF whiskers from 3M production line process P4.

3M P4 Process Coated $Ni_{70}Pt_{30}$ (At.%) NSTF

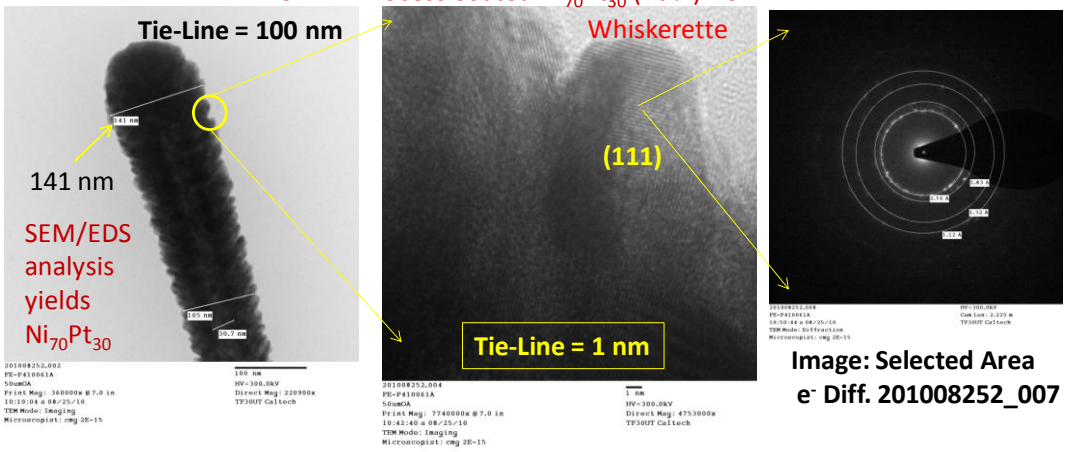

Task 1.3 – New catalysts for increased ORR activity and stability

- JPL/Cal Tech Activities – Charles Hays and Carol Garland (Cal Tech sub.)

1st Sample Set: $Pt_{30}Ni_{70}$ coated NSTF whiskers from 3M production line process P4.

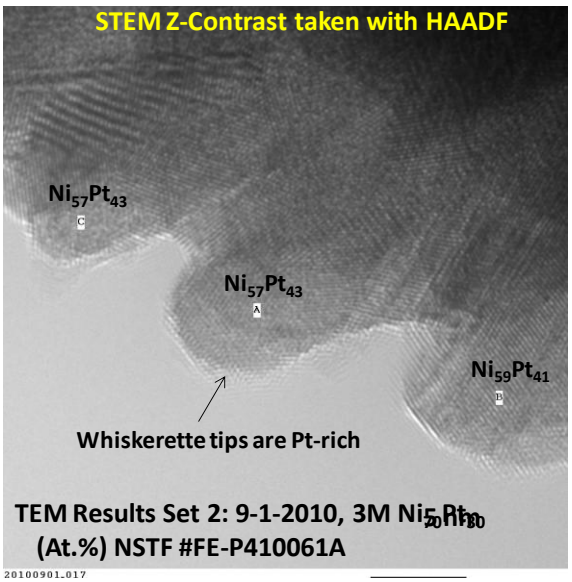

Tips of whiskerettes on sides of whisker are Pt rich vs. the whole whisker coating composition.

Microscopist: CMG ZE-15-A2

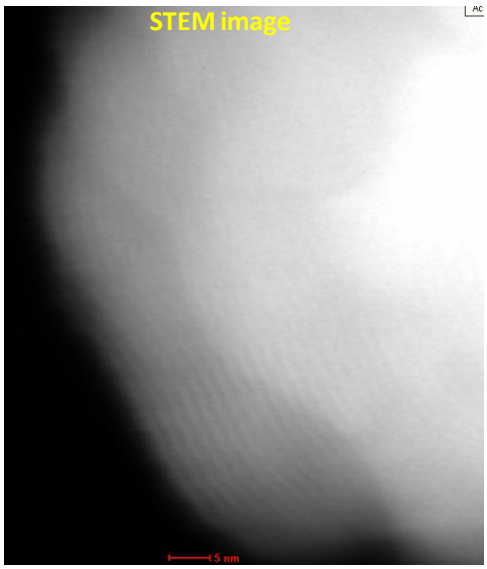

Layering observed at top of whisker from P4 process of sequential deposition.

Task 1.3 – New catalysts for increased ORR activity and stability

- JPL/Cal Tech Activities – Charles Hays and Carol Garland (Cal Tech sub.)

2nd Sample Set: $Pt_{30}Ni_{70}$ coated NSTF whiskers by JPL co-deposition ion guns.

Strong variation of composition in whiskerettes depending on location on whisker !

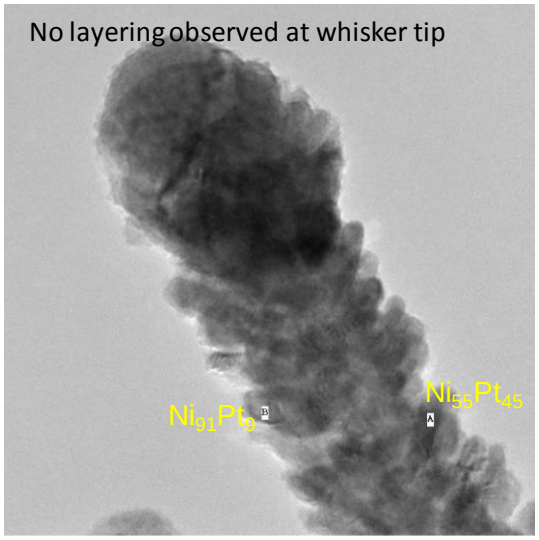

No layering on whisker tip consistent with co-deposition instead of sequential.

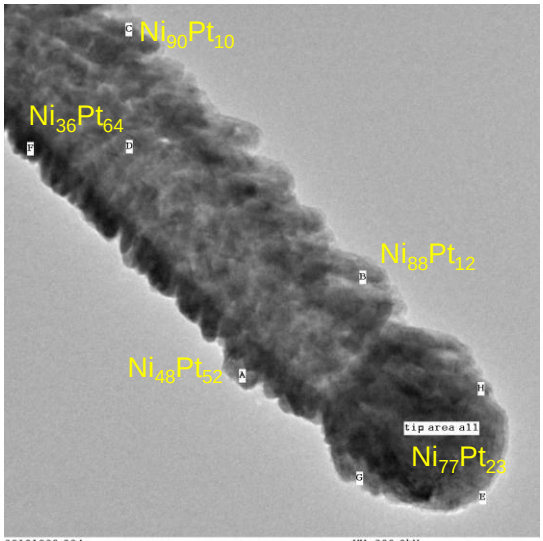

Text boxes denote composition at measurement sites

Task 1.3 – New catalysts for increased ORR activity and stability

- JPL/Cal Tech Activities – Charles Hays and Carol Garland (Cal Tech sub.)

Microstructural Characterization Summary

1st Sample Set: $Pt_{30}Ni_{70}$ coated NSTF whiskers from 3M production line process P4.

- Whiskerettes show strong (111) orientation by e-diffraction (same as PtCoMn)
- SEM/EDS analysis of entire whiskerette yields $Ni_{70}Pt_{30}$ composition, right on target
- Tips of whiskers show layering (consistent with sequential deposition) same as we see for PtCoMn)
- Tips of whiskerettes are Pt-rich, but whole whisker composition is 70:30.

2nd Sample Set: $Pt_{30}Ni_{70}$ coated NSTF whiskers by JPL co-deposition ion guns.

JPL coated $Pt_{30}Ni_{70}$:

- does not show layering on whisker tips as expected.
- shows deposition induced shadowing effects, causing NiPt on one side and $Ni_{90}Pt_{10}$ on the other side (orientation re. Ion guns.)
- NiPt exhibits $L1_0$ Tetragonal superlattice
- $Ni_{70}Pt_{30}$ exhibits $L1_2$ Cubic superlattice

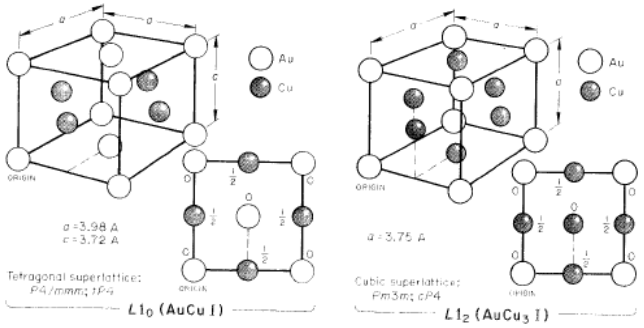

Task 2

Selected Supplementary Information

Task 2 – Voltage Cycling Durability – 4000 cycles, effect of T °C, time

50 cm² 2009 Best of Class CCM's

4000 CV cycles, 0.6 – 1.2 V H_2/N_2, 20 mv/sec, 1 min./cycle, 80 or 95 °C

- Surface area stability similar with either 80 °C or 95 °C protocol
- Absolute ORR activity losses at 900mV similar for 80 °C or 95 °C protocol
- Production coater catalyst vs ML-2 batch coated catalyst (MT or ST) all similar
- Loss after 4000 minutes at OCV much less than after 4000 minutes of cycling (1 min/cycle)

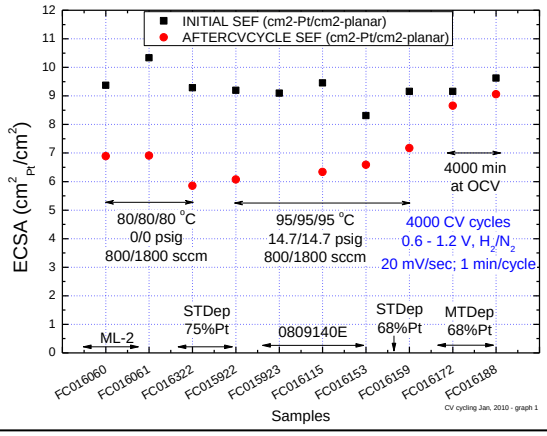

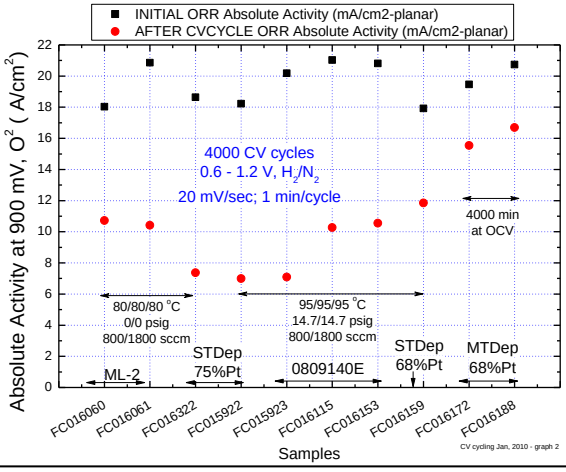

3M Advanced Cathode Catalysts and Supports…… DOE Review, March 16, 2010

Task 2 – Voltage Cycling Durability – 4000 cycles, effect of T °C, time

50 cm² 2009 Best of Class CCM's

4000 CV cycles, 0.6 – 1.2 V H_2/N_2, 20 mv/sec, 1 min./cycle, 80 or 95 °C

- Specific activity stability similar with either 80 °C or 95 °C protocol.
- Cell voltage at 0.02 and 1 A/cm² similar for 80 °C or 95 °C protocol
- Production coater catalyst vs ML-2 batch coated catalyst (MT or ST) all similar
- Loss after 4000 minutes at OCV much less than after 4000 minutes of cycling (1 min/cycle)

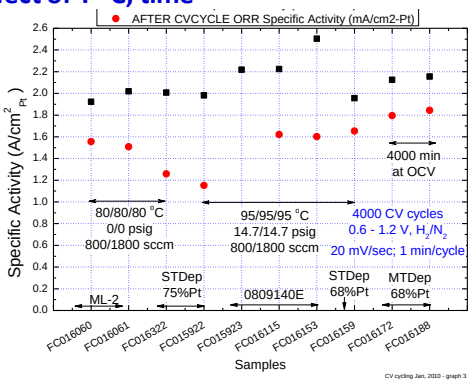

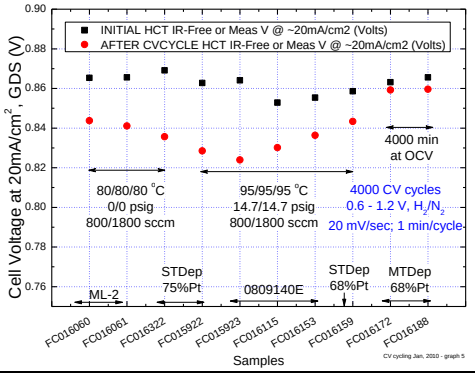

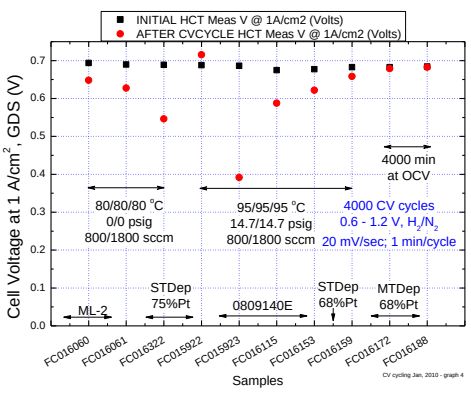

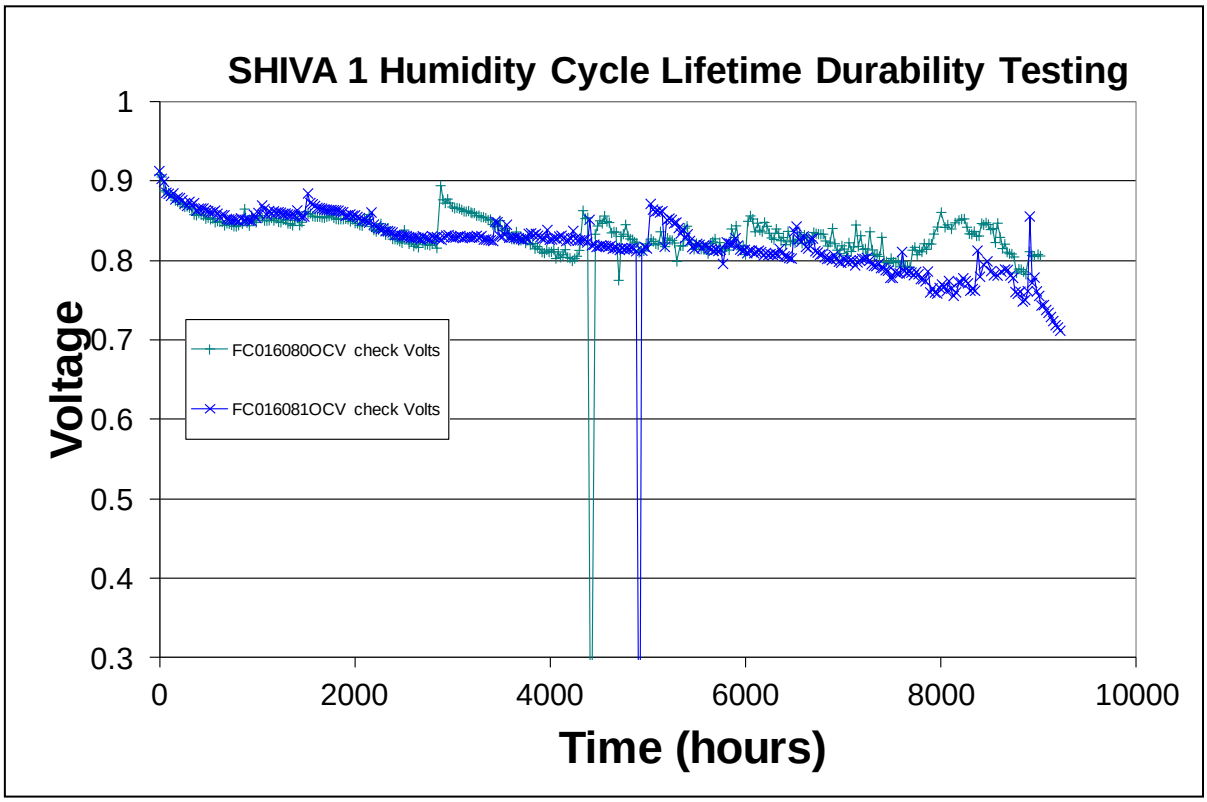

Fig. S5. Open circuit voltage versus time under the SHIVA 1 Load Cycling AST shown in Fig. 7.6, for the last two tested MEA's that reached 9000 hours of lifetime as judged by when the OCV fell below 0.8V.

Task 3

Selected Supplementary Information

Task Summary

Task 3 Full Size (> 250 cm^2) Single or Multi-Cell Tests

Subtask 3.1 Down-selection of cathode catalysts in 50-cm^2 cell tests

The purpose of this subtask is to evaluate MEA's made with subsets of the supports and catalysts down-selected from Tasks 1 and 2, in 50 to 100 cm^2 single cells, using well established testing protocols for performance and durability. The approach will consist of performance and durability load-cycle testing under various pressures, temperatures, stoichiometries and relative humidities. Durability testing will include the accelerated testing recommended by DOE in Appendix D of the solicitation, or more rigorous accelerated tests as may be advised at the time. The expected outcome will be the down-selected cathode catalysts which demonstrate the best overall performance and durability when evaluated as 50 to 100 cm^2 MEA's that could meet the 5000 hour lifetime targets.

Subtask 3.2 Large area accelerated durability tests

The purpose of this subtask is to take the down-selected cathode catalysts from Subtask 3.1 and validate with accelerated testing that the same performance and durability is achieved in large area (> 300 cm^2) single (or at most several) cells, using existing, proven stack hardware at 3M. The approach may include at least three stack builds. The expected outcome will be validation that under non-accelerated testing the full size MEA's would meet the 5000 hour targets.

As in original contract

Task 3 Full Size (> 250 cm^2) Single or Multi-Cell Tests

Subtask 3.2 Large area short stack durability tests

3M NUVERA FUEL CELLS

Initiated as a technology integration project with Nuvera Fuel Cells

Driver for a Technology Integration Project between 3M and Nuvera Corp.

- Key opportunity to evaluate for the first time, the combination of the 3M NSTF electrode technology with the Nuvera open flow field bi-polar plate technology.
- Evaluate the NSTF 2008/9 Best of Class MEA's with Andromeda Stack
- Enables joint assessment of any mutual benefits
- Project began ~ Sept. 2009
- Short stack testing at both 3M and Nuvera now underway:
  - Technical exchange of information
  - Testing facilities upgrades
  - Roll-good parts supplied to Nuvera, gasketed CCM's made by Nuvera
  - Hardware delivery and training at 3M for stack assembly
  - First stack build at 3M on Nov. 17, 2009. Operation tried immediately.
    - 16 cell short stack, Andromeda design
    - used 2008 series of MEA (0.1/0.15 PtCoMn loadings) by default
    - stack operation and conditioning began immediately
      - -- exploring stack cell compression
      - -- stack operating conditions
      - -- feeling the way forward with the new combination
    - NSTF CCMs sent to Nuvera for parallel stack build in late Feb., 2010
      - -- (2009 best-of-class NSTF with 0.05/0.10 PtCoMn loadings)

Task 3 Full Size (> 250 cm^2) Single or Multi-Cell Tests
Subtask 3.2 Large area accelerated durability tests

To date:

Time Assembled: ~ 2,900 hours

Time Operated: 100 hours

Short stack under test at 3M Menomonie

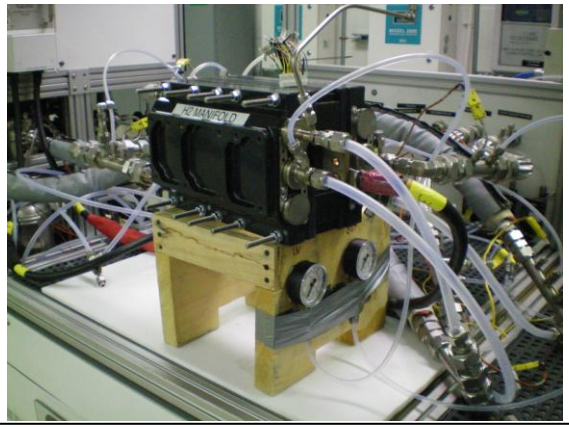

Approximate Event Sequence

Initial Stack Build, 15.5 kgf/cm^2 compression
- Stack operation initiated Nov. 17, 2009
- Break-in conditioning for ~ 25 hrs,

Operation at 3 bar, 75/75/75 for initially for station reasons.

Compression increased to 19 kgf/cm^2
- Operation at 3 bar, various RH, T
- Single cell tests at similar conditions

Compression increased to 22.5 kgf/cm^2
- Operation at various RH, T, P
- Total operating time < 100 hrs to date

Subtask 3.2 Large area short stack durability tests

Excessive H-pump resistance at 2 A/cm^2

Average R ~ 0.096 ohm-cm^2 at 22.5 kgf/cm^2 and 19 kgf/cm^2.

Average R ~ 0.106 ohm-cm^2 at 15 kgf/cm^2

Nuvera Stack Tests with NSTF MEAs. H_2 Pump Experiment. Individual Cell Resistance Values - All Cells. Test conditions: Pressure 1.0 Bar, Stoichiometry 2.0/2.0 (A/C), Stack Humidification 75/75/75 ºC (A/S/C), Stack Compession 15 kgf/cm^2 to 22.5 kgf/cm^2.

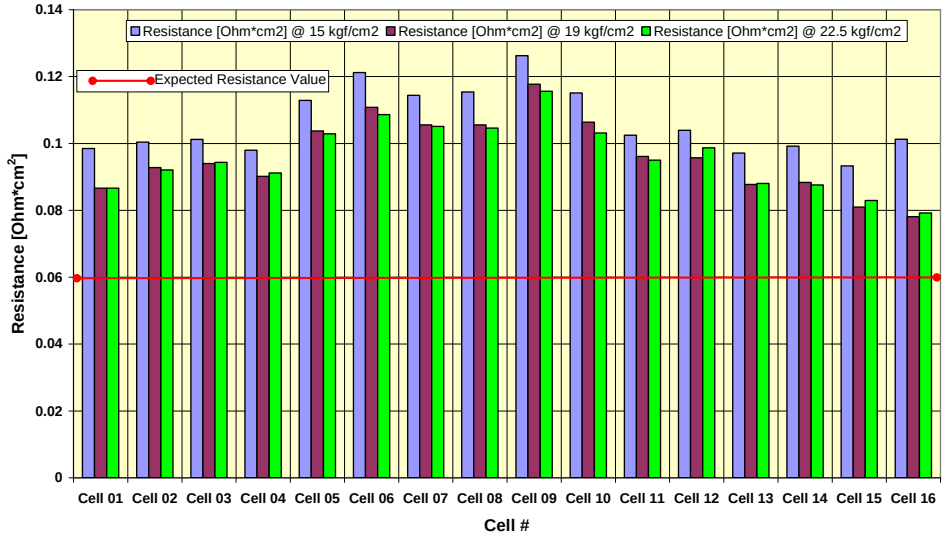

Subtask 3.2 Large area short stack durability tests

3M NUVERA FUEL CELLS

To date:

- Time Assembled: ~ 2,900 hours
- Time Operated: < 100 hours

General Condition

- Stack cell H-pump impedance ~ 80% high
- Performance stable, appears to have conditioned easily
- Exploring stack compression, operating conditions
- Learning to operate safely, understand effects of operating conditions before any durability starts.

Nuvera Stack Tests with NSTF MEAs - Galvanodynamic Polarization (CV) 0-2.0 A/cm^2.
Test conditions: Pressure 3.0 Bar, Stoichiometry 3.0/2.5 (A/C), Stack Humidification 75/75/75ºC (A/S/C), Coolant Flow 25 SLM, Run time 50-75h. Average Cell Voltage Plotted.

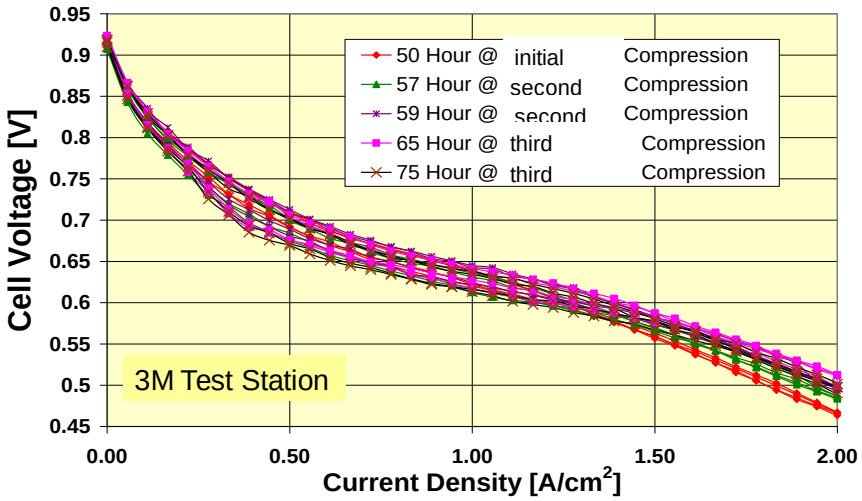

Subtask 3.2 Large area short stack durability tests

3M NUVERA FUEL CELLS

- RH Sensitivity, Temperature Sensitivity Complete
- Lower pressure operation in progress
- Some durability running, then rebuild w/ 2009 BoC CCM

Nuvera Stack Tests with NSTF MEAs - Galvanodynamic Polarization (CV) 0-2.0 A/cm^2.
Test conditions: Pressure 3.0 Bar, Stoichiometry 3.0/2.5 (A/C), Stack Humidification 75/75/75 ºC (A/S/C), Coolant Flow 25 SLM, Third Stack Compession , Run time 75 h.

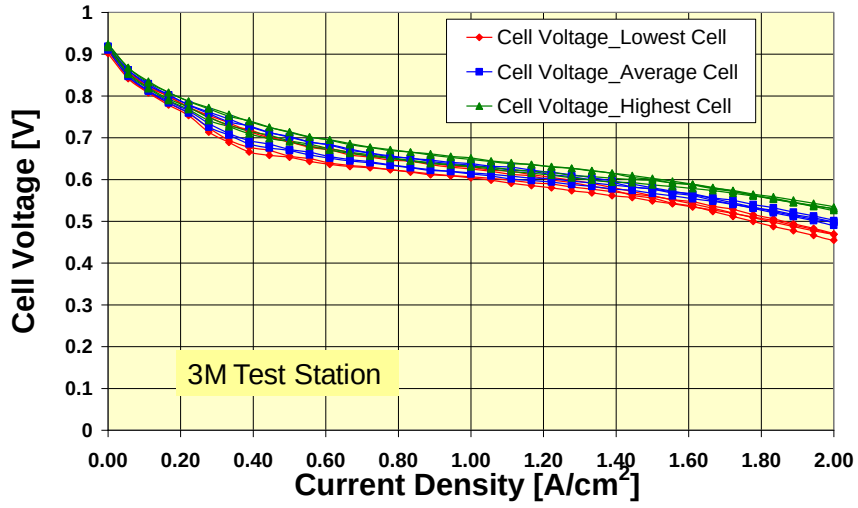

Subtask 3.2 Large area short stack durability tests

Single cell comparisons to Nuvera stack test conditions

Objectives:

- Assess correlation of stack cell voltage deviations from the average at 2 A/cm^2 with H-pump cell resistance deviations:
  - comparison of H-pump resistance sensitivity factors at different compressions,
  - extract estimate of contributions to cell-cell voltage variability from non-resistance factors
- Comparison of best cell performance with 50 cm^2 single cell
- Project performance of stack's **best** cell performance if H-pump impedance could be reduced by 0.040 ohm-cm^2 to ~ 0.05 ohm-cm^2 and compare to single cell performance.

3M Advanced Cathode Catalysts and Supports…… DOE Review, March 16, 2010

Subtask 3.2 Large area short stack durability tests

Single Cell Tests to Compare with Current Andromeda-NSTF Stack Build

- Cell: 50 cm^2, Quad-Serpentine flow fields
- CCM: NSTF "2009 Best of Class"
- GDL: 3M 2979
- Break-in conditioning: Fast start-up protocol #52, Station 1
- Objective: MEA testing at Nuvera stack operating conditions in order to provide insight on impedances and mass transport over-potentials that may be useful in understanding the stack's MEA conditions.

Reduced anode pressure, some anode RH and lower anode stoich.

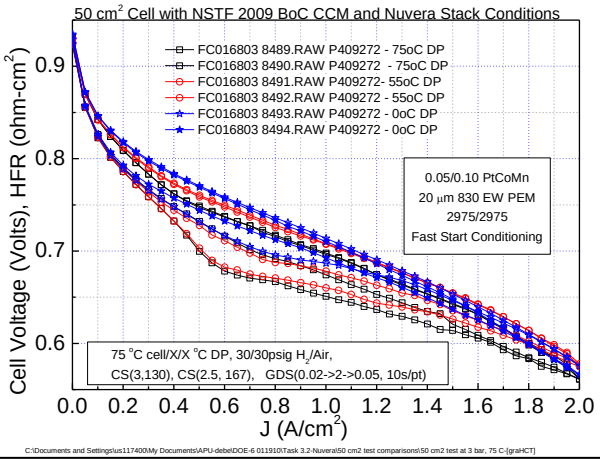

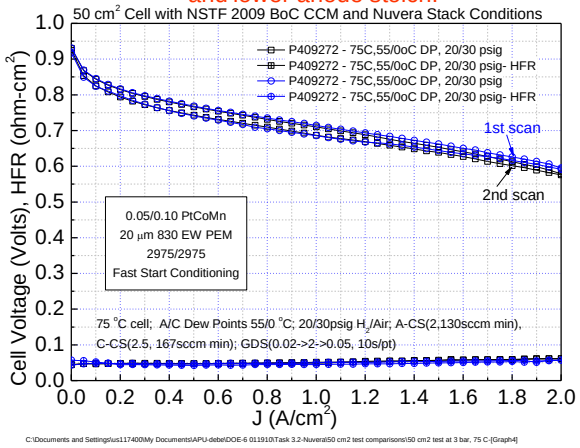

Subtask 3.2 Large area short stack durability tests

Single cell comparisons to Nuvera stack test conditions

Operating at 20/30 psig and 55/0 °C dew points helped by ~ 15 mV at 2 A/cm^2 compared to 30/30 psig and 0/0 °C dew points.

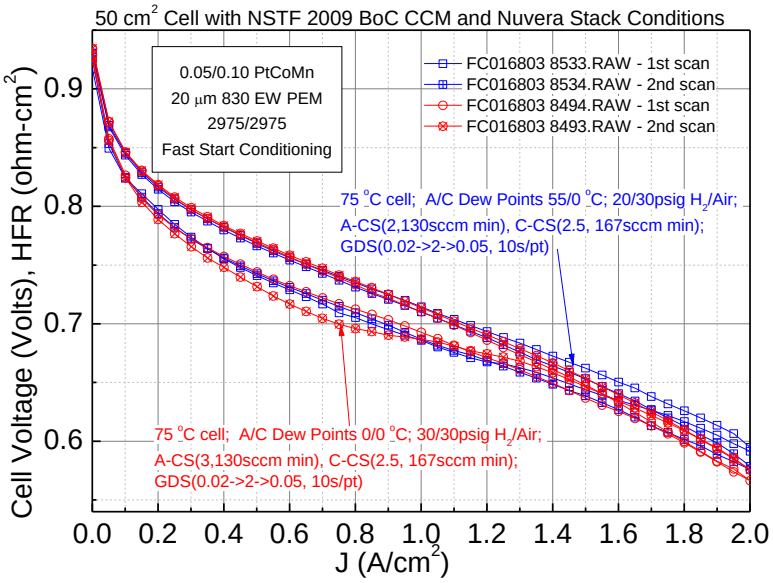

C:\Documents and Settings\us117400\My Documents\APU-debe\DOE-6 011910\Task 3.2-Nuvera\50 cm2 test comparisons\50 cm2 test at 3 bar, 75 C-[Graph6]

From analyses of HFR and IR-corrected ….

To reach 650 mV at 2 A/cm^2 :

- Reduce excess HFR by 0.010 ohm-cm^2
- Reduce MTO from 60 to ~ 30 mV.

3M Advanced Cathode Catalysts and Supports…… DOE Review, March 16, 2010

Subtask 3.2 Large area short stack durability tests

Correlation of Cell Voltage at 2 A/cm^2 with H-pump resistance

- Higher compression does appear progressively improve average stack cell voltage at current densities above 1 A/cm^2. Very clear at 2 A/cm^2.
- Some of the improvement may be due to improved performance over time.

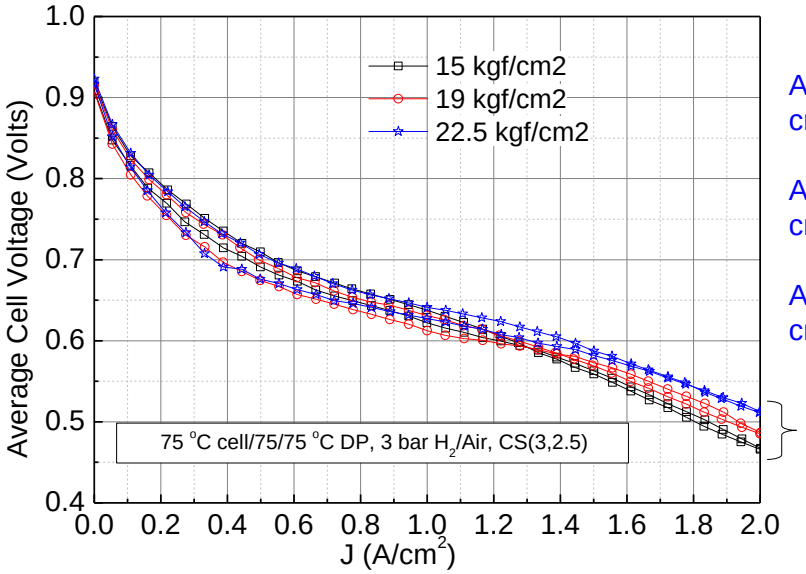

C:\Documents and Settings\us117400\My Documents\APU-debe\DOE-6 011910\Task 3.2-Nuvera\Stack -variable conditions tests\Correlations of R and V-[Graph4]

Average R ~ 0.0959 ohm-cm^2 at 22.5 kgf/cm^2

Average R ~ 0.0962 ohm-cm^2 at 19 kgf/cm^2.

Average R ~ 0.106 ohm-cm^2 at 15 kgf/cm^2

Monotonic increase at 2 A/cm^2 not due to just reduction in average R.

Subtask 3.2 Large area short stack durability tests

Correlation of Cell Voltage at 2 A/cm^2 with H-pump resistance

- There appears to be some correlation of cell voltage with H-pump resistance.
- Plot cell voltage difference about average versus cell resistance difference about average: (next slides)

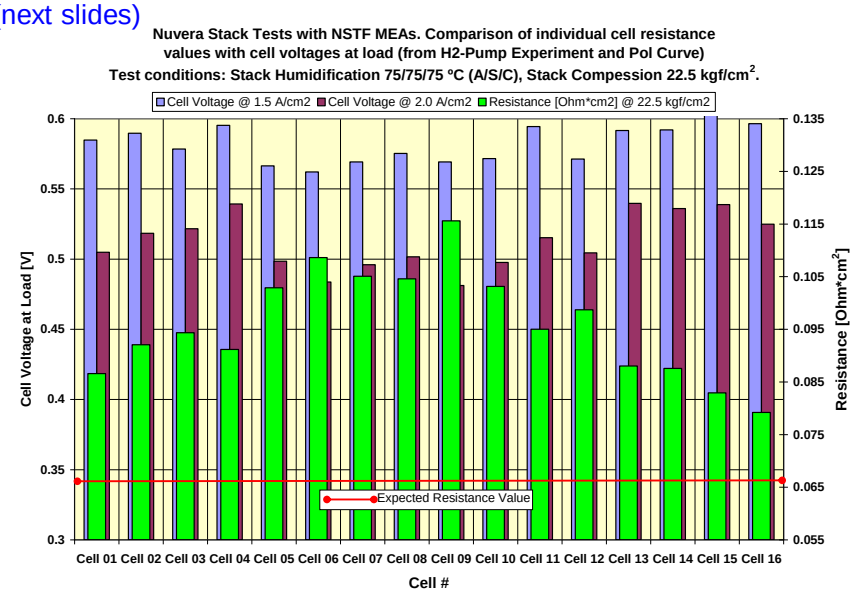

3M Advanced Cathode Catalysts and Supports…… DOE Review, March 16, 2010

Subtask 3.2 Large area short stack durability tests

Correlation of Cell Voltage at 2 A/cm^2 with H-pump resistance

- At 15 kgf/cm^2 compression, the variation of cell voltage about the mean at 2 A/cm^2 appears to correlate fairly well with the variation in H-pump resistance.
- R^2 = only 80.5%, intermediate to the other compression values.

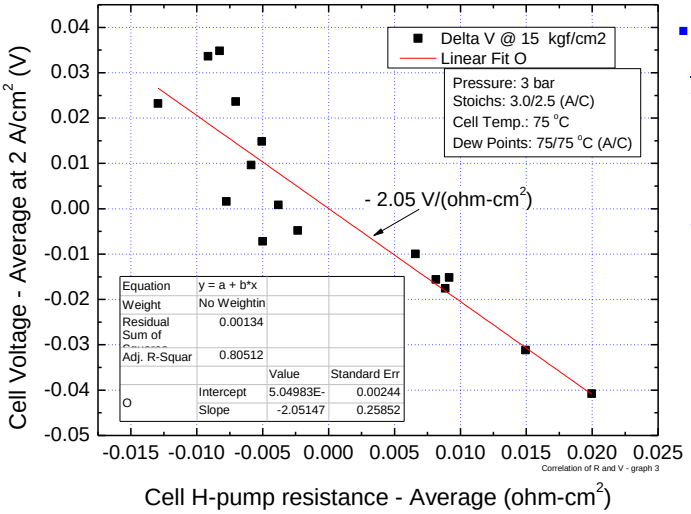

- 1 σ standard deviation of ± 0.26 V/ohm-cm^2 implies that for R = ~ 0.1 ohm-cm^2 resistance, only ± 26 mV variation is due to non-resistance cell to cell variability factors.

Subtask 3.2 Large area short stack durability tests

Correlation of Cell Voltage at 2 A/cm^2 with H-pump resistance

- At 19 kgf/cm^2 compression, the variation of cell voltage about the mean at 2 A/cm^2 appears to correlate well with the variation in H-pump resistance.
- R^2 = 90.5%, higher than at other compression values.

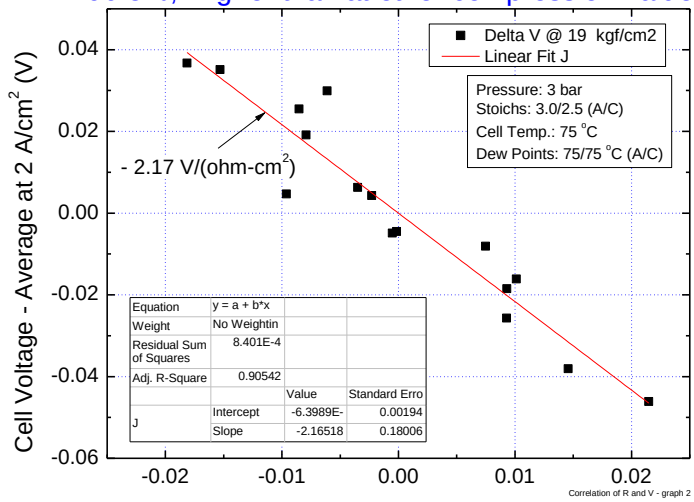

- 1 σ standard deviation of ± 0.18 V/ohm-cm^2 implies that for R = ~ 0.09 ohm-cm^2 resistance, only ± 16 mV variation is due to non-resistance cell to cell variability factors.

Subtask 3.2 Large area short stack durability tests

Correlation of Cell Voltage at 2 A/cm^2 with H-pump resistance

- At 22.5 kgf/cm^2 compression, the variation of cell voltage about the mean at 2 A/cm^2 appears to correlate fairly well with the variation in H-pump resistance.
- R^2 = only 73%, less than at lower compression values.

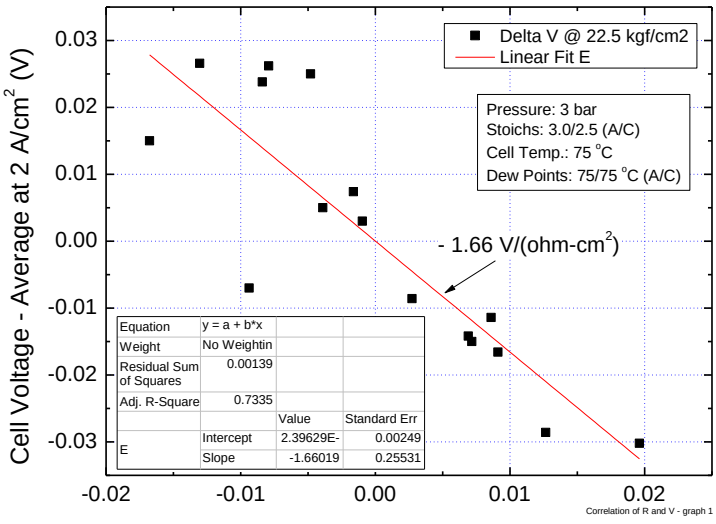

- 1 σ standard deviation of ± 0.26 V/ohm-cm^2 implies that for R = ~ 0.09 ohm-cm^2 resistance, only ± 23 mV variation is due to non-resistance cell to cell variability factors.
- Sensitivity factor of -1.66 V/ohm-cm^2 implies a gain of 83mV at 2 A/cm^2 (or 0.0415/(A/cm^2)) could result if the H-pump resistance was reduced by 0.040 ohm-cm^2.

Subtask 3.2 Large area short stack durability tests

Project stack performance at lower H-pump resistance

Use the H-pump resistance sensitivity of -1.6 V/ohm-cm^2 at 22.5 kgf/cm^2 to project the stack's average cell performance at 75/75/75 ^{o}C:

- If H-pump reduced by 0.040 ohm-cm^2, stack average cell voltage would exceed the 50 cm^2 single cell voltage above 1.2 A/cm^2.
- Lower stack voltage below 1.2 A/cm^2 reduced by drier or hotter operation as on next slide.

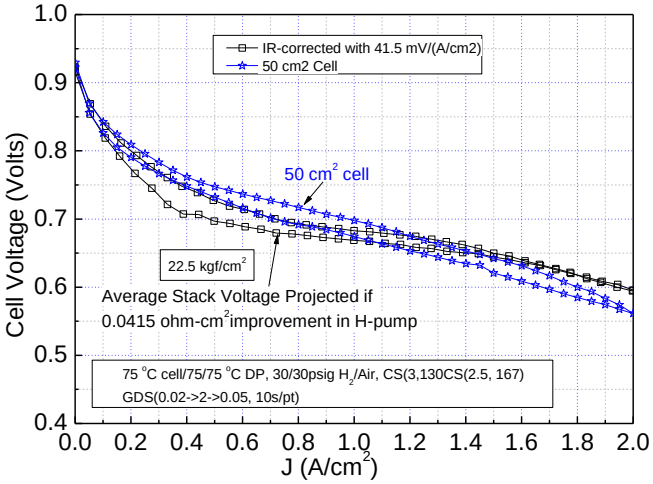

3M Advanced Cathode Catalysts and Supports…… DOE Review, March 16, 2010

Subtask 3.2 Large area short stack durability tests

Correlation of Cell Voltage at 2 A/cm^2 with H-pump resistance

Conclusions:

- Individual cell voltages at 2 A/cm^2 correlate quite well with the H-pump resistances at each compression level for the 75/75/75 ^{o}C, 3 bar conditions.
- Non-resistance contribution to cell to cell voltage variability is ~ 25 mV at 2 A/cm^2. This suggests mass transport variations are small.
- If the average H-pump resistance could be reduced by 0.04 ohm-cm^2, the stack voltage would exceed single cell performance above 1.2 A/cm^2.
- The stack's best individual cell performance at 80/80/80 ^{o}C is within 50mV of the 50 cm^2 cell performance at 75/75/75 ^{o}C.

Subtask 3.2 Large area short stack durability tests

Comparison of stacks best cell performance with single cell performance

Stack's best cell performance at 80/80/80 °C and third compression level is:

- within 50mV of the single cell performance at 75/75/75 °C
- shows less hysteresis than single cell curves.
- improved relative to 75°C stack operation below 1 A/cm^2.

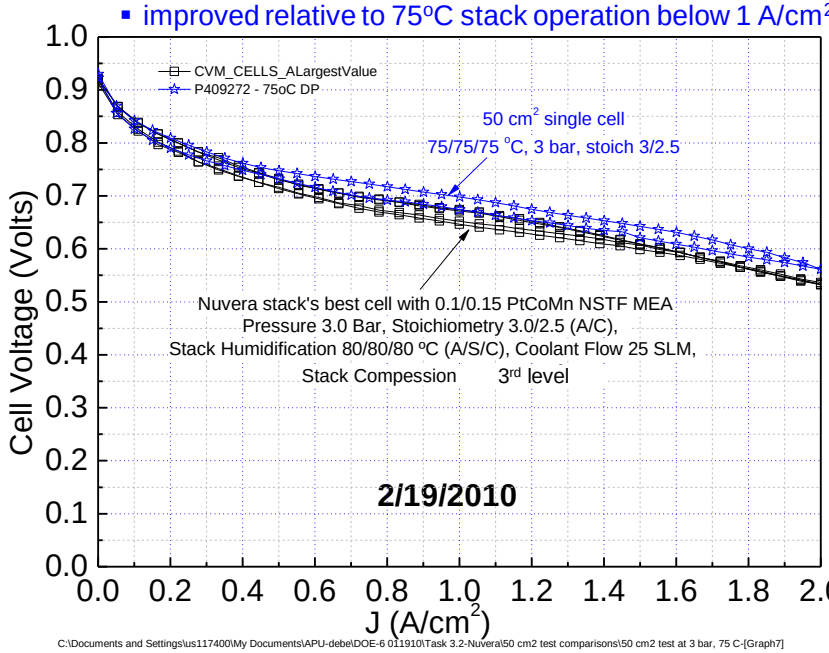

C:\Documents and Settings\us117400\My Documents\APU-debe\DOE-6 011910\Task 3.2-Nuvera\50 cm2 test comparisons\50 cm2 test at 3 bar, 75 C-[Graph7]

Next Steps:

- Lower pressure test series.
- 4th compression level
- Re-build with 2009 BoC CCMs
- Work with Nuvera on their stack testing.

Task 4

Selected Supplementary Information

Subtask 4.1 Durability tests of new NSTF supports

From the statement of work for this project, "the purpose of subtask 4.1 is to specifically evaluate the stability of the new NSTF based catalyst supports derived from Subtask 1.1. The approach will use accelerated tests to evaluate stability of the catalyst activity and surface areas against corrosion of the support from high voltage cycling, stop/start cycling or fuel starvation. Both high through-put characterization methods as well as 50-cm^2 single cell tests will be included in the approach. The expected outcome is a down-selection of the new NSTF catalyst supports from Subtask 1.1 that also meet the durability requirements."

The Tasks 1.1 series of experiments, WAO-1, 2, 3 and 4, explored optimization of the NSTF PR-149 whisker support characteristics for best overall fuel cell performance and was highlighted in Section 9.8. Fig. 9.21(A,B) showed ORR mass activity was linearly dependent on the Pt ECSA coating the support whiskers, but was not a discerning function of the PR-149 thickness until it exceeded about 2000 units. Fig. 9.21(C,D) also showed that the polarization curves were not a strong function of the growth parameter in the range of 1 to 5. Fig. S6 below shows similar results for the intermediate growth parameter value of 3. The fuel cell performance is independent of the PR-149 thickness parameter in the range of 1800 to 2400 units.

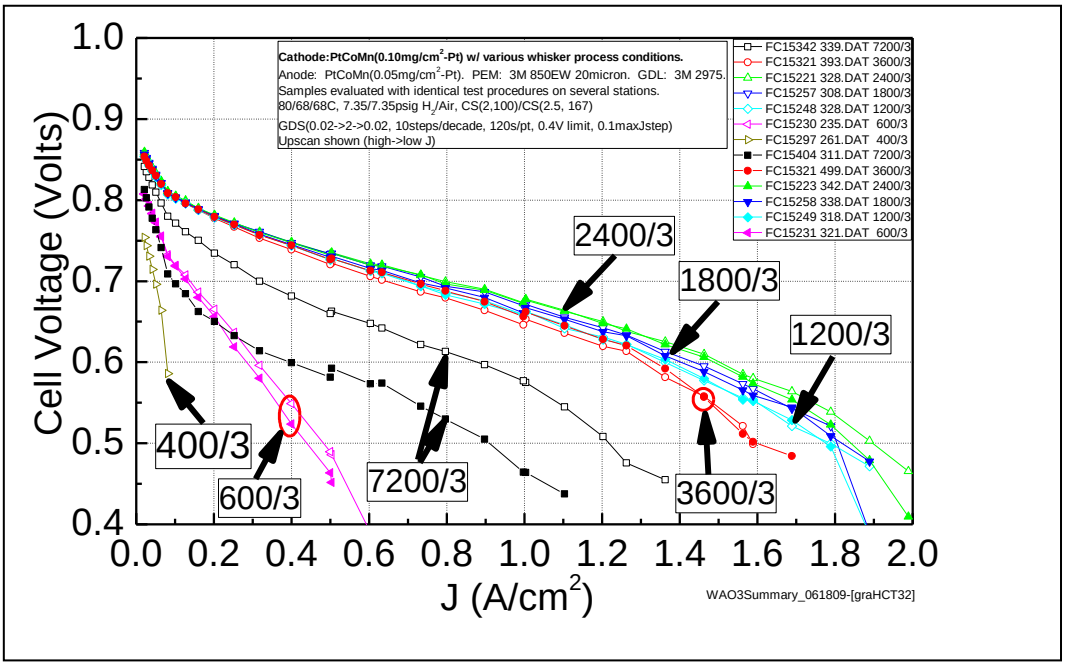

Fig. S6. Polarization curves for the WAO-3.2 series of whisker growth for the thickness range of 400 to 7200 units and the growth parameter value number 3.

Since the PR-149 thickness value and the growth parameter value for the "standard" NSTF whiskers were approximately at the 2000/3 values before this project began, a major conclusion of the Task 1.1 experiments is that there was no substantial improvement to be made by changing these whisker growth parameters. This means that all the durability evaluation work done under Task 2, testing new catalyst compositions on standard whiskers in 50 cm^2 single cells and as compositional spreads applied by Dalhousie University to the NSTF standard whiskers, met the objectives of subtask 4.1.

Task 5

Selected Supplementary Information

Task 5.0 - Optimized NSTF MEA Roll-good and Stack Testing

Tasks: 5.1. NSTF catalyst / low EW membrane interface optimization and 5.2. Optimized anode and cathode GDL's

Tasks 5.1 and 5.2 were critical precursors to Task 5.3 since the membrane, catalysts and GDL's can significantly affect one another. However, when doing catalyst development it is necessary to fix the membrane and GDL in order to screen the catalyst parameter one is studying. Ultimately it is necessary to vary the membrane and GDL properties as well since it otherwise can never be known if the three system components are optimized for working together and meeting such diverse requirements as performance, durability, and operational robustness.

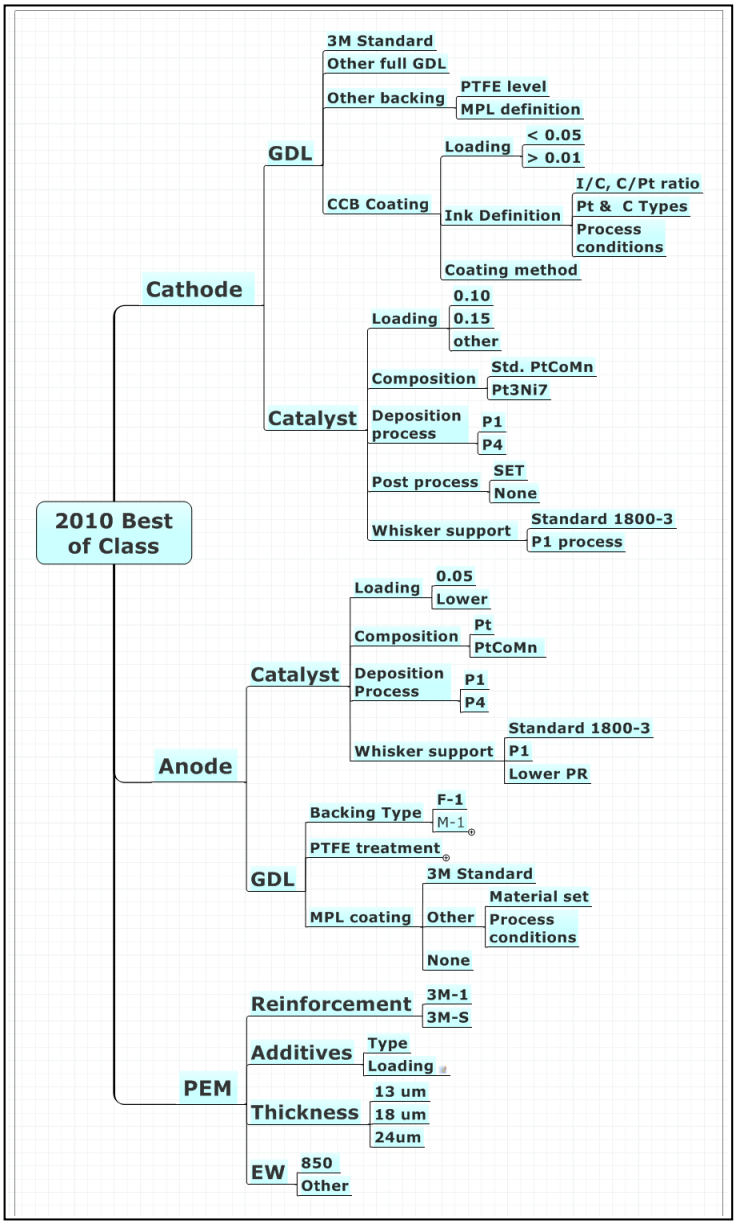

Throughout this project, as improvements were realized in the membranes and GDL's, the new components and a multitude of process and material parameters were evaluated with the continuously improving cathode NSTF catalysts to try and produce the best performing MEA that would go into the final stack testing. The number of variables becomes excessively large, and requires hundreds of different MEA's tested in duplicate at a minimum in order to develop a clear understanding of the component interactions.

In preparation for Task 5.3, the optimization process towards a 2010 best of class MEA went on for over a year as the combinations of material and process decisions illustrated in Fig. S7 below were explored.

Fig. S7. Illustration of the process map used in Tasks 5.1 and 5.2 for optimizing the MEA components for down-selection for stack testing in Task 5.3.

Technical Accomplishments and Progress: GDL Optimization for NSTF CCM

Electrode backing (EB) carbon paper : Designed Experiment

- 7 commercial roll-good papers
  - Variables: wet proofing and MPL coating area weight (necessary due to variable EB)
- 3 commercial fully coated GDLs also evaluated

Results: Fuel cell results for all were significantly poorer than 3M baseline GDL

Baseline carbon paper improvement : Designed Experiment

- Variables : wet proofing and MPL area weights
- Seven fuel cell performance metrics

Results:

- No single set of GDL parameters were optimum for all seven fuel cell metrics.
- For steady state cool performance, optimal GDL parameters were different for dry conditions (0 % RH) and wet conditions (100 % RH).
- Good second order linear regression fits were obtained for three responses (PDS, cathode stoich. sensitivity, and % RH sensitivity at 90/60/60 °C).

Asymmetric anode/cathode GDLs with baseline EB paper : Designed Experiment

- 2^{4-1} factorial with center point replication
- Variables : wet proofing and MPL coating area weight
- **Still in progress -** Largest improvement so far was for extreme difference for anode and cathode GDLs: high wet proofing and MPL weight for cathode and low wet proofing and MPL weight for anode.

Technical Accomplishments and Progress: GDL Optimization for NSTF CCM

Best GDL Approaches Identified to Date

GDL	PDS, 70 C	GDS, 7.35 psig, 80 C	GDS, 14 psig, 85 C	Cathode Stoich Sensitivity	% RH Sens.,	Steady State Cool Start amps/cm^2 at 0.6 V			
	V at J = 1.2	V at J = 1.5	V at J = 1.5	V at 1.4 CS, 80 C	Volts at 90/50/50 C/%RH/%RH	30 C, 0/0	30 C, 100/100	40 C, 0/0	40 C, 100/100
Baseline GDL	0.607	0.540	0.600	0.522	0.588	0.342	0.209	0.540	0.250
GDL A	0.603	0.584	0.625	0.521	0.612	0.305	0.172	0.490	0.203
GDL B	0.623	0.591	0.628	0.531	0.536	0.295	0.120	0.514	0.169
GDL C	0.602	0.578	0.629	0.498	0.596	0.277	0.130	0.467	0.154
GDL D	0.595	0.567	0.614	0.510	0.612	0.334	0.200	0.549	0.235

- Greatest higher temperature improvements were for GDL Type B (15 mV for PDS and 30 to 50 mV for GDS).
- Generally poorer steady state cool performance results than for baseline GDL.
- Overall best results with minimal impact on steady state cool performance was for GDL D.

3M Advanced Cathode Catalysts ..... 2009 DOE Hydrogen Program Review, May 18 - 22

Task 5.2 – Optimized anode and cathode GDL's

"Fundamental" GDL property characterization

One of the areas of research undertaken as part of Task 5.2 for optimizing the GDL's for use with the NSTF CCM's was to obtain basic physical and chemical property measurements of the GDL backing layers to develop understanding of the structural characteristics critical for desired water management. This is distinctly different from screening materials and process factors for functional performance trends which was a major activity of the project Task 5.2. Simple to execute, "easy" to interpret liquid water permeability measurements on as-received GDL backing materials from different manufacturers, and PTFE treated GDL's. The approach here was to start with the most basic and elementary measurements of liquid water permeability to try and see what physical characteristics of the GDL media might be most critical. The work began at the start of the project and has mainly been completed except for most important result of extracting those critical properties. A number of intriguing insights have been gained however.

Water permeability measurements

The basic premise of the approach was to make liquid water permeation measurements through a wide variety of commercially available GDL media based on primarily capillary flow, as illustrated in Fig. S8.

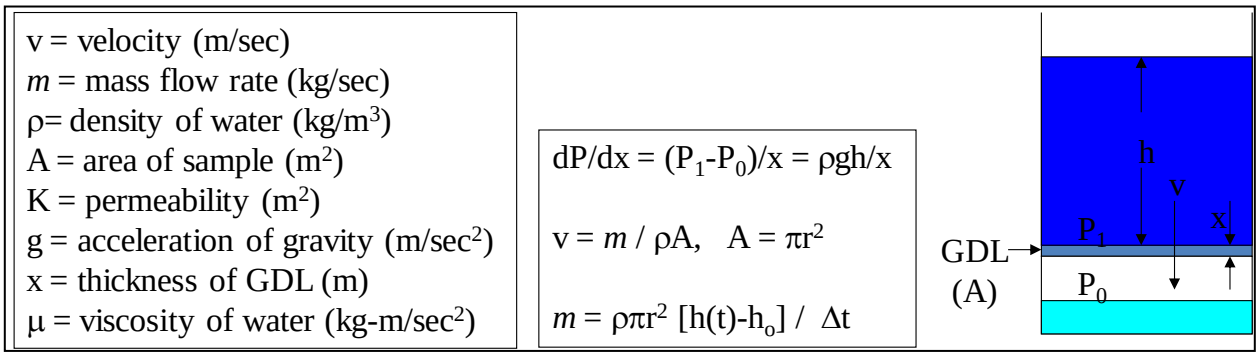

Fig. S8. Concept for simple measurement of liquid water permeability, K, through GDL media.

This flow can be characterized by an effective permeability, K, using Darcy's Equation:

(3) $$v(\text{m/sec}) = -(K/m)dP/dx,$$

where the variables are defined in Fig S8. The velocity of a fluid through a porous media is proportional to the pressure gradient in the media and inversely proportional to the liquid viscosity. In practice, this simple approach involved repeated measurements of the mass flow rate, *m*, of water flowing through an area A of the GDL, due to the pressure generated by a standing column of water of height h placed over the area A, without edge leaks. Fig**.** S9 illustrates this. A test method and assembly were worked out with numerous trials and experiments. Very dramatic hysteresis effects and widely ranging rates of water transmission were observed with all the different types of GDL media. The final methodology was very reproducible. It was applied to twelve types of "as-received" GDL electrode backing materials from seven suppliers. Sample pieces were die-punched from four locations on each sample as illustrated in the plan view in Fig. S9. Then six runs with each sample piece were made, recording the time for a certain volume of water to flow through the sample while maintaining a constant water head constant. Another variation practiced, recorded the time for a given volume to flow through the sample from water head h_1 to h_2.

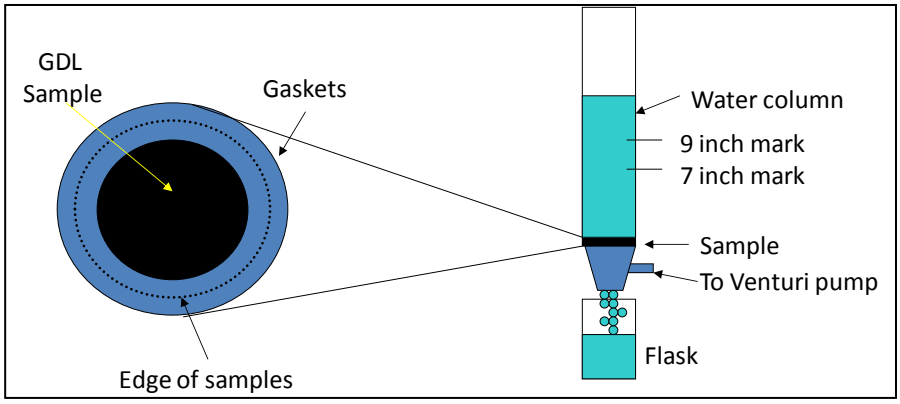

Fig. S9**.** Lab set-up for implementing the concept for measuring the liquid water permeability in Fig. S8. The GDL samples' flow-through area were 1 inch in diameter.

Fig. S10 shows the measured water mass flow rates as a function of trial number for ten of the GDL media. All samples were as-received electrode backings with no hydrophobization or microporous layers (MPL's). The error bars reflect the root means squared deviation from 3 to 4 samples of each type. Flow rates were determined from measured time for 175mL flow volume with ± 10mL uncertainty. All measurements were at ambient temperature.

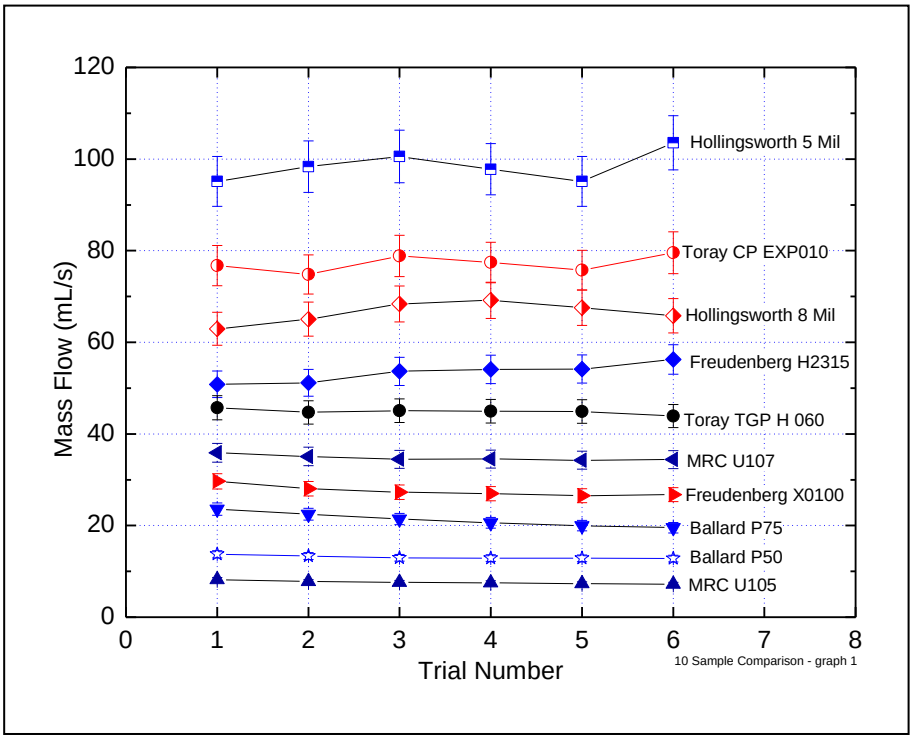

Fig. S10. Mass flow rates as a function of trial number for ten different GDL backing media using the approach shown in Figs. S8 and S9.

Fig. S11 shows SEM images of 6 of the GDL material evaluated showing dramatic variations of microstructure, despite most using common sized carbon fibers. The variations are due to the different types of binder material used by the manufacturer. The pore sizes distributions might be expected to be greatly different among them.

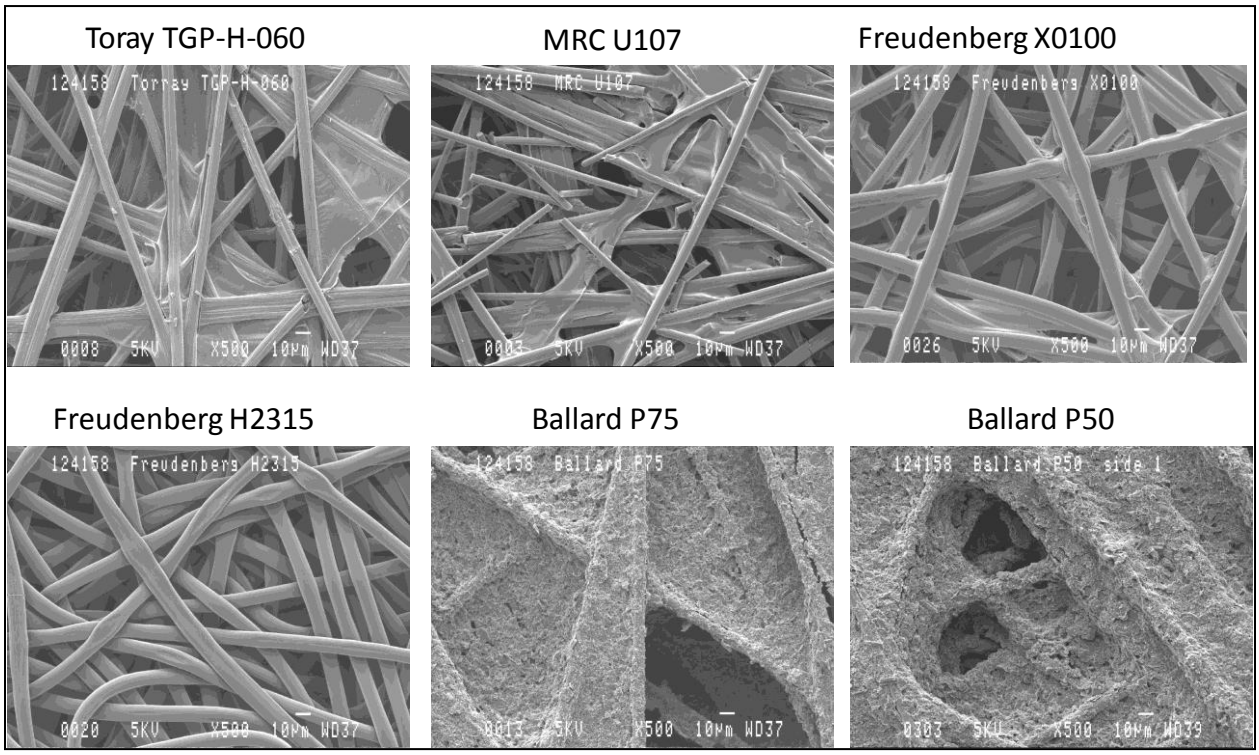

Fig. S11. SEM images at 500 X magnification of six of the GDL media evaluated showing dramatic variations of microstructure, despite most using common sized carbon fibers.

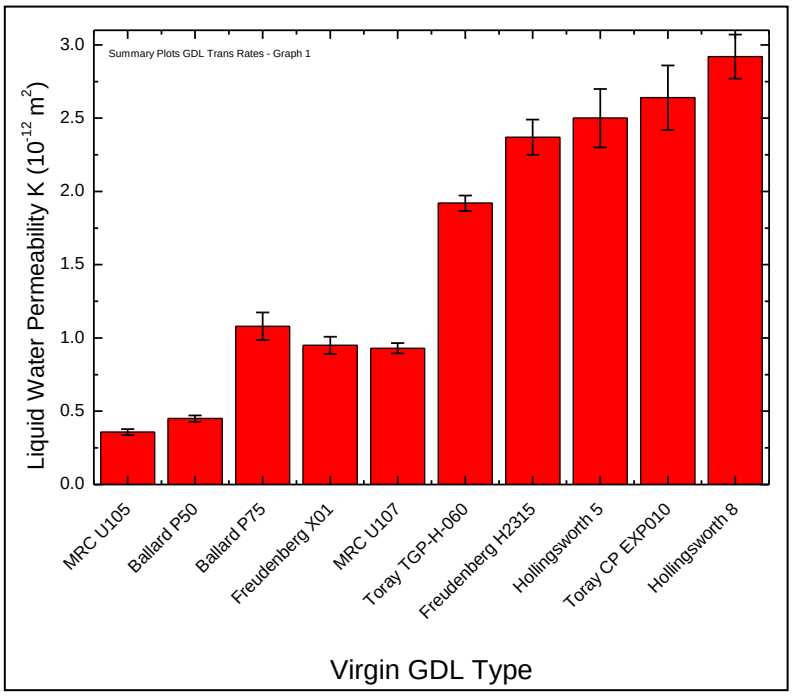

Fig. S12. Liquid water permeability values calculated for 10 as-received carbon paper GDL Backing papers from mass flow measurements in Fig. S10 and Darcy's equation (3).

Using the mass flow data in Fig. S10 and Darcy's equation (3), the liquid water permeability, *K*, can be calculated from:

(4) $K = -\mu\, m x / (\rho^2 A g h)$ and $m = \rho\pi r^2 [h(t)-h_o] / \Delta t$

as shown in Fig. S12. The value of *K* appears to vary an order of magnitude among these types.

The next step is to see if this sizeable difference can be attributed to some physical property of the GDL backing layers. This is a difficult task, as there are aspects of the GDL's composition that cannot be obtained from their suppliers. One intriguing model concept we have been pursuing is that the very large pore porosity and possibly the shape of those pores, is a key parameter since the liquid water would most naturally go through the large pores rather than smaller pores, regardless of surface wetting characteristics of the fibers and binder material comprising them. We consider then, as a first approximation, that the GDL media consist of two solid phases, the very dense carbon fibers, and the different binders of varying density. By large pores we mean the large, irregularly shaped, highly angular apertures with dimensions of 10 to 50 microns seen in the SEM images of Fig. S11. The water will flow completely or substantially only through the large pores or apertures defined by the carbon fibers where binder is not present. It will not flow through the very small pores or cracks in the binder phase of the papers. This is because the smaller holes would have a substantially higher pressure drop to pass water than the larger holes, so it would naturally take less energy to flow at a slightly faster rate through any adjacent large aperture or hole

As stated, the water permeability should be a function only of the large holes or pores defined by the non- carbonized binder areas between the fibers. If so, then this large-pore porosity factor, P_{LP}, would be the primary factor determining the liquid water permeability, *K*.

To explore this further, let P_{LP} be the porosity of the large pores only, V_f and m_f the volume and mass of the carbon fibers respectively, and V_b and m_b the volume and mass of the binder respectively, where the volume of the micro-pores inside the domain of the binder phase is included in the value of V_b. Define also $V_b / V_f = \delta$, and $m_b / m_f = c$, and let *V* = the total sample volume.

Then the measured sample density is $\rho_m = (m_b + m_f) / V = (m_f/V)(1+c)$, and the individual phase densities are $m_f = \rho_f V_f$, and $m_b = \rho_b V_b$ for the fiber and binder respectively. We can assume that the density of the fibers is that of solid carbon, $\rho_f = 2$ g/cm^3. The large pore porosity, P_{LP}, is then defined from the void volume as:

5) $P_{LP} \equiv 1 - V_f / V - V_b / V = 1 - (1+\delta)\, V_f / V$, which can be rewritten as,

(6) $$P_{LP} = 1 - \frac{1+\delta}{\rho_f}\frac{m_f}{V} = 1 - \frac{1+\delta}{\rho_f}\frac{\rho_m}{(1+c)} = 1 - \frac{\rho_m}{h\rho_f}$$, where

7) $h = (1+c)/(1+\delta) = (1+ m_b/ m_f)/ (1+ V_b/ V_f)$.

So we have a single parameter, *h*, that can be used to adjust the single solid phase porosity, $P_s(\%) = 100\%(1-\rho_m/ \rho_f)$. A plot of the permeability values from Fig. S12 versus the measured density (single solid phase) of the GDL media gives no correlation or apparent functional relationship. But assuming a two-phase (solid) media, of dense fibers and less dense binder, we can pose the question of what value of *h* is required to make all data points for the various carbon papers fall on a single linear function of *K* vs $P_s(\%)$. By inverting (6) and solving for *h* with the definition of P_s, it results that

(8) $h = (1- P_s) /(1- P_{LP})$,

where the value of P_{LP} is obtained from the plot of K versus P_s.

Fig. S13 shows the resulting plot of permeability versus the large pore porosity, for the values of h used to bring all the measured points coincident with a straight line drawn between the two Freudenberg papers, since they consist of just the single solid phase carbon fibers, i.e. they do not appear to contain any binder phase. Since they have no secondary resin phase carbon, h = 1 is assumed for these two GDL papers. Fig. S13 shows that with very reasonable values of h a remarkable correlation is revealed between K and the large-pore porosity. The insert table in Fig. S13 shows the calculated values of h that collapse all the K vs P_{LP} data onto a single straight line.

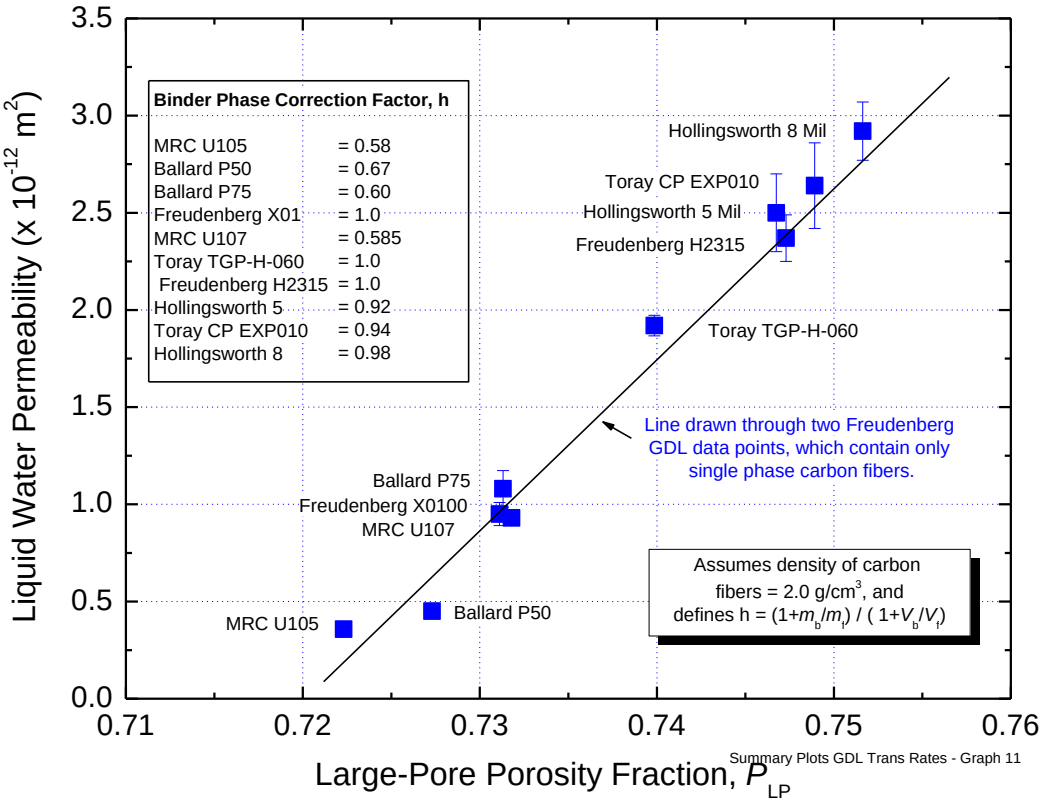

Fig. S13. Plot of the GDL liquid water permeability's vs the large-pore porosity calculated from equations (5)-(8) for the "best fit" values of parameter h listed in the inset table.

If we had measured values of m_b, m_f, and ρ_b, then we could determine the values of h from measured quantities using equation (8). (We do not know of any method to do this currently.) Since the density of the binder is less than the solid carbon fibers, the value of $h \leq 1$. The extracted values of h shown in Fig. S13 are consistent with this constraint. Also, it appears reasonable that the more porous the binder phase appears, the larger the value of h, as in the MRCU105, and the Ballard P50 and P75 cases. The number of solid carbon fibers per unit volume and their size would also affect the large pore volume, and presumably is the reason for the porosity difference of the Freudenberg H2315 and X0100 samples.

There are several important conclusions that can be drawn from this analysis:

1) The steepness of the slope of *K* versus the large pore porosity shows a very sensitive function of the permeability on the structure and volume of the large pores. This may also explain to the sensitivity to compression for some materials.

2) It appears that there is a large-pore porosity percolation threshold value of ~ 72% below which there is negligible liquid water permeability for the small pressure head used for these measurements.

3) Based on the above analysis, it is remarkable that the water permeability is explainable simply on the basis of physical structure and not surface chemistry. This may be explainable if the large pores are sufficiently sized that water can flow through them with minimal effect from the surface or requirement for surface wetting. Also, it suggests that just the overall, effective porosity is what is important, and not the shapes and sizes or topology of the pores. In a second series of measurements, using twelve GDL types hydrophobically treated with PTFE at levels between 0% to 5 wt %, the presence of the PTFE did not dramatically change or affect the water permeability of most of the GDL types, consistent again with the physical structure being the critical factor for liquid water transport.

We believe these results suggest that some physical property of the GDL papers not presently known is critical for determining their ability to transport liquid water. Our own viewpoint is that classical theories that model transport of liquids through these types of porous media using conventional models for interconnected, round, tubular shaped pores, are not adequate to treat these kind of materials, where the pores appear to be more like stacks of irregularly shaped apertures. In this case, it may be more the energy required to deform a column or “tube” of water as it is forced through the matrix of stacked angular apertures, that determines the effective permeability. This may then depend more on some non-intuitive statistically derived characteristic of the GDL’s apertures or pores, such as might be extracted from mass and pore morphological metrics determined from X-ray CT Images. We have made some effort in this regard, but have not found a unique characteristic yet.

Technical Back-Up Slide

Task 5.1/5.2/5.3 – MEA Integration for Final Stack Testing

❑ **2010 Best of Class" MEA component down-selection process**

Example 4: Cathode GDL Options

Cathode GDL Options:

- Backing type: Fixed, 3M Standard
- Hydrophobic treatment - % PTFE
- MPL type – probably fixed
- Hybrid vs non-hybrid (Hybrid CCB)
  - Pt/C type and loading, I/C ratio,
  - C diluent fraction
  - Coating chemistry and method

Deciding Factors:

- Water management metrics (enhanced water out the cathode)
- ORR metrics
- HCT metrics (Mass transfer overpotential) at high temperature
- Pt loading cost/benefit ratio
- Accelerated stress tests

Hybrid Type B: US 6,238,534

- Anode = NSTF Pt, 0.05 mg/cm^2
- **Cathode = 3M Gradient** = NSTF + Pt/C (CCB on 3M GDL)
- PEM = 3M 20 µm,
- Anode GDL = MPL-free type A used as-received

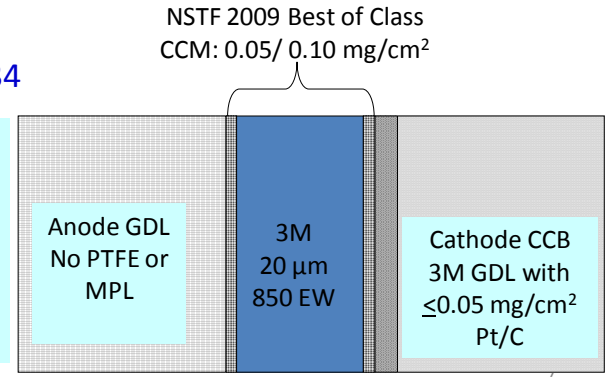

Task 5.1/5.2/5.3 – MEA Integration for Final Stack Testing

❑ 2010 Best of Class" MEA component down-selection process

Example 6: Cathode GDL Options

- At 200 and 270 kPa (peak power) Hybrid B performance and HFR are insensitive to temperature and humidity over ranges shown.
- 0.84 V at 0.1 A/cm^2 at highest pressure,
- Only ~ 40 mV of MTO (η_{tx}) at 200 kPa and 90°C at 2 A/cm^2.

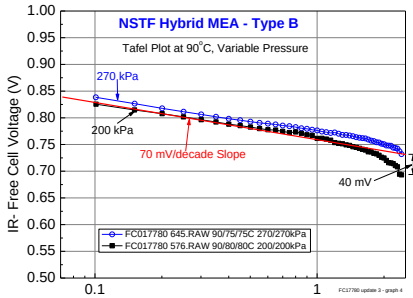

MTO 40 mV @ 2 A/cm^2

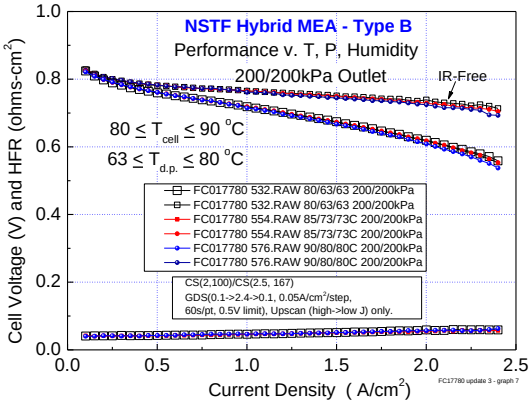

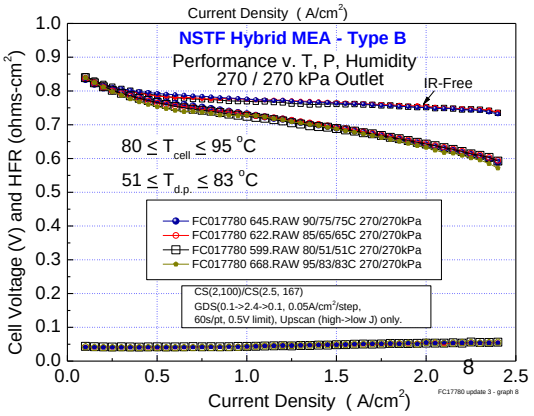

Task 5.1/5.2/5.3 – MEA Integration for Final Stack Testing

❑ 2010 Best of Class" MEA component down-selection process

Example 6: Cathode GDL Options

Cathode GDL Options:

- Backing type: Fixed, 3M Standard
- Hydrophobic treatment - % PTFE
- MPL type – probably fixed
- Hybrid vs non-hybrid (Hybrid CCB)
  - Pt/C type and loading, I/C ratio,
  - C diluent fraction
  - Coating chemistry and method

Deciding Factors:

- Water management metrics (enhanced water out the cathode)
- ORR metrics
- HCT metrics (Mass transfer overpotential) at high temperature
- Pt loading cost/benefit ratio
- Accelerated stress tests

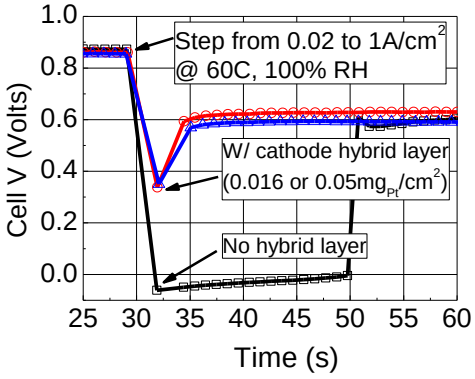

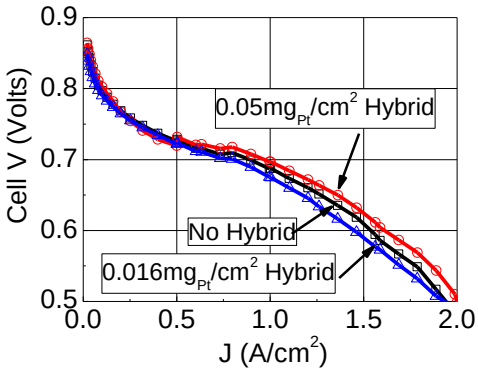

Task 5.1/5.2/5.3 – MEA Integration for Final Stack Testing

❑ 2010 Best of Class" MEA component down-selection process

Example 6: Cathode GDL Options: Hybrid B: 30ºC Steady State vs. P_{Anode}

- Hybrid B MEA's show significant low Temperature benefit relative to NSTF CCM-only.
- Water management effects of cathode CCB and Anode GDL, P_A appear primarily additive:
  - CCB helps take water out cathode
  - Anode GDL and low anode pressure help take water out the anode.

Benefit of water out the anode

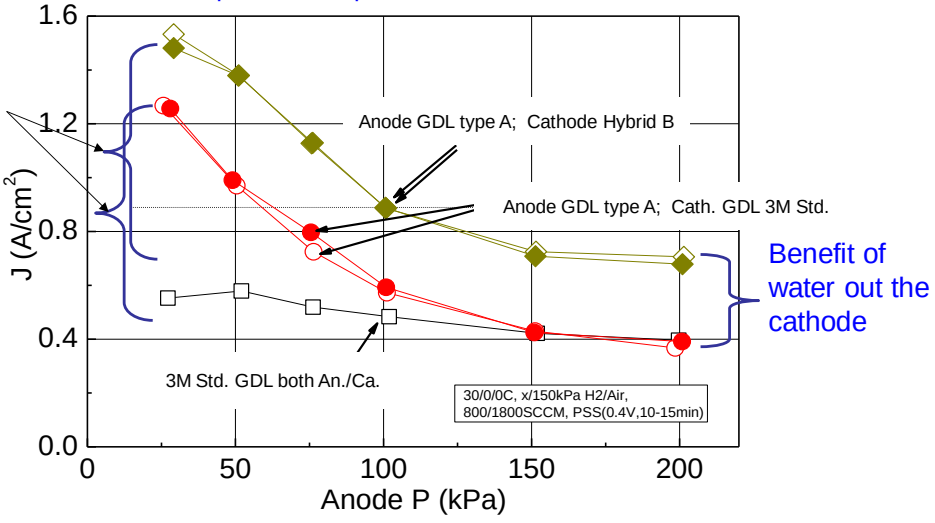

Benefit of water out the cathode

C:\Documents and Settings\us314230\My Documents\publications\2010 ECS\PAPER Water Management - SubAtm Anode SteadyState 020810-[Graph22]

Task 5.1/5.2/5.3 – MEA Integration for Final Stack Testing

❑ 2010 Best of Class" MEA component down-selection process

Example 6: Cathode GDL Options

Summary - Hybrid B CCB Optimization

- With 0.05Pt/C CCB, Pt in CCB is electrochemically H_{upd} active and measurable by surface area and somewhat by ORR activity. However, no benefit is generally observed under H_2/Air pol. curves at low J.
- Presence of CCB improves load transient performance, reversible decay rate, dry performance, cool-dry performance, and high current density-hot performance over non-CCB constructions.
- To date, production CCB's generally have yielded similar or better high J performance than MEAs without CCB, but performance at moderate current densities is suppressed ~10-30 mV.
- Significant performance issues have become evident as the Pt content of the hybrid layer has been reduced to < 0.04 mg/cm^2.
- It is not clear yet if a hybrid MEA construction will meet all the necessary conditions for down-selection for the final 2nd stack durability testing.

Technical Back-Up Slide

Task 5.1/5.2/5.3 – MEA Integration for Final Stack Testing

❑ **2010 Best of Class" MEA component down-selection process**

Low Temperature Water Management Summary

- Strategies to increase the fraction of water moving out the anode and decrease the liquid water moving out the cathode are most effective for increasing cool, wet limiting currents.
  - Natural NSTF hydrophilic property enables this approach
  - Best strategy in principle for any MEA if it can be done – harvests product water to humidify PEM, decreases O_2 mass transport impedance on the cathode.
- Novel effect of sub-atmospheric anode pressure (P_A) operation demonstrated:
  - Several-fold increase in room temperature limiting current
  - P_A effect sensitive to temperature, anode GDL properties. **Useful for screening GDL's.**
  - Conventional "thick" dispersed electrode MEAs do not show same benefit.
  - Water balance mechanistic study
    - Reduced anode pressure decreases total water flux out cathode.
    - Simple model suggests performance improvement due to decreased *liquid* product water flux through cathode GDL.
- Material Factors
  - **Anode GDL backing layer appears to be most significant component affecting control of water flow from cathode to anode at ambient pressure.**
  - Continuing to screen new vendor supplied GDL backing layers and 3M MPL's for best performance and minimal negative factors such as shorting.

Task 5.3 – Stack 1

A primary focus of this project during the period 4/2010-3/2011 was the screening process for down-selecting the final MEA component sets for the final stack testing. Much of the GDL development work, P1 vs P4 catalyst deposition and SET process work (see Sections 7 and 9) were all directed at this objective. The MEA component sets investigated in this process included those bulleted items below:

- Cathode catalyst: composition, loading, deposition process, post process
- Anode catalyst: composition and deposition process (finalized)
- PEM: thickness, supported vs un-supported, chemical additive levels, etc.
- Anode GDL: Backing layer type, MPL properties
- Cathode GDL: Backing layer type and MPL properties, interfacial coatings

As illustrated in Fig. S7, the down-selection process itself involved evaluation of hundreds of MEA's in duplicate covering two dozen or more specific component/process parameter experiments. The results are too extensive and proprietary to discuss here but more information and some examples can be found in this project's 2011 presentation at the DOE annual merit review (http://www.hydrogen.energy.gov/pdfs/review11/fc006_atanasoski_2011_o.pdf).

The other major effort over this same time period was to prepare for and then fabricate roll-good CCMs down-selected for stack 1 testing provided by GM's fuel cell facilities at Honeoye Falls, NY. Two stack tests were planned. The first stack was to enable down-selecting to the final MEA type to be tested in a 2nd stack under an accelerated durability protocol. The first stack compared the six MEA configurations shown in Table S.1, consisting of three different membrane options and three cathode catalyst options. Different GDLs were used for the anodes and cathodes, but only one type of each. The anode catalyst was fixed at NSTF-0.05 mg_{Pt}/cm^2 of the P1 processed PtCoMn. These six MEA types were fabricated as roll-goods and used to populate Stack 1, a 29 cell "Rainbow" stack, one "color" for each MEA type, for initial beginning of life operation under various automotive relevant test protocols for beginning of life testing to enable further down-selection for a second stack (Stack 2 discussed below) that was directed at longer durability studies.

Table S.1. Definition of six MEA configurations evaluated in Stack 1, a 29 cell "rainbow" stack.

CCM ID	PEM	Anode	Cathode	S1622 Cells
Config. 1	3M-24um (w/add. 2)	0.05 P1 PtCoMn	0.15 P4 PtCoMn + SET	9-12
	3M-24um (w/add. 1)	0.05 P1 PtCoMn		
Config. 2	3M-24um (w/add. 2)	0.05 P1 PtCoMn	0.10 P1 PtCoMn	5-8, 22-25
Config. 3	3M-S	0.05 P1 PtCoMn	0.15 P1 PtCoMn	13-16
		0.05 P1 PtCoMn		
Config. 6	3M-X	0.05 P1 PtCoMn	0.15 P1 PtCoMn	17,18
Config. 7		0.05 P1 PtCoMn	0.10 P1 PtCoMn	19-21
Config. 8	3M-24um (w/add. 1)	0.05 P1 PtCoMn	0.15 P1 PtCoMn	1-4, 26-29

The stack 1 performance was a surprise in that it significantly underperformed what we expected based on 50 cm^2 single cells. Figure S14(A) compares polarization curves from the four configuration-1 MEAs in stack 1 with what we and GM had previously measured in 50 cm^2 single cells for similar MEAs under similar conditions. Significant effort was spent by both 3M and GM to "debug" the low performance over a 2.5 month period. A number of confounding issues contributed, including test station water purity, properties or contamination of the ionomer used for the membrane lots used to fabricate the CCMs, and more effective break-in conditioning that is possible with single cells versus large area stacks. Further tests revealed the catalyst ORR metrics and surface areas were as expected, stack compression was nominal, but 50 cm^2 CCMs made in the lab with the same membrane lots as used in roll-to-roll fabrication of the CCM for stack 1 also underperformed what was expected. CCMs from the same roll-to-roll lots were also tested in a 3M short stack (5 cell, 312 cm^2) and found to underperform the single cell results at ambient pressure (Fig. S14(B)) but give similar results at 22 psig (Fig. S14(C)), and slightly better than the GM stack at a similar pressure, as shown in Fig. S14(D).

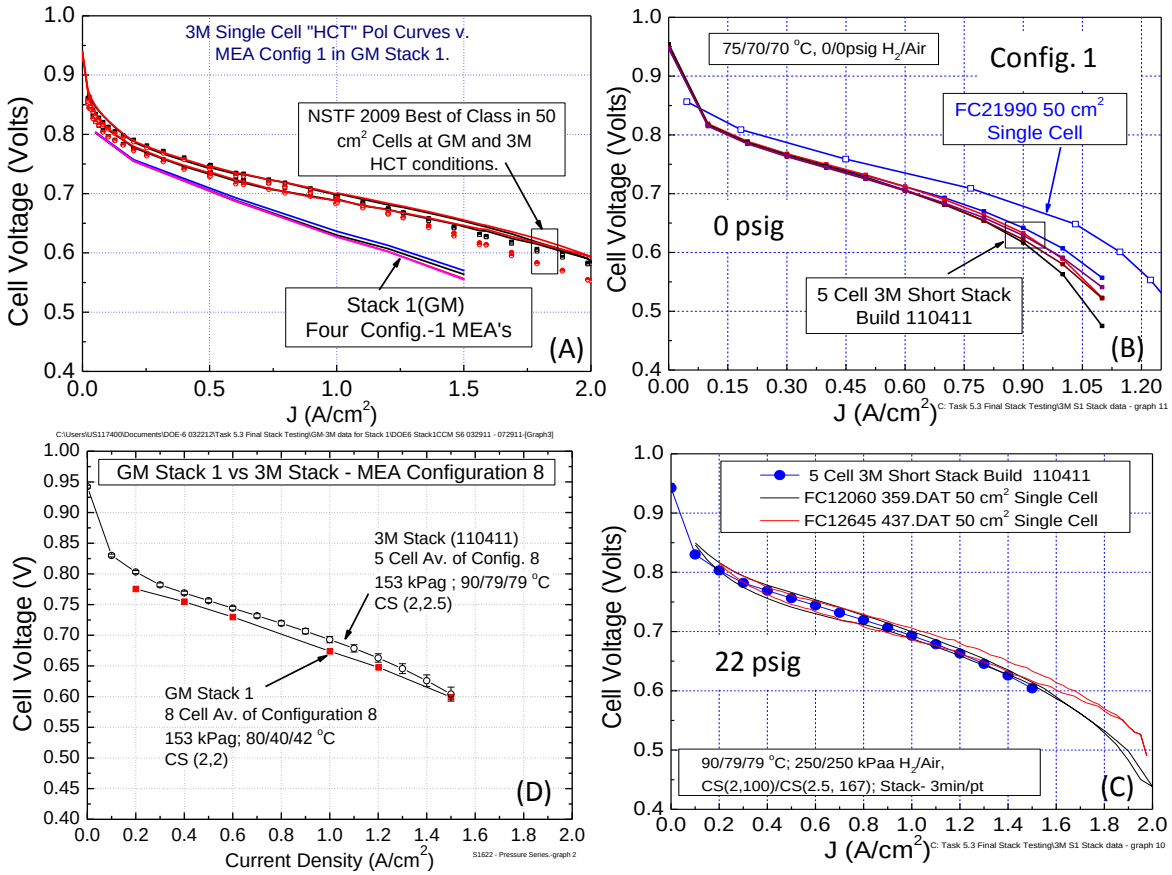

Fig. S14. (A) Comparison of the polarization curves obtained from the four configuration 1 MEAs in stack 1, with the expected performance based on 50 cm^2 single-cell tests measured both at 3M and GM. **(B)** Comparison of ambient pressure polarization curves from the same MEA configuration (made with the same component lot material inputs as used for the GM stack 1 MEA's), but measured at 3M in a 5 cell 312 cm^2 short stack, with the MEA's single cell 50 cm^2 performance. **(C)** Same 5 cell 3M stack and single cell MEA tests as in (B) but at 22 psig. **(D)** Polarization curve averages under nearly the same conditions, from the configuration 8 MEA's tested in the GM stack 1 hardware and in the 3M short stack hardware.

Despite these shortcomings, the GM stack 1 tests were successful in clearly being able to delineate the performance order of the six MEA configuration types, with MEA configuration 1 being the best and down-selected MEA for the eventual stack 2 durability testing. This is illustrated in Fig. S15 which compares the various MEA configuration type average cell voltages at 1.2 A/cm^2 under one particular test condition in the GM stack during the break-in conditioning period.

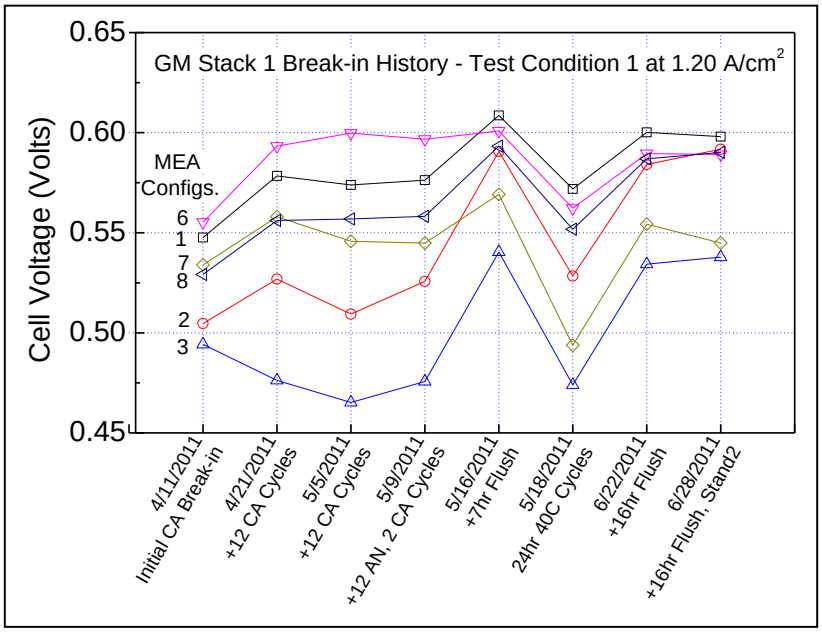

Fig. S15. Comaprison of the six MEA configuration types' average cell voltages at 1.2 A/cm^2 under one particular test condition in the GM stack during the break-in conditioning period.

Figure 7.7 in Section 7 shows a pressure-series of polarization curves, comparing the 4-cell average stack performance of the configuration-1 MEAs with six, 50 cm^2 single-cell tests (done at 3M) having the identical type MEA. (The test conditions used for the data in Fig. 7.7 were those supplied by the systems modeling group at ANL, Ahluwalia et al., and used by 3M for generating other MEA data requested by that group.) Performance improves with pressure similarly in single cells and the stack, consistent with mass transport issues. The stack 1, MEA type 1 performance average underperforms the single-cell tests at all conditions, but not by too much as long as the current density is below ~1.5 A/cm^2. At higher current densities the stack 1 performance falls considerably short of the small single cells.

There is still a question of the possible impact of flow field differences between the quad-serpentine 50 cm^2 cells used at 3M and the flow field of the GM stack. Flow fields had never been systematically optimized for the NSTF type ultra-thin electrodes but as discussed in Section 9.10, they can clearly have a strong effect that might not be considered an issue with conventional thick layer electrodes. This suggests that the different sized lands and channels of the GM flow fields may be part of the difference seen between the short stack 1 test results and the expected single cell test results.

Task 5.3 – Stack 2

The down-selected MEA configuration type 1 in Table S.1 from the stack 1 tests was intended to be the sole MEA type used in the second stack, slated for accelerated durability testing. Due to various issues, this exact MEA configuration 1 did not end up being the final MEA type used in stack 2, as a different membrane was ultimately used. Factoring into the decision were NSTF CCM-production issues with available standard, non-supported PEM lots, which made it attractive to move to the newer generation membrane. This gave the opportunity to switch the membrane type from a standard, non-supported membrane to a new, 3M experimental supported membrane, which previous data had indicated helped improve certain accelerated MEA durability tests. There was risk associated with this decision as these were still

experimental PEMs and optimized integration with the NSTF had not been completed. Work related to resolving these issues required an additional 9 month no-cost extension of the project. The final MEA stack 2 catalysts used were the same as that used in configuration 1 in Table S.1. We subsequently discovered that performance in 50 cm^2 single cells was again much worse than expected. Once the final CCM roll-goods were fabricated, and shortly after shipment to GM, the reason for the underperformance was tracked to the inadvertent production release of an experimental PEM lot to make the CCMs that had been put on hold due to suspected contamination of its ionomer. Due to lack of time and funding to make further MEAs, the decision was made to continue with the stack 2 testing with these CCMs.

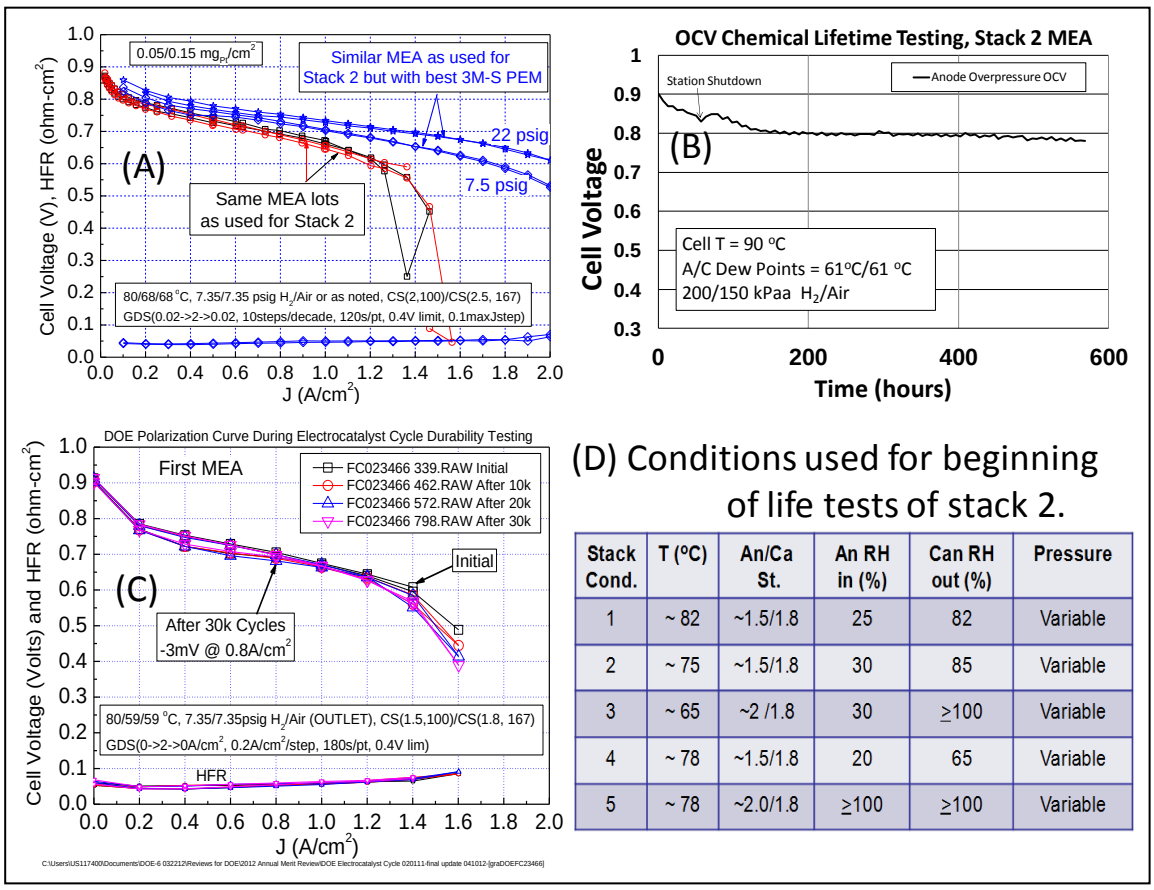

(D) Conditions used for beginning of life tests of stack 2.

Stack Cond.	T (°C)	An/Ca St.	An RH in (%)	Can RH out (%)	Pressure
1	~ 82	~1.5/1.8	25	82	Variable
2	~ 75	~1.5/1.8	30	85	Variable
3	~ 65	~2 /1.8	30	≥100	Variable
4	~ 78	~1.5/1.8	20	65	Variable
5	~ 78	~2.0/1.8	≥100	≥100	Variable

Fig. S16. (A) Single-cell 50 cm^2 GDS polarization curves at 7.5 psig from MEAs taken from the same lot as used for stack 2, compared with a similar MEA that used a known non-contaminated 3M-S membrane, at both 7.5 and 22 psig. **(B)** OCV hold versus time durability test for an MEA identical to that used for stack 2. **(C)** GDS polarization curve and HFR impedance for an MEA identical to that used for stack 2 before, during and after 30,000 CV cycles from 0.6 to 1 volt. **(D)** Conditions used for the beginning of life tests in stack 2.

Figure S16A) compares 50 cm^2 single cell beginning of life performances at 7.5 psig H_2/air from MEAs using the same CCM lots as used in stack 2, with that from MEAs using CCMs made with the same catalyst lots but with normally performing experimental 3M-supported membrane (best 3M-S) at 7.5 and 22 psig H_2/air. In addition to the dramatic loss of limiting current density with the contaminated PEM, the ORR activities were slightly depressed, while the catalyst electrochemical surface areas and MEA HFR were normal. Surprisingly however, as the stack 2 type MEA was tested in a single 50 cm^2 cell using nominally the same

cycling durability protocol discussed below for stack 2, but with periodic recovery, the MEA performance continuously improved for nearly 400 hours and approached that of the best 3M-S curves shown in Figure S16(A).

Despite these issues with beginning of life performance, Figures S16(B) and S16(C) show that the MEAs using CCMs from the same lots as in the stack 2 MEAs, passed both the DOE OCV hold tests and the CV cycling tests. The objective of the OCV hold test is assessment of the whole MEA/membrane durability at OCV at 90°C under 30% RH, 250/200 kPa H_2/air. The target is 500 hours with less than 20% loss of OCV. This MEA went 570 hours with a 13% loss under the 50 kPa H_2 overpressure. The CV cycling accelerated stress test characterizes the resistance of the catalyst to dissolution, agglomeration or loss of activity due to high voltage cycling. The protocol involves cycling the cathode between 0.6 and 1.0 volts and back again at 50 mV/sec under 100/100 kPa H_2/N_2 at 80°C cell and dew points. The target is to have after 30,000 cycles, less than 40% loss of surface area and ORR mass activity and a polarization curve loss of less than 30 mV at 0.8 A/cm^2. The stack 2 lot of MEA's (two were tested) demonstrated a 10±7 mV loss at 0.8 A/cm^2, 16±2% loss of surface area, and 37±2% loss of mass activity. This is the first time we have been able to demonstrate meeting all the targets with this accelerated stress test.

The stack 2 beginning of life performance was evaluated under five different sets of operating conditions as in Fig. S16(D). Consistent with the single cell tests, the beginning of life stack 2 MEA performances were much lower than expected and lower than single cell tests with the same MEA lot, but did not vary significantly from the driest to the wettest conditions, as shown in Fig. S17(A). Average cathode surface areas were approximately normal at 8.2 m^2/g, while in-stack shorting resistances were lower than the standard GM baseline MEAs used as end-cells in the 29-cell short stack.

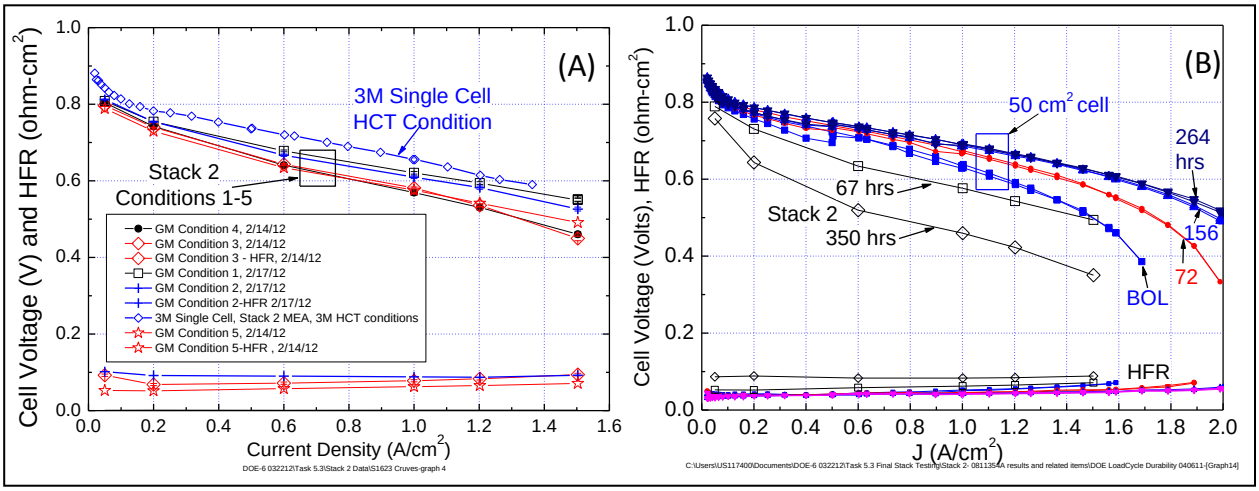

Fig. S17(A) Average MEA beginning-of-life performance in stack 2 at the five conditions shown in Fig. S16(D) compared to the 50 cm^2 single-cell test under GDS high current test conditions of: 80/68/68°C cell temperature/anode/cathode dew points; 150 kPa H_2/air; and anode/cathode stoichiometric flows of 2/2.5. GDS polarization curve conditions are same as in Figure 3.
(B) Comparison of stack 2 performance change after 4 sets of 1,500 load cycles (~300 hours) with the performance change of the same MEA type in a 50 cm^2 single cell (at 3M) after 200 hours of a similar load cycle, interspersed with periodic recovery shutdowns every 12 or 24 hours. Procedure Loop: 1) 5 thermal cycles, 2) polarization curves, 3) 12- or 24-hr cycling under

The objective of stack 2 was to conduct a load-cycling protocol representative of an accelerated stress test for lifetime durability. The protocol chosen was close to that

recommended by the U.S. Drive Fuel Cell Tech Team with some modifications to adapt it to the under-performing MEA and the slower cool-wet transient behavior of the thin layer NSTF electrodes with the GDLs used (see publication numbers four and five in the Appendix for the impact of the anode GDL type on this behavior). Higher pressure, controlled current ramp rate, and minimum voltage control were the main modifications to the protocol. After four sets of 1,500 cycles, ~350 hours of operation, the following observations were made: two point (beginning and end) performance decay rates were much higher than expected (by factors of 3x to 8x); cross-over leak rates and hydrogen take-over in the cells were high; high frequency resistance increased with time but could not account for the lost performance; there were significant fluctuations in performance between each of the 4-cycle sets. Fig. S17(B) shows the beginning-of-life performance (67 hours, open squares) of the stack and that after 350 hours (open diamonds) of cycling, showing extreme decay. Also shown in Fig. S17(B) are the performances of the same stack 2 type MEA tested in a 50 cm^2 single cell at 3M at beginning of life and after 72 hours (red circles), 156 hours (up triangles) and 264 hours (down triangles) with nominally the same load cycling protocol. One key difference in the single cell tests and the stack tests is that the single cell was recovered periodically (12- or 24-hour period) by stopping the load cycling and doing five thermal cycles before resuming the load cycling. Thermal cycling is the typical break-in conditioning protocol used for NSTF MEAs and the large improvement in performance of the single-cell MEA seen with the load cycling is consistent with removal of impurities in the vicinity of the electrodes. The performance of the single cell MEA in Fig. S17(B) continued to improve or stabilized depending on current density for nearly 400 hours, after which its performance started to decay and by 580 hours it had failed due to edge failure of the CCM. This MEA did not have subgasket edge-protection which would be expected to improve lifetime significantly. Low performing cells in the stack 2 prevented going to high current densities and necessitated replacing MEAs and rebuilding the stack on two occasions.

The first rebuild replaced four original NSTF based MEA's with baseline GM MEA's at ~ 330 hours of operation. The second rebuild replaced six more original NSTF stack 2 MEA's with NSTF stack 1 MEA's (which already had ~ 300 Hours on them) at ~ 360 hours of operation. Following the second rebuild, the stack was water-flushed, but another cell failed above 1.2 A/cm^2 while several durability cycles were run. Performance started reasonably well but then quickly diminished. It was observed that the shorting resistance for every cell, including all the GM baseline cells, would significantly worsen (drop in value) after each such rebuild. The reason for this was not determined.

The stack sat for 6 weeks after a wet shut down, then polarization curves were re-ran and one further cycling attempt was made on 8/16/12. Only several hours of cycling were completed before the stack 2 forced a test station E-stop. It was eventually determined that further work with the stack would not be instructive and testing was discontinued.

The following three sets of figures show the final polarization curves obtained with the stack 2 during the last trials. They show stack 2's cell by cell plots of three types of polarization curve voltages at 0.2, 0.6 and 1 A/cm^2 versus time. The NSTF cells are in blue, the control cells in red. Replacement of failed NSTF cells by the GM baseline cells (red curves) can pull the whole stack averages up. Replacing the bad Stack 2 MEA's with (used) Stack 1 MEA's also improved the average. After 300 hours, there was some indication that all cells were improving even the original bad stack 2 MEA's.

Task 5.3 Final Stack Testing (cont.)

Example of degradation versus time with polarization curve type A at 0.2, 0.6 and 1 A/cm^2.

- Some cells appeared to be recovering slightly at all currents, near the end.
- The stack 1 (Performance stack) MEA's were much better when replacing the failed stack 2 (Durability stack) MEA's.

Polarization Curve Type A, 1.0A/cm^2

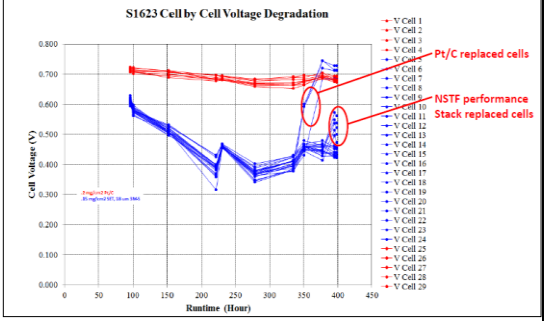

Polarization Curve Type A, 0.2 A/cm^2

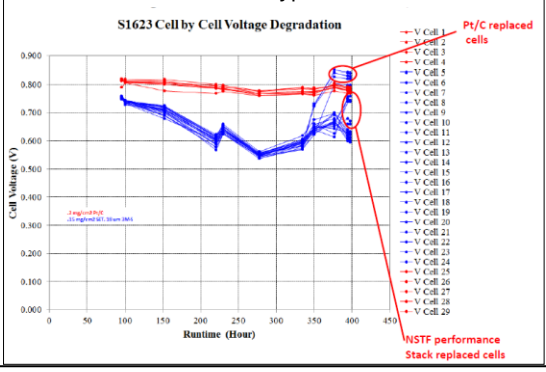

Polarization Curve Type A, 0.6 A/cm^2

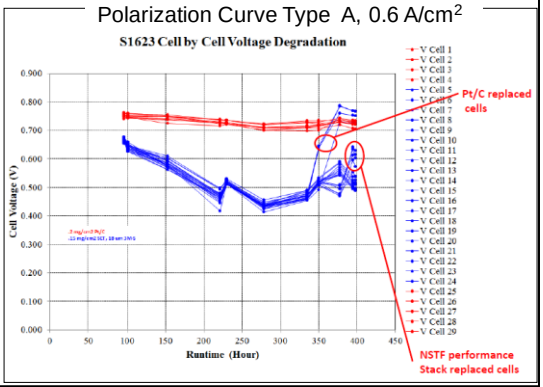

Task 5.3 Final Stack Testing

Example of degradation versus time with polarization curve type B at 0.2, 0.6 and 1 A/cm^2.

- Some cells appeared to be recovering slightly at all currents, near the end.
- The stack 1 (performance) MEA's were much better when replacing the failed stack 2 (durability) MEA's.

Polarization Curve Type B, 1.0 A/cm^2

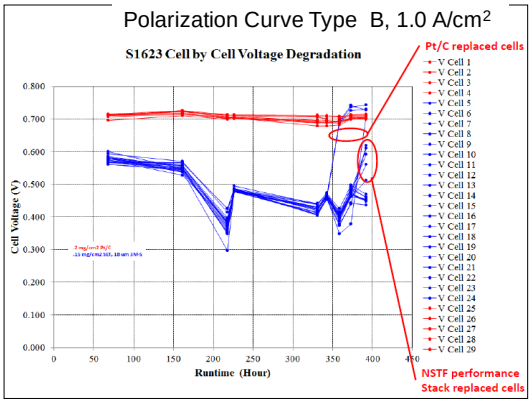

Polarization Curve Type B, 0.2A/cm^2

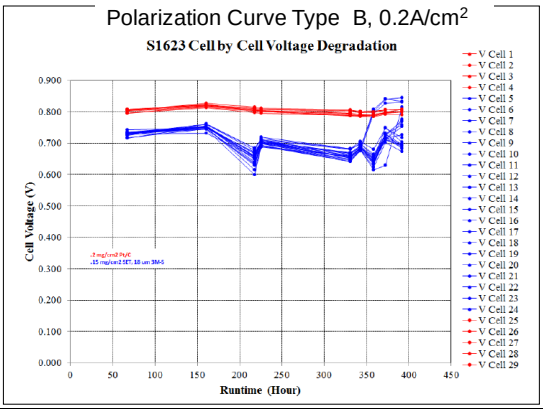

Polarization Curve Type B, 0.6 A/cm^2

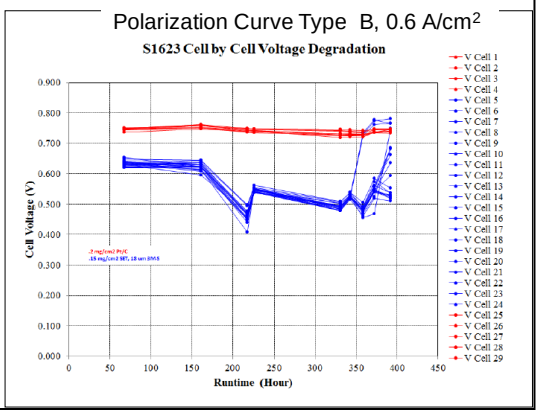

Task 5.3 Final Stack Testing

Example of degradation versus time with polarization curve type A at 0.2, 0.6 and 1 A/cm^2.

- Some cells appeared to be recovering slightly at all currents, near the end.
- The stack 1 (Performance stack) MEA's were much better when replacing the failed stack 2 (Durability stack) MEA's.

Polarization Curve Type C, 1.0 A/cm^2

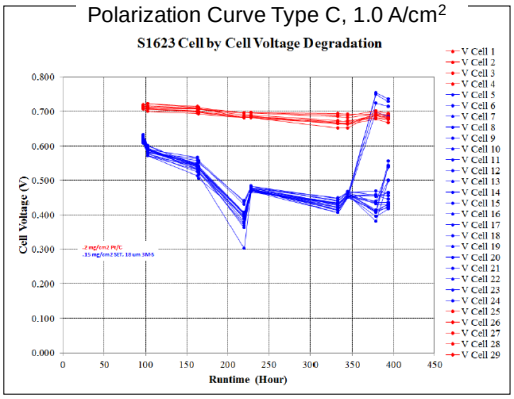

Polarization Curve Type C, 0.2 A/cm^2

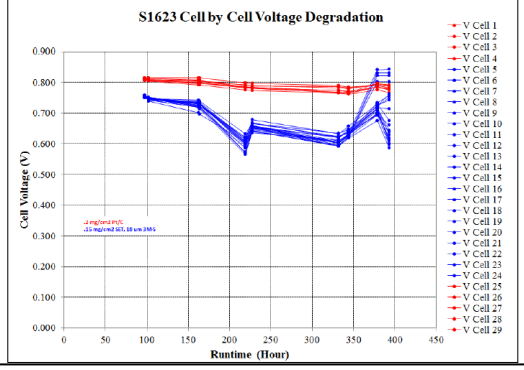

Polarization Curve Type C, 0.6 A/cm^2

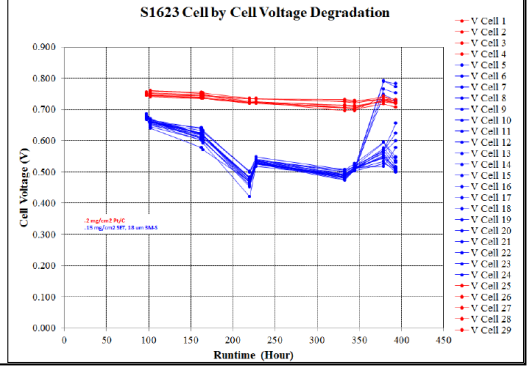

Stack 2 Testing Conclusions provided by Eric Thompson, GM
(Comments in parenthesis added by 3M for clarification.)

"Following the last rebuild, durability cycling data was discouraging. The "Durability NSTF cells" (meaning stack 2) degraded quickly. Cell instability in polarization curves was reported by the technician. On the bright side, data following the last rebuild when "Performance Stack NSTF Cells" (i.e. stack 1) were used to replace the troublesome "Durability NSTF cells", those cells displayed a more expected and reasonable behavior for NSTF. Significant separation in performance (was observed) between the two sets of NSTF parts in the durability cycling data. Also, "NSTF performance stack" (stack 1) MEAs performed higher in polarization curve degradation data. This gives some positive indication that with a healthy membrane, the NSTF can perform much better in the (modified) durability cycling protocol.

In hindsight we may have gotten more hours and more useful data doing a full replacement of "Durability NSTF cells" with "Performance NSTF cells" earlier in the process. (We were headed in this direction and debated doing so.) The presence of any contaminated NSTF Durability cells just held back and limited what could be run and observed with Performance Stack NSTF parts (in the Durability stack 2). This exercise has also given learning as a framework of how the DOE durability cycling protocol should be modified to accommodate and align with NSTF attributes: Higher pressure (200 kPa) as opposed to near ambient pressure; Utilize at least a 5 sec ramp-in in load transients, as opposed to direct step transient; Maintain cell voltage above 0.6 V based on Jingxin's study seems beneficial, although we have not fully confirmed this here."

Task 6

Selected Supplementary Information

Task 6.0 - New Task focused on faster/simpler break-in conditioning

6.1 Improved break-in protocols and conditions

3M Advanced Cathode Catalysts and Supports…… DOE Review Nov. 9, 2010

Task 6 MEA break-in conditioning

Objective: Dramatically reduce the time and simplify the process for initial break-in conditioning of NSTF catalyst based MEA's.

- **Issue:** Low loading and low surface area of NSTF electrodes requires unacceptable times, > 24 hours, to reach peak performance under current break-in and conditioning protocols. Water flushing also is used in our standard "thermal cycling" protocol and may not be available for stack conditioning.

- **Two subtasks focusing on test station protocols and materials:**
  - Subtask 6.1. Break-in conditioning protocol - quantify the effect of test station operating parameters on the time for break-in conditioning of the standard PtCoMn NSTF MEA's in 50 cm^2 single cell tests
  - Subtask 6.2.Component Factors - Identify MEA component factors having greatest effect on break-in conditioning time

Work this period:
- Limited to evaluating success of "stack capable" start-up protocol to wider array of stations and material component sets.
- Effectiveness for wider array of all MEA performance protocols.

3M Advanced Cathode Catalysts and Supports…… DOE Review Nov. 9, 2010

Task 6 MEA break-in conditioning

Development of "Stack-Capable" FAST Conditioning Methodology

- Objective of experiments is to determine if NSTF MEAs can be conditioned using rapid conditioning protocols which should be feasible in stacks
  - Low reactant flows
  - Current rather than voltage control
  - Completely dry inlet gases (simpler conditioning; less expensive conditioning equipment required)

- To allow completely dry operation, water balance calculations suggest that pressurized reactants are required
  - ~200kPa for 70-75C cell with constant stoich 2.0/2.0

- Experiments based on modification of April 2010 baseline "fan-cooling" script, Script #52
  - Script #52: High reactant flows, voltage control, humidified gases

- Tests done with 2009 Best of Class NSTF MEAs (0.05PtCoMn/0.10PtCoMn, 3M 850EW 20u, 2979 GDLs), on single test station (S20).

Task 6 MEA break-in conditioning

Development of "Stack-Capable" FAST Conditioning Methodology

Protocol Definitions

Script #52		
Tcycle	**LoadCycle**	**Duration**
{50/45/45C, 800/1800SCCM, 100/100kPa}, {30/60/60C, 200/400SCCM, 100/100kPa}	OCV(2s), 0.5V(2s), 0.25V(10s) 1 PDS Curve per Tcycle (at max T)	1hr
{75/70/70C, 800/1800SCCM, 100/100kPa}, {55/90/90C, 200/400SCCM, 100/100kPa}	OCV(2s), 0.5V(2s), 0.25V(10s) 1 PDS Curve per Tcycle (at max T)	3hr
{75/70/70C, 800/1800SCCM, 100/100kPa}, {30/60/60C, 200/400SCCM, 100/100kPa}	OCV(2s), 0.5V(2s), 0.25V(10s) 1 PDS Curve per Tcycle (at max T)	16hr

April 2010 FAST Baseline

Fast Startup (Dry VCycle)		
Tcycle	**LoadCycle**	**Duration**
{50/0/0C, 800/1800SCCM, 200/200kPa}, {30/0/0C, 200/400SCCM, 200/200kPa}	OCV(2s), 0.5V(2s), 0.25V(10s) 1 PSS(0.4V) per Tcycle (at max T)	1hr
{75/0/0C, 800/1800SCCM, 200/200kPa}, {55/0/0C, 200/400SCCM, 200/200kPa}	OCV(2s), 0.5V(2s), 0.25V(10s) 1 PSS(0.4V) per Tcycle (at max T)	3hr
{75/0/0C, 800/1800SCCM, 200/200kPa}, {30/0/0C, 200/400SCCM, 200/200kPa}	OCV(2s), 0.5V(2s), 0.25V(10s) 1 PSS(0.4V) per Tcycle (at max T)	16hr

Differences from #52
- Dry gases
- 200kPa Pressure
- PDS curves replaced w/ PSS(0.4V, 5min)
  - •avoid dryout at low J portion of test

3M Advanced Cathode Catalysts and Supports…… DOE Review Nov. 9, 2010

Task 6 MEA break-in conditioning

Development of "Stack-Capable" FAST Conditioning Methodology

Protocol Definitions

Script #52

Tcycle	LoadCycle	Duration
{50/45/45C, 800/1800SCCM, 100/100kPa}, {30/60/60C, 200/400SCCM, 100/100kPa}	OCV(2s), 0.5V(2s), 0.25V(10s) 1 PDS Curve per Tcycle (at max T)	1hr
{75/70/70C, 800/1800SCCM, 100/100kPa}, {55/90/90C, 200/400SCCM, 100/100kPa}	OCV(2s), 0.5V(2s), 0.25V(10s) 1 PDS Curve per Tcycle (at max T)	3hr
{75/70/70C, 800/1800SCCM, 100/100kPa}, {30/60/60C, 200/400SCCM, 100/100kPa}	OCV(2s), 0.5V(2s), 0.25V(10s) 1 PDS Curve per Tcycle (at max T)	16hr

April 2010 FAST Baseline

Fast Startup (Dry CathodeStarve)		
Tcycle	**LoadCycle**	**Duration**
{50/0/0C, 140/124SCCM, 200/200kPa}, {30/0/0C, 140/124SCCM, 200/200kPa}	OCV(2s), 0.1A/cm2(10s), 0.2A/cm2(3s) 1 PSS(0.4V) per Tcycle (at max T)	1hr
{75/0/0C, 140/124SCCM, 200/200kPa}, {55/0/0C, 140/124SCCM, 200/200kPa}	OCV(2s), 0.1A/cm2(10s), 0.2A/cm2(3s) 1 PSS(0.4V) per Tcycle (at max T)	3hr
{75/0/0C, 140/124SCCM, 200/200kPa}, {30/0/0C, 140/124SCCM, 200/200kPa}	OCV(2s), 0.1A/cm2(10s), 0.2A/cm2(3s) 1 PSS(0.4V) per Tcycle (at max T)	16hr

Differences from #52
- "Stack capable"
  - •J Control
  - •Low V induced by cathode starvation
- Low J; low reactant flows
- Dry gases
- 200kPa Pressure
- PDS curves replaced w/ PSS(0.4V, 5min)
  - •avoid dryout at low J portion of test

Task 6 MEA break-in conditioning

Development of "Stack-Capable" FAST Conditioning Methodology

Evaluation of Conditioning Rates

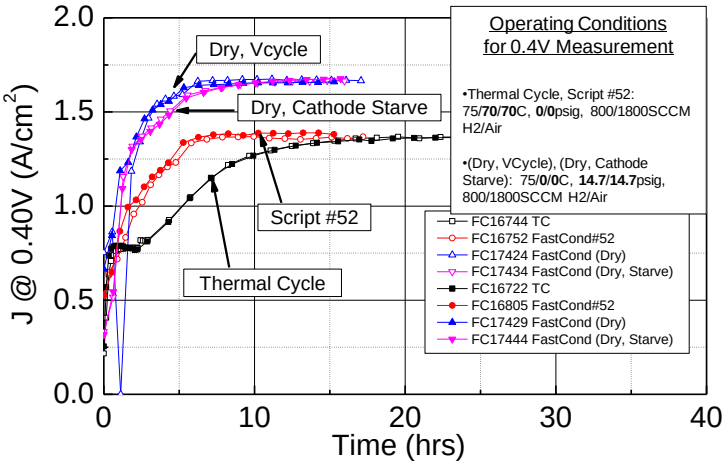

Q:\Projects\0046650001_DOE_VI\Shared\Task1.1.1 OriginPlots\Other\DryConditioning\DryConditioning 040510-[Graph1]

- Startup rates with dry conditioning protocols similar to baseline FAST protocol #52.
- Nominally fully conditioned in <8 hours.
- Absolute performance differences possibly due to different reactant pressures used.

3M Advanced Cathode Catalysts and Supports…… DOE Review Nov. 9, 2010

Task 6 MEA break-in conditioning

Development of "Stack-Capable" FAST Conditioning Methodology

80C Polarization Curve Performance

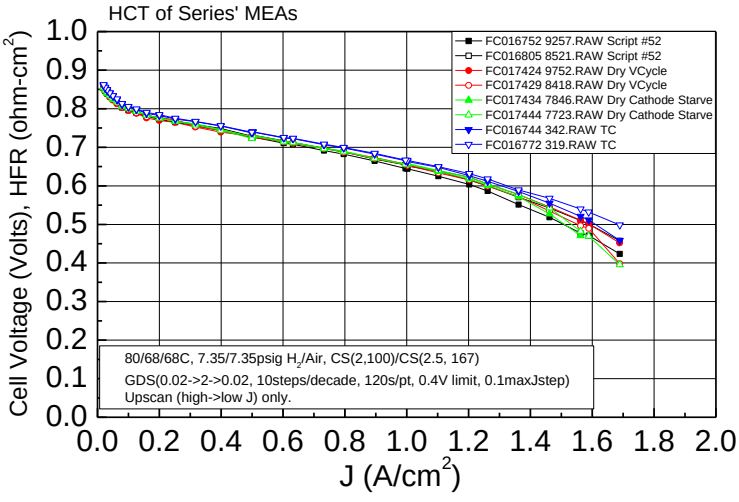

Q:\Projects\0046650001_DOE_VI\Shared\Task1.1.1 OriginPlots\Other\DryConditioning\DryConditioning 040510-[graHCTUS]

- HCT performance at high J slightly lower with FAST than thermal cycle protocol.

Task 6 MEA break-in conditioning

Development of "Stack-Capable" FAST Conditioning Methodology

Activity and HCT Relative Metric Values

Performance Relative to Thermal Cycling (40hrs)	Wet Vcycle (Script #52)		Dry Vcycle		Dry CathodeStarve	
	Abs	%Change	Abs	%Change	Abs	%Change
PDS 0.813V J (A/cm2-planar)	-0.044	-22	-0.032	-16	-0.027	-14
SEF (cm2-Pt/cm2-planar)	-0.314	-3				
ORR Absolute Activity @ 1050s (mA/cm2-planar)	0.496	3	-0.394	-3	-2.378	-16
HCT Meas V @ 0.020A/cm2 (Volts)	-0.006		-0.009		-0.006	
HCT Meas V @ 0.32A/cm2 (Volts)	-0.009		-0.013		-0.007	
HCT Meas V @ 1.00A/cm2 (Volts)	-0.017		-0.011		-0.008	
HCT Meas V @ 1.46A/cm2 (Volts)	-0.031		-0.021		-0.026	

- Tabulated metrics indicate that FAST conditioning generally results in modest reductions in performance v. thermal cycling
- Large losses in low J PDS and high J HCT tests.

3M Advanced Cathode Catalysts and Supports…… DOE Review Nov. 9, 2010

Task 6 MEA break-in conditioning

Evaluation of FAST Conditioning by All Performance Characteristics

Sample ID	Short Sample Description	Anode Catalyst ID	Anode GDL ID	Cathode Catalyst ID	Cathode GDL ID	Cathode Pt Loading (mg/cm2-planar)	PEM ID	Start Date	Station ID
FC017092	0.05PtCoMn/0.10PtCoMn 3M 20u H2315/2979 TC S14	P409281B	H2315	P409272	297995007B	0.1	MM09168B	2/26/2010	14
FC017228	0.05PtCoMn/0.10PtCoMn 3M 20u H2315/2979 TC S14	P409281B	H2315	P409272	297995007B	0.1	MM09168B	3/12/2010	14
FC017910	0.05Pt/0.15PtCoMn 3M/G 2979/2979 TC S14	P1D10145	297995007B	P408344A	297995007B	0.15	A747420	6/2/2010	14
FC018060	0.05Pt/0.15PtCoMn 3M/G H2315/2979 FASTCOND S14	P1D10145	Freudenberg H2315	P408344A	297995007B	0.15	A747420	6/14/2010	14
FC018102	0.05Pt/0.15PtCoMn 3M/G H2315/2979 TC S14	P1D10145	Freudenberg H2315	P408344A	297995007B	0.15	A747420	6/16/2010	14
FC018172	0.05Pt/0.15PtCoMn 3M/G 2979/2979 FASTCOND S14	P1D10145	297995007B	P408344A	297995007B	0.15	A747420	6/24/2010	14
FC018197	0.05Pt/0.15PtCoMn 3M/G H2315/2979 FASTCOND S14	P1D10145	Freudenberg H2315	P408344A	297995007B	0.15	A747420	6/29/2010	14
FC018224	0.05Pt/0.15PtCoMn 3M/G H2315/2979 FASTCOND S14	P1D10145	Freudenberg H2315	P408344A	297995007B	0.15	A747420	7/6/2010	14
FC018235	0.05Pt/0.15PtCoMn 3M/G H2315/2979 TC S14	P1D10145	Freudenberg H2315	P408344A	297995007B	0.15	A747420	7/8/2010	14

- During FAST conditioning protocol development, only typically evaluated high T performance.
- Here, evaluating activity, low and high T water management, performance stability, activities and surface areas.
- Note different material set than protocol development study – 0.05Pt/0.15PtCoMn, 3MG, H2315/2979 – and different test station.

Task 6 MEA break-in conditioning

Evaluation of FAST Conditioning by All Performance Characteristics

80 °C Polarization Curve Performance

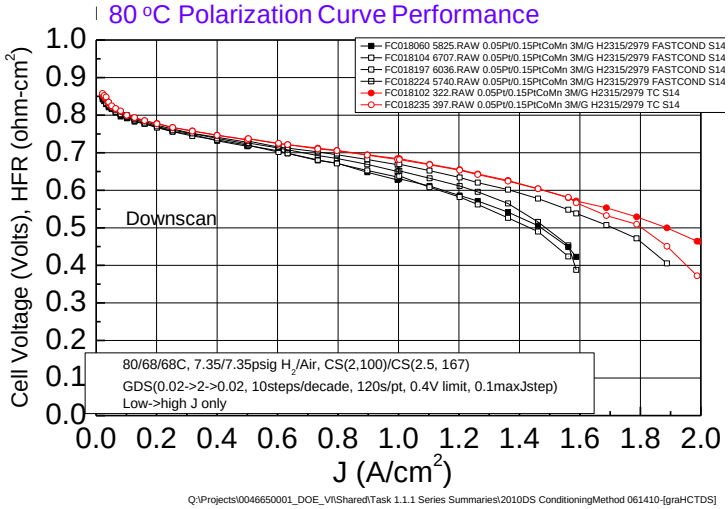

- FAST conditioned samples had significantly reduced limiting current than thermal cycled MEAs.
- Much larger gap than expected based on previous protocol development study
  - Materials?
  - Station?

3M Advanced Cathode Catalysts and Supports…… DOE Review Nov. 9, 2010

Task 6 MEA break-in conditioning

Evaluation of FAST Conditioning by All Performance Characteristics

80C Polarization Curve Metrics

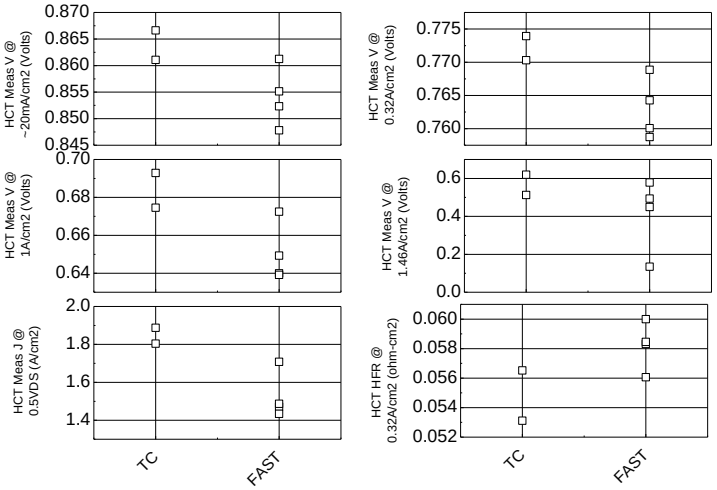

- FAST COND MEAs had lower performance overall.
- HFR was slightly higher with FAST COND MEAs @ 0.32A/cm2 (not enough to explain performance difference)

Task 6 MEA break-in conditioning

Evaluation of FAST Conditioning by All Performance Characteristics

Activity Metrics

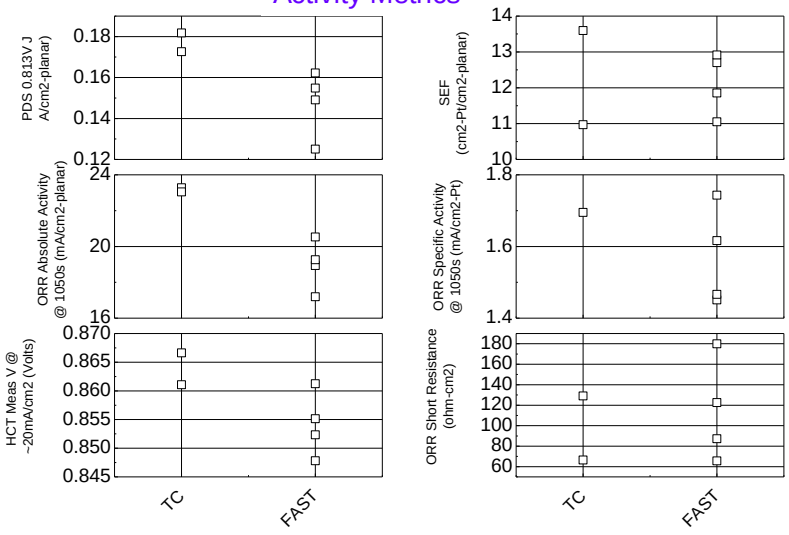

- FAST MEAs typically had lower absolute kinetic performance

Task 6 MEA break-in conditioning

Evaluation of FAST Conditioning by All Performance Characteristics

30 °C Steady State Performance

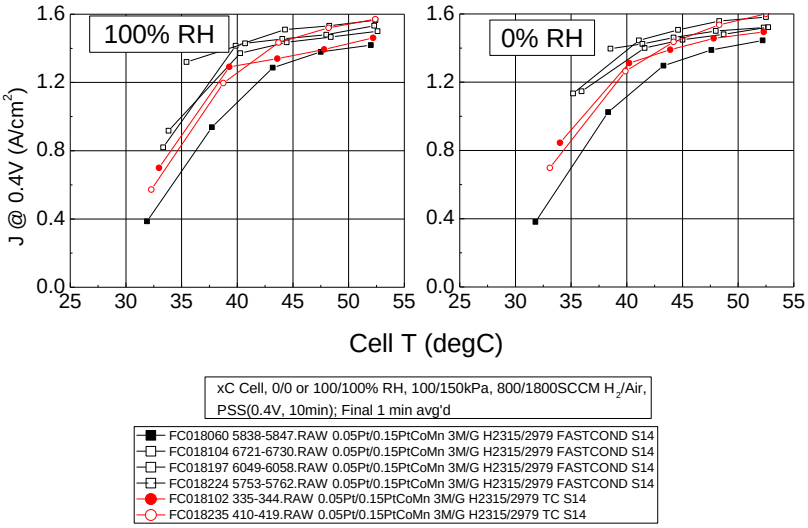

- FAST Conditioned MEAs generally had similar or higher cool PSS performance than MEAs that were conditioned by the standard thermal cycling protocol.

Task 6 MEA break-in conditioning

Evaluation of FAST Conditioning by All Performance Characteristics

30C Startup Transient Performance

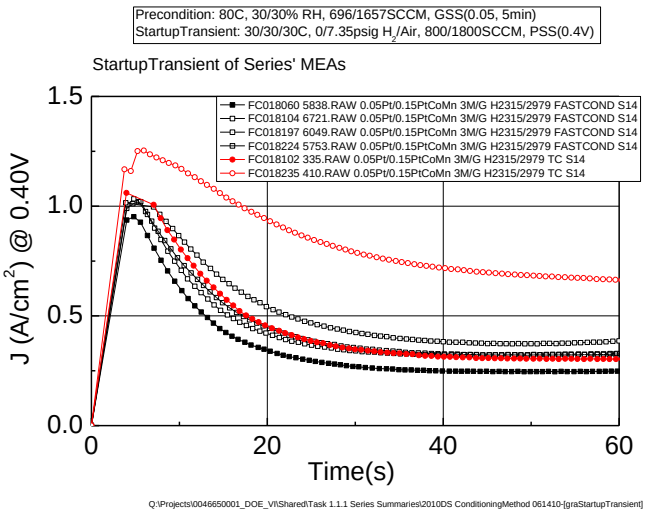

- Other than one thermal-cycled MEA, all MEAs generally had similar startup transients.

3M Advanced Cathode Catalysts and Supports…… DOE Review Nov. 9, 2010

Task 6 MEA break-in conditioning

Evaluation of FAST Conditioning by All Performance Characteristics

Hot and Dry Performance of Series' MEAs

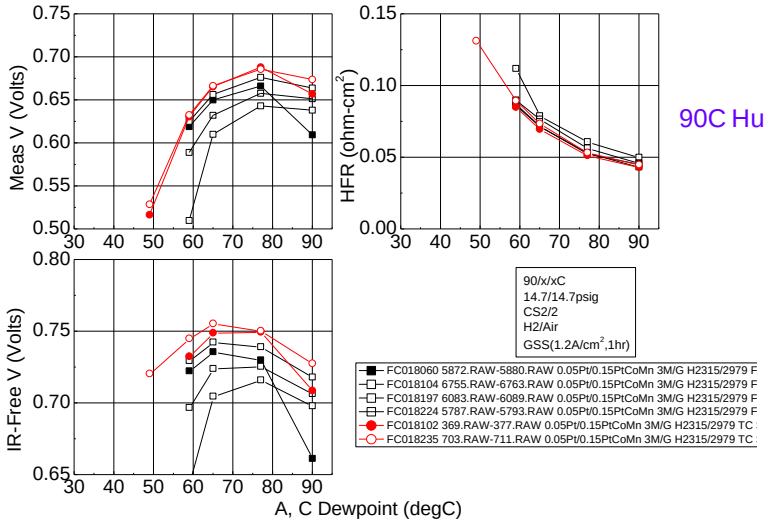

90C Humidification Sensitivity

- FAST COND MEAs generally had worse performance than TCd MEAs, especially at lower RH
- FAST COND MEAs generally had slightly high HFR at all humidities
- Many FAST Conditioned MEAs died during the driest part of this test.

Task 6 MEA break-in conditioning

FAST Conditioning Summary

- Systematic studies of the factors important for FAST conditioning were conducted. Critical factors included rapid and numerous voltage cycles over a sufficiently large range and sufficiently large temperature cycles.
- FAST conditioning methods were further developed which enabled achievement of nominally peak performance in < 8 hours via nominally stack-capable methods.
- However, FAST conditioning does not always achieve performance parity with the slower, historical 3M thermal cycle conditioning procedure. Small but significant reductions in cathode kinetic metrics occur, and depending upon the material set, significant reductions in the high current density performance are observed.
- Further systematic study is needed to determine if the performance gaps can be resolved.

Task 6. MEA break-in conditioning

Protocols

- Protocols' primary repeat sections are shown.
- Protocols are repeated until stable performance is achieved.
- Reactant flows shown for 50cm^2 cell.

Standard Thermal Cycle

```
//WARMUP WITH POL. CURVES AND V HOLDS//
SET_CELL_TEMPERATURE (75C)
SET_ANODE_FLOW (800SCCM)
SET_CATHODE_FLOW (1800SCCM)
SET_ANODE_HUMIDIFICATION (70C)
SET_CATHODE_HUMIDIFICATION (70C)
SET_ANODE_PRESSURE (0 psig)
SET_CATHODE_PRESSURE (0 psig)
COUNT= (0); WHILE_COUNT_< (4)
   COUNT+1 ()
   POL. CURVE (0.85V->0.25V->0.85V, 0.05V/STEP, 10S/STEP)
   V=0.4V,5min
END_WHILE_COUNT ()
//COOL TO ROOM T, GASES OFF, LIQ WATER INJECT//
SET_CELL_TEMPERATURE (25C)
SET_ANODE_FLOW (0SCCM)
SET_CATHODE_FLOW (0SCCM)
SET_ANODE_HUMIDIFICATION (0.26CC/MIN)
SET_CATHODE_HUMIDIFICATION (0.40CC/MIN)
J=0A/cm2, 45min
```

Fast Condition (Dry, Starve)

```
//WARMUP WITH J (CURRENT DENSITY) CYCLE//
SET_CELL_TEMPERATURE (75C)
SET_ANODE_FLOW (140SCCM)
SET_CATHODE_FLOW (124SCCM)
SET_ANODE_HUMIDIFICATION (DRY)
SET_CATHODE_HUMIDIFICATION (DRY)
SET_ANODE_PRESSURE (14.7 psig)
SET_CATHODE_PRESSURE (14.7 psig)
COUNT= (0); WHILE_COUNT_< (22)
   COUNT+1 ()
   J=0A/cm2, 2s
   J=0.1A/cm2, 10s
   J=0.2A/cm2, 3s
END_WHILE_COUNT ()
//PERFORMANCE CHECK//
SET_ANODE_FLOW ( 800SCCM)
SET_CATHODE_FLOW (1800SCCM)
V=0.4V, 5min
//MORE J CYCLE AT 75C//
SET_ANODE_FLOW (140SCCM)
SET_CATHODE_FLOW (124SCCM)
COUNT= (0); WHILE_COUNT_< (22)
   COUNT+1 ()
   J=0A/cm2, 2s
   J=0.1A/cm2, 10s
   J=0.2A/cm2, 3s
END_WHILE_COUNT ()
//COOL CELL TO 55C WITH J CYCLE//
SET_CELL_TEMPERATURE (55C)
COUNT= (0); WHILE_COUNT_< (44)
   COUNT+1 ()
   J=0A/cm2, 2s
   J=0.1A/cm2, 10s
   J=0.2A/cm2, 3s
END_WHILE_COUNT ()
```

Appendix

Appendix

Reproduction of Key Publications Resulting from this Project

Fifteen of the twenty-seven publications resulting from this project are considered sufficiently important to be included in this final report because they provide concise and complete summaries of the progress made in several of the key accomplishment areas discussed in sections 7 and 9 of the project overview. The first one, a tutorial on the NSTF technology, provides all background information necessary to understand the results discussed in the main body of this report. Several in the list below, including numbers 1, 2, 7, and 8, provide a broader perspective of how the NSTF electrocatalyst technology and materials generated in this project compare with the broader field of ORR electrocatalysts for fuel cells, and also opportunities for OER applications on fuel cell anodes and water electrolysis.

A.1 Key 3M Publications

1. Updated version of: Mark K. Debe, "Nanostructured Thin Film Electrocatalysts for PEM Fuel Cells – A Tutorial on the Fundamental Characteristics and Practical Properties of NSTF Catalysts," *ECS Transactions* **45** (2) 47-68 (2012). Prepared for submission to The *JES*.
2. M. K. Debe, R. T. Atanasoski, and A. J. Steinbach, "Nanostructured Thin Film Electrocatalysts – Current Status and Future Potential, *ECS Transactions*, **41**(1) 937-954 (2011).
3. M. K. Debe, A. J. Steinbach, G. D. Vernstrom, S. M. Hendricks, M. J. Kurkowski, R. T. Atanasoski, P. Kadera, D. A. Stevens, R. J. Sanderson, E. Marvel and J. R. Dahn, "Extraordinary oxygen reduction activity of Pt_3Ni_7," *J. Electrochem. Soc.* **158**(8) B910-B918 (2011), and *ECS Trans*., **33** 143 (2010).
4. A. J. Steinbach, M. K. Debe, J. L. Wong, M. J. Kurkowski, A. T. Haug, D. M. Peppin, S. K. Deppe, S. M. Hendricks, and E. M. Fischer, "A New Paradigm for PEMFC Ultra-Thin Electrode Water Management at Low Temperatures," *ECS Trans.*, **33**(1), 1179-1188 (2010).
5. A. Steinbach, M. Debe, M. Pejsa, D. Peppin, A. Haug, M. Kurkowski and S. Maier-Hendricks, "Influence of Anode GDL on PEMFC Ultra-thin Electrode Water Management at Low Temperatures," *ECS Transactions*, **41**(1) 449-457 (2011).
6. Mark K. Debe, "Effect of Electrode Structure Surface Area Distribution on High Current Density Performance of PEM Fuel Cells," *J. Electrochemical Society* **159**(1) B54-B67 (2011).
7. M. K. Debe, S. M. Hendricks, G. D. Vernstrom, M. Meyers, M. Brostrom, M. Stephens, and Q. Chan, Jason Willey, Monjid Hamden, and Cortney K. Mittelsteadt**,** Christopher B. Capuano, Katherine Ayers and Everett Anderson, "Initial Performance and Durability of Ultra-low Loaded NSTF Electrodes for PEM Electrolyzers," *J. Electrochem. Soc.,* **159**(6) K165-K176 (2012).
8. Mark K. Debe, "Electrocatalyst Approaches and Challenges for Automotive Fuel Cells," invited review article, *Nature,* **486**(9401) 43-51(2012).

A.2 Key Dalhousie Publications

9. Gary Chih-Kang, D. A. Stevens, J. C. Burns, R. J. Sanderson, G. D. Vernstrom, R. T. Atanasoski, M. K. Debe and J. R. Dahn, "Oxygen reduction activity of dealloyed $Pt_{1-x}Ni_x$ catalysts." *J. Electrochem. Soc.* **158**(8) B919-B26 (2011).
10. Arnd Garsuch, D. A. Stevens, R. J. Sanderson, S. Wang, R. T. Atanasoski, S. Hendricks, M. K. Debe, and J. R. Dahn, "Alternative Catalyst Supports Deposited on Nanostructured Thin Films for Proton Exchange Membrane Fuel Cells," *J. Electrochemical Society* **157**(2) B187-B194 (2010).

11. Arman Bonakdarpour, Tara R. Dahn, Radoslav Atanasoski, Mark K. Debe, and Jeff R. Dahn, "H_2O_2 Release During Oxygen Reduction Reaction on Pt Nano Particles," *Electrochemical and Solid-State Letters*, **11**, B208-B211, 2008.
12. D. A. Stevens, R. Mehrotra, R. J. Sanderson, G. D. Vernstrom, R. T. Atanasoski, M. K. Debe and J. R. Dahn, "Dissolution of Ni from high Ni content $Pt_{1-x}Ni_x$ alloys," *J. Electrochem. Soc.* **158**(8) B905-B909 (2011).

A.3 Key ANL Publications

13. Dennis van der Vliet, Chao Wang, Mark Debe, Radoslav Atanasoski, Nenad M. Markovic and Vojislav R. Stamenkovic, "Platinum-alloy Nanostructured Thin Film Catalysts for the Oxygen Reduction Reaction," *Electrochimica Acta*. **56** 8695-8699 (2011).
14. R.K. Ahluwalia, X. Wang, A. Lajunen, A.J. Steinbach, S.M. Hendricks, M.J. Kurkowski, and M.K. Debe, "Kinetics of Oxygen Reduction Reaction on Nanostructured Thin-Film Platinum Alloy Catalyst," *Journal of Power Sources* **215** (2012) 77-88.
15. Dennis van der Vliet, Chao Wang, Dusan Tripkovic, Dusan Strmcnik, Xiaofeng Zhang, Mark Debe, Radoslav Atanasoski, Nenad M. Markovic and Vojislav R. Stamenkovic, "Metallic Nanotubes with Tunable Composition and Structure as Advanced Electrocatalysts," *Nature Materials*, **in press** (2012).

The publications listed on the previous two pages of the Appendix have been deleted due to copyright protection protocol.